Copyright

by

Chung-Yon Lin

2016

**The Dissertation Committee for Chung-Yon Lin Certifies that this is the approved version of the following dissertation:**

# Progress towards a highly efficient and accurate platform for enantiomeric excess determination

**Committee:**

Eric V. Anslyn, Supervisor

Jonathan L. Sessler

Richard A. Jones

Adrian Keatinge-Clay

# Progress towards a highly efficient and accurate platform for enantiomeric excess determination

**by**

**Chung-Yon Lin, B.S.**

**Dissertation**

Presented to the Faculty of the Graduate School of

The University of Texas at Austin

in Partial Fulfillment

of the Requirements

for the Degree of

**Doctor of Philosophy**

**The University of Texas at Austin**

**May 2016**

# Dedication

For Morimoto and unconditional love.

## Acknowledgements

I would like to gratefully acknowledge my mentor Eric Anslyn. I am extremely fortunate to have had the opportunity to grow under his tutelage. Similarly, my undergraduate chemistry professors have been hugely influential in my career, particularly Erland Stevens and Felix Carrol. Also, my high school chemistry teacher Jill Shore, I wouldn't have turned to chemistry if it weren't for her. I would also like to acknowledge those who have stood by me through the good and the bad of graduate school. This dissertation is made possible only through the support and guidance of those mentioned above.

**Progress towards a highly efficient and accurate platform for enantiomeric excess determination**

Chung-Yon Lin, Ph.D.

The University of Texas at Austin, 2016

Supervisor: Eric V. Anslyn

Enantiomeric excess (ee) determination remains as the bottleneck for high throughput screening of asymmetric catalysts. The work described herein sought to expand on two previously developed ee sensing assays from our lab– an iron based amine assembly and a zinc based multicomponent assembly. To start, the substituent effect of the zinc multicomponent dynamic assembly for secondary chiral alcohol ee determination was investigated. A new assembly with a higher dynamic range and smaller error was observed. Additionally, potential cooperative binding to the multicomponent assembly was investigated. Furthermore, this work included some preliminary results for a concurrent sensing platform for molecules with chiral amine and alcohol moieties.

# Table of Contents

# List of Tables

# List of Figures

# List of Schemes

# Chapter 1[1]

## 1. INTRODUCTION

Due to the potential adverse effect of one enantiomer in a racemate pharmaceutic, asymmetric catalysis has been at the forefront of organic chemistry research. Many efficient asymmetric transformations have been developed recently.[1] These asymmetric transformations are often carried out with either a chiral catalyst or chiral auxiliary. [2,3] High-throughput screening (HTS) of chiral catalyst or auxiliary requires rapid quantification of product enantiomeric excess (*ee*) and yield to achieve high efficiency. [4,5] Currently, the use of chiral chromatographic methods is the most common strategy to measure *ee* values.[6-10] These methods are associated with high cost (solvent, column replacement) and low duty cycle (equilibration time), and therefore are not ideal for HTS. To achieve the speed required for true HTS, methods that avoid elution are desirable.

Short analysis time and the potential to eliminate chromatographic separation make optical spectroscopy based ee determination methods attractive. These methods, however, often require derivatization of the analyte, which add additional steps to the screening process.[5] Hence, host-guest systems that selectively target the asymmetric transformation products are ideal. Recently, our group has developed optical spectroscopy based host-guest systems with the aim of rapid determination of enantiomeric excess. In these systems, *ee* values can be easily determined with reproducible calibration curves or appropriate patterning techniques; exact association constants for the two enantiomers are not required. For further reading about host-guest based *ee* determination, several reviews and primary literature are available. [11-13]

---

[1] This introduction chapter is adopted from the previously published account, see Jo, H. H.; Lin, C.-Y.; Anslyn, E. V. *Acc. Chem. Res.* **2014**, *47*, 2212-2227. Jo and Lin wrote the review together; Lin wrote the IDA section while Jo wrote the CD section.

This introduction chapter covers enantioselective indicator displacement assays (eIDAs) that target α-hydroxycarboxylates,[14-16] vicinal diols,[14-18] and α-amino acids.[19-22] This is followed by circular dichroism (CD) and exciton coupled circular dichroism (ECCD) techniques for diamines, amines, carboxylic acids, amino acids, secondary alcohol, cyclohexanones, and aldehydes. Additional highlights of other ee based sensors are included at the end. This chapter is adopted from a previously published account, where Hyun-Hwa Jo authored the CD and ECCD based ee sensors aspect to the account and I wrote the rest.

## 2. Enantioselective Indicator Displacement Assay (eIDA) as Detection Methods

In an enantioselective indicator displacement assay (eIDA), the quantification of enantiomeric excess is based on displacement of an indicator by a chiral analyte. This displacement of an indicator is monitored through either the absorbance or fluorescence changes. These changes can then be employed to quantify the amount of chiral analyte of interest.

### 2.1. eIDA for α-Hydroxycarboxylates and Vicinal Diols

One of our first eIDAs exploited the binding of boronic acids to α-hydroxyacids and vicinal diols.[14-16] The assay was developed with boronic acid receptors and catechol indicators. A representative example is shown in **Figure 1.1**. It was hypothesized that the presence of stereocenters neighboring the boron atom in the host would result in enantioselective association with chiral guests. In addition, *o*-aminomethyl functionality was used to aid the association equilibria.[15] In the initial study with boronic acid receptor (*S*,*S*)-**1** and various α-hydroxycarboxylates, using PV as the colorimetric indicator, an average of ±15% error was observed for the determined *ee* values.

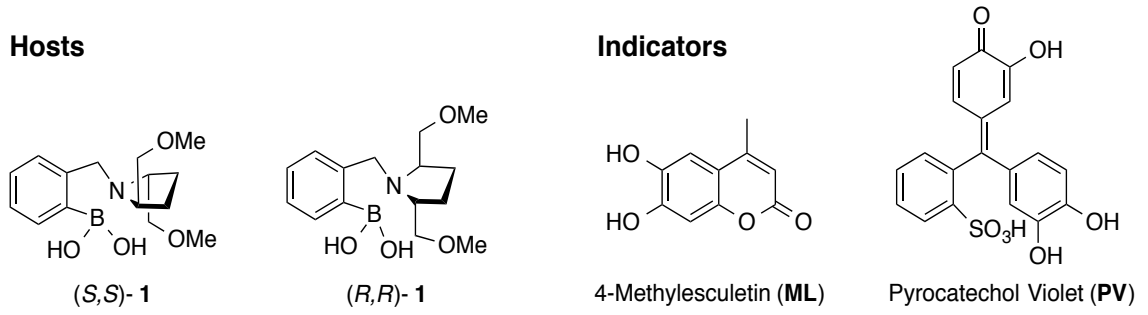


**Figure 1.1** Examples of structures of the hosts and indicators used in the study.

In an effort to enhance the assay's sensitivity and improve the accuracy in *ee* measurements, fluorescent indicators were investigated.[14] 4-Methylesculetin ML, along with receptor (*S,S*)-1, was used to develop mathematical relationships that correlate optical signal to *ee* and concentration. It was found that iterative fitting the curve of fluorescence intensity vs *ee* using Origin® software gave the best results. Through this approach, the average error in *ee* was found to be ±7%. Further studies with a series of receptors, a series of indicators, and other guest substrates gave a protocol that could be used to optimize indicator selection, concentration of the indicator, and the chiral receptor concentration.[16]

The boronic acid and vicinal diol host-guest eIDA was further explored to extend the scope of detection and practicality.[17,18] In the reported study,[17] four pairs of syn-vicinal diol enantiomers were selected as guests along with three indicators (**Figure 1.2**). Two additional chiral hosts, (*S,S*)-**2** and (*R,R*)-**2**, were introduced to the system along with the previously reported host (*S,S*)-**1** to enhance the enantioselectivity. Using 96-well plates and a UV-Vis plate reader, absorbance data were collected at different wavelengths with each host-indicator pair (3 for each pair, 9 total). The wavelengths were selected on the basis of the largest absorbance changes. Principal Component Analysis (PCA) on the absorbance

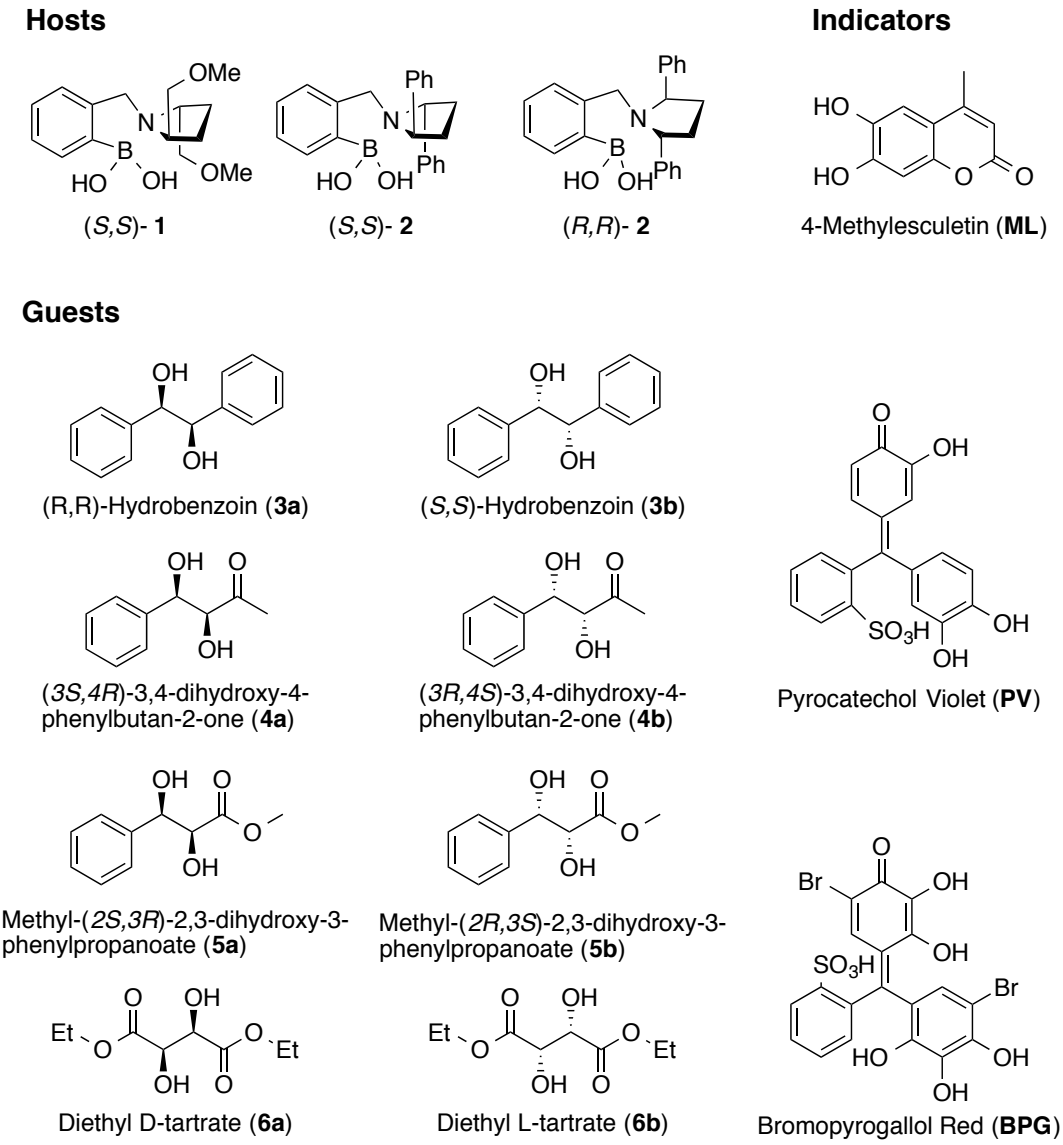


**Figure 1.2** The hosts, guest enantiomers, and indicators used for developing HTS protocol.

data showed excellent differentiation of both the identity of the diols and their enantiomers (**Figure 1.3**). Furthermore, the eIDA successfully differentiated samples with different guest concentration at various *ee* values on a PCA score plot (**Figure 1.4**). To demonstrate the predictive power of this system, artificial neural network (ANN) analysis with 14

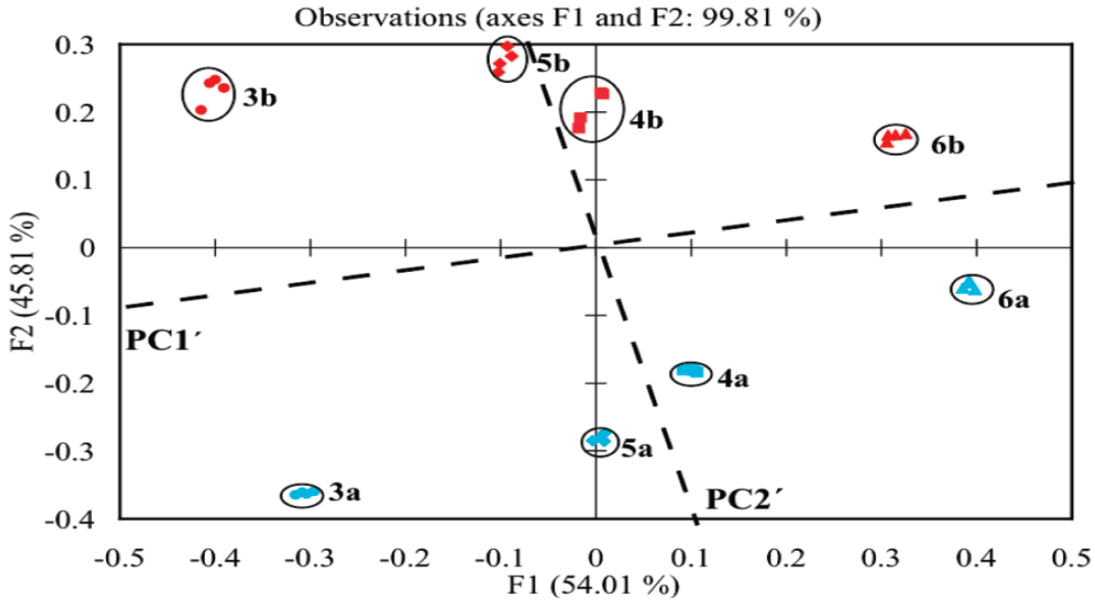


**Figure 1.3** The PCA plot of the diol enantiomers discriminated with (*S*,*S*)-1-PV, (*R*,*R*)-2-ML, and (*S*,*S*)-2-PV receptor-inidcator pair. The study was conducted in 10 mM p-toluenesulfonic acid/Hunig's base buffer (pH 7.4) in 100% MeOH at 25 °C.

absorbance inputs yielded an average absolute error of ±0.08 mM for sample concentration and ±7% for *ee*.

In an effort to perform HTS utilizing this eIDA procedure, a stepwise process for a protocol development for concentration and *ee* determination was published.[18] The protocol described a 5 step process that includes optimization of the eIDA host and indicator concentration using UV-Vis titrations, screening for the best host-indicator combination to discriminate the enantiomers of interest, training of an ANN, analyzing unknown *ee* analytes, and, lastly, loading the absorbance results onto the trained ANN to determine *ee* and concentration. Except for the first step, which is only required to be done once per host-indicator pair, all the steps can be performed on a well-plate reader allowing for true HTS. The developed protocol was used to analyze samples of hydrobenzoin with

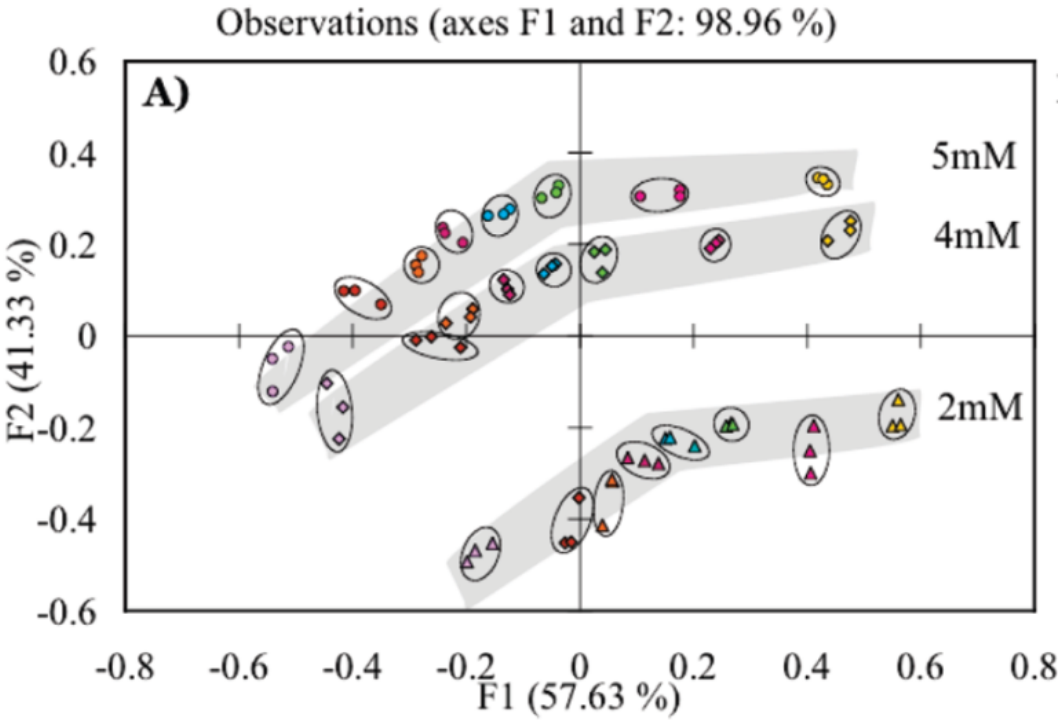


**Figure 1.4** The PCA plot of diol 5 with varying *ee* and at three different concentrations discriminated by (*S*,*S*)-1-BPG, (*R*,*R*)-2-ML, and (*S*,*S*)-2-PV receptor-inidcator pair. The study was conducted in 10 mM p-toluenesulfonic acid/Hunig's base buffer (pH 7.4) in 100% MeOH at 25 °C.

unknown *ee* and an average error of ±0.17 mM in the range of 3-8 mM concentration and ±2.4% for *ee*. When tested with samples synthesized with established Sharpless asymmetric dihydroxylation reactions, the protocol was able to identify the best ligand as reported by literature.[17]

## 2.2. eIDA for α-Amino Acids

Another system of eIDAs was developed for *ee* determination of α-amino acids.[19-22] The system utilized $Cu^{II}$ with chiral ligands **7** and **8** as hosts complexed to chromazurol S to form the receptor (**Figure 1.5**). Upon enantioselective coordination of chiral α-amino acids to form diastereomeric complexes, the selected colorimetric indicators were released, thus resulting in changes in absorbance. Using X-ray crystallographic data, the enantioselectivity was postulated to have arisen from both the favored positioning of the dimethoxybenzylic rings on ligand **7** and the steric interactions of the phenyl groups on ligand **8** with the amino acid side chain. Using this eIDA, 13 out of the 17 examined amino acids were enantioselectively discriminated. Further study with *ee* calibration curves showed around ±11.9% average error for *ee* determination. To further demonstrate the practicality, a high throughput screening protocol utilizing this eIDA was developed with 96-well plates and four α-amino acids. (**Figure 1.6**).[22] The average absolute error of *ee* determination for all four of the amino acids was ±9.7% using only receptor $[Cu^{II}((R,R)\text{-}\mathbf{7})]^{2+}$; receptor $[Cu^{II}((R,R)\text{-}\mathbf{8})]^{2+}$ had unsatisfactory results. ANN analysis was applied to the data collected in hopes to improve the eIDA's predictive power. With ANN, the average absolute error of *ee* was found to be ±10.0%. An asymmetrically synthesized α-amino acid with unknown *ee* was subjected to the eIDA. The determined *ee*, from the reported eIDA, was found to be in good agreement with values measured with chiral HPLC and a $^1$H NMR chiral shift agent.

In our research, focus for *ee* determination switched from UV-Vis and fluorescence based systems to Circular Dichroism (CD) based methods. One reason was the signal dependence on the concentration of chiral analyte. Further, with UV-Vis based systems, anything that can absorb in the region of detection could interfere with the signal of interest. This fact, in the context of HTS for chiral catalysts, would mean additional purification

steps, which are not ideal for the process. A second reason for the change was simplification in host design. The hosts for eIDAs were often not commercially available and required synthesis, whereas most of our CD based hosts are formed with commercially available compounds or ligands that can be made with simple synthetic procedures. For the reasons given here, we moved the focus of our work to various forms of CD spectroscopy.

### 3. CIRCULAR DICHROISM (CD) AS A DETECTION METHOD

Circular dichroism (CD) spectroscopy is an optical technique that is inherently sensitive to chirality, enables one to analyze and differentiate analytes in a chiral host-guest system, and is applicable to high-throughput screening (HTS). Most chiral building blocks do not display strong Cotton effects in CD spectroscopy. However, intense Cotton effects can be produced when metal complexes have MLCT bands, or when identical

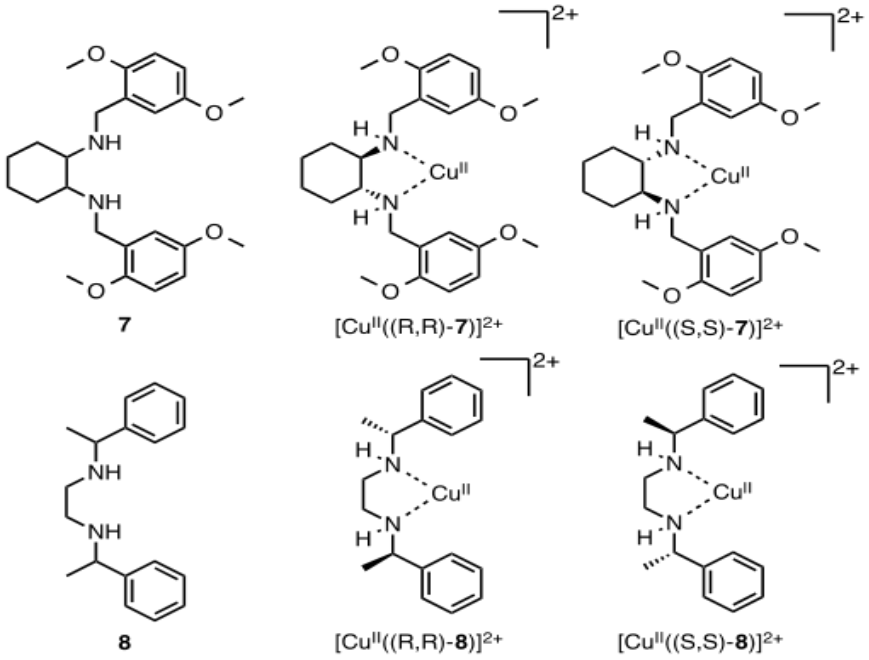


**Figure 1.5** Structures of the chiral ligands (7 and 8) and the receptors formed with $Cu^{II}$ and chiral ligand.

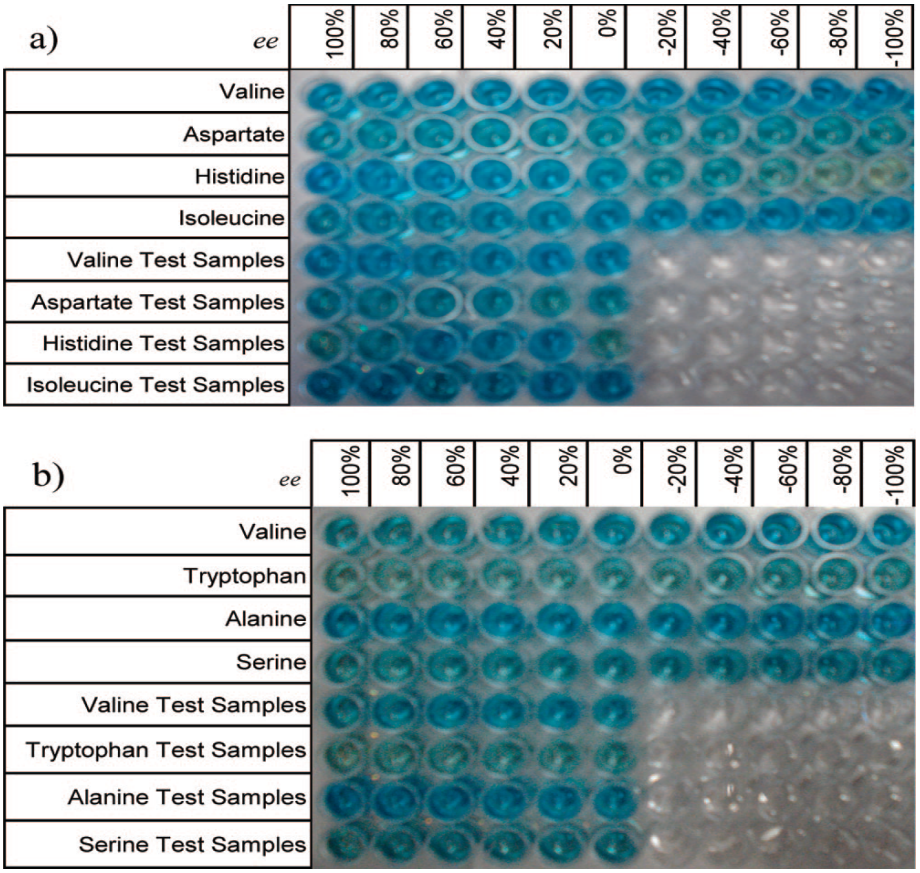


**Figure 1.6** The 96-well plate used for making the *ee* calibration curves. Each plate had 4 rows of amino acids samples for making the calibration curve with 6 test samples on the bottom. (a)$[Cu^{II}((R,R)\text{-}7)]^{2+}$ was used as the receptor. (b) $[Cu^{II}((R,R)\text{-}8)]^{2+}$ was the receptor.

chromophores have a helical twist, leading to exciton-coupled circular dichroism (ECCD). The sign of the Cotton effect gives valuable information for determining the absolute configuration of the chiral analyte, and the CD signals can be directly correlated to the *ee* of the sample. For our CD based sensors, titration studies are typically performed to find the saturation point and the binding stoichiometry of the host-guest interaction. The use of guest concentrations beyond the saturation point leads to concentration independent spectral responses.

In combination with statistical and chemometric techniques, such as linear discriminant analysis (LDA), artificial neural networks (ANNs), and principal component analysis (PCA), the CD spectral data can be further analyzed to find trends in the data as well as uncover characteristics of the data that best differentiate the chemo- and enantio-identity of the products. LDA is a technique to find linear combinations of features that maximize the separation between classes and minimizes the separation within classes,[23,24] and PCA is a tool that can classify and identify variance in data.[25] These analysis techniques allow for highly accurate discrimination of chemoselectivity and enantioselectivity in sample reactions.

### 3.1. Metal-to-Ligand-Charge Transfer (MLCT) CD Assays

Our first CD-based assay for *ee* involved analysis of a metal complex that has CD-active metal-to-ligand-charge transfer (MLCT) bands.[26,27] The MLCT band in the visible region of the CD spectrum was of interest because most organic functional groups are CD-silent in this range, showing signals only in the 190-220 nm region. A simple inorganic coordination complex with *R*- or *S*- BINAP (2,2'-diphenylphosphino-1,1'-binaphthyl), a binaphthyl diphosphine ligand with axial chirality, was used as a host system to discriminate the chirality of diamines, primary amines, and cyclohexanones.[26-30] The axial

chirality of BINAP arises from the limited rotation at room temperature of the bond linking the two sterically hindered two napthyl rings. The coordination complex with a transition metal, such as copper or palladium, introduces structural rigidity to the BINAP and its ligands derivatives.[28] Upon addition of chiral guest, the MLCT bands were modulated, allowing enantiomeric differentiation. BINAP was also chosen because both of its enantiomerically pure forms are commercially available. The guest molecules can be directly used with the metal complex when the number of host binding sites and the number of functional handles of the guest are the same. Otherwise, the guests need to be derivatized in order to bind to the metal complex.

### *3.1.1. Racemic and Chiral Metal Complexes as Hosts for Diamines*

Chiral metal complexes that have CD active MLCT bands, such as $[Cu^{I}(BINAP)(MeCN)_2]PF_6$ (**9**) or $[Pd^{II}(BINAP)(MeCN)_2]PF_6$ (**10**), were used to differentiate enantiomers of chiral vicinal 1,2-diamines (**Figure 1.7**).[26] Both enantiomers of **9** have MLCT bands around 340 nm in the CD spectrum, giving opposite Cotton effects for the *R* and *S* copper-coordinated complexes (**Figure 1.8**). Because there are no CD signals above 300 nm for the diamine analytes tested, or for the metal alone with diamines, the signals above 300 nm are indicative of the chemical identity, chirality, and concentration of the guests. Distinctive CD-active MLCT bands were observed for each diamine and its enantiomer when complexed with *R*- or *S*- **9**. Also, by comparing the intensity difference between CD signals of the complexes of diamine enantiomers with *R*-**9** or *S*-**9**, *ee* for diamines was evaluated with an average error of ±3.8%.

The LDA plot in **Figure 1.9**, generated from the CD data of all the receptors at chosen wavelengths, showed chemical identification and chiral discrimination of all of the diamine analytes, which was determined by their individual clustering through the four

quadrants. When the same data was analyzed with multilayer perceptron (MLP) ANNs, *ee* and concentration ($[G]_t$) were determined with average errors of ±3.8% and ±18.6%, respectively.

The racemic mixtures of **9** and **10** were also employed to discriminate enantiomers of chiral diamines.[27] Of course, the racemic mixture does not show any CD signals alone, but upon binding with enantiopure vicinal 1,2-diamines, CD active MLCT bands are observed. The LDA plot successfully classified the diamines and their handedness.

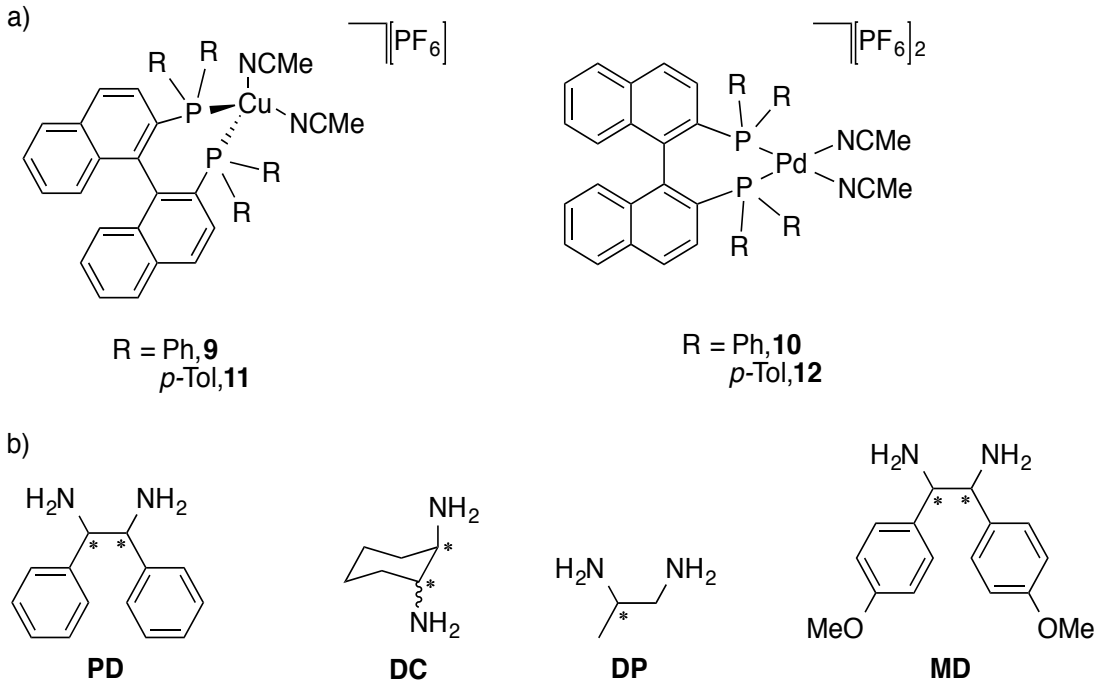


**Figure 1.7** (a) Racemic-metal complexes sensors employed in this study. (b) Diamine analytes used in this study included 1,2-phenylethylene-diamine (PD), 1,2-diaminocyclohexane (DC), 1,2-diaminopropane (DP), bis(4-methoxyphenyl)-1,2-diaminoethane (MD).

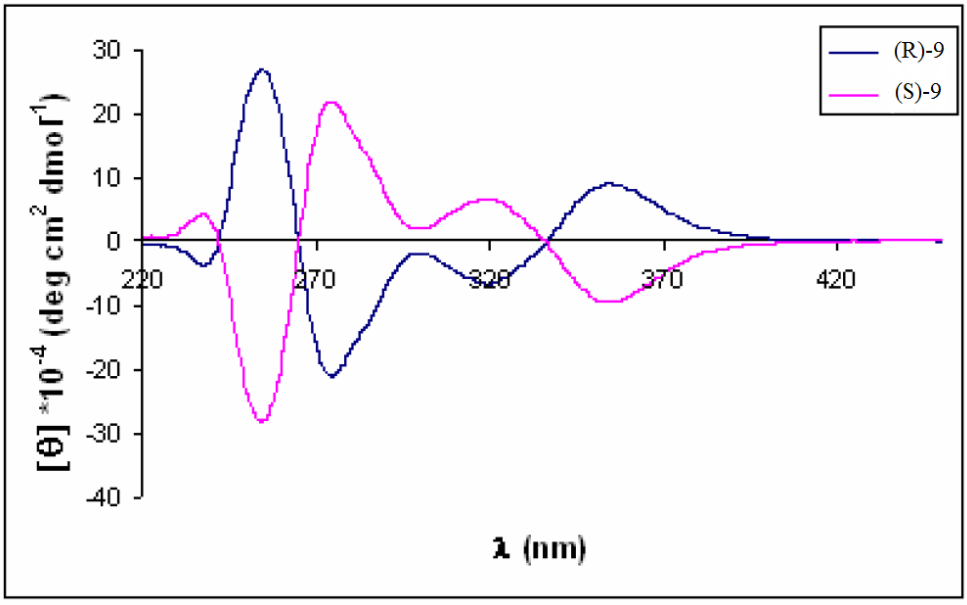


**Figure 1.8** CD spectra of *R*-9 [0.4mM] and *S*-9 [0.4mM] between 220 nm and 450 nm.

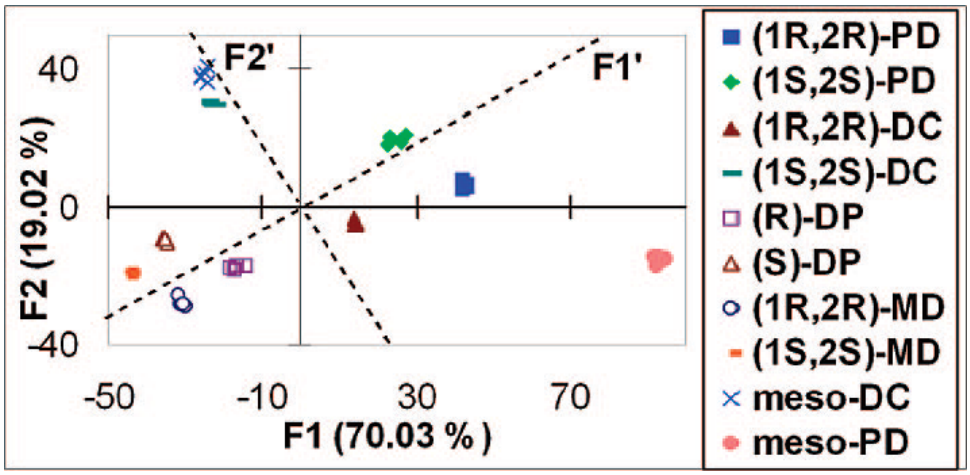


**Figure 1.9** Response patterns for all the analytes using (*R*)-9 receptor obtained by LDA.

### *3.1.2. Chiral Metal Complexes as a Host for α-Chiral Primary Amines*

The same metal complex **9** was employed to discriminate α-chiral primary amines.[29] However, the addition of underivatized chiral amines to *R*-**9** does not show any signal modulation by CD spectroscopy. Therefore, a simple derivatization of chiral amines to form imines that can coordinate with *R*-**9** was necessary. Chiral imines were formed from the condensation of chiral amines with 2-pyridinecarboxaldehyde *in situ* (**Scheme 1.1**). The modulated MLCT signal, which is indicative of the coordination of the imines with *R*-**9**, was observed in the CD spectrum (**Figure 1.10**). The CD signals were characteristic to each analyte, and the data was further analyzed with LDA and PCA. In the PCA plot, F1 axis defines chirality with negative values for *R*-enantiomers and positive values for *S*-enantiomers, and F2 axis defines concentration. The average error for *ee* was ±17%, which led us to develop a method that could give a more accurate enantiodiscrimination.[31]

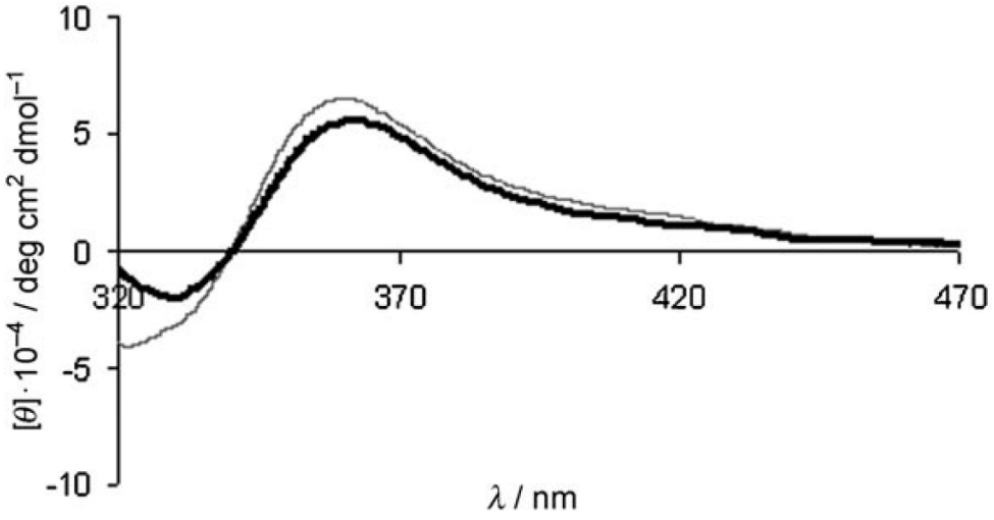


**Figure 1.10** CD spectrum for (*R*)-9 [0.4mm] and the enantiomers of CPI [0.8 mm](regular line=(*R*)-CPL, bold line=(*S*)-CPL)

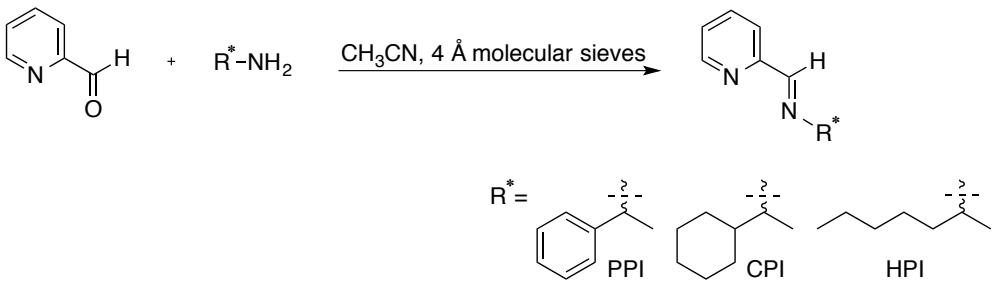


**Scheme 1.1** Derivatization of the amines to form the corresponding Schiff bases.

### *3.1.3. Chiral Cu(I) Metal Complexes as Hosts for α-Chiral Cyclohexanones*

Complex **9** was also applied to the enantiodiscrimination of α-chiral cyclohexanones.[30] In order to create bidentate ligands, that produce a twist upon binding with *R*- or *S*-**9**, enantiomerically pure α-chiral cyclohexanones were derivatized with 1-methyl-1-(2-pyridyl) hydrazine to form hydrazones (**Scheme 1.2**). The nitrogen atoms in the pyridyl group and hydrazone moieties coordinate to a $Cu^{I}$, forming a metal complex. Upon addition of hydrazone to enantiomerically pure **9**, diastereomers will be produced with different twist angles. Different twist angles between the naphthyl rings in BINAP were predicted based upon steric interactions between the phosphine ligand and the R group on the ketones. The degree of twist is reflected in the CD spectrum, allowing for discrimination between the two enantiomers. The *R*-enantiomers of hydrazones with *S*-**9**, compared to *S*-enantiomers, will cause a larger change in the twist, inducing a larger change in the CD signals from the original MLCT band of **9** (**Figure 1.11**). The enantiomeric host *R*-9 produces a mirror image CD spectrum. Through the use of calibration curves, these studies allow *ee* determination of the chiral cyclohexanones to be performed with an absolute error of ± 7%.

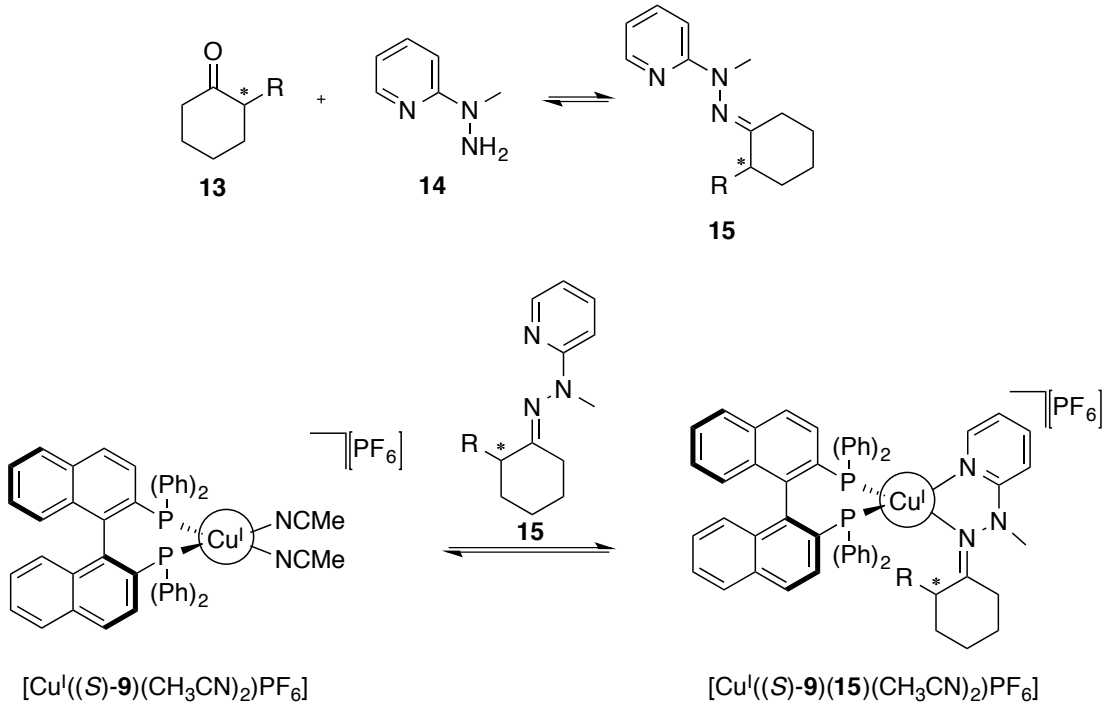


**Scheme 1.2** Derivatization of *R*-chiral cyclohexanones (**13**) with 1-methyl-1-(2-pyridyl) hydrazine (**14**) to produce a bidentate analyte (**15**), followed by complexation to (**9**)

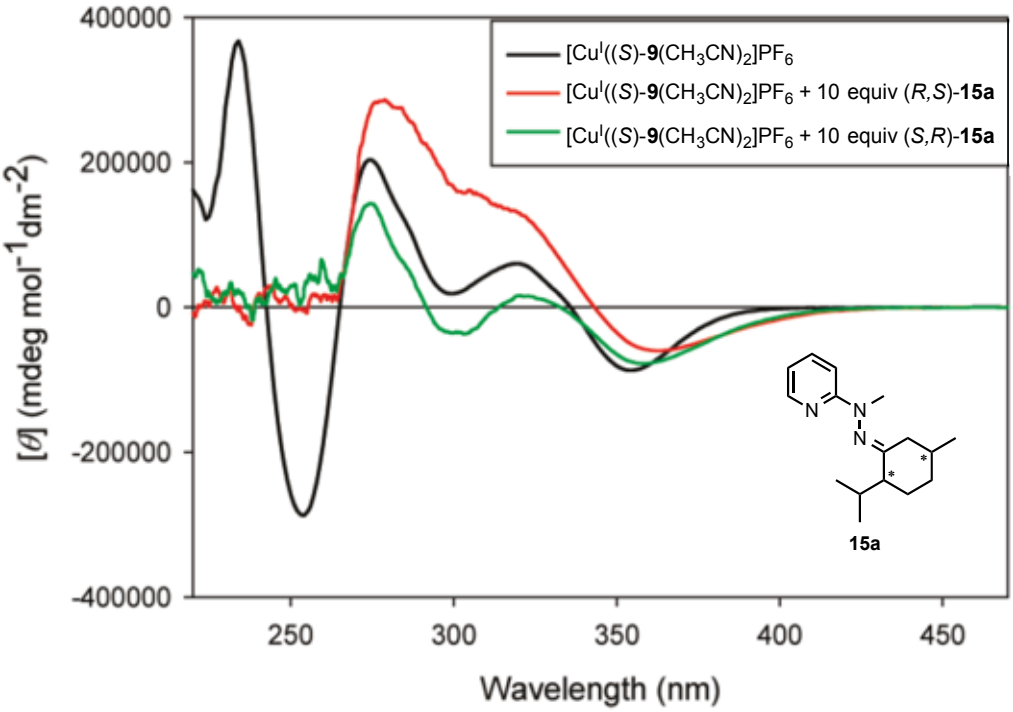


**Figure 1.11** CD spectra of 9 (401 μM) in $CH_3CN$ (black), *S*-9 (401 μM) mixed with (*R*,*S*)-6 (4 mM) (red), and *S*-9 (401 μM) mixed with (S,R)-6 (4 mM) (green).

### 3.2. Boronic Acid Receptors for Chiral Primary Amines

Another method for the analysis of chiral primary amines was created using an assembly from the Bull and James groups,[32,33] where enantiopure 1,1'-bi-2-naphthol (BINOL) assembles with *o*-formylphenyl boronic acid (FPBA) and α-chiral primary amines (**Scheme 1.3**). Enantiomerically pure a BINOL and BINOL-FPBA mixture both have a CD signal that is modulated upon addition of *R* or *S* guest amines.[34] The three-component assembly forms an imine coordinated boronate ester, and it was hypothesized that the absolute configuration of the amine would modify the torsional angles of *S* or *R*-BINOL to cause modulation in CD. However, molecular modeling experiments using Spartan showed no evidence of distortion of the dihedral angle of BINOL in the product assembly. The change in CD occurs from extending the chromophore ability of the chiral amine through the condensation with the aromatic boronic acid (**Figure 1.12**).

Various amine analytes were assembled with BINOL and analogues, and with FPBA (**Figure 1.13**). The CD spectra of the resulting complexes showed differences in intensity and shape, making it possible to discriminate their identities and chirality. With all data obtained from varying hosts and guests, PCA and LDA plots were generated to classify the amines. The *ee* analysis done was highly accurate, giving an average absolute error of ±5.8% using the calibration curves generated.

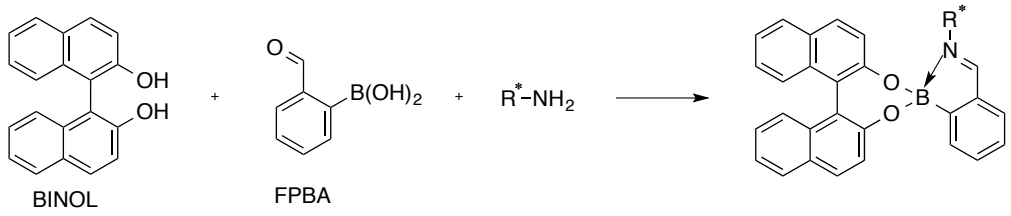


**Scheme 1.3** Formylphenylboronic acid (FPBA) based assembly for chiral amine sensing reported by Bull and James.

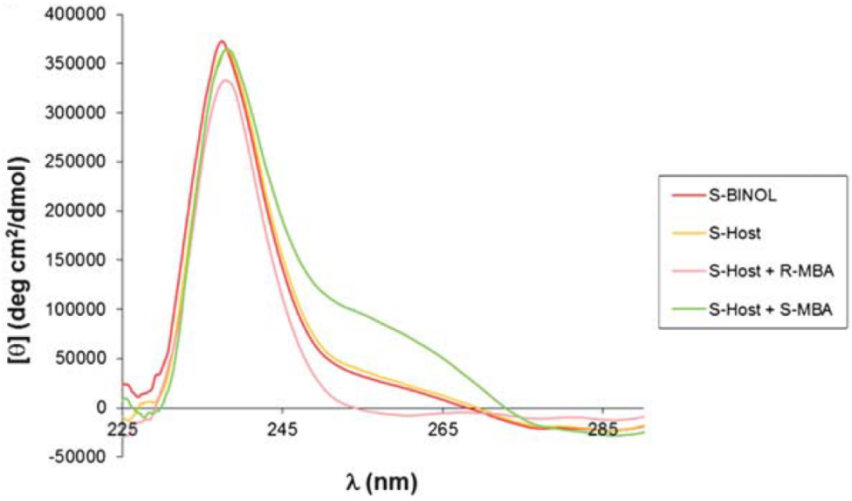


**Figure 1.12** CD spectra of the assembly of MBA with (*S*)-BINOL-FPBA.

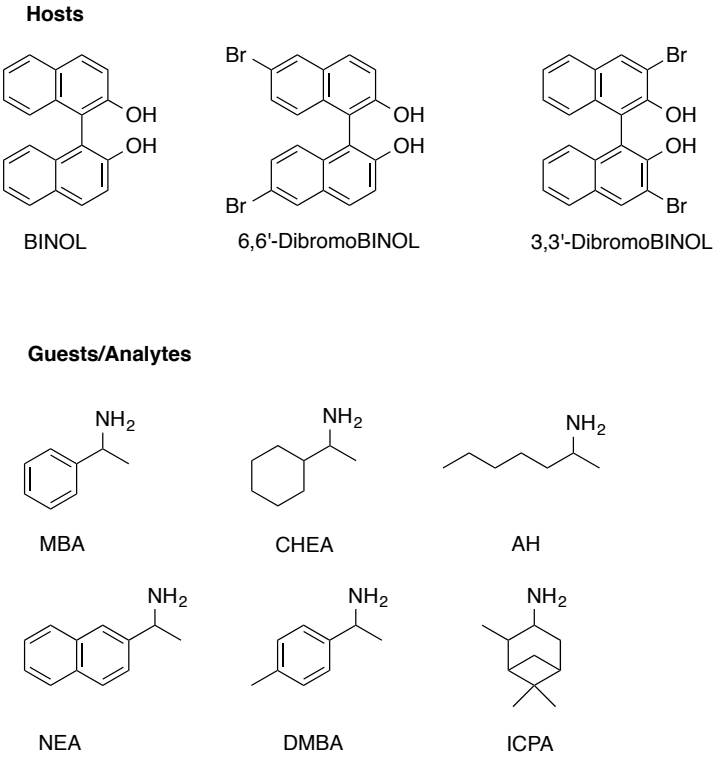


**Figure 1.13** Structures of the compounds used as hosts and guests/ analytes.

### 3.3. Exciton-Coupled Circular Dichroism (ECCD)

One form of CD, namely exciton-coupled circular dichroism (ECCD),[35] has been widely employed in chirality sensing for various analytes.[36-55] When a compound contains two or more chromophores that can be oriented in a helical fashion, ECCD signals are generated. This phenomenon leads to bisignate CD curves centered at the UV-Vis absorption maximum. Enantiomers have mirror image CD spectra, and the sign of the Cotton effect is used to determine the absolute configuration of the analyte. Practically, chiral analytes must be derivatized with chromophores or need to be bound to receptors containing chromophores through supramolecular interactions.

#### *3.3.1. In Situ Generated $Fe^{II}$ Complexes as a Host for Chiral Amines*

The method described in section *3.1.2* for chiral monoamines[29] suffers from several drawbacks. First, the derivatization of 2-pyridinecarboxaldehyde to form bidentate imines takes 2 hours. Second, it gave a moderately high average error of ±17%. Lastly, the calibration curves are concentration dependent. In an effort to eliminate the need for the synthesis of a host and to create a simple and quick assay, our group has turned to self-assembly. In one example, $Fe^{II}$ was used as a metal center to coordinate three equivalents of bidentate imines, which were created from the condensation between a chiral amine and aldehyde **16**.[31] In order to reduce derivatization time, 3-hydroxy-2-pyridinecarbaldehyde was allowed to react with the chiral primary amines to form chiral imines (**Scheme 1.4**). Followed by this in situ amine derivatization, $Fe^{II}$ was added to form octahedral complexes that possess different helical twists. There are four possible stereoisomers for enantiomerically pure amines, and 24 possible stereoisomers for mixtures of *R* and *S* amines. These isomers result from helical isomerism (clockwise, counterclockwise), configurational isomerism (*fac* and *mer*), as well as *R* and *S* amines. However, this complexity does not interfere in *ee* determination and enantiomeric differentiation because

the isomers interchange rapidly in equilibria. The three asymmetrically oriented ligands bonded to $Fe^{II}$ generate ECCD signals, which correlate with the identity of the stereogenic center of the imines and the helicity of the complex (**Figure 1.14**). Imines with an *R* stereogenic center induce a counterclockwise twist and have a negative ECCD couplet, and vice versa.

Amines with aromatic, cyclic, and acyclic functionality were differentiated by the CD signal intensity and shape (**Figure 1.15**). A concentration-independent calibration curve was generated to determine *ee* with low average error of ±5%.

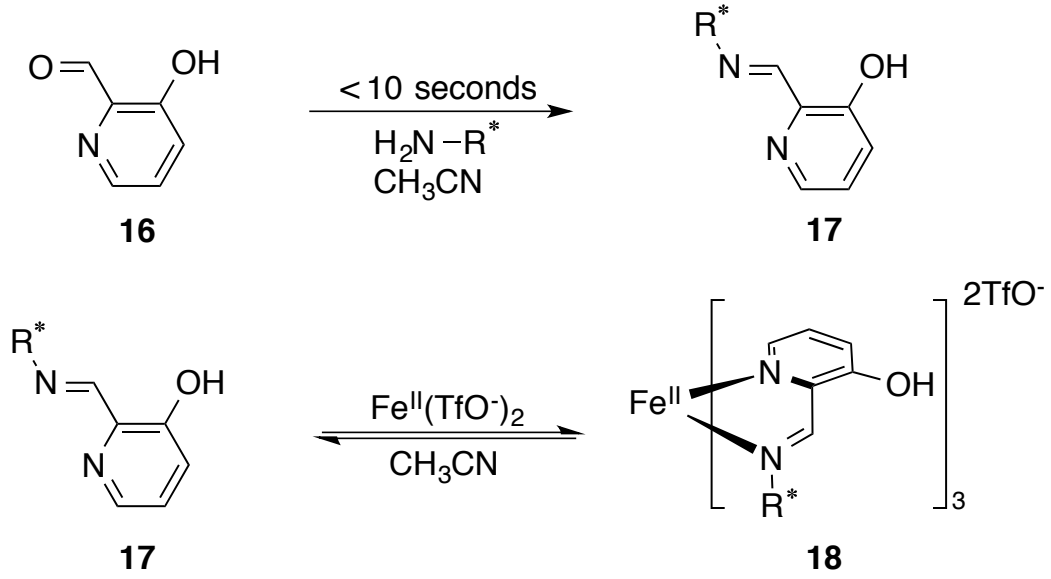


**Scheme 1.4** Aldehyde **16** reacts rapidly with an amine to form imine **17**, followed by complexation with $Fe^{II}$ to form **18**

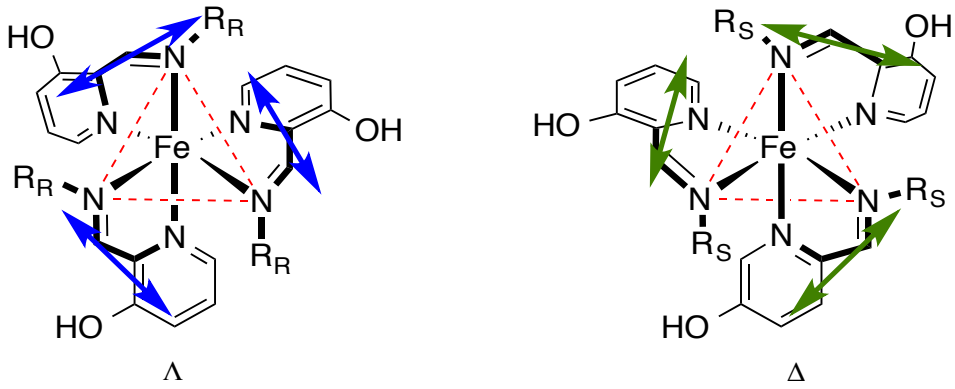


**Figure 1.14** Helical arrangements of the transition dipoles that couple to give rise to the positive and negative ECCD couplets for the Δ-(*R*)- and Λ-(*S*)-fac isomers, respectively.

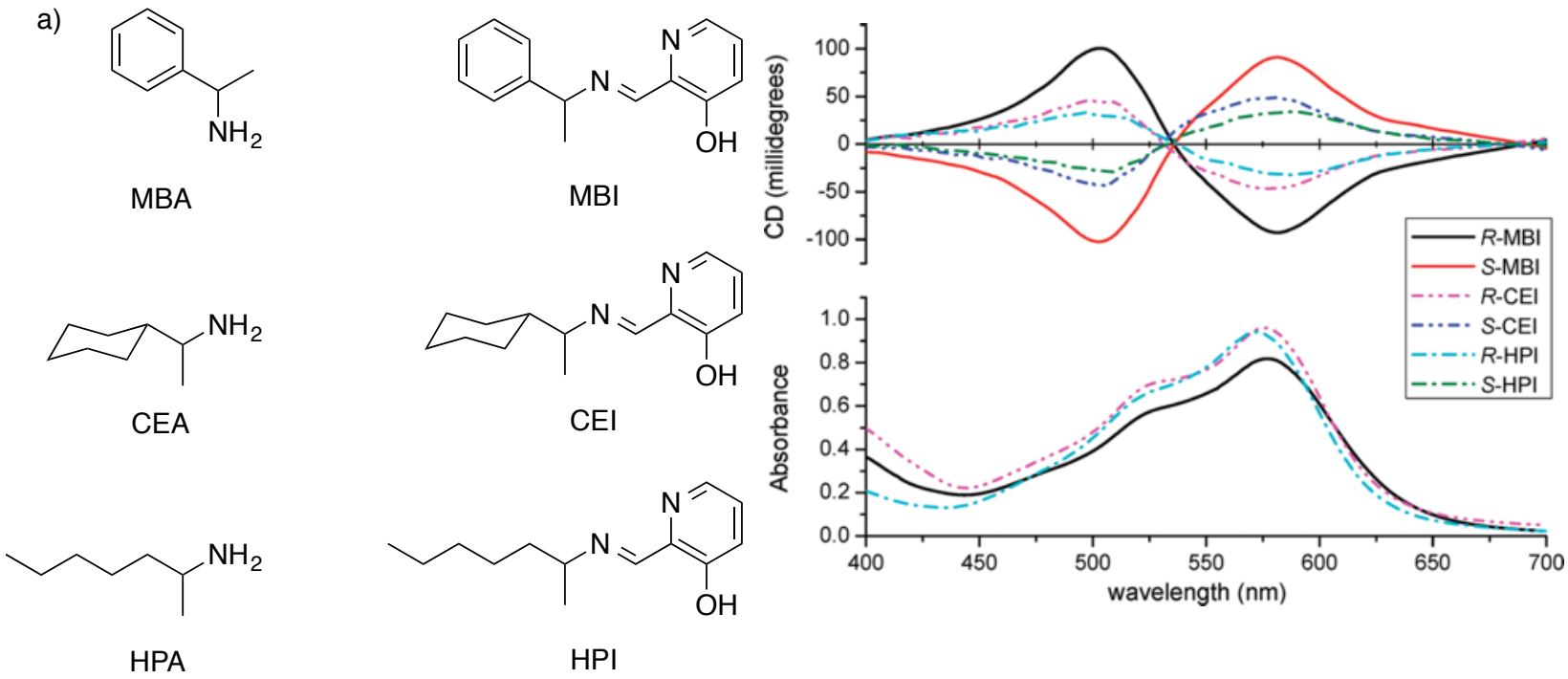


**Figure 1.15** a) Structures of (left) MBA, CEA, and HPA, the three amines studied, and (right) MBI, CEI, and HPI, the three imines formed after reaction of the amines with aldehyde 16. b) UV–vis and CD spectra of the MLCT bands for the three different imines studied, MBI (3 mM), CEI (6 mM), and HPI (7 mM), at 100% and –100% *ee* in acetonitrile with 1 mM $Fe^{II}$ in a 0.1 cm quartz cell from 400 to 700 nm

### *3.3.2. $Fe^{II}$ complexes as a host for α-chiral aldehydes*

Adapting two protocols previously discussed,[29,31] an assay for chiral aldehydes was created.[56] Imines generated from compound **14** with various chiral aldehydes coordinate with metal upon the addition of $Fe^{II}$ triflate (**Scheme 1.4** and **Figure 1.16**). Compared to our previous approach,[29] this assay was advantageous because the derivatization of the amine to form an imine was reduced from 2 hours to 30 mins. The complexation of synthesized bidentate imines **19**-**21** with $Fe^{II}$ led to large CD signals, which were used to determine *ee* of α-chiral aldehydes. The CD signal was used to discriminate absolute configuration of the α-chiral aldehydes as well as their *ee* values with an absolute average error of ±5%.

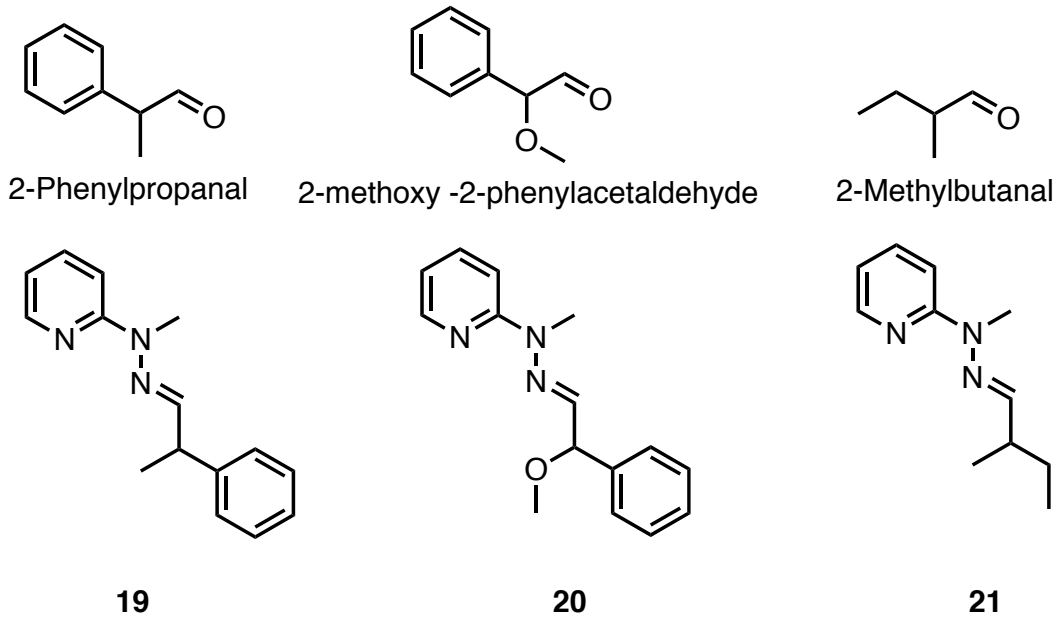


**Figure 1.16** Structure of aldehydes and their corresponding hydrazine imine adducts formed.

### *3.3.3. A $Cu^{II}$ Complex as a Host for Chiral Carboxylates and α-Amino Acids*

Our group has also exploited ECCD for the analysis of chiral carboxylates.[57] Achiral host [(BQPA)$Cu^{II}(ClO_4)$] **22** is easy to synthesize and has an empty coordination site for monodentate carboxylate binding (**Scheme 1.5**). Host complex **22** alone has two different helical isomers that exchange rapidly in equilibria resulting in no CD signal. However, binding of a chiral guest causes one twist to dominate, and thereby generate the corresponding ECCD couplet (**Figure 1.17**). This method has the advantage of avoiding an analyte derivatization step. The guest forms a complex that has a minimum steric interaction with the groups on the stereocenter, thus dictating the helicity. *R*-enantiomers gave negative CD couplets, which are indicative of a P helical isomer with a counterclockwise twist, and vice versa. The difference in steric size of the groups attached to the stereocenter is directly correlated to the magnitude of the CD signal. Calibration curves for the determination of *ee* of carboxylates were generated, and gave an average absolute error of ±3%.

Amino acids contain carboxylate groups, and hence host **22** was also used as a sensor for α-amino acids and β-homoamino acids.[58] Boc-protected α-amino acids and Boc-protected β-amino acids follow the same operating principles as the previously studied carboxylates. For both α-amino acids and β-homoamino acids, D-isomers led to a P-type helix whereas L-isomers led to an M-type helix. However, due to the increase in the degrees of rotational freedom in β-homoamino acids, reduced CD signals were observed (**Figure 1.18** and **1.19**). γ-Amino acids were not suitable for this system.

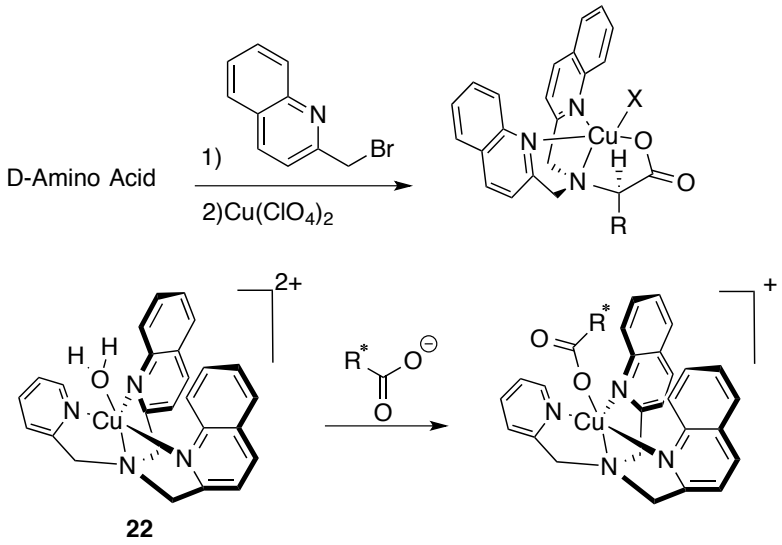


**Scheme 1.5** Protocol to determine absolute configuration of chiral amino acids (Top) and proposed complex formation between [(BQPA)$Cu^{II}(ClO_4)_2$] host **22** and chiral carboxylate guest.

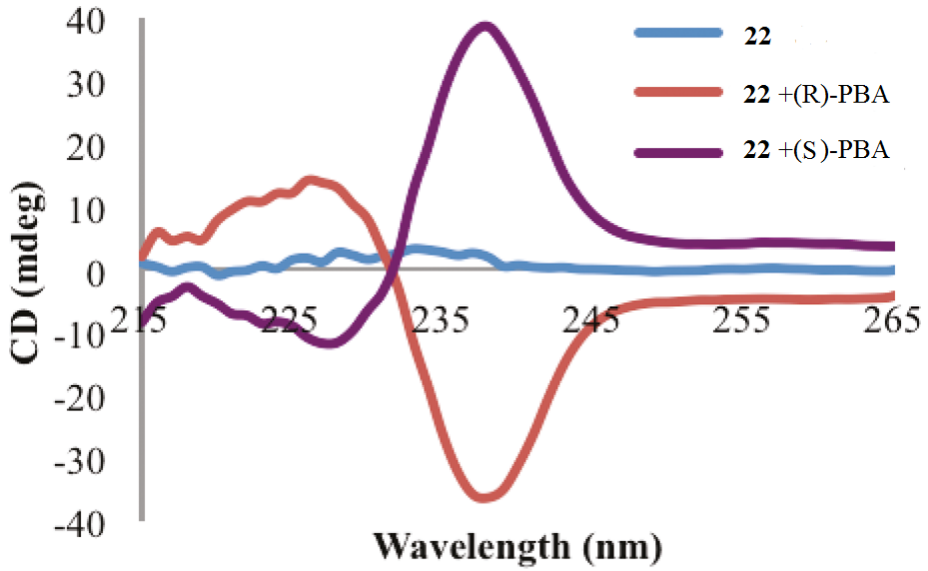


**Figure 1.17** CD spectra of host 22 (0.5 mM) by itself and with each enantiomer of PBA (1.0 mM) in default buffer (75% MeCN/$H_2O$ with 20 mM HEPES buffer at pH 7.4).

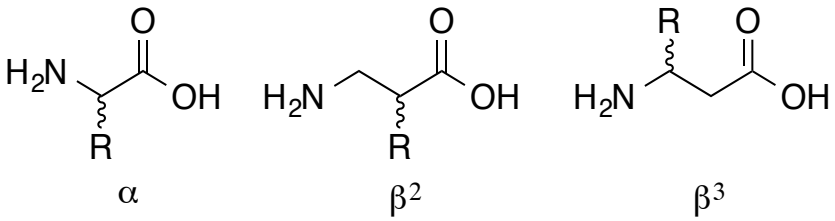


**Figure 1.18** Types of amino acids discriminated using the CuBQPA complex.

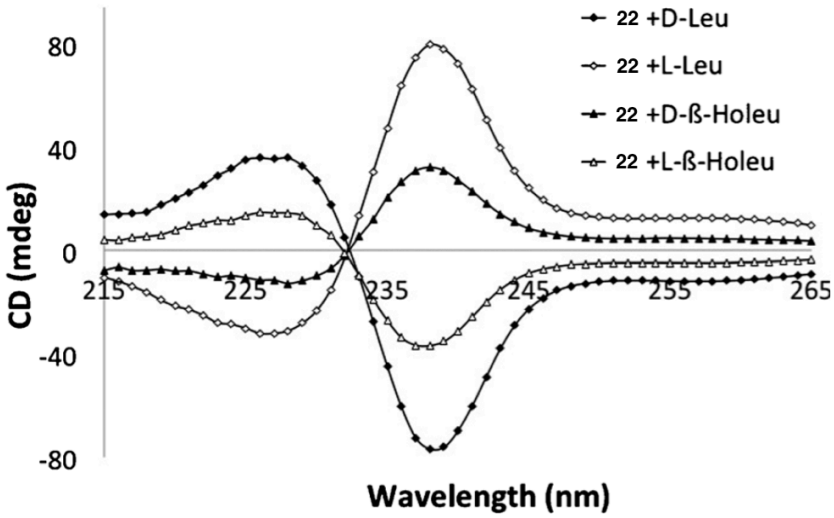


**Figure 1.19** CD spectra for each indicated guest (1.0 mM) with host 22 (0.5 mM) in default buffer.

### *3.3.4. A $Zn^{II}$ Mediated Multi-Component Assembly as a Host for Chiral Secondary Alcohols*

Our most recent ECCD-based sensor targets chiral secondary alcohols and was formed via a dynamic multi-component assembly process.[59] Four components: 2-pyridinecarboxaldehyde, di-(2-picolyl)amine, $zinc^{II}$ triflate and the chiral alcohol were mixed together, and reversible covalent bonding formed assembly **23** (**Scheme 1.6**). The assembly possesses a helical twist of the pyridines that depends on the handedness of the stereocenter at the hemiaminal ether carbon. The stereocenter, in turn, is dictated by the handedness of the alcohol. The helical twist of the tris-pyridine complex induces a large Cotton effect in the CD spectrum resulting from ECCD. *R*-Alcohols lead to a preference of an *S*-stereocenter at the hemiaminal ether carbon, giving a preferential P twist of the tris(pyridine) ligand and a negative ECCD couplet, while the opposite is true for *S*-alcohols.[60] The sign of the Cotton effect is therefore indicative of the handedness of the alcohol stereocenter and the unique CD signals for each alcohol allow determination of alcohol identity. This system has successfully been used to quantify *ee* values of chiral secondary alcohols with a ±3% error.

The diastereomeric ratio (dr) of the assembly with chiral alcohols was linearly correlated with the magnitude of the CD signal (**Figure 1.20**).[61] Further, Charton steric parameters linearly correlate with the dr values and thereby also the ECCD intensity. From these correlations, the magnitude of CD values of various alcohols could be predicted with average absolute error of ±9.5%.

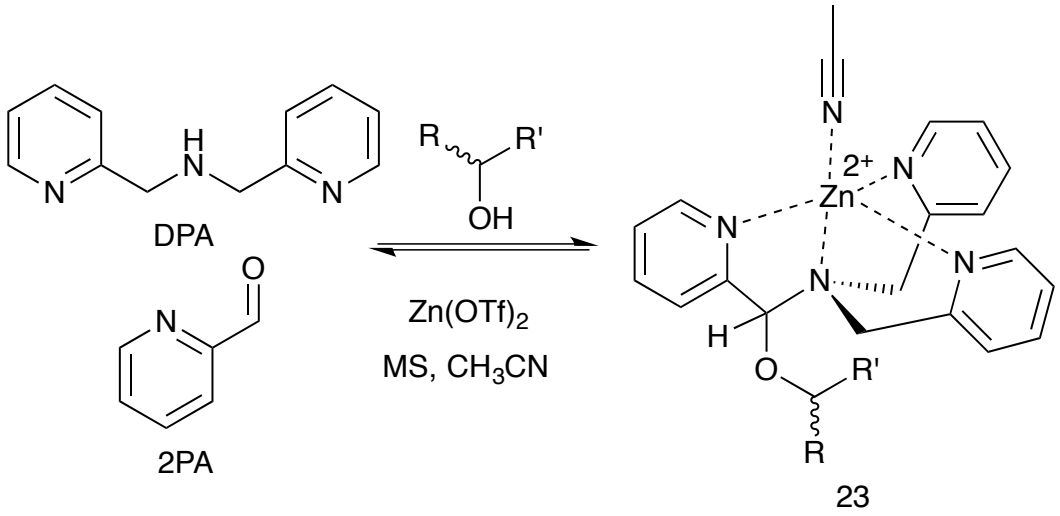


**Scheme 1.6** Secondary chiral alcohol ee sensor composed of 2-pyridinecarbaldehyde (2PA), di-(2-picolyl)amine (DPA), and Zn(II).

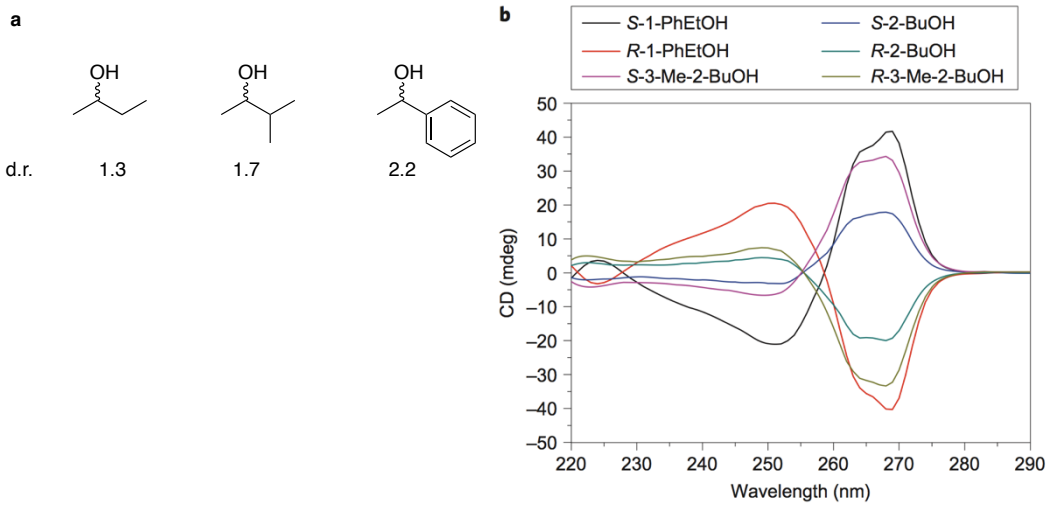


**Figure 1.20** a) Dr values for assemblies with chiral mono-ols (*R* or *S*) obtained from $^{1}$H NMR. b) CD spectra of assembly derived from three alcohols (0.175 mM 2-PA, 0.525 mM mono-ol).

## 4. Other Relevant Works

In addition to the works done by the Anslyn group, there have been quite a few ee sensors reported by other groups. This section will highlight some of the recent works done on the forefront of ee sensing research.

### 4.1 Pu

Pu has reported multiple 1,1'-bi-2-napthol (BINOL) based fluorescent ee sensors for amino alcohols, α-hydroxycarboxylates, and α-amino acids.[62] Most recently, Pu reported a perfluoroalkyl-BINOL based chiral sensor in fluorous phase.[63] As shown in **Figure 1.21**, chiral sensor **24** forms the hemiaminal or aminal adduct with the introduction of aminoalcohol or diamine analytes. In this case, one enantiomer induced a 50-fold fluorescent increase while 2000-fold increase in fluorescence was observed for the other enantiomer. In addition to the fluorous phase probe, another recent BINOL based sensor was shown to be able to determine ee and concentration of the analyte.[64] The fluorescent silent bisnaphthylimine-BINOL conjugate **25** is turned on with the addition of chiral diamine analyte and Zn(II) (**Figure 1.22**). Through monitoring the fluorescence for the displaced aminonaphthalene and newly formed BINOL-imine adduct, Pu et. al was able to determine ee and concentration of the chiral analyte.

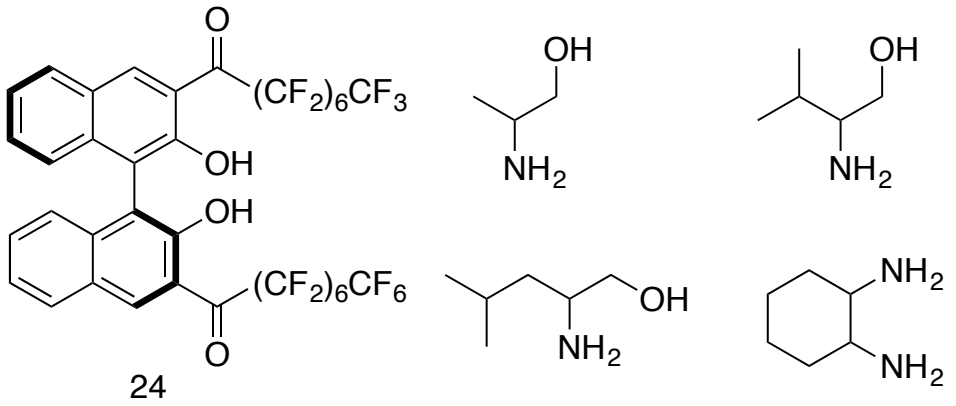


**Figure 1.21** Perfluorosubstituted BINOL ketone (**24**) and the chiral aminoalcohols and diamine used in the enantiomeric excess determination study.

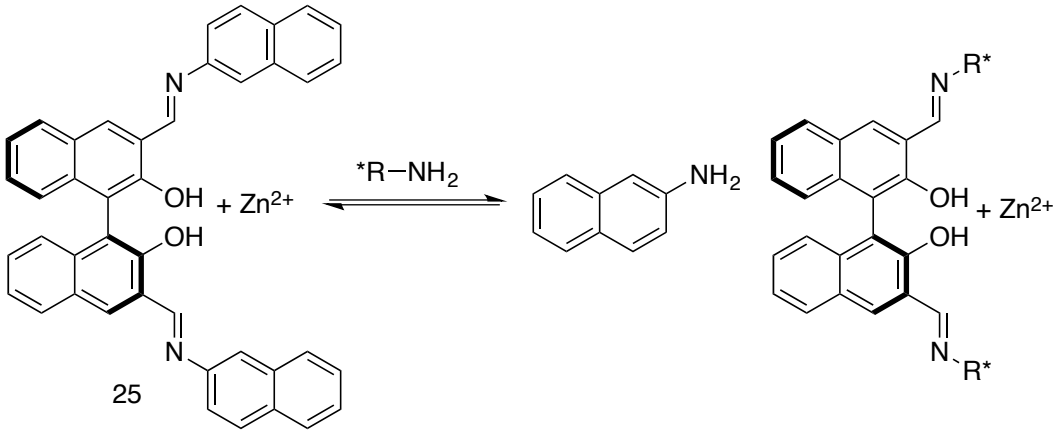


**Figure 1.22** Fluorescent silent bisnaphthaimineBINOL (**25**) sensor is turned on with the addition of chiral amine.

### 4.2 Wolf

Wolf group has published several stereodynamic chiral sensing probes for chiral amines, diamines, amino acids, and amino alcohols.[13,65-69] In their latest work, Wolf and Bentley utilize bis(2-hydroxy-1-naphthyl)ketone complexed with Zn or $Ti^{4+}$ to conccurently determine the yield and ee of chiral diols (**Figure 1.23**). Upon addition, the chiral analyte coordinates to the metal complex, which induces CD and fluorescence turn-on. The chiral analyte ee and concentration are determined through monitoring the CD and fluorescence. Sample screens of Sharpless asymmetric dihydroxylation was conducted to demonstrate the practicality of this method.

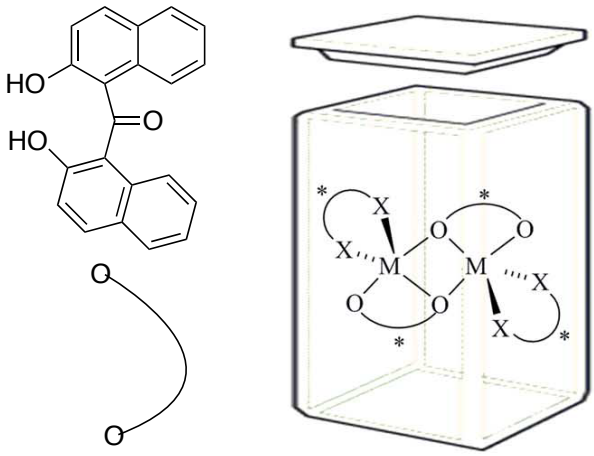


**Figure 1.23** The Bis(2-hydroxy-1-naphthyl)ketone ligand and a graphical representation of the ligand complexed with a metal and chiral ligand.

## 5. Conclusions and Outlook

The use of optical spectroscopy for the determination of enantiomeric excess values has the potential to revolutionize reaction and catalyst discovery. Our group, among others, has pioneered this effort with a focus on either colorimetric or circular dichroism approaches. Within our own group a series of assays targeting several chiral functional groups have been created: diols, diamines, amines, alcohols, carboxylic acids, aldehydes and ketones. In addition, a series of strategies for optical modulations have been implemented: indicator-displacement assays, CD-active MLCT excitation, and exciton-coupled circular dichroism. While the absolute errors in *ee* values are not yet as low as those traditionally associated with chiral HPLC analysis, advances in lowering the errors can be anticipated in the near future. The error in ee values arises primarily from variations in quantitative syringing and pipetting during sample generation. These variations can be reduced by adopting a fully automated protocol often seen in HTS. Even with errors of 5% to 10% one can still quickly identify trends in data and find the "hits" within hundreds of samples. Although the error seem relatively large compared to HPLC, chemists in big-pharma have routinely told our group that they are perfectly acceptable to HTS. Thus, true high-throughput screening is right around the corner.

## 6. Reference


(1) Jaroch, S.; Weinmann, H.; Zeitler, K. Asymmetric organocatalysis. *Chem. Med. Chem.* **2007**, *2*, 1261–1264.

(2) Lin, G.-Q.; Li, Y.-M.; Chan, A. S. C. *Principles and Applications of Asymmetric Synthesis*; John Wiley & Sons, 2003.

(3) Christmann, M.; Bräse, S. *Asymmetric Synthesis*; Wiley-VCH, 2008.

(4) Tsukamoto, M.; Kagan, H. B. Recent advances in the measurement of

enantiomeric excesses. *Advanced Synthesis & Catalysis* **2002**.

(5) Finn, M. G. Emerging methods for the rapid determination of enantiomeric excess. *Chirality,* **2002**, *14*, 534–540.

(6) Welch, C. J.; Szczerba, T.; Perrin, S. R. Some recent high-performance liquid chromatography separations of the enantiomers of pharmaceuticals and other compounds using the Whelk-O 1 chiral stationary phase. *J. Chromatogr. A* **1997**, *758*, 93–98.

(7) Welch, C. J.; Grau, B.; Moore, J.; Mathre, D. J. Use of chiral HPLC-MS for rapid evaluation of the yeast-mediated enantioselective bioreduction of a diaryl ketone. *J. Org. Chem.* **2001**, *66*, 6836–6837.

(8) Welch, C. J.; Fleitz, F.; Antia, F.; Yehl, P. Chromatography as an enabling technology in pharmaceutical process development: expedited multikilogram preparation of a candidate HIV protease inhibitor. *Org. Process Res. Dev.* **2004**, *8*, 186– 191.

(9) Sigman, M. S.; Jacobsen, E. N. Schiff base catalysts for the asymmetric Strecker reaction identified and optimized from parallel synthetic libraries. *J. Am. Chem. Soc.* **1998**, *120*, 4901– 4902.

(10) Wolf, C.; Hawes, P. A. A high-throughput screening protocol for fast evaluation of enantioselective catalysts. *J. Org. Chem.* **2002**, *67*, 2727–2729.

(11) Pu, L. Fluorescence of organic molecules in chiral recognition. *Chem. Rev.* **2004**, *104*, 1687–1716.

(12) Wolf, C.; Bentley, K. W. Chirality sensing using stereodynamic probes with

distinct electronic circular dichroism output. *Chem. Soc. Rev.* **2013**, *42*, 5408–5424.

(13) Bentley, K. W.; Wolf, C. Stereodynamic chemosensor with selective circular dichroism and fluorescence readout for in situ determination of absolute configuration, enantiomeric excess, and concentration of chiral compounds. *J. Am. Chem. Soc.* **2013**, *135*, 12200–12203.

(14) Zhu, L.; Anslyn, E. V. Facile quantification of enantiomeric excess and concentration with indicator-displacement assays: an example in the analyses of alpha-hydroxyacids. *J. Am. Chem. Soc.* **2004**, *126*, 3676–3677.

(15) Zhu, L.; Zhong, Z.; Anslyn, E. V. Guidelines in implementing enantioselective indicator-displacement assays for alpha-hydroxycarboxylates and diols. *J. Am. Chem. Soc.* **2005**, *127*, 4260–4269.

(16) Zhu, L.; Shabbir, S. H.; Anslyn, E. V. Two methods for the determination of enantiomeric excess and concentration of a chiral sample with a single spectroscopic measurement. *Chem. Eur. J.* **2007**, *13*, 99–104.

(17) Shabbir, S. H.; Joyce, L. A.; da Cruz, G. M.; Lynch, V. M.; Sorey, S.; Anslyn, E. V. Pattern-based recognition for the rapid determination of identity, concentration, and enantiomeric excess of subtly different threo diols. *J. Am. Chem. Soc.* **2009**, *131*, 13125–13131.

(18) Shabbir, S. H.; Regan, C. J.; Anslyn, E.V. A general protocol for creating high-throughput screening assays for reaction yield and enantiomeric excess applied to hydrobenzoin. *Proc. Nat. Acad. Sci.* **2009**, *106*, 10487.

(19) Folmer-Andersen, J. F.; Lynch, V. M.; Anslyn, E. V. Colorimetric enantiodiscrimination of alpha-amino acids in protic media. *J. Am. Chem. Soc.* **2005**, *127*, 7986–7987.

(20) Folmer-Andersen, J. F.; Kitamura, M.; Anslyn, E. V. Pattern-based discrimination of enantiomeric and structurally similar amino acids: an optical mimic of the mammalian taste response. *J. Am. Chem. Soc.* **2006**, *128*, 5652–5653.

(21) Leung, D.; Folmer-Andersen, J. F.; Lynch, V. M.; Anslyn, E. V. Using enantioselective indicator displacement assays to determine the enantiomeric excess of alpha-amino acids. *J. Am. Chem. Soc.* **2008**, *130*, 12318–12327.

(22) Leung, D.; Anslyn, E. V. Transitioning enantioselective indicator displacement assays for alpha-amino acids to protocols amenable to high-throughput screening. *J. Am. Chem. Soc.* **2008**, *130*, 12328–12333.

(23) Coomans, D.; Massart, D. L.; Kaufman, L. Optimization by statistical linear discriminant analysis in analytical chemistry. *Anal. Chim. Acta.* **1979**, *112*, 97-122.

(24) Li, Y.; Jiang, J. H.; Chen, Z. P.; Xu, C. J. Robust linear discriminant analysis for chemical pattern recognition. *J. Chemom.* **1999**, *13*, 3-13.

(25) Ringnér, M. What is principal component analysis? *Nat. Biotechnol.* **2008**, 26, 303-304.

(26) Nieto, S.; Lynch, V. M.; Anslyn, E. V.; Kim, H. High-throughput screening of identity, enantiomeric excess, and concentration using MLCT transitions in CD

spectroscopy. *J. Am. Chem. Soc.* **2008**, *130*, 9232-9233.

(27) Nieto, S.; Lynch, V. M.; Anslyn, E. V.; Kim, H.; Chin, J. Rapid enantiomeric excess and concentration determination using simple racemic metal complexes. *Org. Lett.* **2008**, *10*, 5167–5170.

(28) Dezhahang, Z.; Merten, C.; Poopari, M. R.; Xu, Y. Vibrational circular dichroism spectroscopy of two chiral binaphthyl diphosphine ligands and their palladium complexes in solution. *Dalton Trans.* **2012**, *41*, 10817–10824.

(29) Nieto, S.; Dragna, J. M.; Anslyn, E. V. A facile circular dichroism protocol for rapid determination of enantiomeric excess and concentration of chiral primary amines. *Chem. Eur. J.* **2010**, *16*, 227–232.

(30) Leung, D.; Anslyn, E. V. Rapid determination of enantiomeric excess of α-chiral cyclohexanones using circular dichroism spectroscopy. *Org. Lett.* **2011**, *13*, 2298–2301.

(31) Dragna, J. M.; Pescitelli, G.; Tran, L.; Lynch, V. M.; Anslyn, E. V.; Di Bari, L. In situ assembly of octahedral Fe(II) complexes for the enantiomeric excess determination of chiral amines using circular dichroism spectroscopy. *J. Am. Chem. Soc.* **2012**, *134*, 4398–4407.

(32) Pérez-Fuertes, Y.; Kelly, A. M.; Johnson, A. L.; Arimori, S.; Bull, S. D.; James, T. D. Simple protocol for NMR analysis of the enantiomeric purity of primary amines. *Org. Lett.* **2006**, *8*, 609–612.

(33) Pérez-Fuertes, Y.; Kelly, A. M.; Fossey, J. S.; Powell, M. E.; Bull, S. D.; James, T. D. Simple protocols for NMR analysis of the enantiomeric purity of chiral

primary amines. *Nat. Protoc.* **2008**, *3*, 210–214.

(34) Metola, P.; Anslyn, E. V.; James, T. D.; Bull, S. D. Circular dichroism of multi-component assemblies for chiral amine recognition and rapid *ee* determination. *Chem. Sci.* **2012**, *3*, 156-161.

(35) Berova, N.; Di Bari, L.; Pescitelli, G. Application of electronic circular dichroism in configurational and conformational analysis of organic compounds. *Chem. Soc. Rev.* **2007**, *36*, 914–931.

(36) Zahn, S. S.; Canary, J. W. J. Absolute configurations of N,N-dialkyl alpha-amino acids and beta-amino alcohols from exciton-coupled circular dichroism spectra of Cu(II) complexes. *Org. Lett.* **1999**, *1*, 861–864.

(37) Zhang, J.; Holmes, A. E.; Sharma, A.; Brooks, N. R.; Rarig, R. S.; Zubieta, J.; Canary, J. W. Derivatization, complexation, and absolute configurational assignment of chiral primary amines: application of exciton-coupled circular dichroism. *Chirality,* **2003**, *15*, 180–189.

(38) Huang, X. X.; Nakanishi, K. K.; Berova, N. N. Porphyrins and metalloporphyrins: versatile circular dichroic reporter groups for structural studies. *Chirality,* **2000**, *12*, 237–255.

(39) Balaz, M.; De Napoli, M.; Holmes, A. E.; Mammana, A.; Nakanishi, K.; Berova, N.; Purrello, R. A cationic zinc porphyrin as a chiroptical probe for Z-DNA. *Angew. Chem. Int. Ed.* **2005**, *44*, 4006–4009.

(40) Matile, S.; Berova, N.; Nakanishi, K.; Novkova, S.; Philipova, I.; Blagoev, B. Porphyrins: Powerful Chromophores for Structural Studies by Exciton-Coupled

Circular Dichroism. *J. Am. Chem. Soc.* **1995**, *117*, 7021–7022.

(41) Furusho, Y.; Kimura, T.; Mizuno, Y. Chirality-Memory Molecule: AD 2-Symmetric Fully Substituted Porphyrin as a Conceptually New Chirality Sensor. *J. Am. Chem. Soc.* **1997**, *119*, 5267-5268.

(42) Tanasova, M.; Yang, Q.; Olmsted, C. C. An Unusual Conformation of α-Haloamides Due to Cooperative Binding with Zincated Porphyrins. *Eur. J. Org. Chem.* **2009**, 4242-4253.

(43) Borovkov, V. V.; Lintuluoto, J. M.; Inoue, Y. Supramolecular chirogenesis in zinc porphyrins: mechanism, role of guest structure, and application for the absolute configuration determination. *J. Am. Chem. Soc.* **2001**, *123*, 2979–2989.

(44) Li, X.; Borhan, B. Prompt determination of absolute configuration for epoxy alcohols via exciton chirality protocol. *J. Am. Chem. Soc.* **2008**.

(45) Li, X.; Burrell, C. E.; Staples, R. J.; Borhan, B. Absolute configuration for 1,n-glycols: a nonempirical approach to long-range stereochemical determination. *J. Am. Chem. Soc.* **2012**, *134*, 9026–9029.

(46) Tartaglia, S.; Padula, D.; Scafato, P.; Chiummiento, L.; Rosini, C. A chemical/computational approach to the determination of absolute configuration of flexible and transparent molecules: aliphatic diols as a case study. *J. Org. Chem.* **2008**, *73*, 4865–4873.

(47) Ghosn, M. W.; Wolf, C. Chiral amplification with a stereodynamic triaryl probe: assignment of the absolute configuration and enantiomeric excess of amino alcohols. *J. Am. Chem. Soc.* **2009**, *131*, 16360–16361.

(48) Ghosn, M. W. M.; Wolf, C. C. Synthesis, conformational stability, and asymmetric transformation of atropisomeric 1,8-bisphenolnaphthalenes. *J. Org. Chem.* **2011**, *76*, 3888–3897.

(49) Yoon, H.; Lee, C.-H.; Jang, W.-D. Absolute stereochemical determination of chiral carboxylates using an achiral molecular tweezer. *Chem. Eur. J.* **2012**, *18*, 12479–12486.

(50) Fujiwara, T.; Taniguchi, Y.; Katsumoto, Y.; Tanaka, T.; Node, M.; Ozeki, M.; Yamashita, M.; Hosoi, S. Induced circular dichroism in chiralN-methyl amides possessing an achiral binaphthyl chromophore and its application to absolute configuration determination of aliphatic chiral amines. *Tetrahedron:Asymmetry* **2012**, *23*, 981–991.

(51) Iwaniuk, D. P.; Wolf, C. A stereodynamic probe providing a chiroptical response to substrate-controlled induction of an axially chiral arylacetylene framework. *J. Am. Chem. Soc.* **2011**, *133*, 2414–2417.

(52) Wezenberg, S. J.; Salassa, G.; Escudero-Adán, E. C.; Benet-Buchholz, J.; Kleij, A. W. Effective chirogenesis in a bis(metallosalphen) complex through host-guest binding with carboxylic acids. *Angew. Chem. Int. Ed.* **2011**, *50*, 713–716.

(53) Cysewski, R.; Kwit, M.; Warzajtis, B.; Rychlewska, U.; Gawroński, J. Synthesis, conformation and chiroptical properties of diaryl esters of tartaric acid. *J. Org. Chem.* **2009**, *74*, 4573–4583.

(54) Kim, H.; So, S. M.; Yen, C. P.-H.; Vinhato, E.; Lough, A. J.; Hong, J.-I.; Kim, H.-J.; Chin, J. Highly stereospecific generation of helical chirality by imprinting

with amino acids: a universal sensor for amino acid enantiopurity. *Angew. Chem. Int. Ed.* **2008**, *47*, 8657–8660.

(55) Berova, N.; Pescitelli, G.; Petrovic, A. G.; Proni, G. Probing molecular chirality by CD-sensitive dimeric metalloporphyrin hosts. *Chem. Commun.* **2009**, 5958–5958.

(56) Barman, S.; Anslyn, E. V. Rapid determination of enantiomeric excess of α-chiral aldehydes using circular dichroism spectroscopy. *Tetrahedron*. **2014**, *70*, 1357–1362.

(57) Joyce, L. A.; Maynor, M. S.; Dragna, J. M.; da Cruz, G. M.; Lynch, V. M.; Canary, J. W.; Anslyn, E. V. A simple method for the determination of enantiomeric excess and identity of chiral carboxylic acids. *J. Am. Chem. Soc.* **2011**, *133*, 13746–13752.

(58) Joyce, L. A.; Canary, J. W.; Anslyn, E. V. Enantio-and Chemoselective Differentiation of Protected α-Amino Acids and β-Homoamino Acids with a Single Copper (II) Host. *Chem. Eur. J.* **2012**, *18*, 8064-8069.

(59) You, L.; Berman, J. S.; Anslyn, E. V. Dynamic multi-component covalent assembly for the reversible binding of secondary alcohols and chirality sensing. *Nature. Chem.* **2011**, *3*, 943–948.

(60) You, L.; Pescitelli, G.; Anslyn, E. V.; Di Bari, L. An exciton-coupled circular dichroism protocol for the determination of identity, chirality, and enantiomeric excess of chiral secondary alcohols. *J. Am. Chem. Soc.* **2012**, *134*, 7117–7125.

(61) You, L.; Berman, J. S.; Lucksanawichien, A.; Anslyn, E. V. Correlating sterics

parameters and diastereomeric ratio values for a multicomponent assembly to predict exciton-coupled circular dichroism intensity and thereby enantiomeric excess of chiral secondary alcohols. *J. Am. Chem. Soc.* **2012**, *134*, 7126–7134.

(62) Pu, L. Enantioselective fluorescent sensors: a tale of BINOL. *Acc. Chem. Res.* **2012**, *2*, 150-163.

(63) Wen, K.; Yu, S.; Huang, Z.; Chen, L.; Xiao, M.; Yu, X.; Pu, L. Rational Design of a Fluorescent Sensor to Simultaneously Determine Both the Enantiomeric Composition and the Concentration of Chiral Functional Amines. *J. Am. Chem. Soc.* **2015**, *137*, 4517-4524.

(64) Wang, C.; Wu, E.; Wu, X.; Xu, X.; Zhang, G.; Pu, L. Enantioselective fluorescent recognition in the fluorous phase: Enhanced reactivity and expanded chiral recognition. *J. Am. Chem. Soc.* **2015**, *137*, 3747-3750.

(65) Bentley, K. W.; Zhang, P.; Wolf, C. Miniature high-throughput chemosensing of yield , ee , and absolute configuration from crude reaction mixtures. *Sci. Adv.* **2016**, 2.

(66) Bentley, K. W.; Nam, Y.; Murphy, J.; Wolf, C. Chirality Sensing of Amines, Diamines, Amino Acids, Amino Alcohols, and hydroxy Acids with a single probe. *J. Am. Chem. Soc.,* **2013**, *135*, 18052-18055.

(67) De Los Santos, Z.; Ding, R.; Wolf, C. Quantitative chirality sensing of amines and amino alcohols via Schiff base formation with a stereodynamic UV/CD probe. *Org. Biomol. Chem.,* **2016**, *14*, 1934-1939.

(68) Bentley, K. W.; Wolf, C. Comprehensive Chirality Sensing: Development of

Stereodynamic Probe with a Dual (Chir)optical Response. *J. Org. Chem.* **2014**, *79*, 6517- 6531.

# Chapter 2[2]

## 1. INTRODUCTION

In the development of asymmetric catalysis, certain families of catalysts have been found to behave similarly in catalyzing different transformations.[1] While the understanding behind such a transferable catalyst is still unclear, a common feature shared by these catalyst is restriction of the orientations of reacting molecules in solution in the key bond-forming steps. However, there are many asymmetric transformations in which the initial bond-forming steps of a reaction are not stereodetermining, and thus these scaffolds and/or rational design-based approaches have not been particularly successful. One such reaction is the venerable Baeyer–Villiger (B–V) oxidation,[2] which remains a formidable challenge to asymmetric catalysis.[3]

The Miller lab employed a combinatorial approach to develop aspartic acid containing peptide oxidation catalysts that address chemical transformations that are often recalcitrant to rational design approaches.[4] The catalysts operate via in situ generation of peracids from the reaction of a DIC-activated aspartic acid side-chain with hydrogen peroxide (Figure 2.1a). While initially developed for asymmetric epoxidation reactions,[5] we have also applied this catalytic cycle to the B–V oxidation of a variety of cyclic ketones.[6] Very recently, Miller lab reported on the application of this combinatorial approach to the discovery of an aspartic acid-containing peptide B–V oxidation catalyst.[6b] This catalyst was proficient at overcoming the substrates' inherent regioselectivity biases by means of directing group interactions (Figure 2.1b).[7] Catalyst-substrate interactions predicated on hydrogen-bonding interactions seem to be at the heart of the observed high selectivity in our earlier studies. Substrates that lack functionality for the same type of

[2] This chapter is adopted from the published article. ref. Giuliano, M. W.; Lin, C.-Y.; Romney, D. K.; Miller, S. J.; Anslyn, E. V. *Adv. Synth. Catal.* **2015**, *357*, 2301-2309. Lin conducted the ee experiments and Giuliano conducted the HPLC ee catalysis.

phenomena present a special challenge. Herein we report the synergistic use of combinatorial screening, rational library design, HPLC analysis, and a recently reported chiroptical assay that involves a multi-component assembly, all of which lays the foundation for the use of peptide B–V oxidation catalysts to substrates which lack directing groups (Figure 2.1c). The assay[8] played a crucial role in evaluating catalyst performance, and uniquely provided stereochemical information about oxidation products that will inform our future efforts in catalyst development for the B–V oxidation. Its successful implementation also sets the stage for ultra-high throughput screening in the future with hundreds of ee values determined per hour.[9]

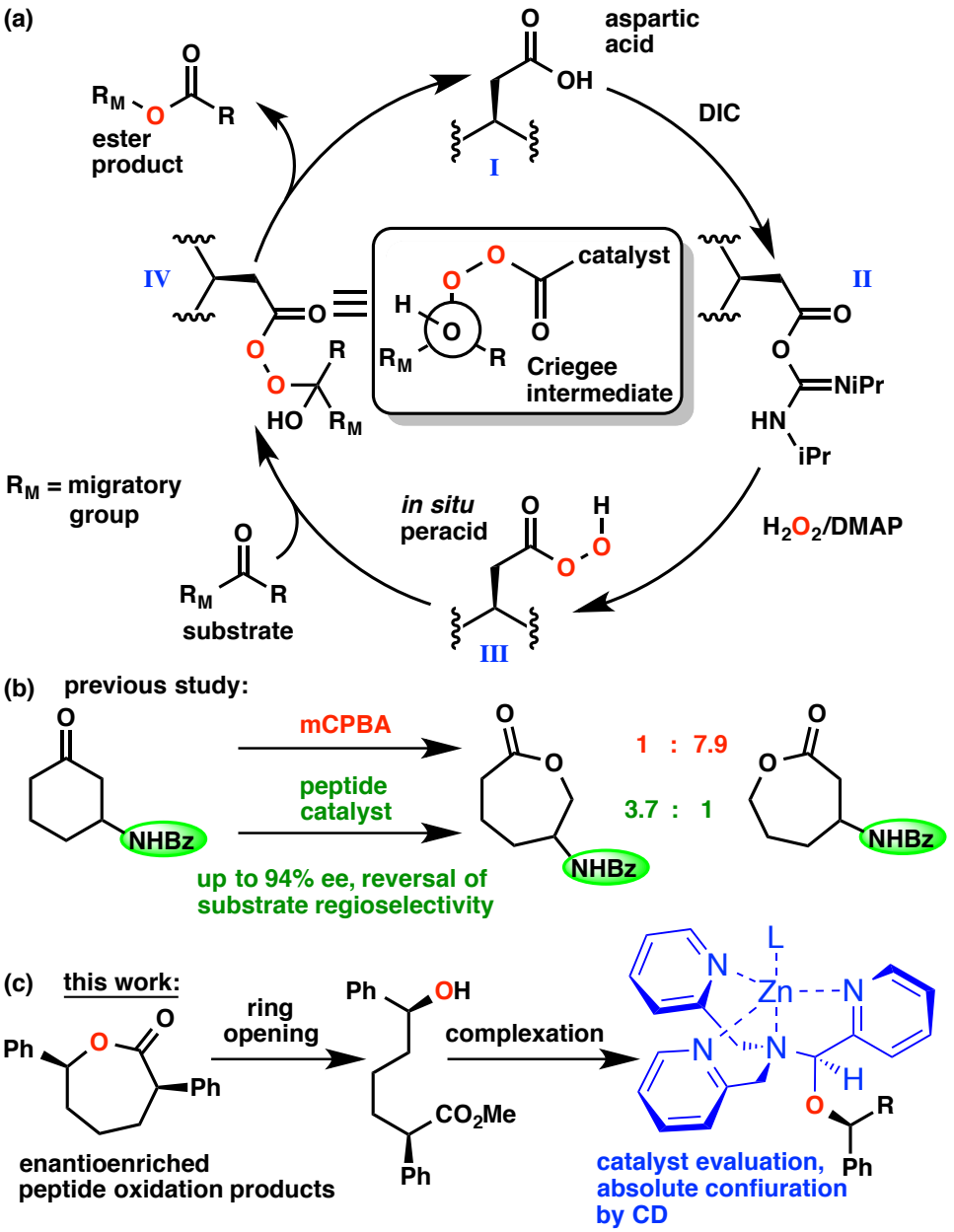


**Figure 2.1** (a) Catalytic cycle for peracid-mediated B–V oxidations based on DIC/$H_2O_2$ activation of aspartic acid. Inset – Newman projection of the Criegee intermediate. (b) Inversion of inherent substrate regioselectivity preferences *via* use of a combinatorially discovered peptide catalyst and a benzamide directing group (green ovals).[6b] (c) Work up and assembly used herein to measure ee values via CD spectroscopy.

## 2. Results and Discussion

### 2.1 Catalyst Design and Screening

Our attention was drawn to a body of literature concerning protein-anion interactions.[10] Specifically, a number of different protein loop sequences have been observed to interact with phosphate, sulfate, and other anions (e.g., Figure 2.2a).[10b,c] We wondered if this sequence space could be reappropriated for the purposes of a peptide-catalyzed asymmetric B–V oxidation, owing to the structural similarities between tetrahedral anions and Criegee intermediates (IV in Figure 2.1a). We prepared a combinatorial library based on a bioinformatic analysis of a so-called CαNN' motif,[10b,c] in which the first two variable residues were biased toward helix-preferring amino acids and the last position incorporated Val to accommodate β-strand torsion angles. The C-terminal residue of the library was chosen as alanine to account for the helical preferences of a number of the anion-binding protein loops.[10c] The N-terminal residues consisted of the catalytically active Asp followed by an L-Pro residue, preempting the possibility of aspartimide rearrangement11 under the reaction conditions. This library comprised 450 unique sequences immobilized onto Rink linker-functionalized polystyrene macrobeads (Figure 2.2b).

Our on-bead screening commenced with the B–V oxidation of the sterically challenging ketone substrate, cis-2,6-diphenylcyclohexanone (Figure 2.2c); the previously reported peptide B–V catalyst was unable to convert this ketone under on-bead conditions.[12] After screening only fifty beads, a number of catalysts were observed to converge into two groups. Each favored opposite enantiomers of the lactone product up to approximately 30% ee, despite the library being composed solely of amino acids with the L configuration. MS/MS sequencing indicated that the two groups of sequence-shad distinct preferences at the (i+2) position. One group universally had an O-benzyl serine

(i+2) residue while the other group favored a (i+2) leucine residue (Table 2.1, entries 1–12).

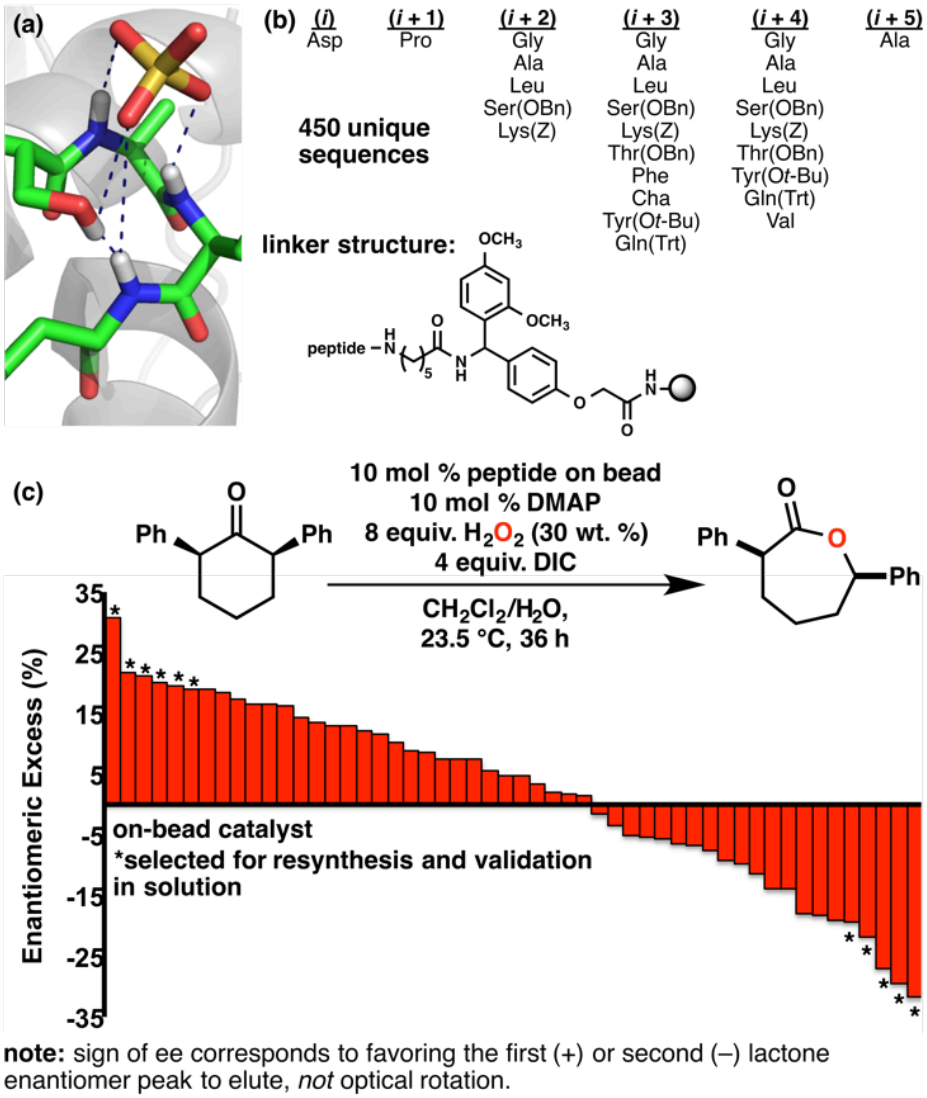


**note:** sign of ee corresponds to favoring the first (+) or second (–) lactone enantiomer peak to elute, *not* optical rotation.

**Figure 2.2** (a) Tetrahedral sulfate anion bound by helical protein loop. PDB: 1YCC. (b) Library composition informed by bioinformatics analysis of protein binding loop sequences. (c) Screening results using 50 beads from combinatorial peptide library. Reactions were 0.1 M in ketone substrate on a scale of 0.69 μmol ketone. Each bead contained 69 nmol peptide catalyst, corresponding to a loading of 10 mol %. $H_2O_2$ was added from a stock solution at a concentration of 3.0 M.

**Table 2.1** Solution-phase validation and focused library screening of peptide catalysts for the B–V oxidation.

| entry | sequence[a] ($i+2$, $i+3$, $i+4$) | conv.[c,d] (%) | ee[c,d] (HPLC, %) | ee[c,e] (CD, %) | entry | sequence[a] ($i+2$, $i+3$) | conv.[c,d] (%) | ee[c,d] (HPLC, %) | ee[c,e] (CD, %) |
|---|---|---|---|---|---|---|---|---|---|
| 1 | **Leu**-Phe-Tyr(O*t*-Bu) | 75 | 46 | --[g] | 13 | Pro-Ser(O*t*-Bu) | 82 | –8 | –9 |
| 2 | **Leu**-Phe-Thr(OBn) | 63 | 42 | 43 | 14 | Hyp(O*t*-Bu)-Ser(O*t*-Bu) | 90 | 9 | 8 |
| 3 | Lys(Z)-Lys(Z)-Ala | 70 | 24 | 22 | 15 | Pip-Ser(O*t*-Bu) | 90 | 5 | 3 |
| 4 | **Leu**-Lys(Z)-Thr(OBn) | 59 | 39 | 36 | 16 | Ala-Ser(O*t*-Bu) | 59 | 4 | 1 |
| 5 | **Leu**-Leu-Thr(OBn) | 74 | 33 | 29 | 17 | Pro-Ser(OH) | 85 | –10 | –5 |
| 6 | **Leu**-Cha-Ala | 77 | 40 | 36 | 18 | Hyp(O*t*-Bu)-Ser(OH) | 41 | –6 | –6 |
| 7 | Boc-Asp(OH)-OBn | > 99 | –2 | --[g] | 19 | Pip-Ser(OH)[f] | 47 | –3 | –4 |
| 8 | **Ser(OBn)**-Gly-Val | 55 | –35 | –32 | 20 | Ala-Ser(OH) | 20 | 1 | 1 |
| 9 | **Ser(OBn)**-Lys(Z)-Ser(OBn) | 76 | –41 | –42 | 21 | Pro-Thr(OBn) | 88 | –10 | –8 |
| 10 | **Ser(OBn)**-Cha-Tyr(O*t*-Bu) | 82 | –37 | –42 | 22 | Hyp(O*t*-Bu)-Thr(OBn) | 91 | 1 | 0 |
| 11 | **Ser(OBn)**-Leu-Ser(OBn) | 77 | –47 | –44 | | | | | |
| 12 | **Ser(OBn)**-Leu-Leu | 75 | –51 | --[g] | | | | | |

[a]Parent sequence of library hits: Boc-Asp-Pro-Xaa-Xaa-Xaa-Ala-Gly-OMe. [b]Parent sequence of focused library: Boc-Asp-Xaa-Xaa-Leu-Leu-Ala-Gly-OMe. [c]Average of two runs. [d]Determined from HPLC traces of worked up reactions. [e]Determined from CD intensity at 270 nm of complex that incorporated lactone-derived secondary alcohol. All runs carried out on a scale of 0.3 mmol ketone. [f]Single run due to limited catalyst material. [g]Catalyst used to develop CD calibration curve. **Note:** sign of ee corresponds to favoring the first (+) or second (–) lactone enantiomer to elute on an HPLC assay, not optical rotation.

## 2.2 Catalyst Bioinformatics

In designing the sequence of the peptide catalysts, Denessiouk et al. have described a sequence loop, referred to as a Cα NN' motif (further described in reference 10b in short model peptides), that is observed to bind to tetrahedral sulfate and phosphate anions in protein crystal structures. We hypothesized that the sequence space occupied by this motif might be repurposed for an asymmetric Baeyer-Villiger oxidation; this was based on the structural similarity between tetrahedral anions and the key Criegee intermediate of the BV oxidation, whose rearrangement governs the enantiodetermining step of the reaction. We carried out an amino acid frequency analysis of the sequences studied by Denessiok et al. (Figure 2.3a). We noted a high population of Gly at all positions. The N position, Gly aside, did not exhibit strong sidechain preferences. However, Denessiouk et al. suggested N-position residues preferred the dihedral angles of the α-helix. Ser residues were found in particularly high frequency at the Cα-position, and it is believed that this is due to sidechain participation in anion binding, which was intriguing for our catalyst design purposes. The Cα-position also appeared to prefer amino acids that occupy the dihedral angles of the α-helix, similarly to the N position. The N' position showed higher frequency of Ser and Thr residues. Denessiouk et al. also observed that residues that prefer β-sheet dihedral angles, such as Val, occupied the N' position. Thus, with some side chain preferences gleaned from this frequency analysis and the dihedral angle preferences of each position provided by the work of Denessiouk et al. we designed the library shown below (Figure 2.3b). Aspartic acid at the N-terminus is the catalytically active residue, and proline was chosen as the (i+1) residue to eliminate the possibility of aspartimide rearrangement interfering with the catalytic cycle. All sequences terminated in an Ala-Ahx (Ahx = ε -aminohexanoic acid) for two reasons. First, the mass of the dipeptide fragment was just above the

observation threshold of the instrumentation used to sequence peptidies. Second, the Ahx would act as a spacer between the surface of the bead and the peptide while the Ala may remotely affect the ability of the peptides to interact with tetrahedral species near their N-terminii, based on additional analysis of the CαNN' motif.[10b] Lastly, the peptides were attached to Rink linker to facilitate acid-mediated cleavage during hit sequencing.

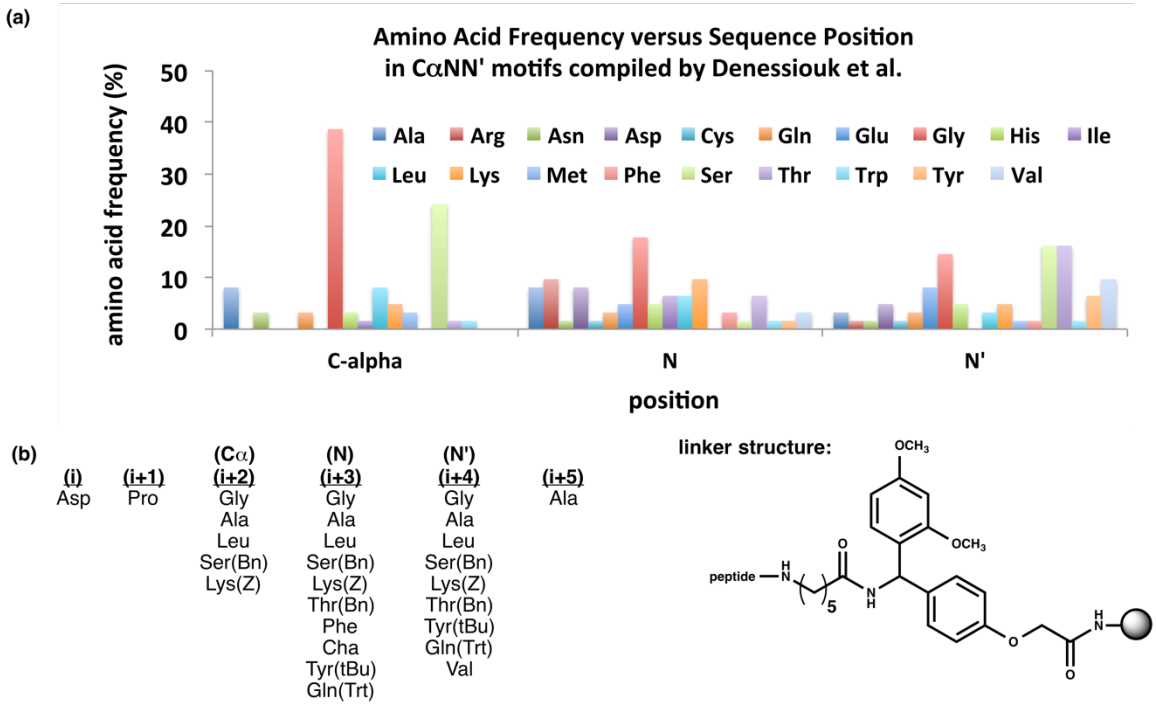


**Figure 2.3** (a) Frequency analysis of the CαNN' motif sequences studied by Denessiouk et al. (b) Combinatorial library designed toward repurposing the CαNN' motif for interaction with theCriegee intermediate in an asymmetric Baeyer-Villiger oxidation.

## 2.3 Peptide Catalyst Analyses

To determine the absolute configuration and the ee of these two distinct stereochemical preferences, we turned to a recently described CD assay (Figure 2.4a).[8] Incorporation of chiral secondary alcohols into a tren-like ligand creates a dynamically assembled zinc(II) complex that exhibits characteristic Cotton effects at 270 nm.[8] The intensity of this signal varies linearly with the ee of the incorporated alcohol, while its sign correlates to the M or P twist of the pyridyl ligands about the zinc(II) center. In turn, this twist is indicative of the absolute configuration, S or R respectively, of the enantiomer of alcohol that is in excess. Our plan was to utilize this assay in the screening of peptide catalysts in solution to develop models of catalyst-Criegee intermediate interactions. Further, we were intrigued to compare the accuracy of this very rapid CD assay with our HPLC assay.

Eleven peptide hits from our combinatorial screen were synthesized, except with a glycine methyl ester residue replacing the aminohexanoic acid linker used in solid phase screening. These peptides were contrasted to N-Boc aspartic acid benzyl ester as a negative control catalyst. Catalyst performance in solution was markedly improved compared to the on-bead sequences, with ee for the best catalysts increasing to 46% for the Leu series (Table 2.1, entry 1) and 51% for the Ser(OBn) series (Table 2.1 entry 12); such improvements are a common phenomeneon in bead-based optimization of catalyst architecture.[4]

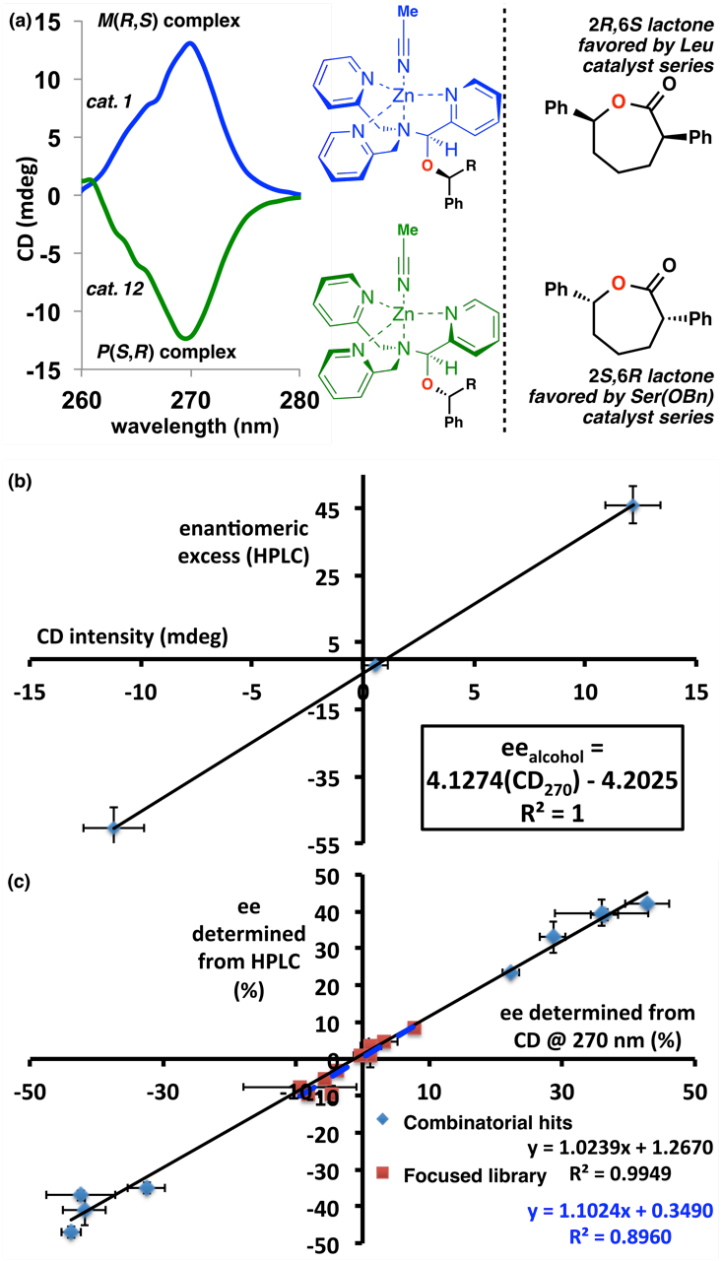


**Figure 2.4** (a) Derivation of lactone absolute configuration from CD spectra of complexed lactone-derived 2° alcohols with catalysts **2** and **13** (Table 1). (b) Calibration curve of ee vs CD intensity using catalysts **2**, **8**, and **13** (Table 1). (c) Comparison of ee by HPLC and ee by CD for duplicate screened combinatorial hits and focused library. Error bars in b and c indicate standard deviation from the average of duplicate runs.

### *2.3.1 CD Assay and Comparison with HPLC Results*

Because we were in the advantageous situation of having catalysts that favored opposite enantiomers, we used a high-yielding ee example of each catalyst and N-Boc aspartic acid benzyl ester to establish a three-point calibration curve. The curve relates CD signal intensity at 270 nm to the ee of the alcohols derived from our product lactones via methanolysis (Figure 2.4b, Table 2.1, entries 1, 7, and 12).[12] The y-intercept of the calibration curve corresponded to approximately a 4% error in ee (Figure 2.4b, from the expected value of 0 for racemic), which is clearly useable for a rapid screening method. In addition, we observed equivalent performance of the CD-assay when comparing to HPLC for the remaining 9 combinatorial hits (Figure 2.4c, black trendline). Alcohols derived from the lactones produced by peptide catalysts with (i + 2) Ser(Bn) residues favored negative CD signals, while those with (i + 2) Leu residues favored positive CD signals (Figure 2.4a). We thus assign the stereochemistry of the lactones produced by Ser(OBn) catalysts as (2S,6R) and that produced by Leu catalysts as (2R,6S).[8] The excellent correlation we observe between the CD and HPLC data is key to another feature of the CD assay – the additional stereocenter in the lactone-derived alcohols does not interfere because the assembly is only responsive to alcohol functional groups. Further, all of the alcohol samples were analyzed without the need for removal of ketone starting material, which remains a spectator; oxidation and methanolysis-related byproducts/reagents were removed via a simple silica plug.

### *2.3.2 Catalyst Stereochemical Analysis*

Previous study of peptide-catalyzed epoxidations of the terpene natural product farnesol led to the discovery of a remotely directed catalyst that implicated an (i + 2) ether sidechain in its mode of stereochemical induction.[4c] We were intrigued by a possible parallel observation in the Ser(OBn) series of catalysts. Additionally, we were curious if

any changes to the (i + 1) L-Pro residue might alter the stereochemical outcome. We screened ten additional peptide catalysts targeted to address these questions (Table 2.1, entries 14–23), maintaining the (i + 3) and (i + 4) Leu residues of the best performing sequence of the Ser(OBn) series. We found that, once again, the CD and HPLC assay of product ee were equivalent in performance, with a strong linear correlation between the ee values obtained with each method (Figure 2.4c, dashed blue trendline).

We were intrigued by catalysts 13, 17, and 21 (Table 1), which, relative to peptide 12, varied the (i+2) position residue to Ser(Ot-Bu), Ser(OH, and Thr(OBn), respectively. In all three cases, we observed lower product ee, which directly implicates this side-chain in the enantiodetermining C–C bond migration. Based on the aforementioned precedent involving ether-containing peptide oxidation catalysts,[4c] we entertained the possibility of the (i+2) sidechain acting as a hydrogen bond acceptor in light of these results. It would seem that increased steric bulk about the side-chain oxygen, as for 13 and 21, decreases the ability of this atom to act as an H-bond acceptor, if such an interaction is important. This putative directing H-bond between the Criegee intermediate and the (i + 2) side-chain would also be weakened if the Lewis basicity of the oxygen were reduced. This may be the case for peptide 17 although we cannot discount potentially deleterious interference of a free hydroxyl group with the catalytic cycle.

Peptides with non-Pro (i + 1) residues and altered (i + 2) residues were not drastically changed relative to peptides 13, 17, and 21. The nature of these effects, although small, may suggest that a determinant of asymmetric induction in the directing group free peptide-catalyzed B-V oxidation is interaction between the aspartic peracid-bound Criegee intermediate and the (i + 2) residue sidechain of the Ser(OBn) catalyst series. While speculative, some thoughts about this series include the possibility of a hydroxylether H-bond between the (i+2) Ser(OBn) residue and a catalyst-bound Criegee intermediate,

potentially directing migration of the pro-R C–C bond (Figure 2.5a). Hence, there is an intriguing parallel with the mode of action of B–V monooxygenases, which direct flavin-bound Criegee intermediate rearrangement via interaction with an active site arginine side-chain (Figure 2.5b).[13] Further study including structural characterization of the catalysts is a focus of our ongoing efforts to explore this intriguing possibility.

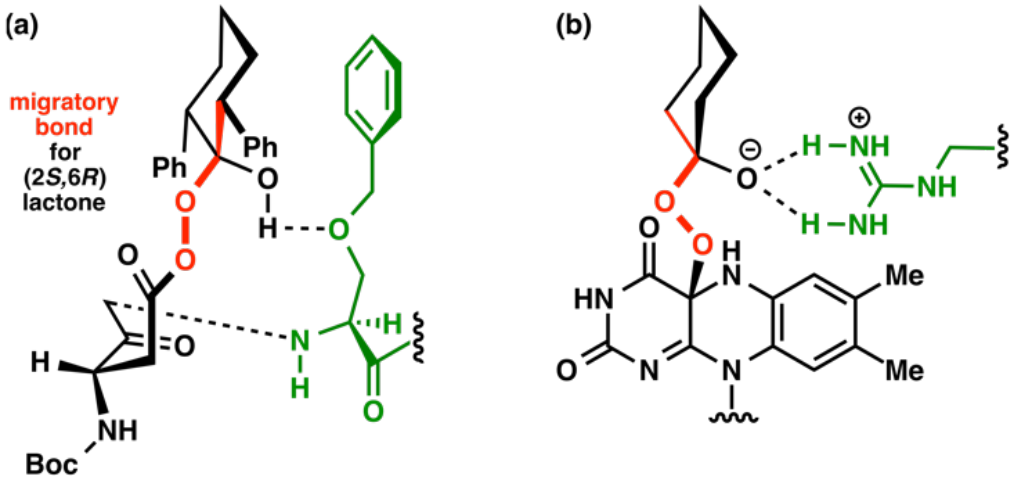


**Figure 2.5** (a) Putative H-bonding between Criegee intermediate and Ser(OBn) sidechain. (b) Drawing of an Arg sidechain interacting with FAD-bound Criegee intermediate; the key stereodetermining interaction in B–V monooxygenases.[13]

## 3. Conclusion

We have reported two families of peptide catalysts that induce enantioselective B–V oxidation by virtue of what we believe to be direct peptide-Criegee intermediate interactions. Both series of catalysts readily oxidize a highly encumbered ketone, which is itself a minimal model of the encumbered ketones found in terpene and polyketide natural products. The design principles used in our combinatorial library, namely targeting sequence space involved in the recognition of moieties similar to the key intermediate of our reaction, led to the discovery of two distinct catalyst families by screening only fifty beads. Our previous B–V and epoxidation reaction efforts based on de novo sequence discovery each required the screening of hundreds of beads to yield hits.[4,6b]

The CD assay we employed proved crucial in our analysis of the stereochemical course of reactions as it yielded the absolute configuration of the lactone products. We find that its ability to evaluate catalyst performance is equivalent to HPLC, even for samples with low ee. The assay provided enormous time savings in the analysis of alcohol samples, reducing the time from ~30 minutes to just a few seconds per sample. The added configurational information, available even for samples with low levels of enantioenrichment, combined with the operational simplicity and per sample speed of the assay itself make a case for wide implementation of this method in the synthetic chemistry community.

## 4. Experimental

### 4.1 Cicular Dichroism Assay

General Notes and Sample Preparation. CD spectra were obtained on a Jasco J-815 CD Spectrometer with Starna Type 1 GL14-S 10-mm quartz cells at 25ºC. The assembly stock solution was prepared by mixing 2-pyridinecarboxaldehyde (1 equiv.), 2,2'-

dipicolylamine (1.2 equiv.), $Zn(OTf)_2$ (1 equiv.), and 4-(2-chloroethyl)morpholine hydrochloride (1 equiv.) in acetonitrile at 50 mM with respect to 2-pyridinecarboxaldehyde. The stock solution was then added to a sample containing 3-5 equiv. methyl 6-hydroxy-2,6-diphenylhexanoate of unknown enantioenrichment with molecular sieves (3 Å) and left at room temperature (20 °C) for 12-16 hours. The alcohol assembly was then diluted to 0.175 mM, with respect to 2-pyridinecarboxaldehyde, before taking CD measurements. Note: This arrangement of testing allowed for the blind testing of samples by CD, which, as discussed in the manuscript, provided equivalent data to HPLC with added information regarding the absolute configuration of the incorporated alcohol stereocenter.

In order to carry out blind testing of lactone-derived secondary alcohols, we required a calibration curve describing the linear relationship between CD intensity and ee. Therefore, ringopened samples of methyl 6-hydroxy-2,6-diphenylhexanoate were analyzed for ee by HPLC and then analyzed for CD at 270 nm. Catalysts 1 and 12 along with Boc-Asp-OBn, tested in duplicate and averaged, served as a three-point set of data for which to determine this relationship. The close correlation of ee by HPLC and ee by CD suggest that this minimal dataset is all that was needed to determine the calibration curve for our samples. Figure 2.6a shows all six full CD spectra obtained for the complexes that incorporated each alcohol sample. We have included the data points and reproduced the calibration curve shown in the manuscript in Figure 2.6b and c.

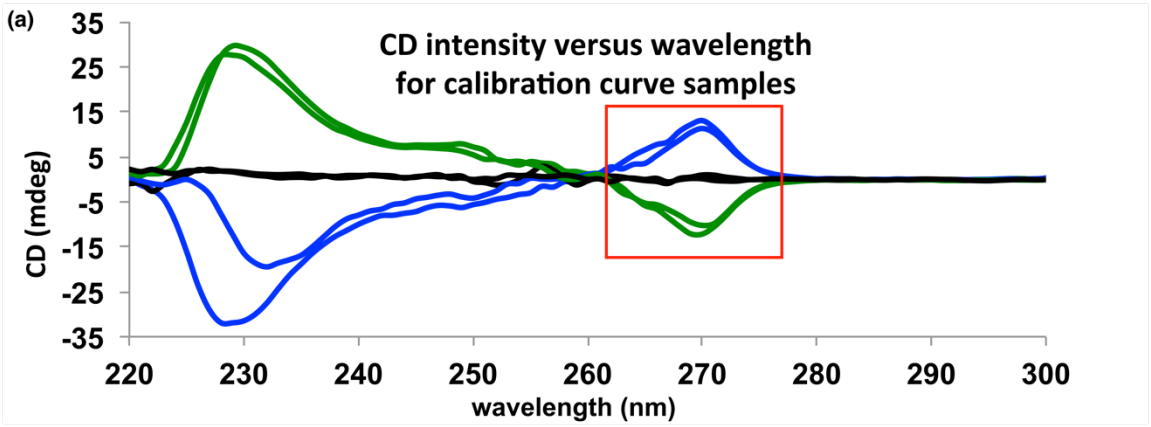


(b)

| catalyst | $CD_{270}$ (mdeg) | ee (%, HPLC) |
|---|---|---|
| 1 | 12 ± 1 | 46 ± 6 |
| Boc-Asp-OBn | 0.5 ± 0.6 | 2 |
| 12 | -11 ± 1 | -51 ± 6 |

(values are averages of duplicate runs)

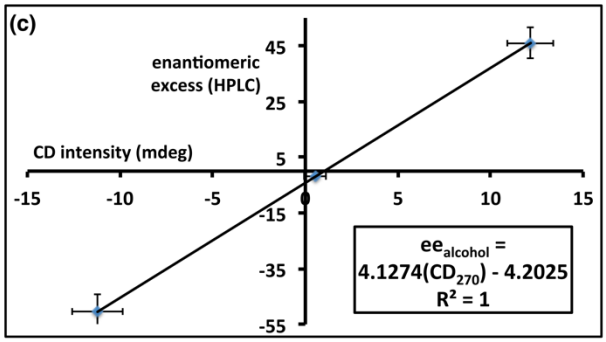


**Figure 2.6** (a) CD spectra of incorporation complexes of samples of methyl 6-hydroxy-2,6-diphenylhexanoate derived from lactones produced by peptides 1 and 12 and Boc-Asp-OBn. (b)Tabulated ee and CD values with errors. (c) Calibration curve related ee to CD intensity at 270 nm, reproduced from the manuscript. Color scheme matches that used in the paper for the Leu and Ser(OBn) series of catalts. Red box indicates the characteristic Cotton effect at 270 nm.

### 4.2 $CD_{270}$ Derived and HPLC determined ee Values

The calibration curve was used to generate ee values from the CD intensity at 270 nm of incorporated alcohols generated from the oxidation products of peptide catalysts 2-6, 8 -11, and 13-22. A summary of the hplc data and ee values of the lactones produced by these catalysts, the CD intensity at 270 nm of the alcohols derived from the lactones, and the ee derived using our calibration curve is presented in Table 2.2.

**Table 2.2** Summary of HPLC and CD data for screening of hit catalysts and focused library.

| entry | catalyst | Int. ketone[a] | Ent. 1[a] (lactone) | Ent. 2[a] (lactone) | Conv.[b] (%) | $CD_{270}$[c] (nm) | ee (HPLC)[b] (lactone) | ee (CD)[d] (alcohol) |
|---|---|---|---|---|---|---|---|---|
| 1 | **1** | | | | | 13.0439 | | -- |
| 2 | **1** | | | | | 11.2848 | | -- |
| 3 | **2** | | | | | 11.9538 | | 45 |
| 4 | **2** | | | | | 10.809 | | 40 |
| 5 | **3** | | | | | 6.64202 | | 23 |
| 6 | **3** | | | | | 6.21763 | | 21 |
| 7 | **4** | | | | | 10.1827 | | 38 |
| 8 | **4** | | | | | 9.47737 | | 35 |
| 9 | **5** | | | | | 8.27517 | | 30 |
| 10 | **5** | | | | | 7.63068 | | 27 |
| 11 | **6** | | | | | 10.9264 | | 41 |
| 12 | **6** | | | | | 8.50589 | | 31 |
| 13 | **Boc-Asp-OBn** | | | | | 0.946928 | | -- |
| 14 | **Boc-Asp-OBn** | | | | | 0.115988 | | -- |
| 15 | **8** | | | | | -6.36278 | | -30 |
| 16 | **8** | | | | | -7.33005 | | -34 |
| 17 | **9** | | | | | -9.67089 | | -44 |
| 18 | **9** | | | | | -8.57125 | | -40 |
| 19 | **10** | | | | | -8.35279 | | -39 |
| 20 | **10** | | | | | -10.1491 | | -46 |
| 21 | **11** | | | | | -9.34748 | | -43 |
| 22 | **11** | | | | | -9.86016 | | -45 |
| 23 | **12** | | | | | -12.1799 | | -- |
| 24 | **12** | | | | | -10.2522 | | -- |
| 25 | **13** | 1847.1217 | 7526.01367 | 8595.5918 | 90 | 0.193427 | -7 | -3 |
| 26 | **13** | 2585.11621 | 3376.17432 | 3979.66846 | 74 | -2.728 | -8 | -15 |
| 27 | **14** | 1686.33386 | 8710.68066 | 7331.7832 | 90 | 2.98403 | 9 | 8 |
| 28 | **14** | 522.39066 | 2507.16138 | 2141.20483 | 90 | 2.84304 | 8 | 8 |
| 29 | **15** | 1186.92847 | 6809.07764 | 6128.55615 | 92 | 1.40974 | 5 | 2 |
| 30 | **15** | 1630.76294 | 6368.66406 | 5853.09277 | 88 | 2.13983 | 4 | 5 |
| 31 | **16** | 6562.52832 | 6295.271 | 5863.29932 | 65 | 1.58751 | 4 | 2 |
| 32 | **16** | 7407.20313 | 4236.146 | 3967.20459 | 53 | 1.05278 | 3 | 0 |
| 33 | **17** | 4187.6 | 6949.7 | 8158.93848 | 78 | -0.0534 | -8 | -4 |
| 34 | **17** | 51721.9 | 33069.2 | 41350.6 | 59 | -0.1377 | -11 | -5 |
| 35 | **18** | 10557.9 | 3957.06396 | 4484.05225 | 44 | -0.279876 | -6 | -5 |
| 36 | **18** | 11662.5 | 3375.17725 | 3756.25391 | 38 | -0.488357 | -5 | -6 |
| 37 | **19** | 10989.3 | 4628.3 | 4939.8 | 47 | 0.0878 | -3 | -4 |
| 38 | **20** | 13465.2 | 2441.2 | 2297.3 | 26 | 1.31206 | 3 | 1 |
| 39 | **20** | 30341.5 | 2418.6 | 2485.6 | 14 | 1.31949 | -1 | 1 |
| 40 | **21** | 2401.1 | 7962.3 | 9594.9 | 88 | -1.22352 | -9 | -9 |
| 41 | **21** | 3049.3 | 9782.5 | 11908.9 | 88 | -0.66669 | -10 | -7 |
| 42 | **22** | 2059.2 | 12942 | 12491.4 | 93 | 0.77786 | 2 | -1 |
| 43 | **22** | 6452.3 | 24974.2 | 24812.7 | 89 | 1.14464 | 0 | 1 |

[a] Raw integrations from HPLC of BV oxidation reaction extracts. [b] Determined from HPLC integrations. [c] Measured for samples of alcohols incorporated into zinc(II) complexes as described above. [d] Calculated using line equation from calibration curve shown in figure S8c.

### 4.3 Reaction Procedures

Preparation of cis -2,6-diphenylcyclohexanone:

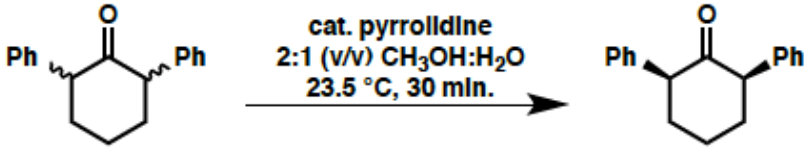


A mixture of the cis and trans isomers of 2,6-diphenylcyclohexanone (5.0 g, 20 mmol, 1.0 equiv.) was slurried in 150 mL 2:1 (v/v) $CH_3$ OH:$H_2$ O at 23.5 ºC (room temperature). 30 drops of pyrrolidine (quantity was adapted from the cited procedure in which stated 3 drops were added on a scale of 2.0 mmol ketone) was added from 12-gauge needle. The reaction was equipped with a water reflux condenser, heated, and held at reflux (oil bath temperature of ~95-105 ºC) for thirty minutes. The reaction was removed from heat and allowed to slowly cool to room temperature without stirring. Over this time a large quantity of colorless/pale yellow crystals (needles) formed. The flask was sealed with a septum at cooled for 12 hours in a 4 ºC refridgerator to maximize product crystallization. Crystals were isolated onto a filter paper in a porcelain Buchner funnel and washed with ~10 mL ice-cold 2:1 (v/v) $CH_3$ OH:$H_2$ O. Product was transferred to a tared vial and dried on high vacuum. 2.3072 g isolated, 46 % yield. $R_f$ (3:1 v/v pentane:$Et_2$ O) = 0.55 $^1$H NMR (600 MHz, $CDCl_3$ ): δ 7.32 (t, J = 7.5 Hz, 4H), 7.25 (t, J = 7.5 Hz, 2H), 7.18 (d, 7.2 Hz, 4H), 3.82 (dd, J = 5.4 Hz, 13.2 Hz, 2 H), 2.41 (m, 2 H), 2.16 (m, 3H), 2.09 (m, 1H). $^{13}$C NMR (150 MHz, $CDCl_3$ ): δ 208.3, 138.6, 128.9, 128.3, 127.0, 58.1, 36.5, 26.2. HRMS (Calculated/Found for $C_{18}H_{19}O_+$; [M+$H_+$]): 251.1436/251.1443. Crystallization: 4 mg cis -2,6-diphenylcyclohexanone was weighed into a 4 mL (1 dram) glass vial equipped with a Teflon-lined cap. 1 mL $H_2$ O was added to the vial and the mixture was heated to boiling with a heat gun. $CH_3$ OH was added drop-wise via Pasteur pipet until the sample became a homogenous solution. The vial was set on the bench-top and capped, vented only slightly

to air. Colorless needle-like crystals were observed within 18 hours of slow evaporation. HPLC trace (210 nm) for the product is shown below.

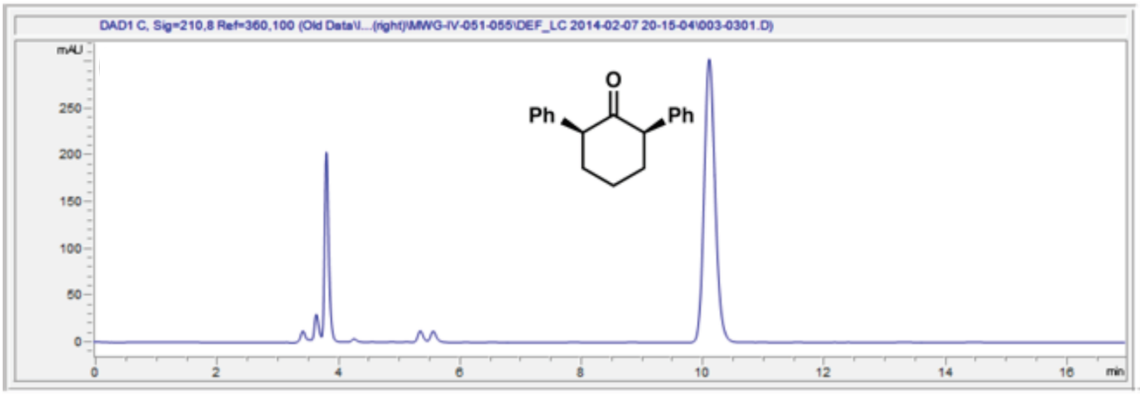

Procedure for peptide-catalyzed Baeyer-Villiger oxidation in solution (screening of hit peptides and focused library) and ring opening to secondary alcohol:

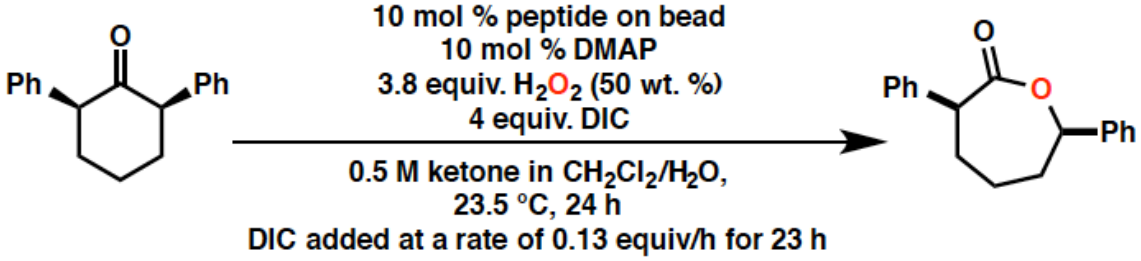


Peptide catalyst (0.03 mmol, 0.1 equiv.), cis-2,6-diphenylcyclohexanone (75 mg, 0.3 mmol, 1.0 equiv.) and DMAP (3.7 mg, 0.03 mmol, 0.1 equiv.) were weighed into a 4 mL vial equipped with a Teflon-coated magnetic stirbar. The mixture was dissolved in 0.6 mL CH2Cl2 and H2O2 was added (50 wt % (aq.); 64.8 μL, 1.14 mmol, 3.8 equiv.). The vials were sealed with Teflon tape and septum caps and stirred at 23.5 ºC (room temperature). DIC (135 μL, 0.9 mmol, 3.0 equiv.) was added via syringe pump at a rate of 0.13 equiv. per hour (5.9 μL/h) over a period of 23 hours. The reactions were stirred one hour past this time for a total reaction time of 24 hours, over which time white precipitate formed.

Quench and workup: Reactions were quenched with 200 μL saturated aqueous Na2SO3. The mixtures were transferred to a separatory funnel quantitatively by rinsing several times with a total volume of 10 mL ethyl acetate (EtOAC). The mixture was diluted to a total volume of 30 mL with EtOAc and washed twice each (15 mL each wash) with saturated aqueous Na2SO3 and saturated aqueous NaHCO3. The organic layer was dried over Na2SO4, filtered, and sampled for HPLC analysis (~100 μL from the worked up solution).

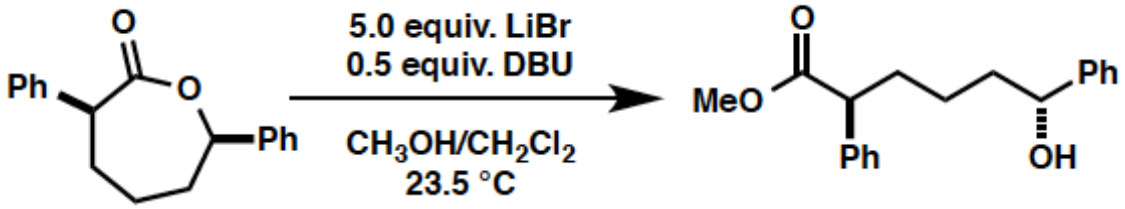


Lactone opening: The worked up reactions were concentrated to afford a solid white residue by rotovap. This residue was pushed through a plug of 10-15 mL (dry volume) silica in a 2.5 cm diameter column that was packed with 3:1 (v/v) Pentane:$Et_2O$. Ketone/lactone mixtures were fully eluted with a total volume for 150-175 mL 3:1 (v/v) Pentane:$Et_2$ O. The plug was necessary to remove peptide, DMAP, and DIC-related reaction byproducts that could coordinate and potentially interfere with the CD assay. We note that ketones and esters do not interfere with the assay, which is designed specifically for alcohol functional groups. The eluent was concentrated, transferred to a 24 mL glass vial, and full concentrated to a white residue. The residue was rinsed into the bottom of the vial with 2-3 mL with $CH_2$ $Cl_2$ and allowed to evaporate to dryness in the fume hood. This step was necessary as in the course of our study we discovered that the racemate of the lactone product was substantially less soluble than the enriched material. If all solid was not dissolved in the ring-opening step, the information obtained by either HPLC or the CD assay led to falsely high ee values. The dried residue was then ring opened (we note that other common lactone-opening methods led to full or partial epimerization of the C2 stereocenter, confounding the analysis of our data.). According to a modification of the procedure of Seebach, a solution in $CH_3OH$ of 0.1 M DBU (1,8-Diazabicyclo[5.4.0]undec-7-ene) and 1.0 M LiBr was prepared in a volumetric flask. An aliquot of this solution was added to lactone sample to afford a reaction mixture that was 0.2 M in lactone (1.0 equiv.), 0.1 M in DBU (0.5 equiv.), and 1.0 M in LiBr (5.0 equiv.). The mixture was sonicated for

1 minute and then stirred for 30 minutes at room temperature with occasional sonication to break up agglomerated solids. At 30 minutes, 1-2 mL $CH_2Cl_2$ was added to the mixture and the reaction was stirred 15 minutes further over which time all solids dissolved. The reaction was quenched with 1 mL of 1 N HCl (aq.). 1 mL brine was added and the mixture was extracted three times with 3 mL (each extract) $CH_2Cl_2$. Extracts were passed through a Pasteur pipet filter containing silica and $Na_2SO_4$ into a 24 mL glass vial. Solvent was removed via rotovap and the remaining residue for the calibration curve samples was analyzed by HLPC. All samples were dried on high-vacuum and then evaluated in the CD assay for ee.

HPLC Sample preparation: < 1 mg of each ring-opened product mixture was dissolved in~250 mL o f 15% (v/v) EtOH in Hexanes. Samples were analyzed on a Chiralcel OD-H column, eluting with 3 % (v/v) EtOH in Hexanes at a flowrate of 1 mL/min. at ambient temperature.

## 5. REFERENCE


1) Yoon, T. P.; Jacobsen, E. N.; *Science*, **2003**, *299*, 1691-1693.
2) (a) Baeyer, A.; Villiger, V. *Chem. Ber*. **1899**, *32*, 3625-3633. (b) Krow, G. R. *Org. React.* **1993**, 43, 251-798. (c) ten Brink, G. J.; Arends, I. W. C. E.; Sheldon, R. A. *Chem. Rev*. **2004**, *104*, 4105-4124. (d) Uyanik, M.; Ishihara, K. *ACS Catal*. **2013**, *3*, 513-520. Key mechanistic studies: (e) Doering, W. von E.; Dorfman, E. *J. Am. Chem. Soc*. **1953**, *75*, 5595-5598. (f) Goodman, R. M.; Kishi, Y. *J. Am. Chem. Soc*. **1998**, *120*, 9392-9393. (g) Crudden, C. M.; Chem, A. C.; Calhoun, L. A. *Angew. Chem., Int. Ed*. **2000**, *39*, 2851-2855.
3) Recent review: (a) Ito, K. in *Comprehensive Chirality*, Carreira, E. M.; Yamamoto, H. Eds. **2012**, *5*, 1-35. Selected examples: (b) Gusso, A.; Baccin, C.; Pinaa, F.;

Strukul, G. *Organometallics*, **1994**, *13*, 3442-3451. (c) Bolm, C.; Schlingloff, G.; Weickhardt, K. *Angew. Chem., Int. Ed.* **1994**, *33*, 1848-1849. (d) Murahashi, S.-I.; Ono, S.; Imada, Y. *Angew. Chem., Int. Ed.* **2002**, *41*, 2366-2368. (e) Watanabe, A.; Uchida, T.; Irie, R.; Katsuki, T. *Proc. Nat. Acad. Sci.* **2004**, *101*, 5737-5742. (f) Xu, S.; Wang, Z.; Zhang, X.; Zhang, X.; Ding, K. *Angew. Chem., Int. Ed.* **2008**, *47*, 2840-2843. (g) Xu, S.; Wang, Z.; Li, Y.; Zhang, X.; Wang , H.; Ding, K. *Chem. Eur. J.* **2010**, *16*, 3021-3035. (h) Reetz, M. T.; Wu, S. *J. Am. Chem. Soc.* **2009**, *131*, 15424-15432. (i) Zhou, L.; Liu, X.; Ji, J.; Zhang, Y.; Hu, X.; Lin, L.; Feng, X. *J. Am. Chem. Soc.* **2012**, *134*, 17023-17026.

4) a) Lichtor, P. A.; Miller, S. J. *ACS Comb. Sci.* **2011**, *13*, 321-326. (b) Lichtor, P. A.; Miller, S. J. *Nat. Chem.* **2012**, *4*, 990-995. (c) Lichtor, P. A.; Miller, S. J. *J. Am. Chem. Soc.* **2014**, *136*, 5301-5308. (d) Abascal, N. C.; Lichtor, P. A.; Giuliano, M. W.; Miller, S. J. *Chem. Sci.* **2014**, *5*, 4504-4511.

5) (a) Peris, G.; Jakobsche, C. E.; Miller, S. J. *J. Am. Chem. Soc.* **2007**, *129*, 8710-8711. (b) Jakobsche, C. E.; Peris, G.; Miller, S. J. *Angew. Chem., Int. Ed.* **2008**, *47*, 6707-6711.

6) (a) Peris, G.; Miller, S. J. *Org. Lett.* **2008**, *10*, 3049-3052. (b) Romney, D. K.; Colvin, S. M.; Miller, S. J. *J. Am. Chem. Soc.* **2014**, *136*, 14019-14022.

7) Hoveyda, A. H.; Evans, D. A.; Fu, G. C. *Chem. Rev.* **1993**, *93*, 1307-1370.

8) (a) You, L.; Berman, J. S.; Anslyn, E. V. *Nat. Chem.* **2011**, *3*, 943-948. (b) You, L.; Pescitelli, G.; Anslyn, E. V.; Di Bari, L. *J. Am. Chem. Soc.* **2012**, *134*, 7117-7125. (c) You, L.; Berman, J. S.; Lucksanawichien, A.; Anslyn ,E. V. *J. Am. Chem. Soc.* **2012**, *134*, 7126-7134.

9) Metola, P.; Nichols, P.M.; Khar, B.; Anslyn, E. V. *Chem. Sci.* **2014**, *5*, 4278-4282.

10) (a) Watson, J. D.; Milner-White, E. J. *J. Mol. Biol.* **2002**, *315*, 171-182. (b) Denessiouk, K. A.; Johnson, M.S.; Denesyuk, A.I. *J. Mol. Biol.* **2005**, *345*, 611-629. (c) Sheet, T.; Supakar, S.; Banerjee, R. *PLoS One*, **2013**, *8*, e57366.

11) Tam, J. P.; Riemen, M. W.; Merrifield, R.B. *Pept. Res.* **1988**, *1*, 6-18.

12) Seebach, D.; Thaler, A.; Blaser, D.; Ko, S. Y. *Helv. Chim. Acta*, **1991**, *74*, 1102-1118.

13) (a) Polyak, I.; Reetz, M. T.; Thiel, W. *J. Am. Chem. Soc.* **2012**, *134*, 2732-2741. (b) Orru, R.; Dudek, H.; Martinoli, C.; Torres Pazmiño, D. E.; Royant, A.; Weik, M.; Fraaije, M. W.; Mattevi, A. *J. Biol. Chem.* **2011**, *286*, 29284-29291. (c) Walsh, C. T.; Chen, Y.-C. J. *Angew. Chem., Int. Ed.* **1988**, *27*, 333-343.

# Chapter 3[3]

## 1. Introduction

The rapid determination of absolute configuration and enantiomeric excess (ee) for chiral molecules has been a bottleneck for high-throughput screening (HTS) of chiral catalysts.[1] Currently, the most commonly used methods for enantiomeric excess determination are high performance liquid chromatography (HPLC) and supercritical fluid chromatography, both using chiral stationary phases.[2–4] Although chiral chromatographic methods are often highly accurate, with error averaging around ±1% for rigorously optimized cases, the major drawback of these methods is their speed and cost.[5] Techniques such as serial injection and multiplexing have significantly improved the analysis time[6–8], but they require additional instrumentation. Subsequently, a wide variety of methods that utilize alternative protocols amenable to HTS are being developed.[9–18]

Sensors based on optical spectroscopic techniques are attractive due to their short analysis time and low cost. For example, various stereodynamic systems that utilize circular dichroism (CD) for ee determination have been published.[12,13,17] Recently, our group developed a chiral alcohol sensor involving a multicomponent assembly that incorporates the alcohol into a hemiaminal ether (1) under equilibrium conditions[13–15] (Scheme 3.1). The incorporation of a chiral alcohol influences the trispyridyl ligand helicity of 1. Because the enantiomers of the alcohol induce opposite twists, their inverse exciton coupled CD (ECCD) spectra enable absolute configuration designation. Furthermore, a calibration curve of this multicomponent assembly determined ee with average ±3% absolute error.

---

[3] This Chapter is adopted from the published article by Lin, C.-Y.; Giuliano, M. W.; Ellis, B. D.; Scott, M. J.; Anslyn, E. V. *Chem. Sci.*, **2016**, DOI: 10.1039/c5sc04629g. In this paper, Giuliano provided secondary chiral alcohol samples while Lin conducted the experiments.

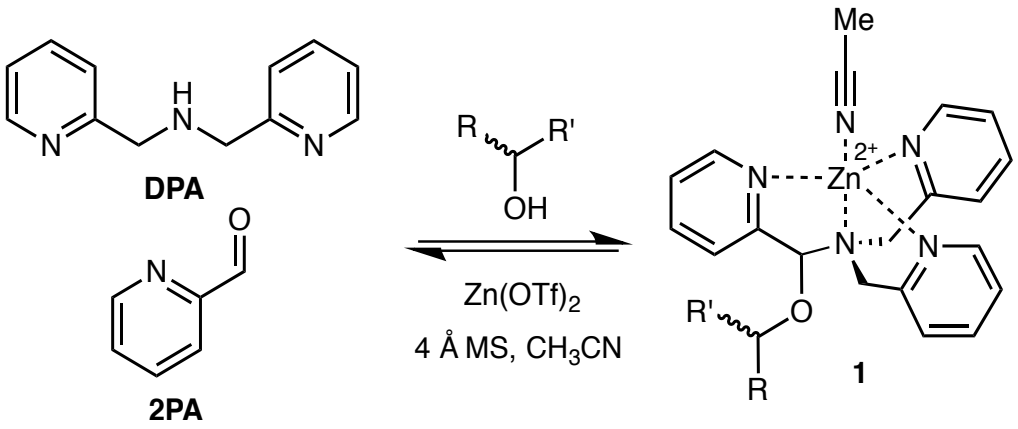


**Scheme 3.1** Multicomponent hemiaminal ether assembly (**1**), formation from 2-pyridinecarbaldehyde (**2PA**), di(picolyl)amine (**DPA**), $Zn^{2+}$, molecular sieves (3Å), and a chiral alcohol analyte.

With the success of multicomponent assembly 1, we turned our attention to improve the analytical power of the technique. One major limitation of this original assembly was a low CD intensity for chiral alcohols with similar sized substituents at the stereocenter. When an alcohol substrate has similar substituents, a slight preference toward one tris-pyridyl helicity is observed, which results in a small dynamic range for the CD ellipticities and an increased error in ee determination. To counter this problem, we investigated the effect of 3- and 6- substituents on the heterocyclic ligand 2PA. Given the tripodal geometry of the assembled complex 1, it was hypothesized that, due to proximity to the hemiaminal ether, altering the 3- position substituent (Scheme 3.2, Z) would enhance the assembly sensitivity to the differences in the steric size of the alcohol substrates, thereby increasing the diastereomeric ratio (dr) values. Additionally, the 6-substitution (Scheme 3.2, Y) was expected to similarly alter the dr values due to different interactions with the axial metal ligand (L). Because we have previously found that larger dr values result in larger CD signals and lower errors in ee determination,[13-15] the goal of our substitutent effect studies was to enhance the dr's.

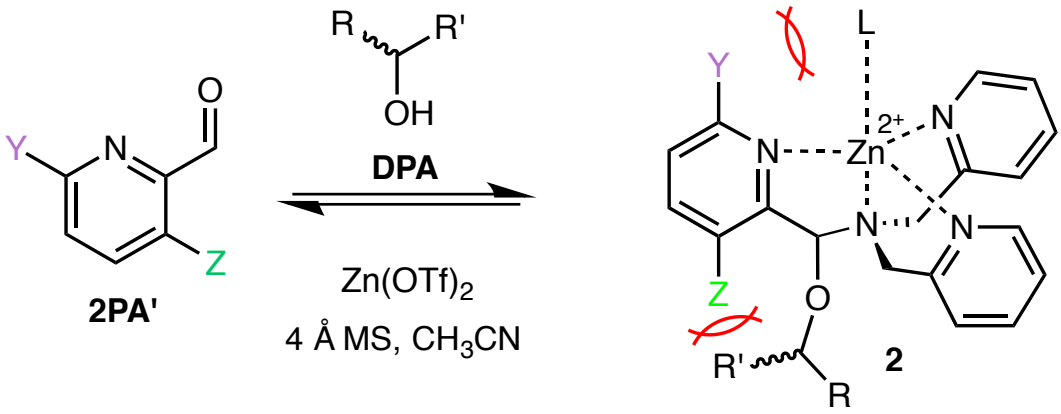


**Scheme 3.2** 3- or 6- substituted **2PA** (shown as **2PA'**) were hypothesized to alter the multicomponent assembly (**2**) differently leading to altered *dr* and CD. The 3- substituent (represented by **Z**) introduces steric bulk proximal to the alcohol substrate while the 6- substituent (**Y**) interacts with the axial metal ligand **L**.

## 2. Results and Discussion

### 2.1 Substituent Effects Studies

The effects of 3- and 6- substituents were examined in assemblies formed with different 2PA derivatives (2PA'). The conditions for assembly formation followed closely that of the previously published protocol.13 Each 2PA' (1 equiv. at 35mM) was mixed with DPA (1.2 equiv.), followed by addition of $Zn(OTf)_2$ (1 equiv.), molecular sieves (3 Å), and 4-(2-chloroethyl)morpholine HCl (1 equiv.) in acetonitrile at 35 mM. (R)-1-Phenylethanol (3 equiv.) was used as the standard analyte. Rather than 18 hours at room temperature equilibration as previously reported, it was found that incubating the assembly for 1 hour at 40 °C yielded the same result. Thus, all the multicomponent assembly experiments described herein presumed to reach equilibrium in this manner.

Each new assembly was characterized by $^1$H NMR and CD (see Characterization section). Additionally, dr's and yields of the assemblies were calculated by $^1$H NMR. Assembly 2 exists as diastereomers, and the dr value is defined as the ratio of the major and minor diastereomer at equilibrium, while the yield is defined as the extent of formation of 2 (Figure 3.1). To calculate the yield, The proton peaks of interest are identified, integrated, then used to calculate the yield. Using the following 1H NMR spectrum as an example, the aldehyde (10.2 ppm), hemiaminal methine (6.1 ppm), and hemiaminal ether diastereomeric methines (5.9 ppm and 6.3 ppm) were identified and integrated. The integrated values are used to calculate the yield (Figure 3.1).

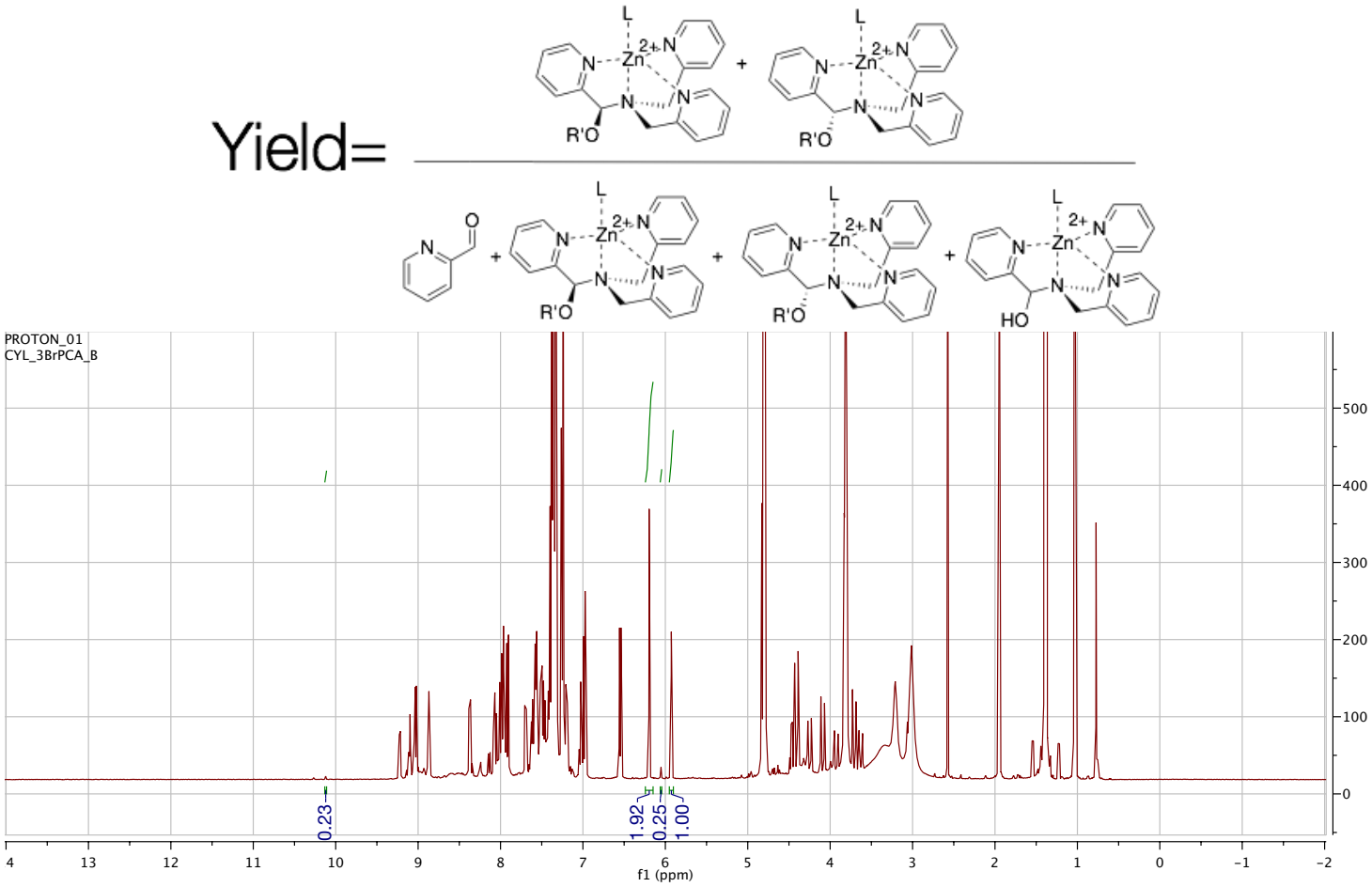


**Figure 3.1** Example proton spectrum and formula for calculating the yield of assembly formation.

Note, the yield here is not isolated yield but rather a measure of thermodynamic preference for the hemiaminal ether assemblies. Systematic examination of CD, yield, and dr values allowed us to gain insights on the properties of these multicomponent assemblies. While CD is the ultimate signal response of interest for ee determination, the assembly yield represents a measure of the relative thermodynamic preference for formation of the hemiaminal ether complexes, while the dr value provides information on the relative stabilities of the two diastereomers formed in each assembly.

The assembly yield and dr values are shown in Table 3.1. Low extents of assembly formation (<5%) were observed for quinoline-2-carbaldehyde (QA) and phenanthridine-6-carbaldehyde (PNA). The lack of complex formation was attributed to the aromatic hydrogen blocking the coordination of the Zn metal (Scheme 3.3). Although this is a thermodynamic issue inhibiting assembly, it is in accord with our recent finding of the involvement of Zn(II) in the rate determining step of assembly formation.[19] In the instance of no such proton obstruction, the assembly formed with isoquinoline-1-carbaldehyde (IQA) and exhibited similar CD, dr, and yield as 2PA. However, due to the comparable or lower performances of these ligands, we turned our attention to non-benzofused substituents.

| Code | Substituent | **2PA$^3$** assembly | | **2PA$^6$** assembly | |
|---|---|---|---|---|---|
| | | Yield | *dr* | Yield | *dr* |
| **2PA'$^F$** | F | 87% | 1.51 | 73% | 1.45 |
| **2PA'$^{Cl}$** | Cl | 87% | 1.62 | 58% | 1.71 |
| **2PA'$^{Br}$** | Br | 86% | 1.92 | 52% | 1.61 |
| **2PA'$^{MeO}$** | MeO | 96% | 1.41 | 52% | 1.89 |
| **2PA'$^{Me}$** | Me | 97% | 2.01 | 83% | 2.28 |
| **2PA** | H | 83% | 1.41 | 83% | 1.41 |
| **IQA** | 3,4-benzo | 79% | 1.45 | n/a | n/a |
| **QA** | 5,6-benzo | <5% | n/a | n/a | n/a |
| **PNA** | dibenzo | <5% | n/a | n/a | n/a |

**Table 3.1** Multicomponent assembly hemiaminal ether yield and *dr* formed with various pyridine carbaldehyde derivatives (**2PA$^3$**, **2PA$^6$**, **IQA**, **QA**, **2PA**, and **PNA**) and 1-phenylethanol. *The 3 and 6 subscribes designate the regiochemistry of **PA** substitution.

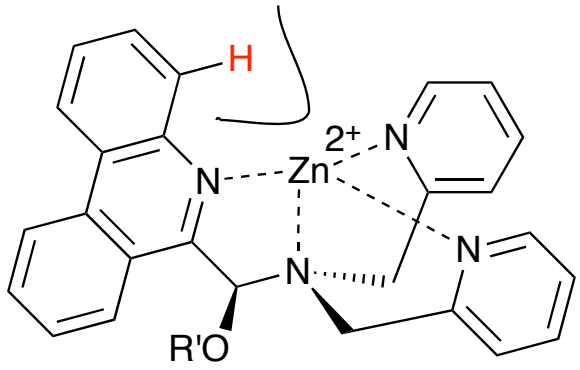


**Scheme 3.3** The unfavorable positioning of aromatic hydrogen for 5, 6-benzo fused ligands (PNA shown above) resulted in the lack of assembly formation. The axial metal ligand was omitted for clarity.

All of the non-benzofused ligands (Table 3.1) formed the multicomponent assembly. However, the assemblies formed with 3-substituted ligands ($2PA^3$) consistently outperform in yield their 6-substituted counterparts ($2PA^6$). This discrepancy potentially carries the same explanation for why QA and PNA give poor yields; an alteration at the 6 position introduces steric bulk that hinders Zn(II) coordination.

To further understand the nature of these substituent effects, the observed assembly dr was correlated with linear free energy relationships (LFERs) (Figure 3.2). Because the interaction between ligands $2PA^6$ and L resembles the 1,3-diaxial interaction of substituted cyclohexanes,[20] A-values were used as the corresponding substituent parameter (Figure 3.2 a). A linear correlation ($R^2$=0.95, slope = 0.12) was observed between log(dr) and A-values. The strong linearity affirms that the assembly responds to changes in substituent in the same manner as the cyclohexane system, but that the assembly is 12% as sensitive as cyclohexane to substituent changes. Similarly, $2PA^3$ correlated linearly (R2=0.86, slope = -0.13) with Taft steric parameters (Figure 2.3b) with approximately 13% the sensitivity as the substituent changes with respect to the reference reaction. These linear correlations with two different steric LFERs affirmed our hypothesis that there are two different modes of steric effects in the multicomponent assembly.

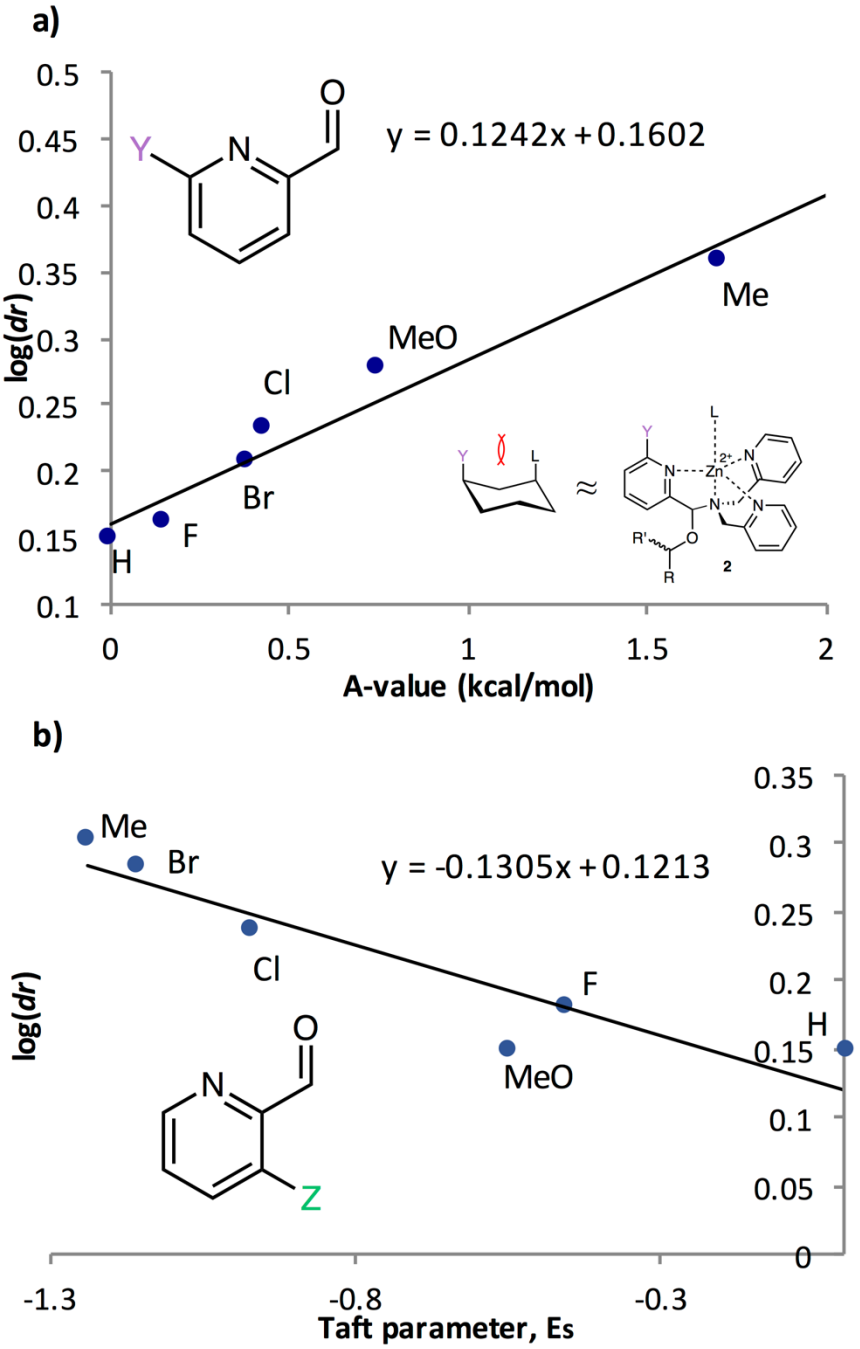


**Figure 3.2** Linear plots showing log(*dr*) values for assemblies involving **a**) 6-substituted pyridine-2-carbaldehydes plotted against A-values corresponding to the substituents, and **b**) 3-substituted pyridine-2-carbaldehydes plotted against corresponding Taft steric parameters.

## 2.2 LEFRs Analyses

Following the substituent effect studies, 3-methylpyridine-2-carbaldehyde ($2PA^{3Me}$) was the ligand that most significantly improved the assembly dr (Scheme 3.4), with bromide as a close second ($2PA^{3Br}$). Thus, we expected the CD signals for assemblies using 3-Me and 2-Br to be similar. However, broadening of the ECCD signal was observed with Br due to the nature of exciton coupling, where the signal originates from the coupling of excited chromophores. When the chromophores participating in ECCD are identical, a sharp couplet is observed. If the three participating pyridyl chromophores do not share identical absorbance spectrum, a broadening in the ECCD signal is observed[21] (see Characterization section), as is evident for Br substitution. However, methyl does not alter the absorbance of pyridine significantly, and therefore the ECCD remains sharp. Efforts to form the assembly with matching di- and tri- substituted bis-3-methyl and bis-3-bromo DPA-like ligands were unsuccessful, likely due to steric limitations (Scheme 3.5).

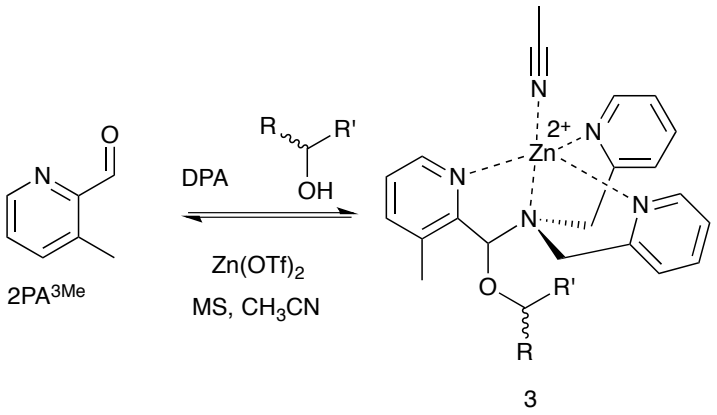


**Scheme 3.4** Multicomponent assembly **3** formed with ligand **$2PA^{3Me}$**, **DPA**, $Zn(OTf)_2$, and chiral alcohol following the same protocol as reported above.

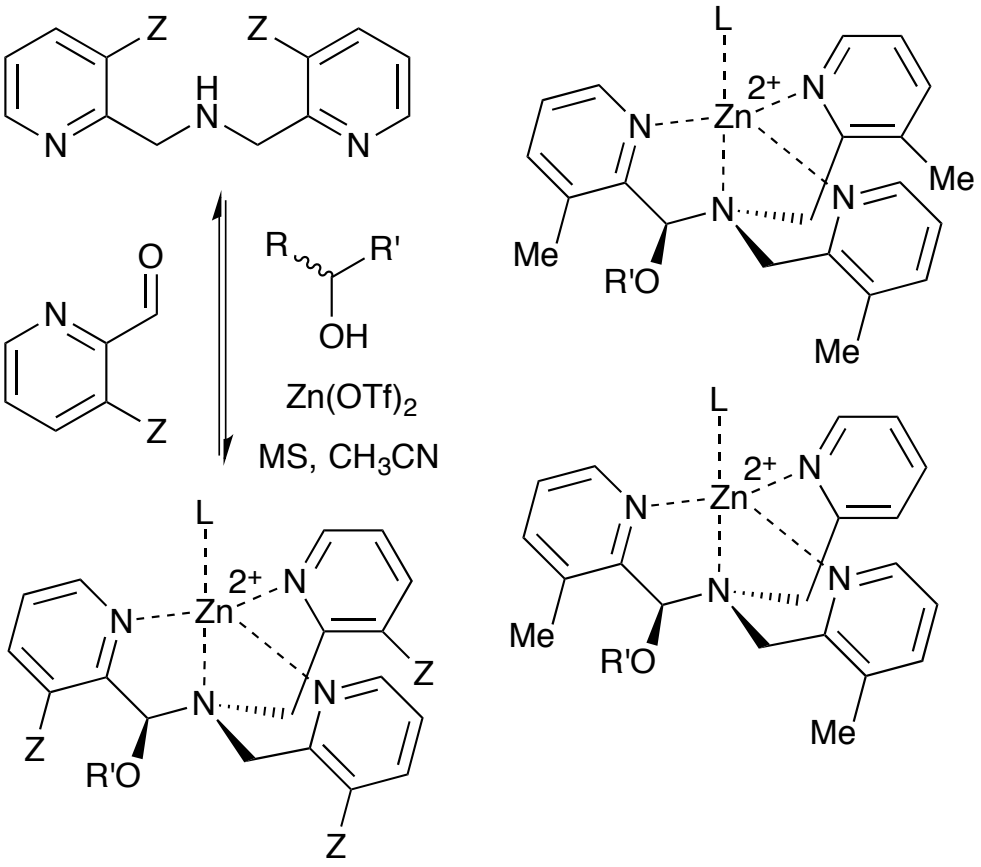


**Scheme 3.5** Lack of assembly formation was observed when attempted with di- or tri- substituted ligands. Methyl substituted variants are shown above.

## 2.3 Linear Model for CD Correlation

In an effort to extend the utility of assembly 3, a model was developed to correlate the ECCD signal and dr values to the steric size of the groups on the stereocenter of chiral alcohols. Six alcohols were chosen to cover aromatic, cyclic aliphatic, linear alkyl, and branched alkyl side chains (Scheme 3.6). First, it should be noted that the CD signal for the assembly has an inherent maximum, because the pyridine rings in 3 can twist only to a certain extent before the ligand no longer binds Zn(II) and the complex disassembles. Therefore, the magnitude of the CD does not correlate to dr value linearly, but rather by a half sigmoid (Figure 3.3). That is, the CD intensity approaches a maximum asymptote as the dr value approaches infinity, and conversely, as the dr approaches one, the signal drops to zero. Given this logic, Eq. 1 was developed where ΔCD is the difference between CD signals at 270 nm for enantiopure R and S samples of the chiral alcohols and CDmax is the theoretical CD maximum of an assembly.[15] For all the alcohol samples, dr values were plotted against ΔCD ($R^2$=0.86, Figure 3.4). The plot predicts a maximum CD of 186.6 mdeg, for 3, which is significantly higher than the reported maximum CD for the original assembly 1 (113.5 mdeg).

$$\frac{\Delta CD}{2CD_{\max}} = 1 - \frac{2}{1 + d.r.} \quad (1)$$

Once a linear relationship between dr and CD had been established, we turned our attention to correlate alcohol sterics to their corresponding assembly dr value. Charton parameters were used to calculate the absolute value of the difference in the size of the non-hydrogen substituents (Δv) on the stereogenic α-carbon of each alcohol (Table 3.2)[22].

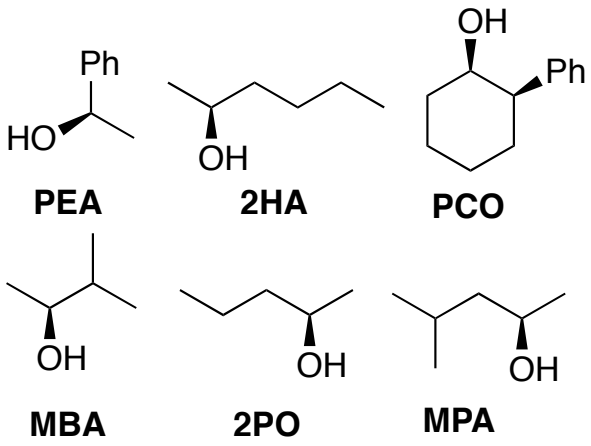


**Scheme 3.6** The alcohols used in the correlating alcohol steric size to their corresponding CD signal.

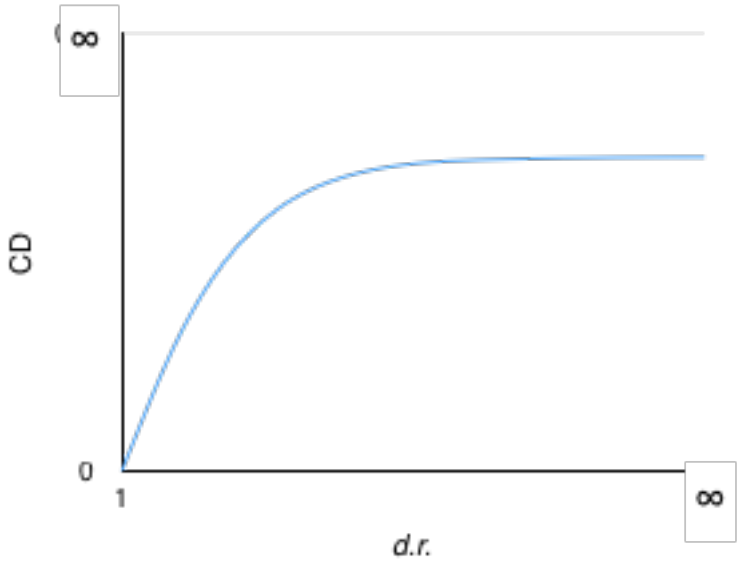


**Figure 3.3** Theoretical relationship between the assembly dr value and CD signals.

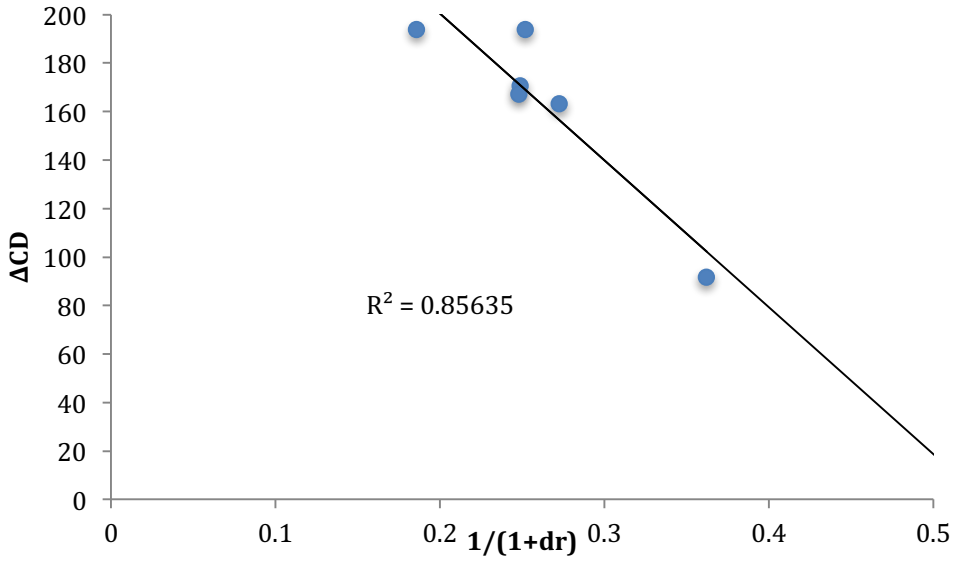


**Figure 3.4** The alcohol *dr* value was correlated to their enantiopure sample CD value at 270 nm using assembly **3**.

| Alcohol | $\Delta v$ | dr |
|---|---|---|
| PCO | 0.57 | 3.02 |
| MPA | 0.46 | 4.38 |
| 2HA | 0.16 | 2.97 |
| 2PA | 0.16 | 2.67 |
| PEA | 0.05 | 2.01 |
| MBA | 0.24 | 3.03 |

**Table 3.2** The difference in substituent Charton parameter ($\Delta v$) and their corresponding hemiaminal ether *dr* value for **3**.

A poor linear correlation ($R^2$=0.49) between Δv and log(dr) of the alcohols was observed, caused by inaccurate estimation in Δv for PCO and 2HA. For the conformationally restricted PCO, considering only the 2 and 6 position substituents significantly overestimates Δv versus the higher degree of freedom alkyl chains. In the case of 2HA, Charton parameters predict the linear butyl substituent to be the same size as the linear propyl substituent (same value for n-propyl and n-butyl), resulting in 2HA having the same Δv as 2PO. This results in an underestimation of Δv for 2HA. Dramatic improvement in the correlation ($R^2$=0.93, Figure 3.5) was observed once PCO (red square in Figure 3.5) was removed from the data set, while removing 2HA (green diamond) from the set further improved the correlation ($R^2$=0.99).

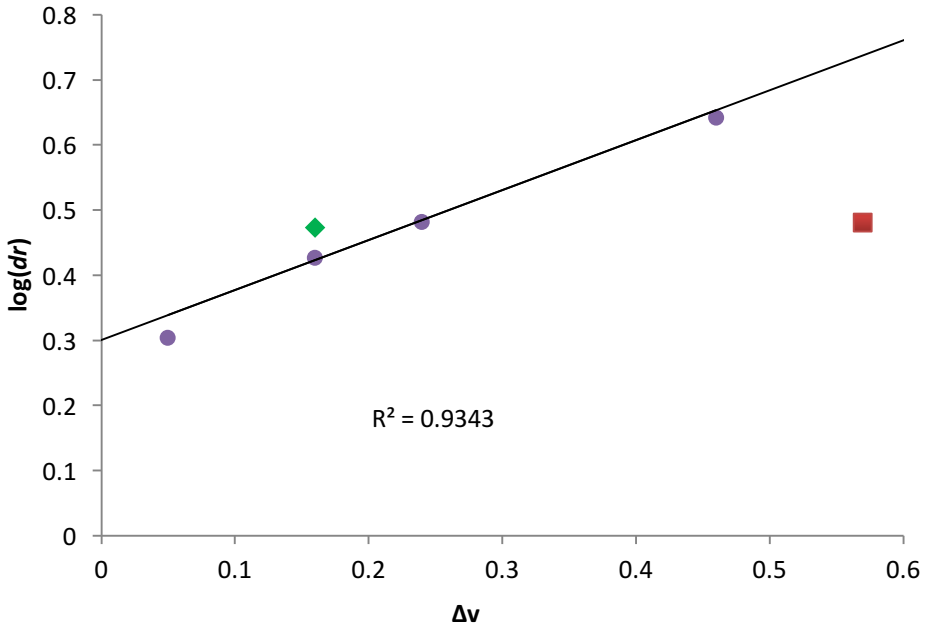


**Figure 3.5** Linear correlation was established between the alcohol substituent Charton parameters (*Δv*) and their corresponding log(*dr*) value.

Examining the LFERs involving correlations of phenyl steric size versus other substituents on the stereocenter of the alcohol pointed to a curious difference between assemblies 1 and 3. There are two reported steric values for phenyl. The larger Charton valve of v=1.73, pertaining to a freely rotating phenyl, was previously applied to the analysis of assembly 1.[13-15] However, we found that the pyridinyl methyl group in 3 restricts the rotation of the β-phenyl substituents on the alcohol substrates. Therefore, the smaller phenyl Charton parameter, v= 0.57, gave a better linear fit to the data in Figure 3.5. This smaller steric value describes interactions with a rotationally restricted phenyl ring, such that only one face of the ring is presented to the reactant. Thus, while the original assembly 1 exhibits free rotation of the phenyl group, the congested environment of assembly 3 forces the phenyl substituent to adopt a conformation with minimal steric interactions (Figure 3.6 and Scheme 3.7).

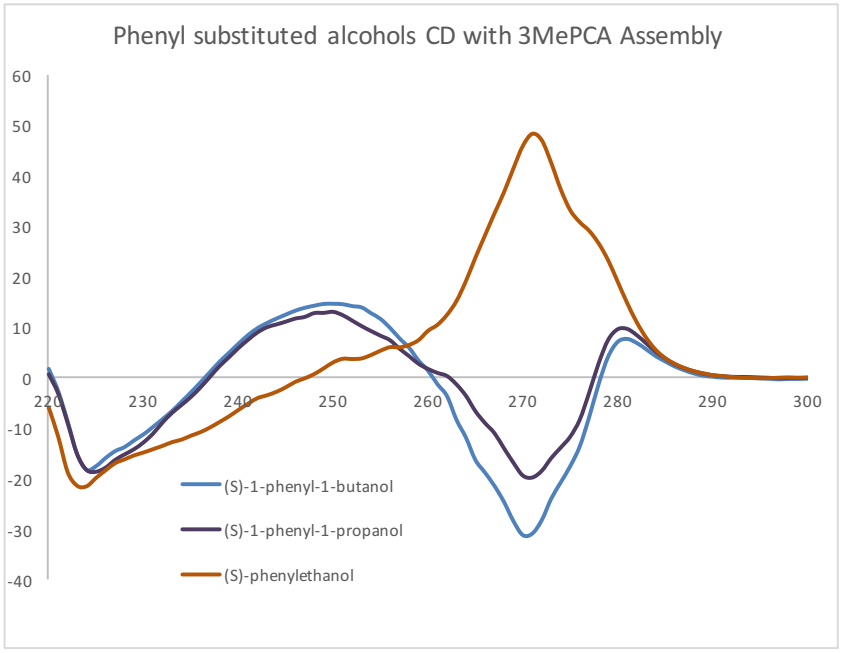


**Figure 3.6** CD spectra of 3MePA with various enantiopure (S)-1-phenyl alcohols. As the alkyl chain grows, the assembly Cotton effect grows in opposite direction indicating the phenyl group size is between a methyl and ethyl substituent.

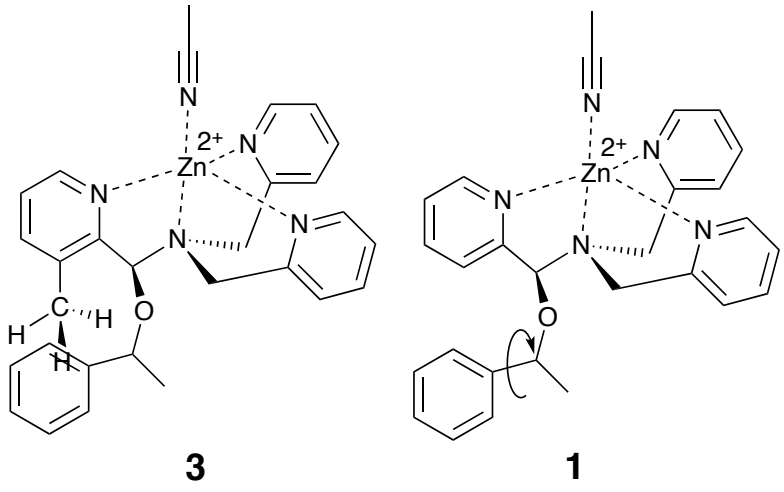


**Scheme 3.7** Proposed origin of context dependent steric size. Assembly **3**, with an additional proximal methyl group, hinders the alcohol phenyl substituent rotation.

This change in the perceived steric size of a phenyl ring for different assemblies had a further ramification when studying a chiral alcohol we had previously analysed with assembly 1. In recent studies, we had measured the ee values of several catalysts for an asymmetric Baeyer-Villager reaction, that after lactone hydrolysis, led to a 1-phenyl substituted alcohol (DPHA, Figure 3.7).[23] An opposite Cotton effect in the CD spectra of assembly 3 was observed for the same enantioenriched sample of DPHA as that for assembly 1 (Figure 3.7). While initially puzzling, further investigation revealed that assembly 3 recognizes a phenyl group sterically as between a methyl (v=0.52) and an ethyl (v=0.56) group. Assembly 3 reverses the helical twist of the pyridine rings when a methyl is changed to an ethyl in a 1-phenyl alkanol chain (Scheme 3.7). Further increase in the chain length continues to increase the magnitude of the CD values, but still with a negative Cotton effect for assembly 3. This effect is evident even though the Charton parameter for phenyl is similar to ethyl (0.57 vs. 0.56). Thus, we find another example that steric size is context dependent, and the Charton parameters do not perfectly predict the size differences of the groups on the stereocenters of the chiral secondary alcohols within the context of 3. In fact, a closer examination of phenyl substituted alcohols in the linear model leads to similar conclusion (Figure 3.5, shown in blue).

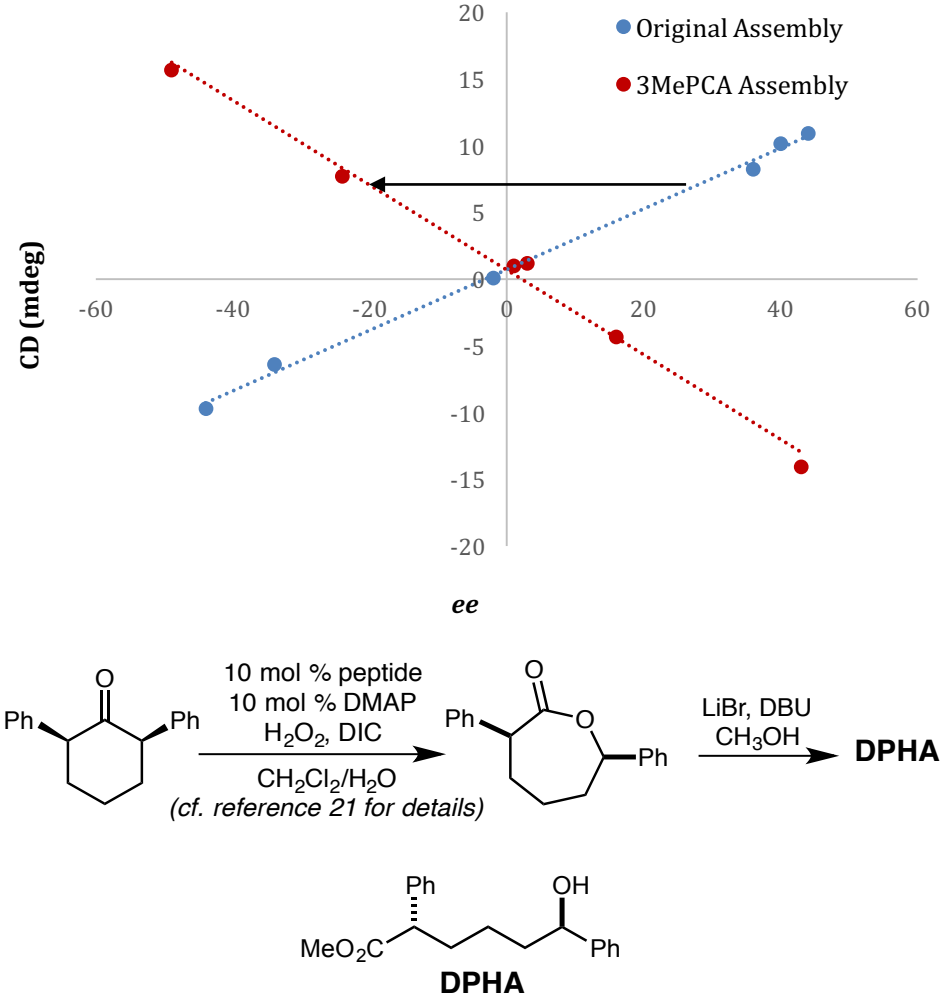


**Figure 3.7** Calibration curves of the previously published alcohol analyte with assemblies **3** and **1,** $R^2 = 0.99$[21]. The assembly was formed at 35 mM (with 3 equiv. excess of alcohol), and CD at 270 nm was taken with a 175 μM assembly solution in MeCN. The **slope** of the calibration curve for **3** flipped in comparison to that for **1**.

## 2.4 Dynamic Range Comparison with 2PA Assembly

After developing models that correlate analyte steric size to their corresponding ECCD signals in assembly 3, we shifted our focus to demonstrate the enhanced dynamic range for ee determination and the corresponding lowering of the error, as was the initial goal of the project. Calibration curves were constructed for alcohols 2OA and 2BA using assembly 3 (Figure 3.8 and 3.9). The results were compared to the original assembly calibration curve (R2=0.99 for all assemblies, Figure 3.10). The values of ee ranged from 100% (100% (R)-enantiomer) to -100% (100% (S)-enantiomer), and were plotted against the signal observed at 270 nm. The optical response to ee using assembly 3 is about 3-4 times as large to that using assembly 1. The 2OA calibration curve for assembly 3 was used to calculate the ee of three blind samples, and the average absolute error was found to be 1.7%. This improvement in error over 1 results from the enhanced dynamic range of 3.

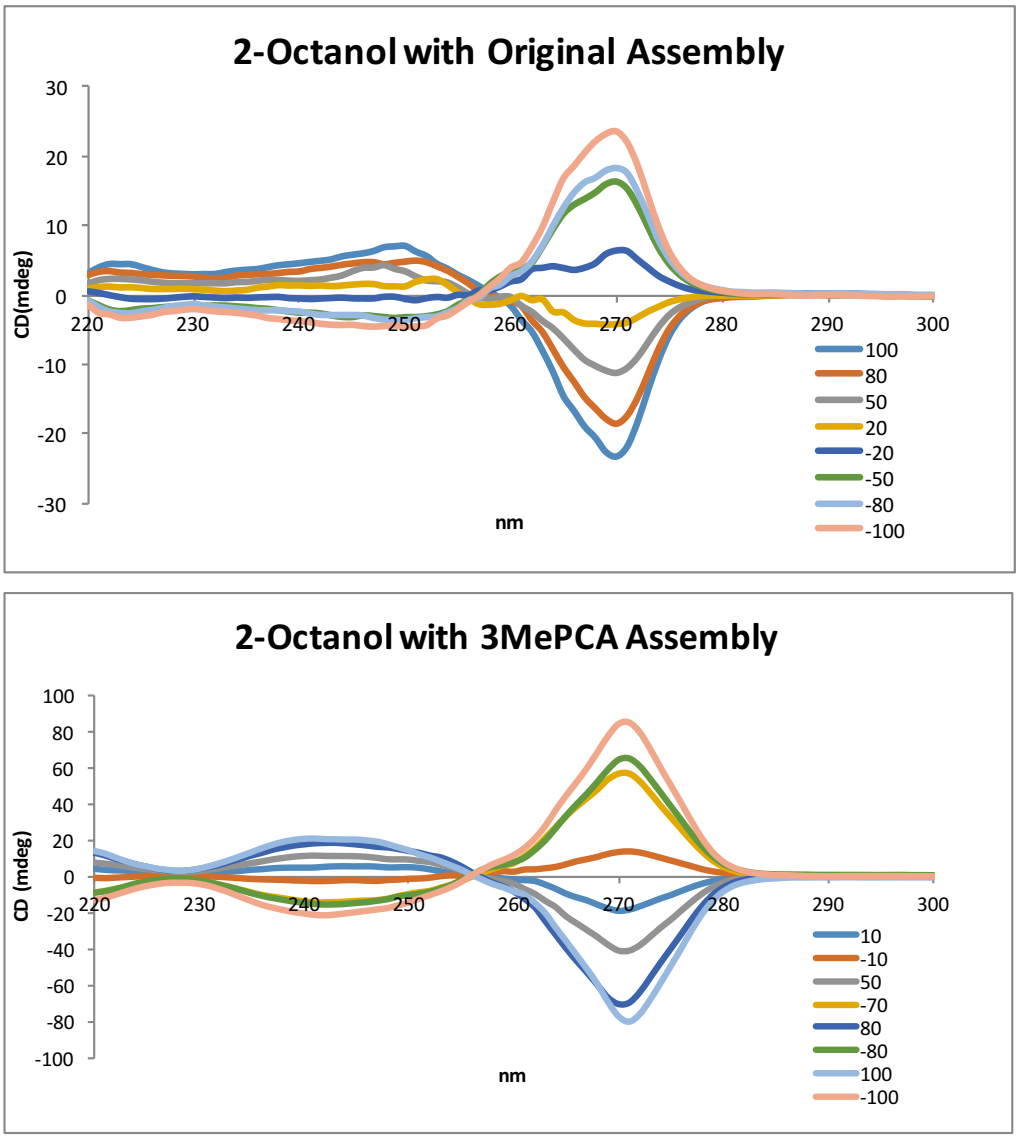


**Figure 3.8** CD spectra of the original assembly and the 2PA$^{3Me}$ assembly with 2-octanol. The assembly was formed at 50 mM and the CD spectra was taken following the procedure described in the main text.

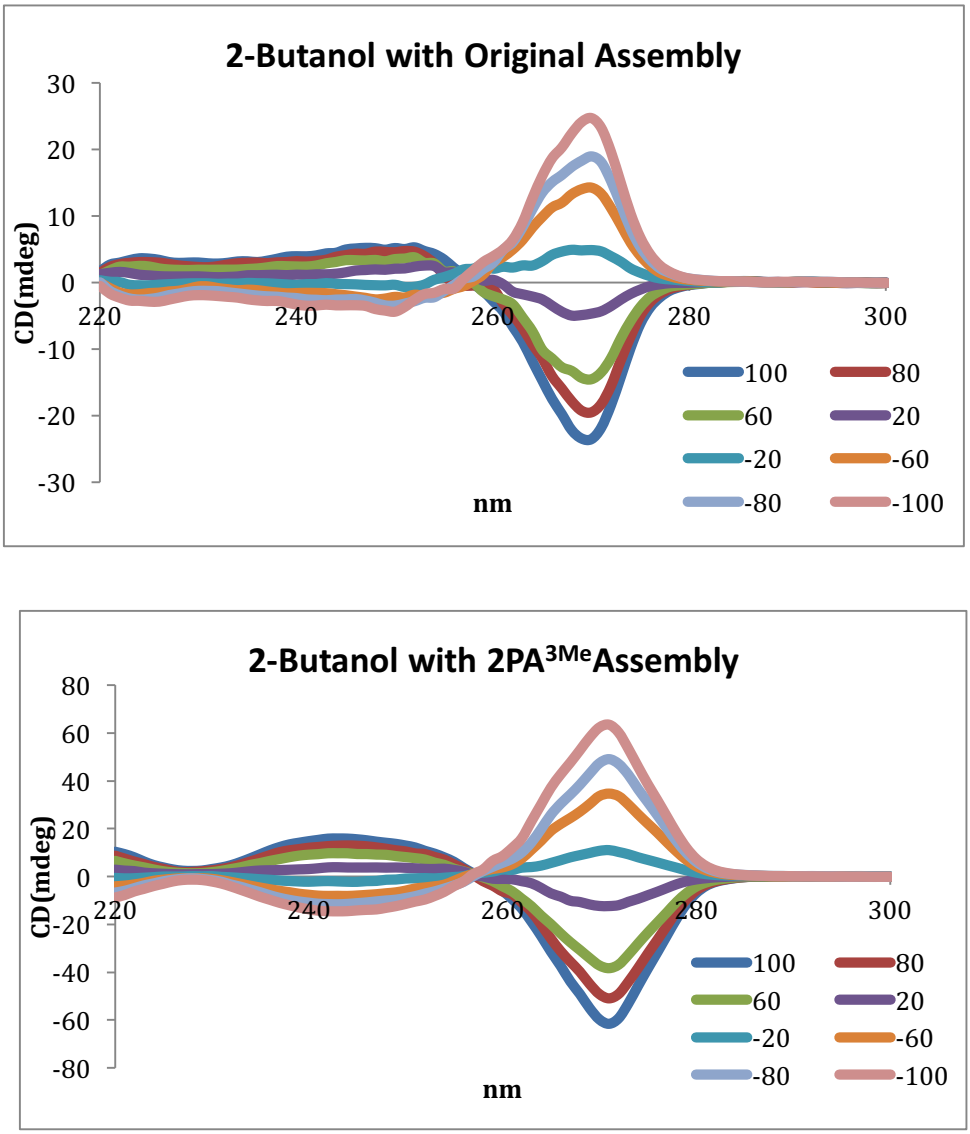


**Figure 3.9** CD spectra of the original assembly and the 2PA$^{3Me}$ assembly with 2-butanol. The assembly was formed at 50 mM and the CD spectra was taken following the procedure described in the main text.

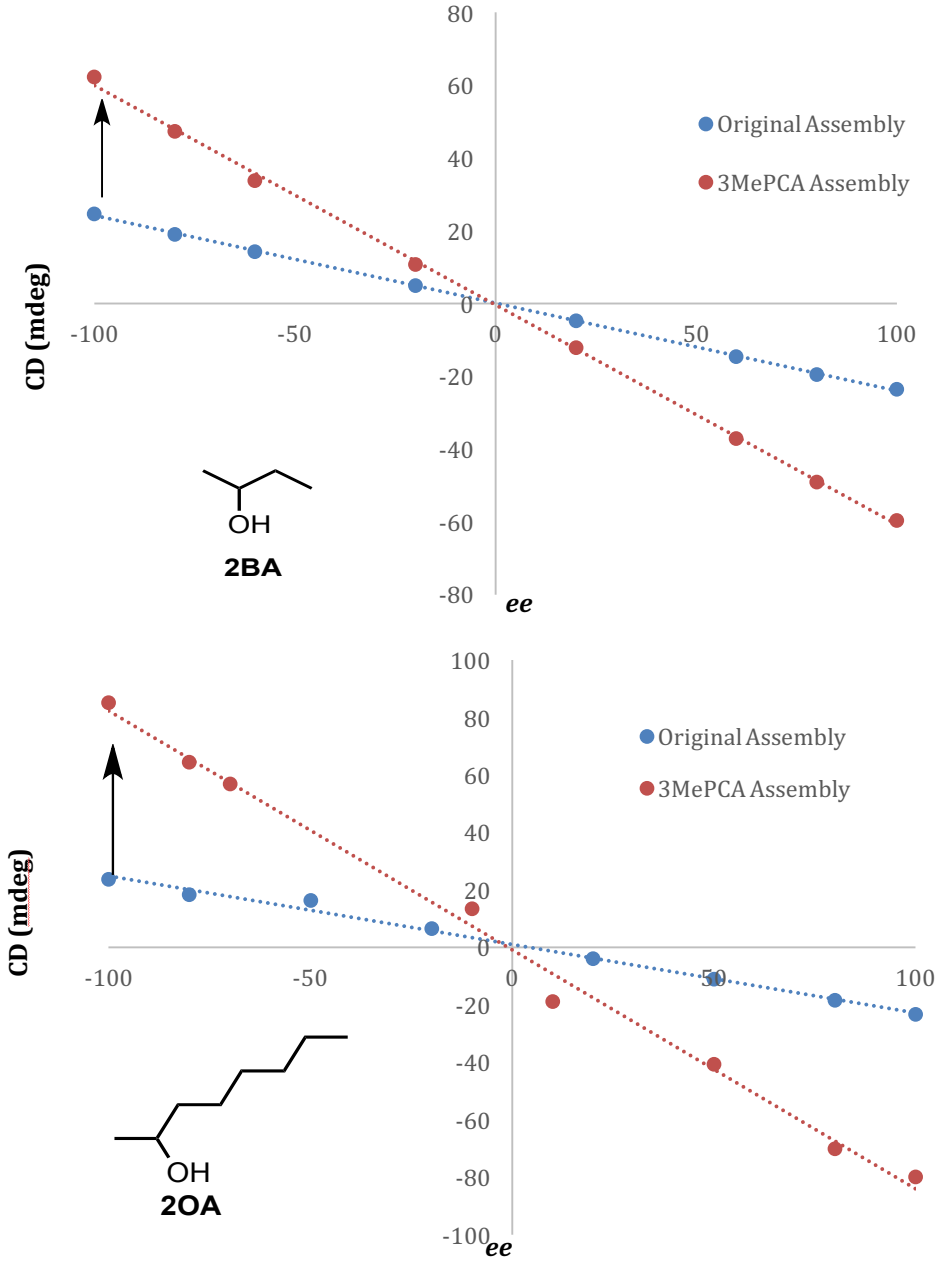


**Figure 3.10** Linear calibration curves of **2OA** and **2BA** with assemblies **1** and **3** were constructed with maximum cotton effect CD at 270 nm ($R^2$= 0.99). The assemblies were formed at 35 mM (with 3 equiv. excess of alcohol), and CD was taken with a 175 μM assembly solution in MeCN. Assembly **3** calibration curves showed an increase in dynamic range in comparison to their original assembly counterparts.

## 3. Conclusions

The studies described herein demonstrate that linear free energy relationships that reflect steric size can correlate the magnitude of the dr values for the 4-component assemblies represented by Scheme 3.4. The steric sizes of the substituents on the 3- and 6-positions of 2PA as well as the groups on the stereocenter of the alcohol dictate the dr and CD optical response. The dependence on sterics was such that two different steric sizes for phenyl were necessary, depending upon the assembly, to model the data properly. Through these studies, we found the assembly containing $2PA^{3Me}$ had the most improvement in the dynamic range of the optical response, resulting in lower errors for ee determination.

## 4. Characterizations and Spectra

### 4.1 Assembly $^{1}$HNMR Spectra

$^{1}$H NMR and CD spectra were used to characterize each multicomponent assembly formation in acetonitrile at 50mM, and the assemblies formation protocol followed the procedure described in the text above. The protons of interest are shown in Scheme 3.8, and the number in the figure is used to identify all the proton of interest in the NMR spectra.

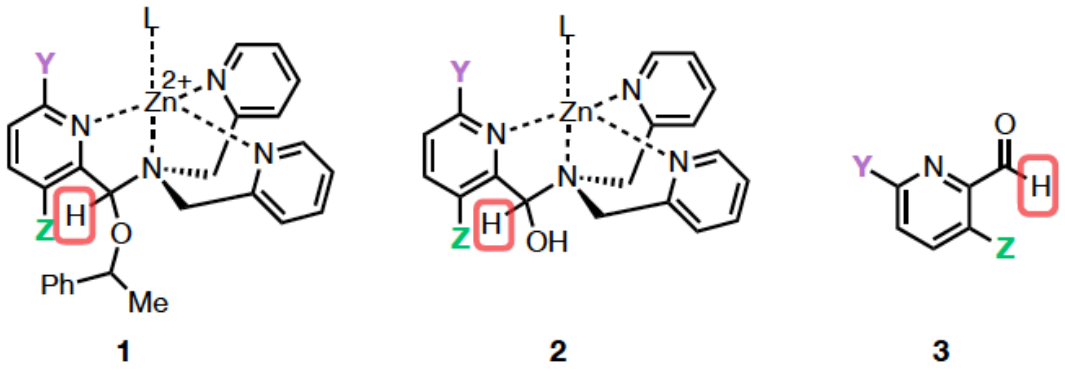


**Scheme 3.8** The protons used in calculating the yield or the extent of assembly formation. These included the hemiaminal ether methine (1), hemiaminal methine (2), and the aldehyde proton (3).

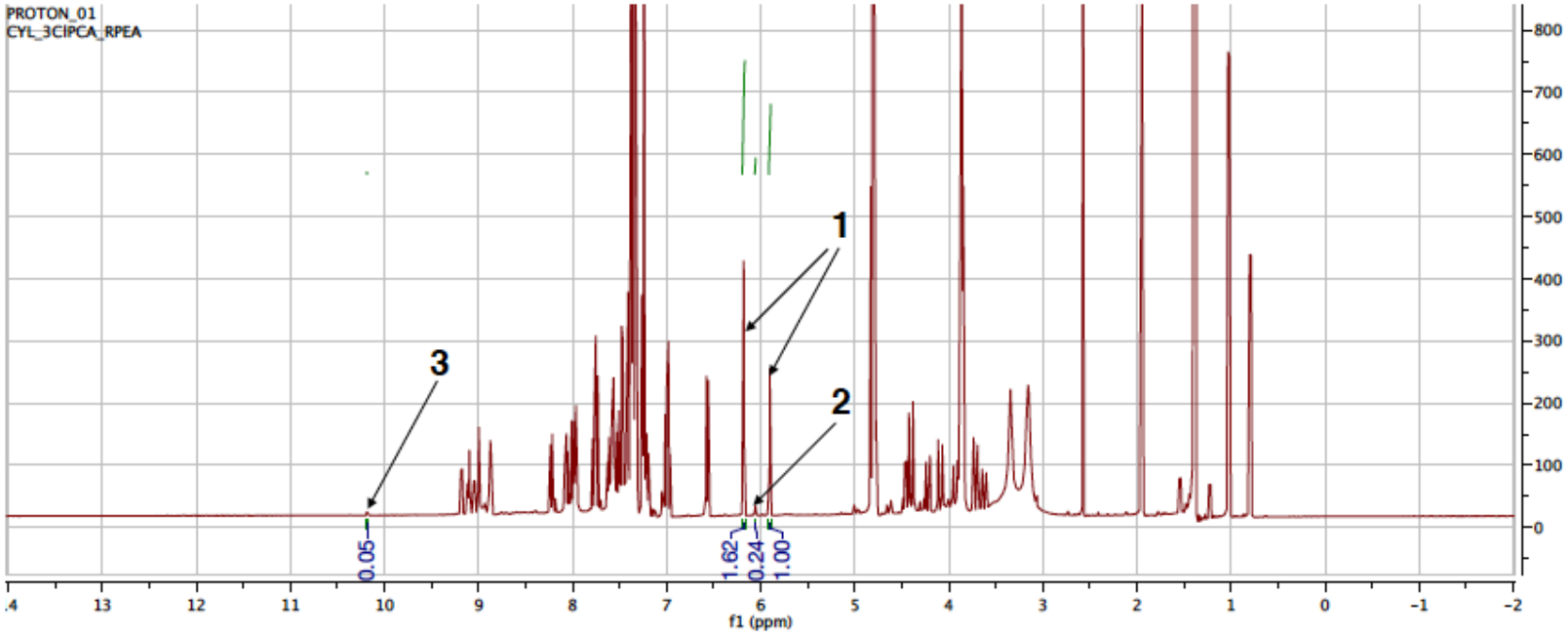


**Figure 3.11** [1]HNMR of the assembly formed with 3-chloropyridine-2-carbaldehyde.

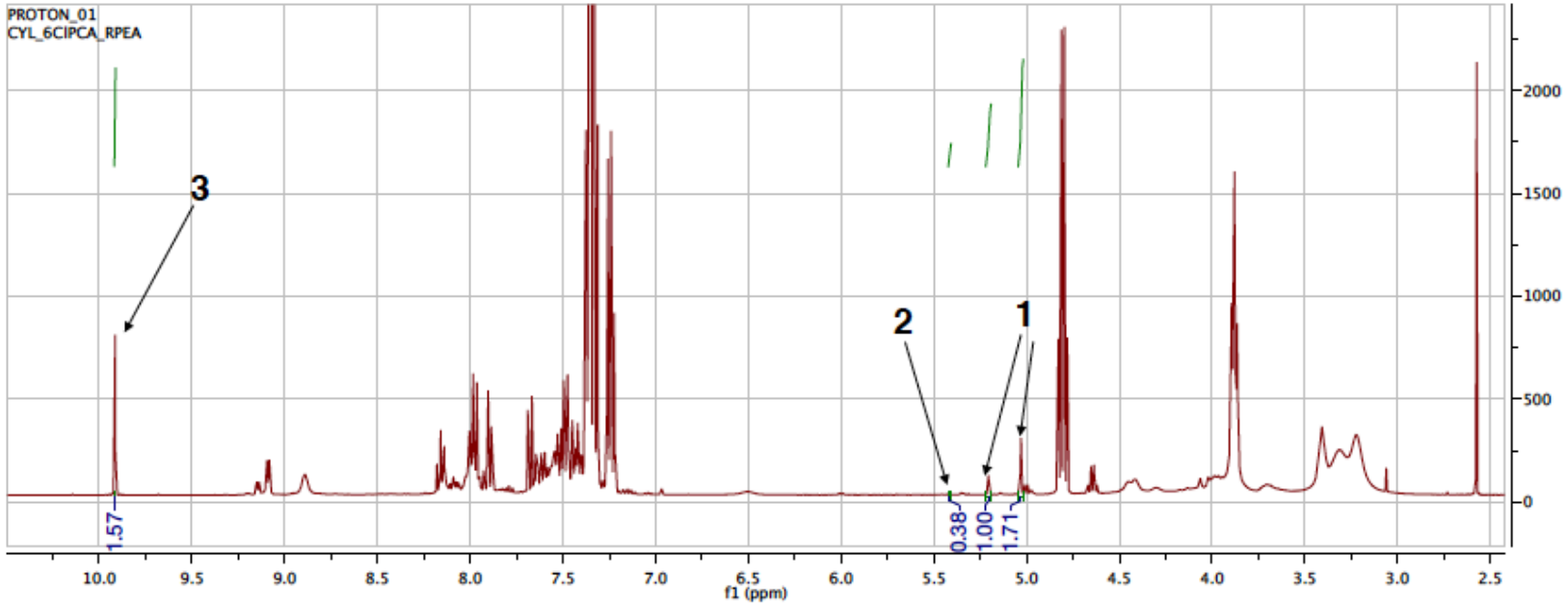


**Figure 3.12** [1]HNMR of the assembly formed with 6-chloropyridine-2-carbaldehyde.

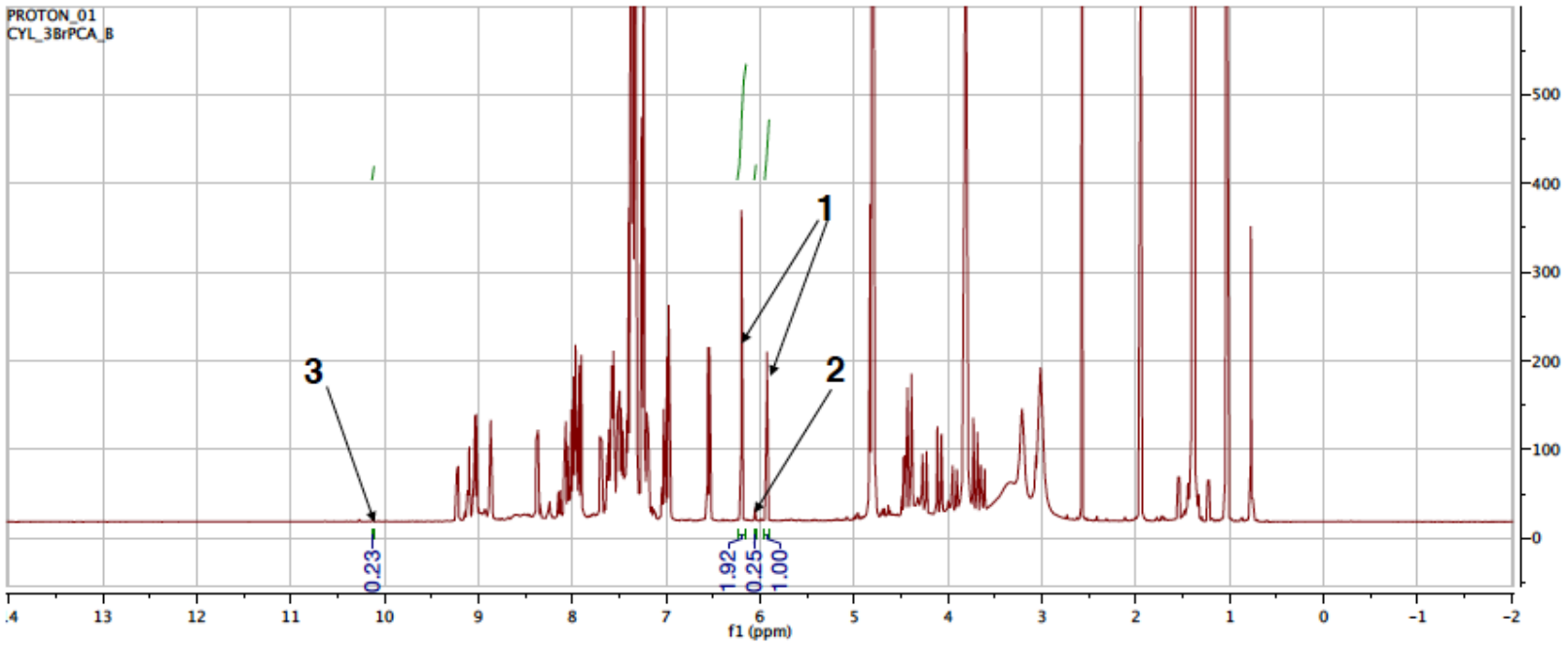


**Figure 3.13** [1]HNMR of the assembly formed with 3-bromopyridine-2-carbaldehyde.

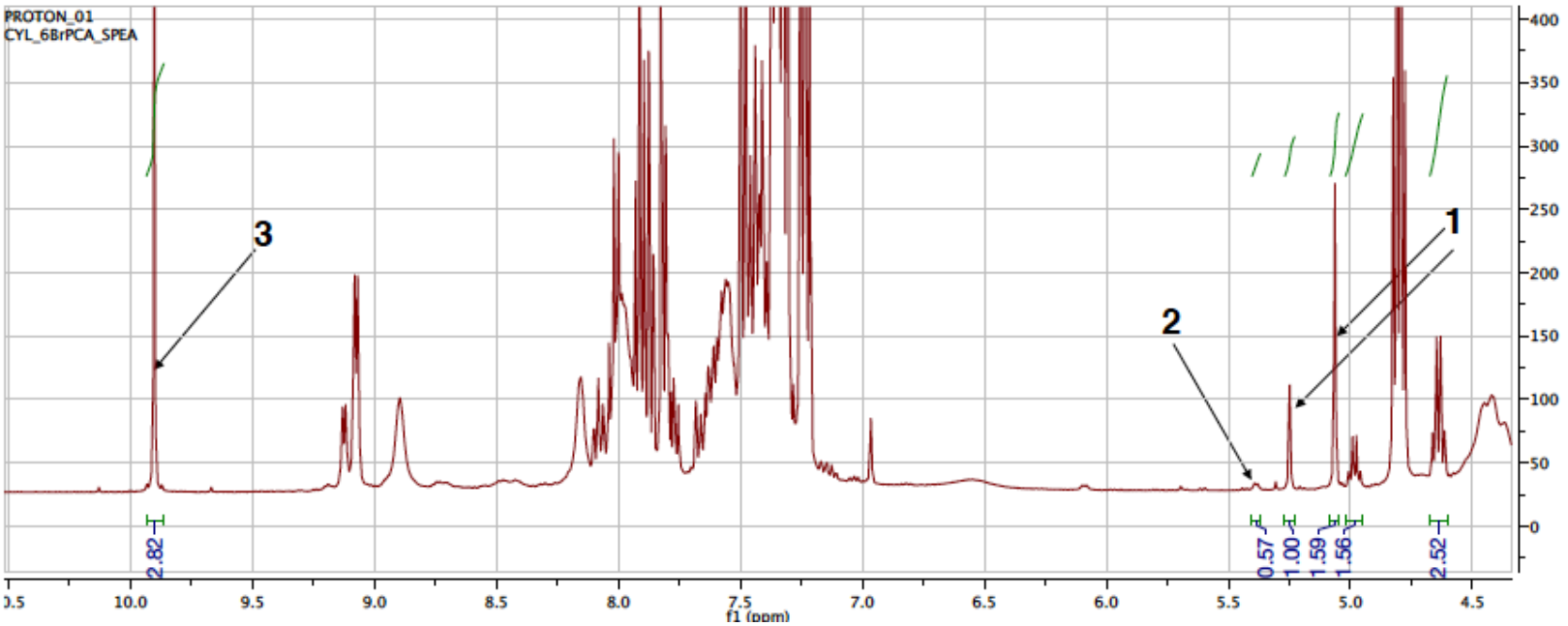


**Figure 3.14** [1]HNMR of the assembly formed with 6-bromopyridine-2-carbaldehyde.

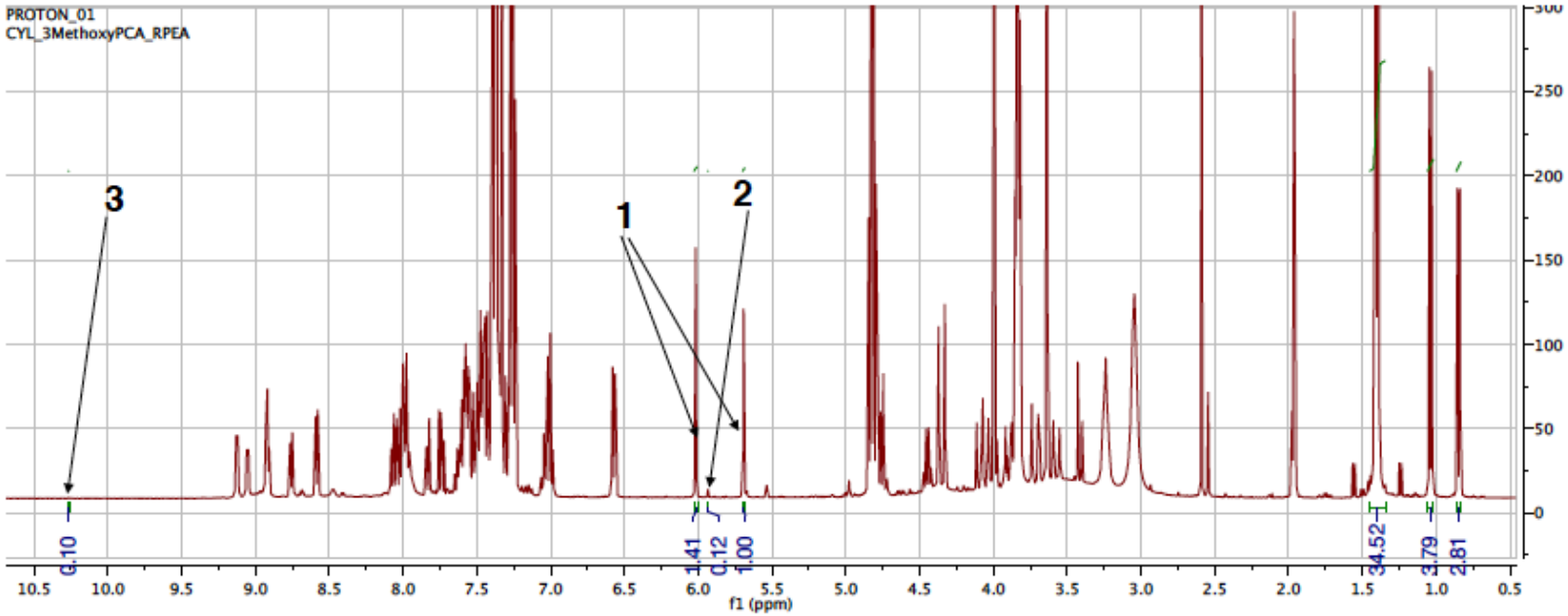


**Figure 3.15** [1]HNMR of the assembly formed with 3-methoxypyridine-2-carbaldehyde.

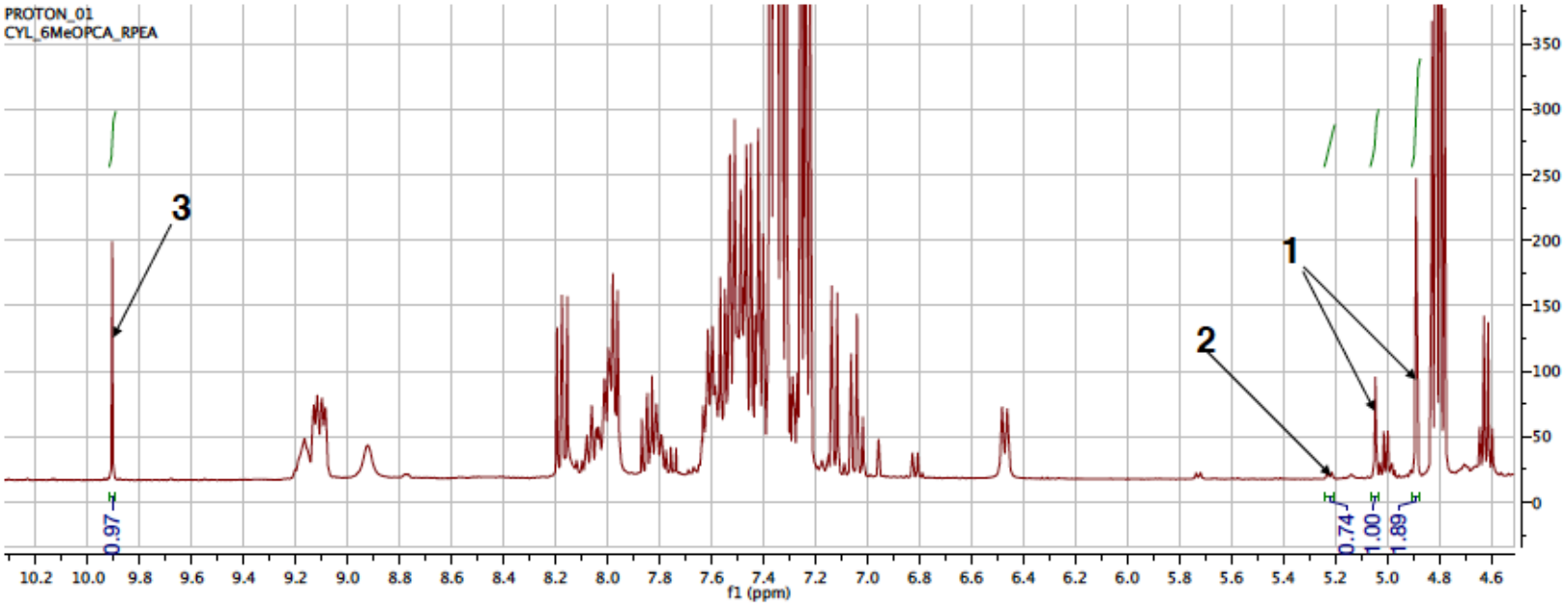


**Figure 3.16** [1]HNMR of the assembly formed with 6-methoxypyridine-2-carbaldehyde.

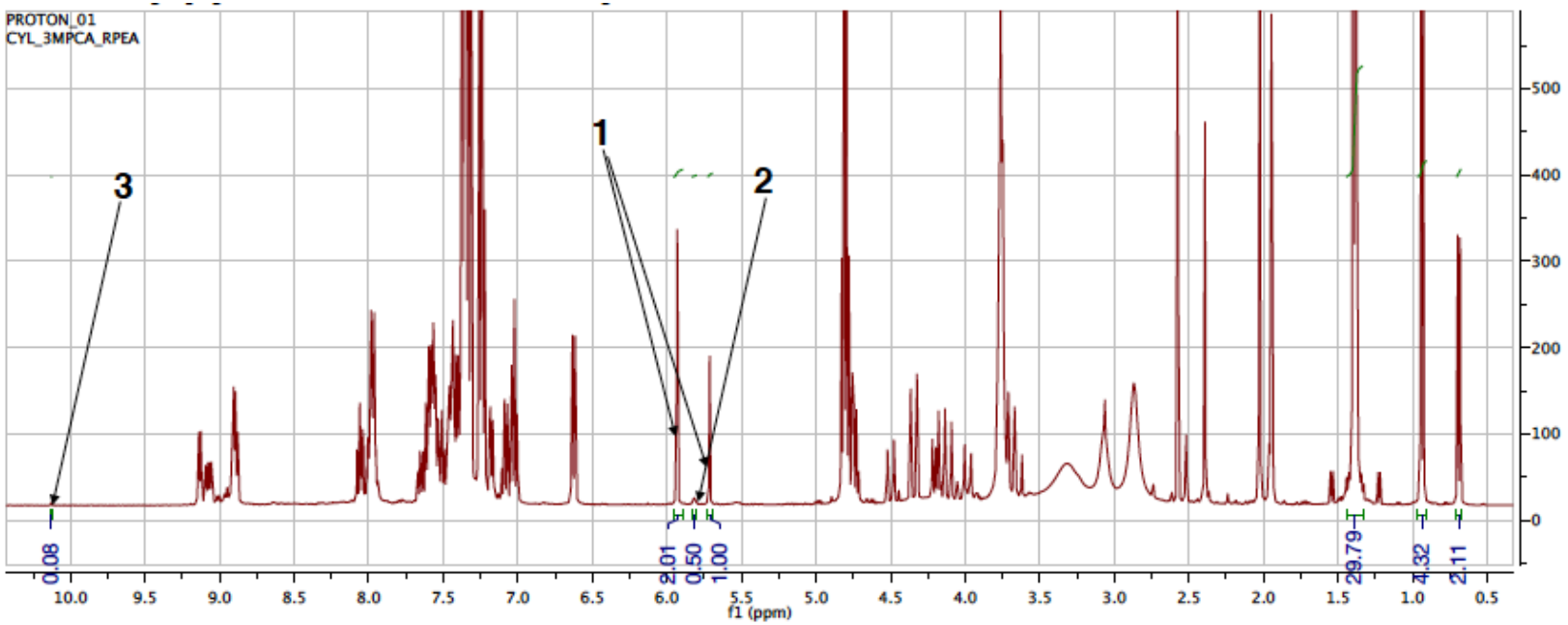


**Figure 3.17** [1]HNMR of the assembly formed with 3-methylpyridine-2-carbaldehyde.

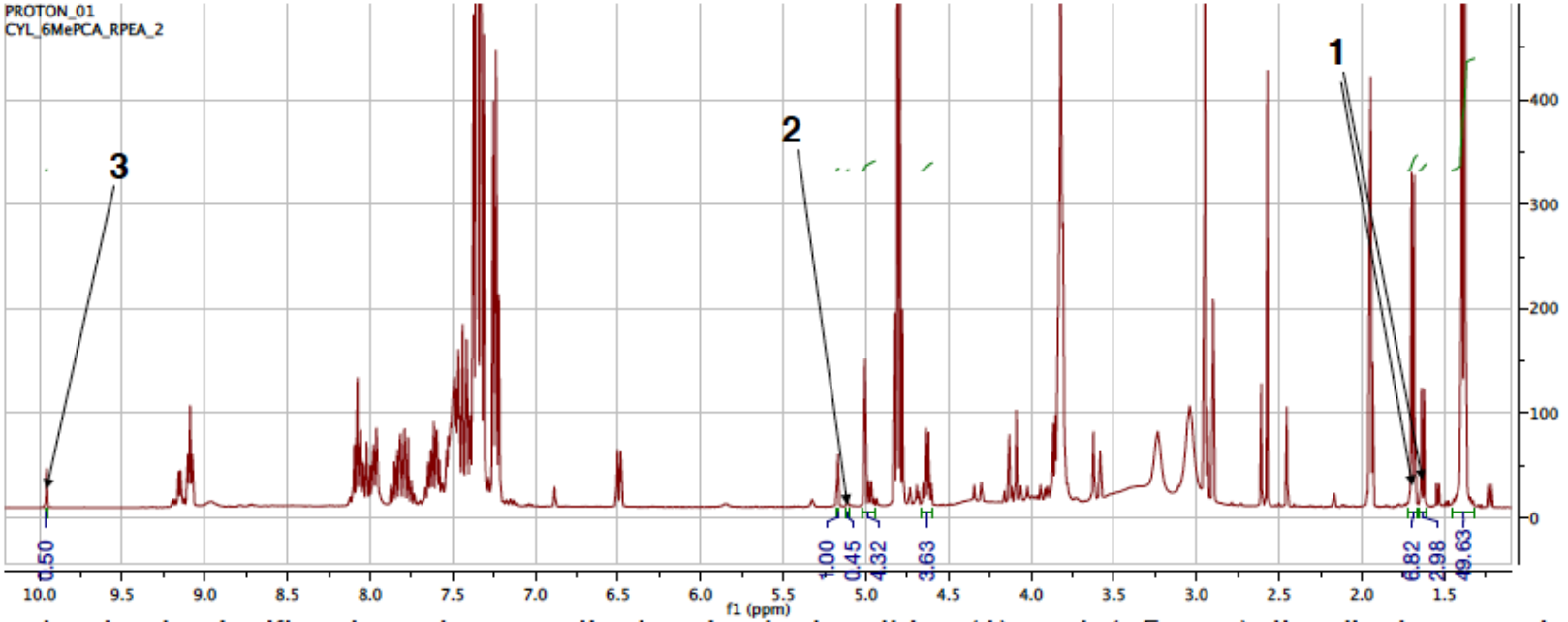


note: due to significant overlap near the hemiaminal methine (1) peak (~5 ppm), the diastereomeric ratio was determined using the diastereomeric methyl peaks (~1.7 ppm).

**Figure 3.18** [1]HNMR of the assembly formed with 6-methylpyridine-2-carbaldehyde.

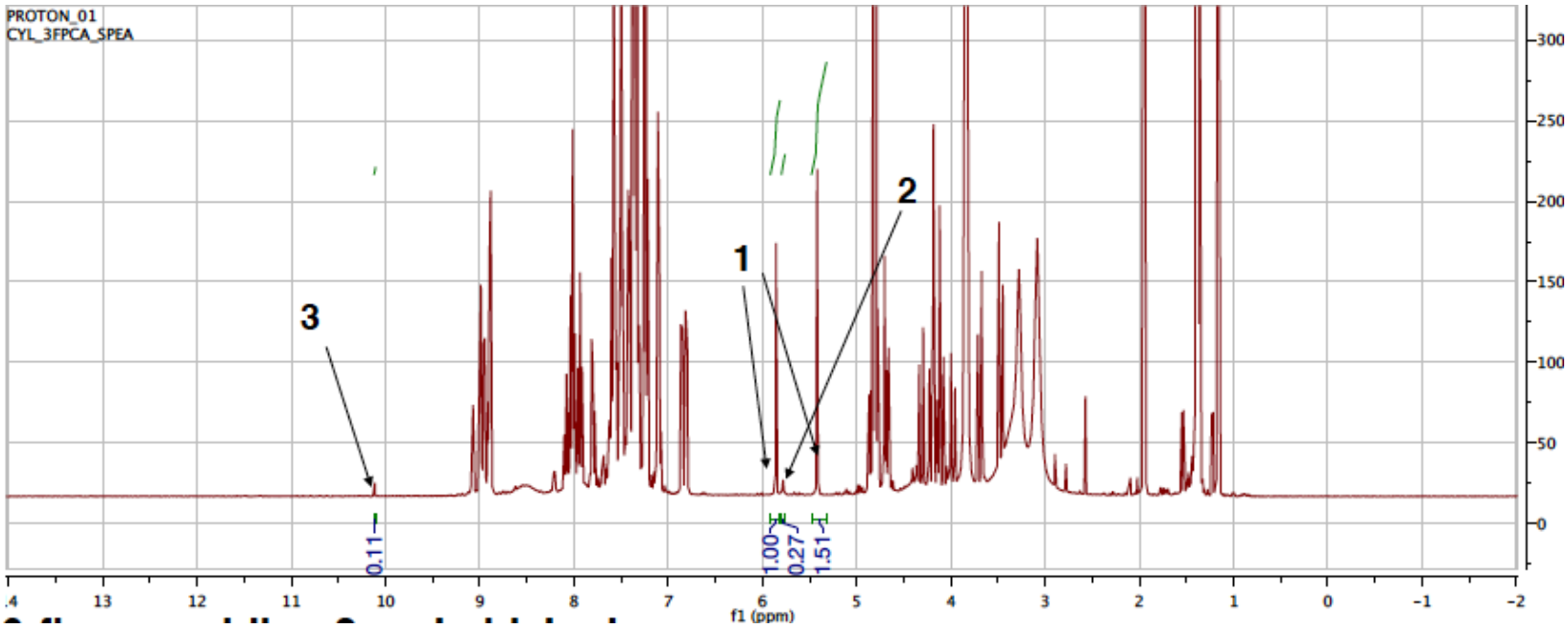


**Figure 3.19** [1]HNMR of the assembly formed with 3-fluoropyridine-2-carbaldehyde.

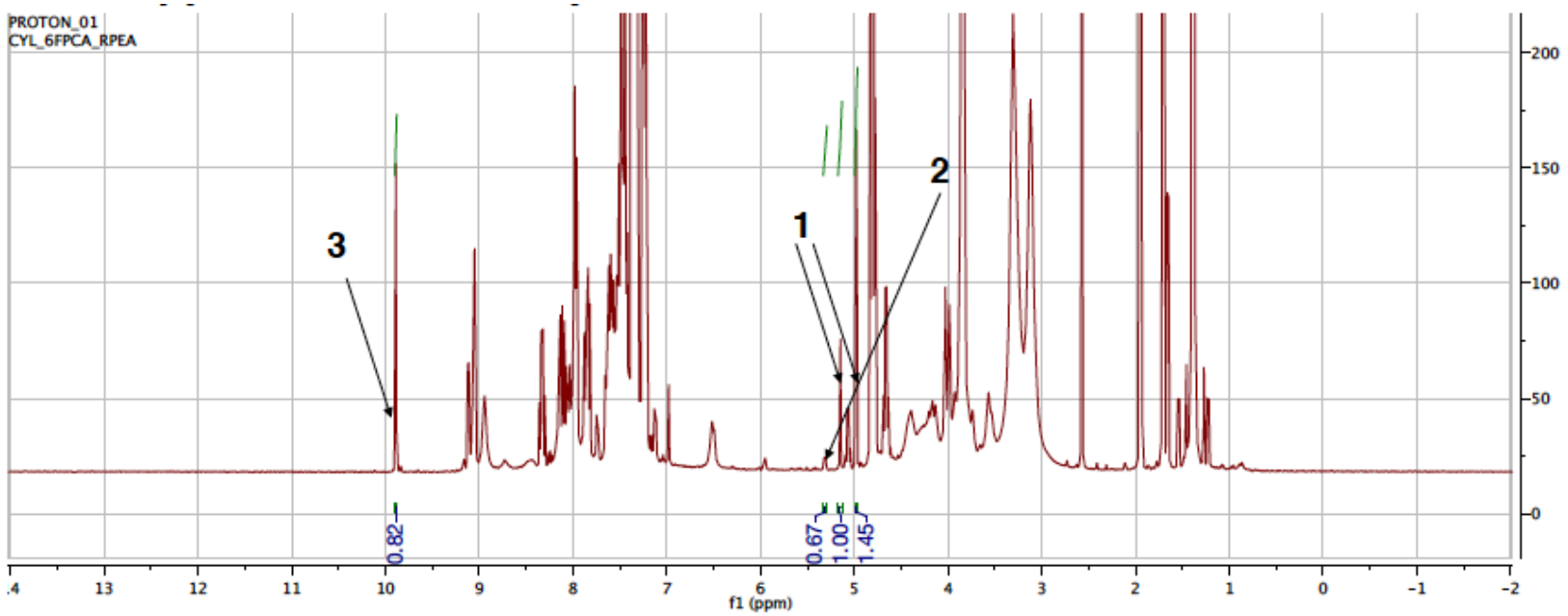


**Figure 3.20** [1]HNMR of the assembly formed with 6-fluoropyridine-2-carbaldehyde.

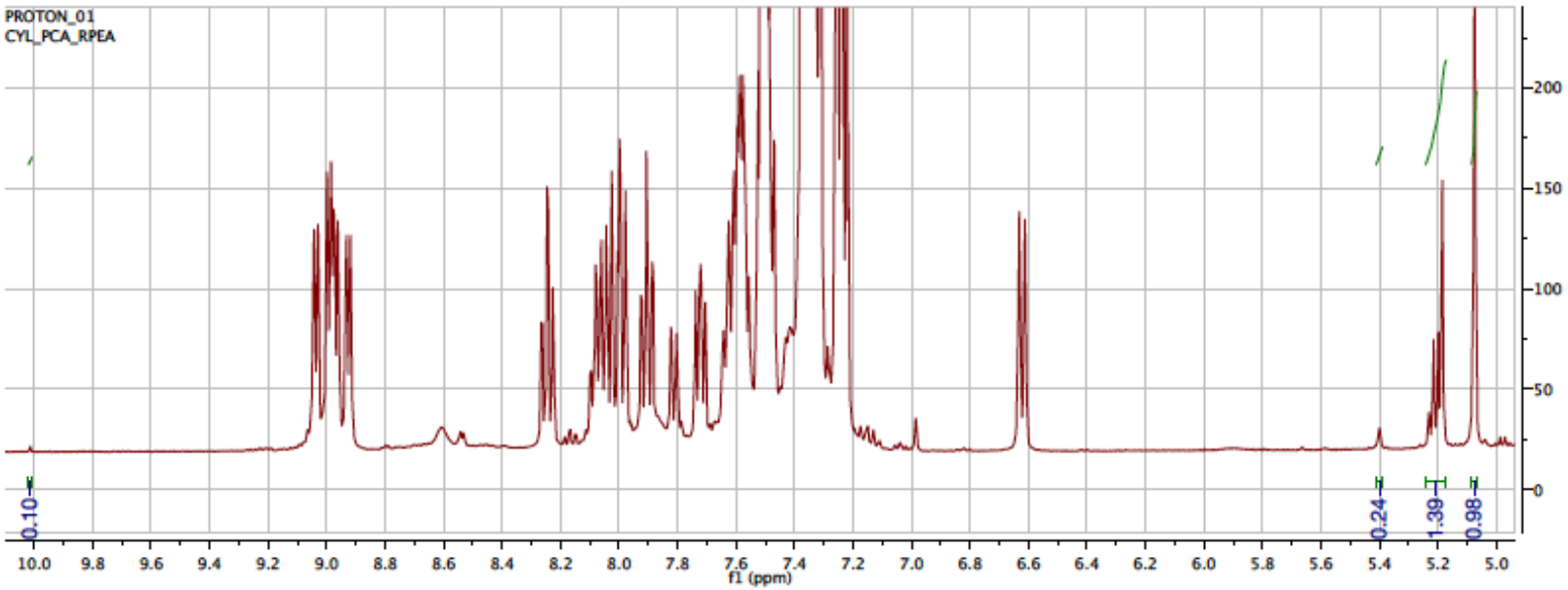


**Figure 3.21** [1]HNMR of the assembly formed with pyridine-2-carbaldehyde.

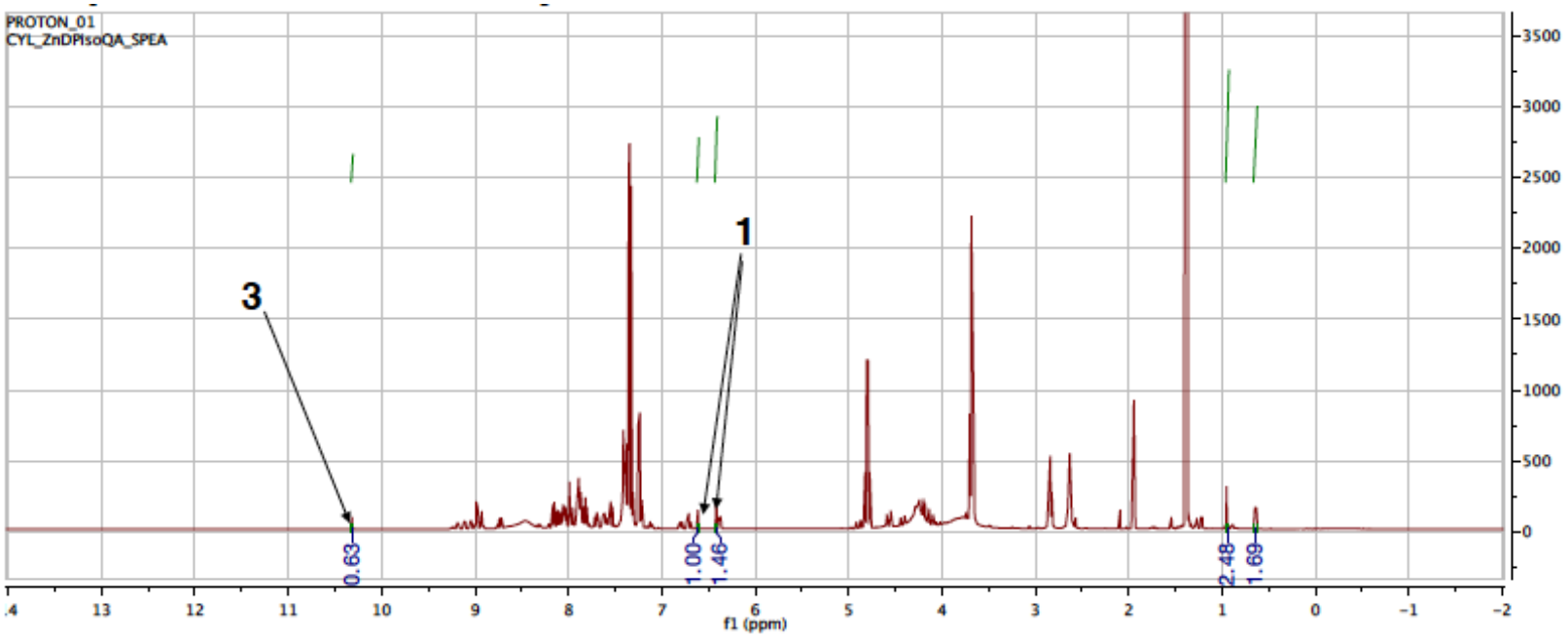


**Figure 3.22** [1]HNMR of the assembly formed with isoquinoline-1-carbaldehyde.

### 4.3 CD Studies of 2PA' Ligands

CD spectra were taken with Jasco J-815 CD Spectrometer with Starna Type 21 1-mm quartz cuvette at 25 °C in acetonitrile at 175 μM. The assemblies were formed with protocols described in the main text of the article. CD spectra of assemblies with varying 2PA' ligand are shown below. In the following spectra, PEA is 1-phenylethanol and 3MeBA is 3-methylbutanol.

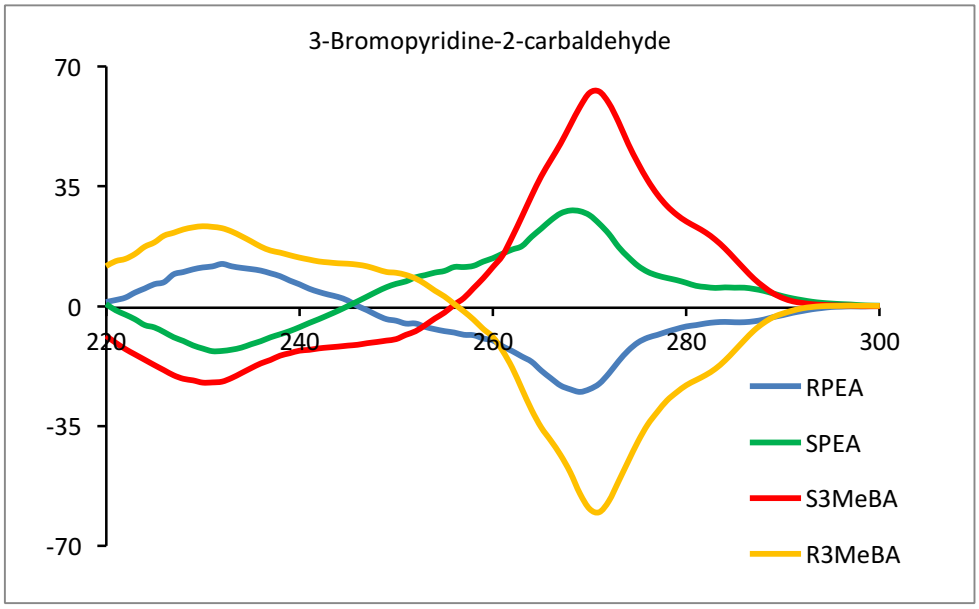


**Figure 3.23** CD spectra of assembly formed with 3-bromopyridine-2-carbaldehyde.

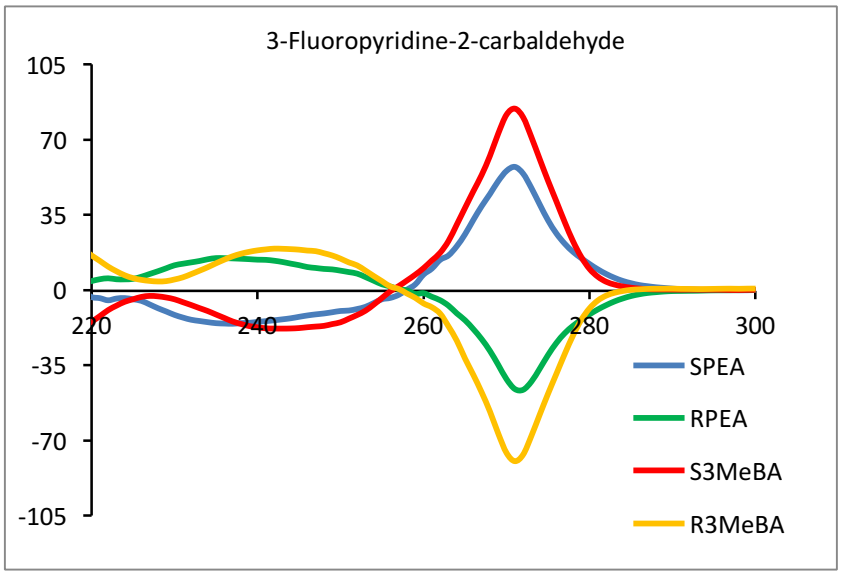


**Figure 3.24** CD spectra of assembly formed with 3-fluoropyridine-2-carbaldehyde.

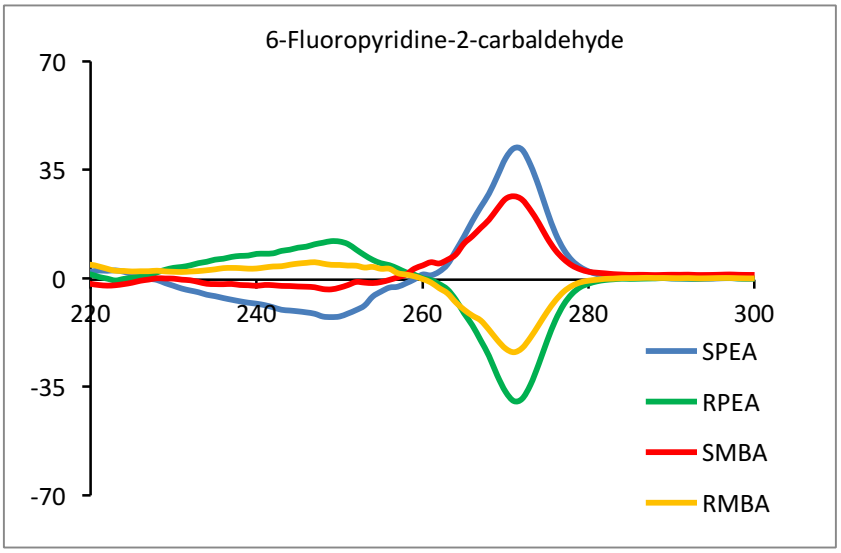


**Figure 3.25** CD spectra of assembly formed with 6-fluoropyridine-2-carbaldehyde.

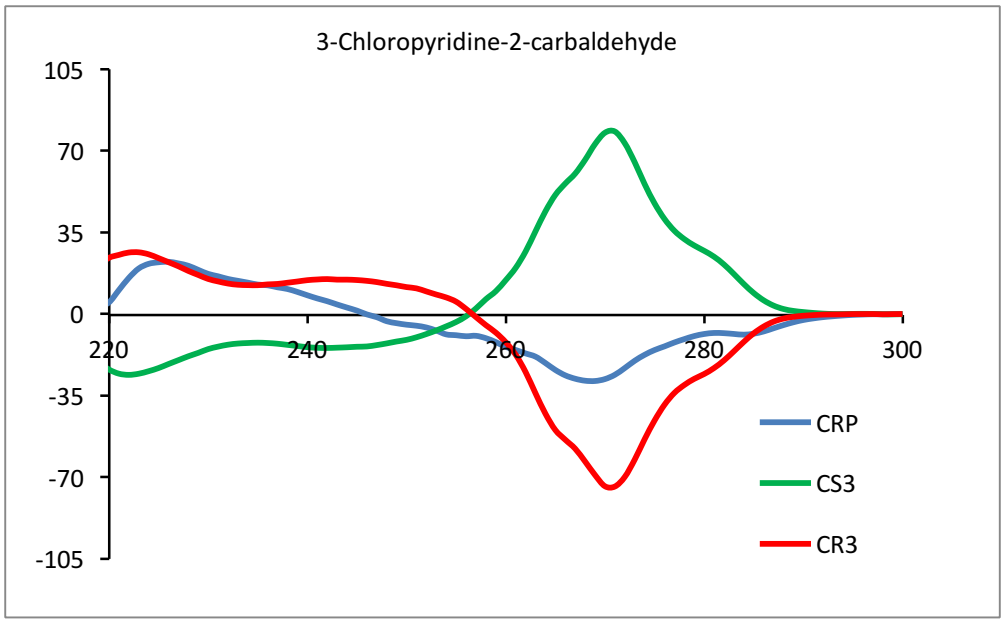


**Figure 3.26** CD spectra of assembly formed with 3-chloropyridine-2-carbaldehyde.

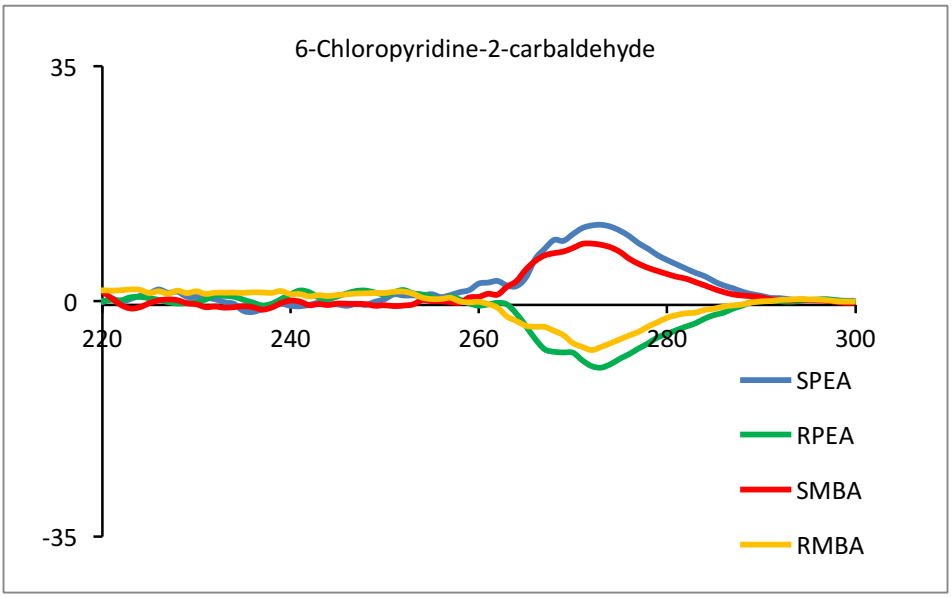


**Figure 3.27** CD spectra of assembly formed with 6-chloropyridine-2-carbaldehyde.

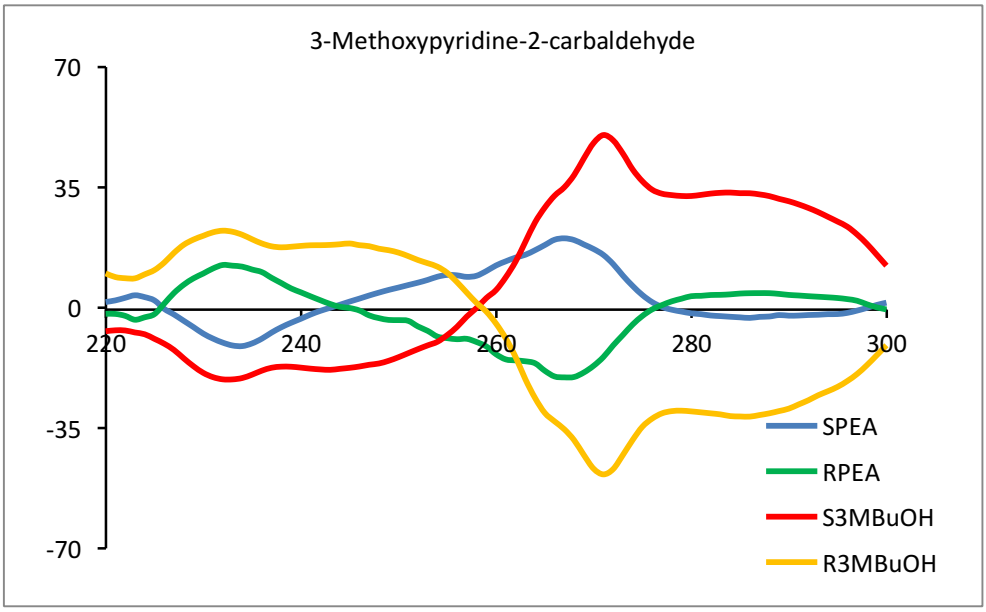


**Figure 3.28** CD spectra of assembly formed with 3-methoxypyridine-2-carbaldehyde.

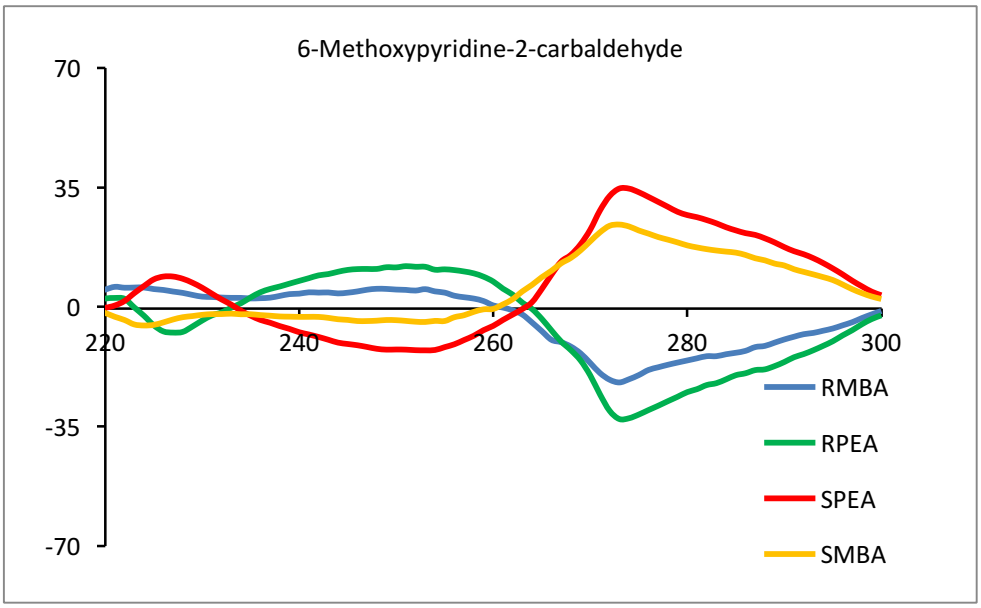


**Figure 3.29** CD spectra of assembly formed with 6-methoxypyridine-2-carbaldehyde.

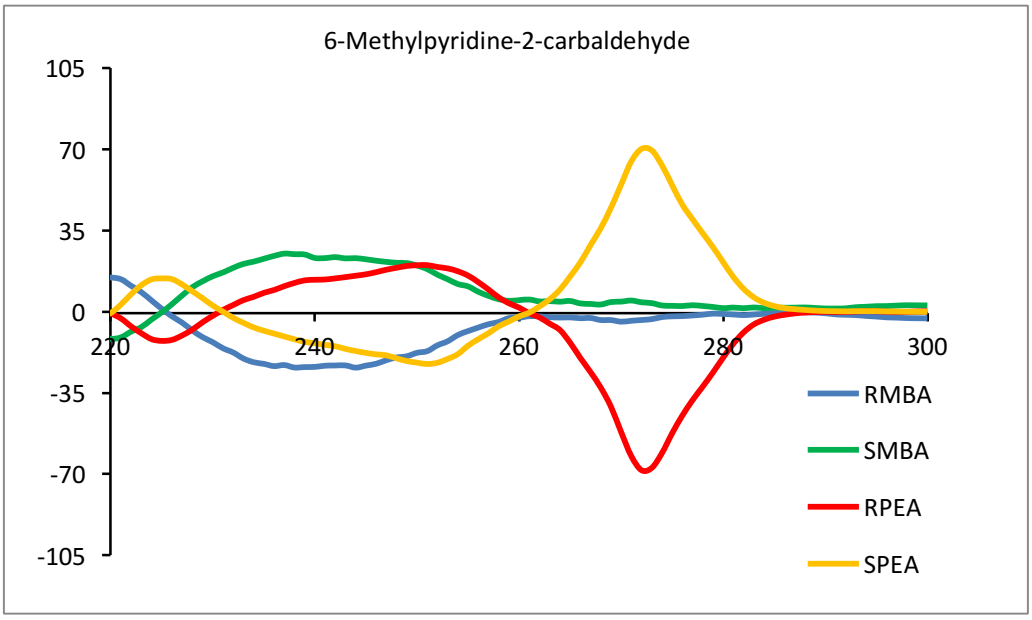


**Figure 3.30** CD spectra of assembly formed with 6-methylpyridine-2-carbaldehyde.

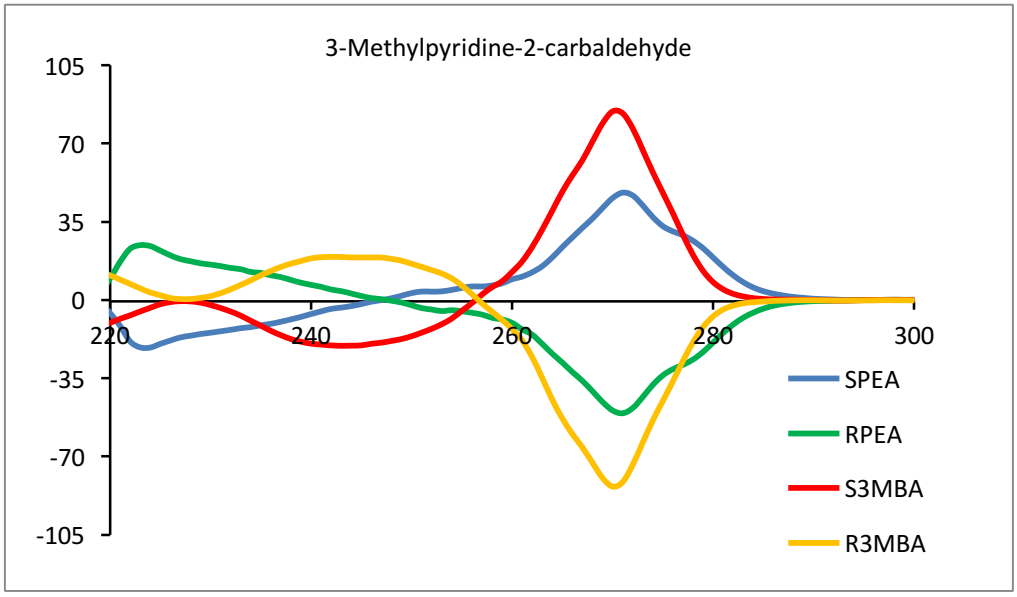


**Figure 3.31** CD spectra of assembly formed with 3-methylpyridine-2-carbaldehyde.

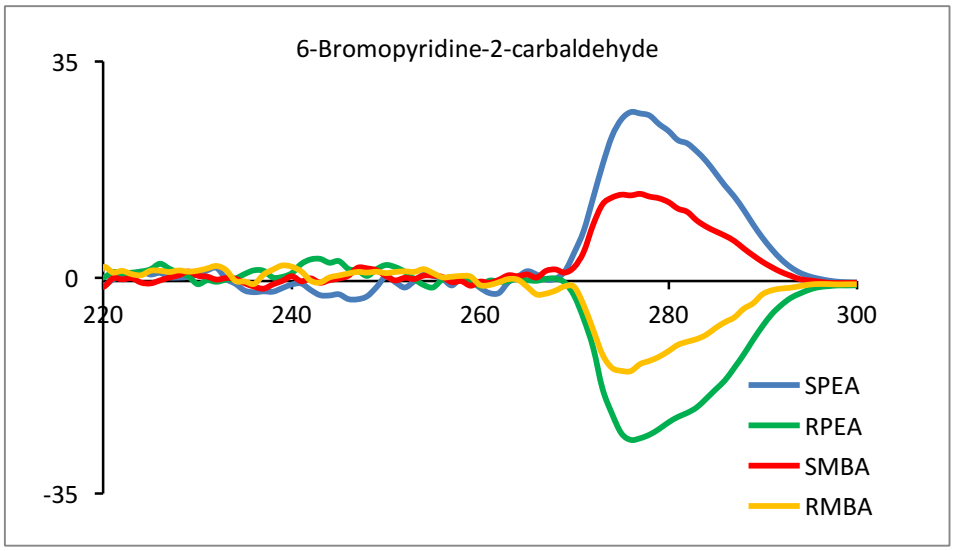


**Figure 3.32** CD spectra of assembly formed with 6-bromopyridine-2-carbaldehyde.

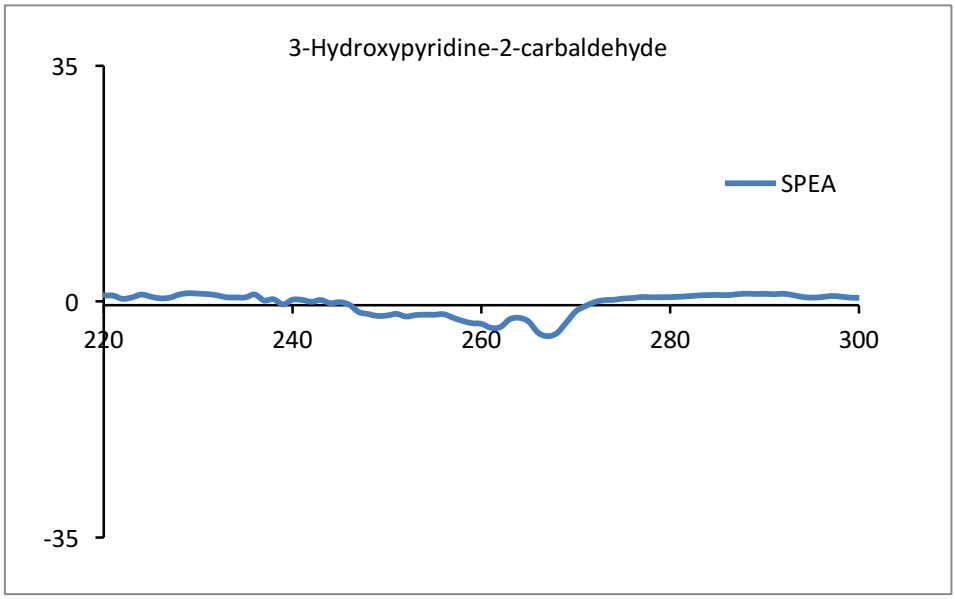


**Figure 3.33** CD spectrum of assembly formed with 3-hydroxypyridine-2-carbaldehyde.

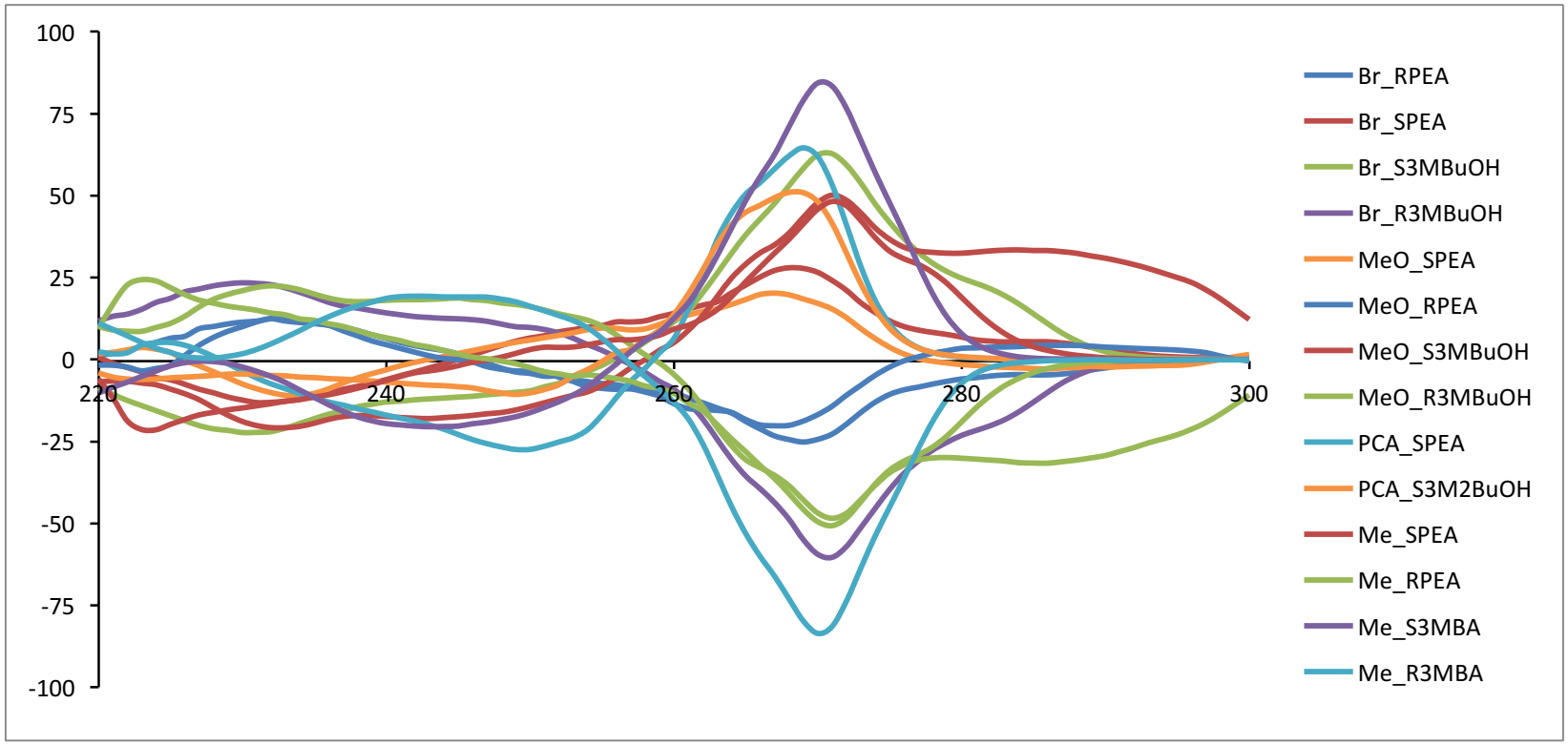


**Figure 3.34** Overlay of all the CD spectra above.

## 4.4 3-Methylpyridine-2-carbaldehyde Assembly Linear Model $^{1}$HNMR and CD Spectra

The 3-methylpyridine-2-carbaldehyde assembly was formed with described procedure in the main text in acetonitrile at 50 mM, and the *dr* was derived from $^{1}$H NMR spectra. Only the diastereomeric methine peaks are integrated in the following spectra. CD spectra were taken with Jasco J-815 CD Spectrometer with Starna Type 21 1-mm quartz cuvette at 25 °C in acetonitrile at 250 μM. The assemblies were formed with protocols described in the main text of the article. CD spectra of $2PA^{3Me}$ assembly with various alcohol are shown below.

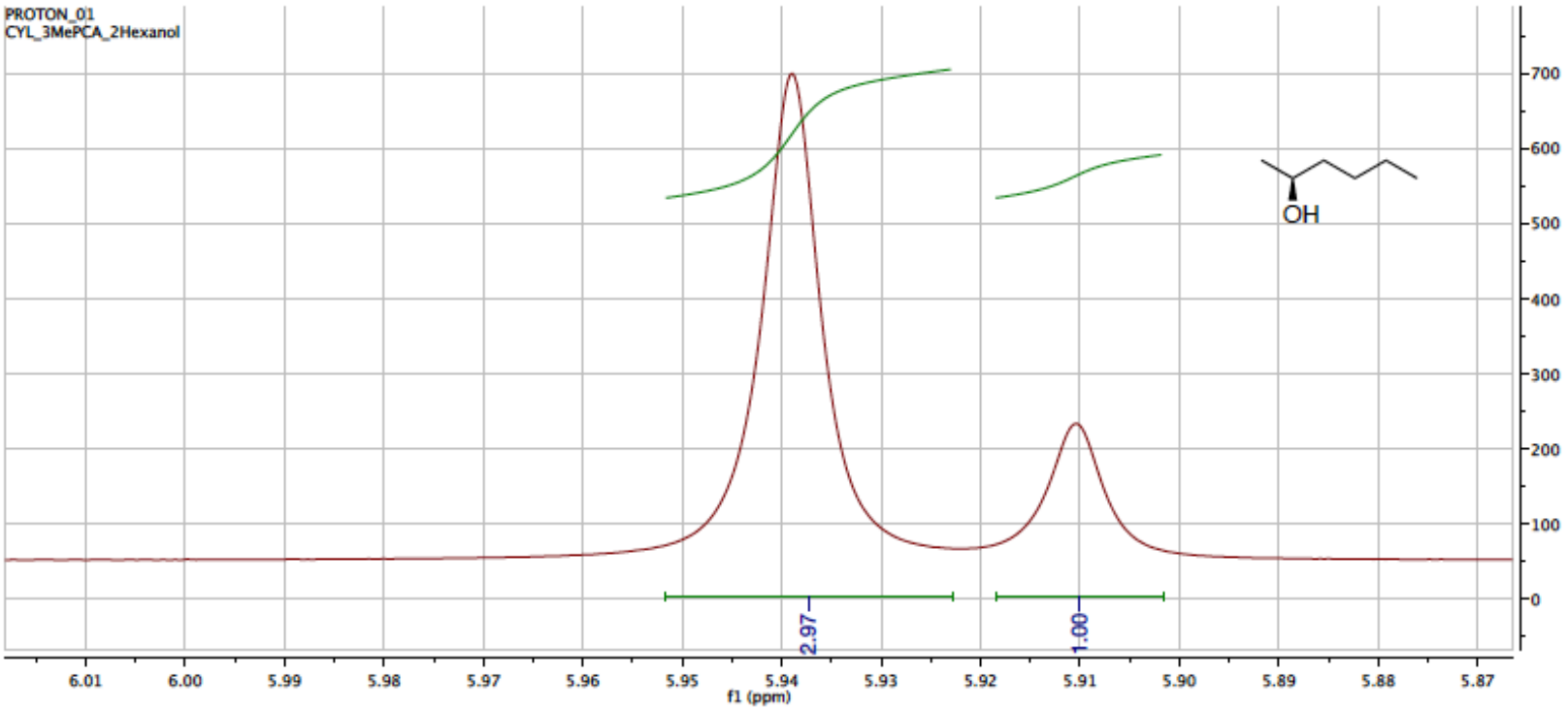


**Figure 3.35** [1]HNMR spectrum of 2-hexanol with 3-methylpyridine-2-carbaldehyde assembly.

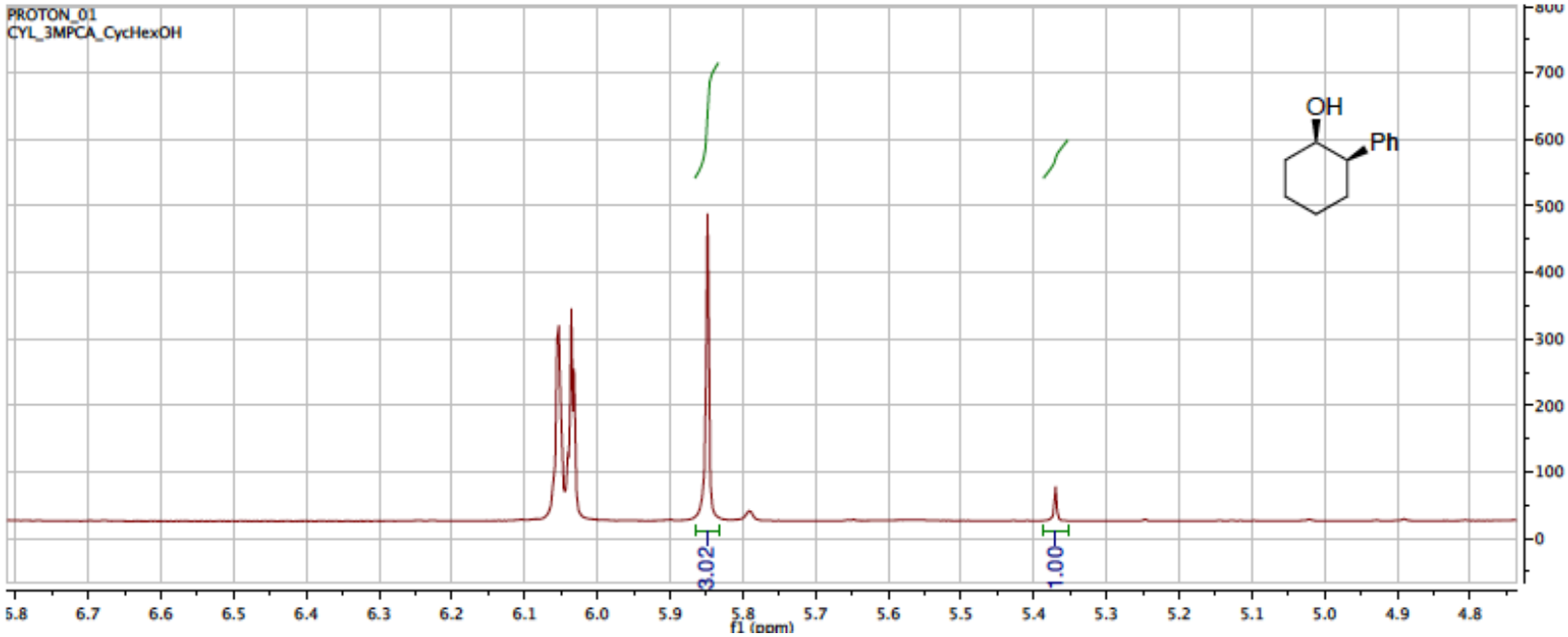


**Figure 3.36** [1]HNMR spectrum of *trans*-2-phenylcyclohexanol with 3-methylpyridine-2-carbaldehyde assembly.

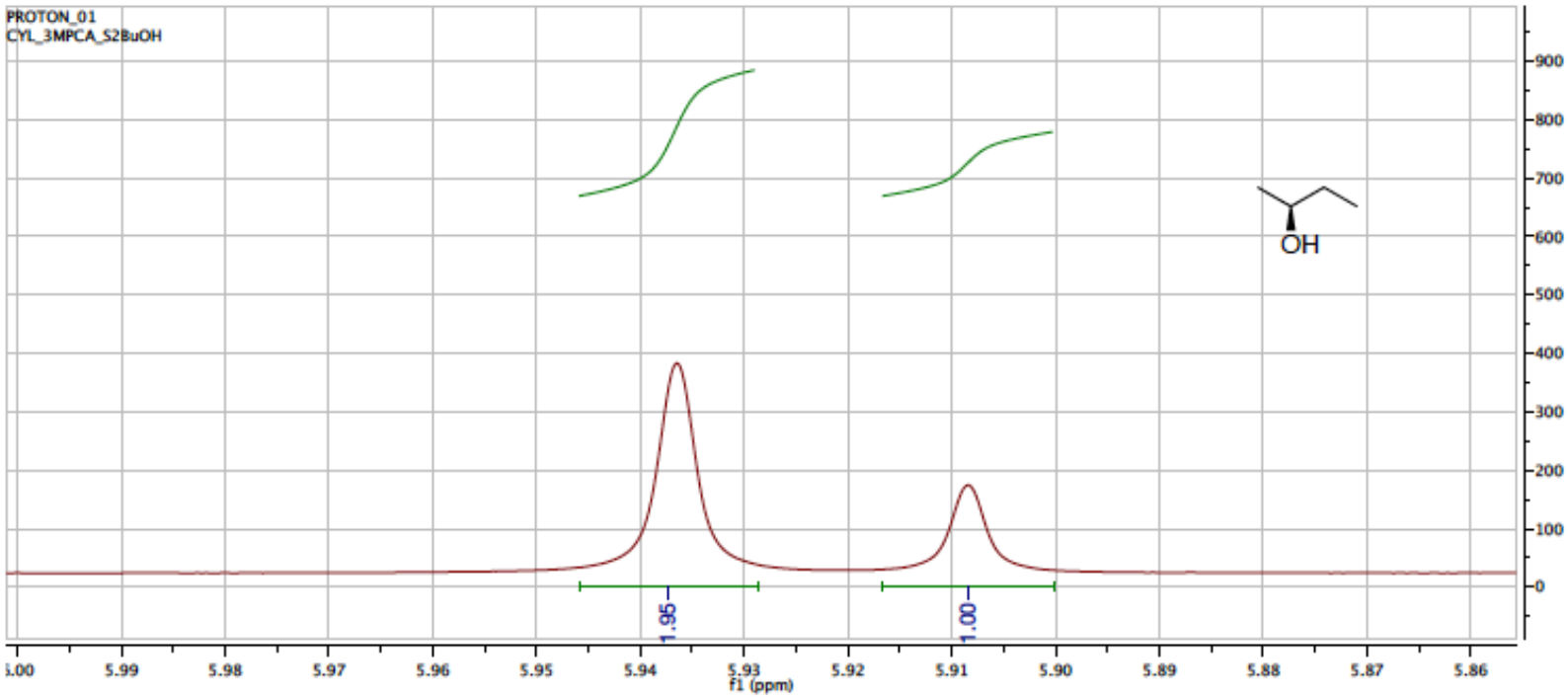


**Figure 3.37** [1]HNMR spectrum of 2-butanol with 3-methylpyridine-2-carbaldehyde assembly.

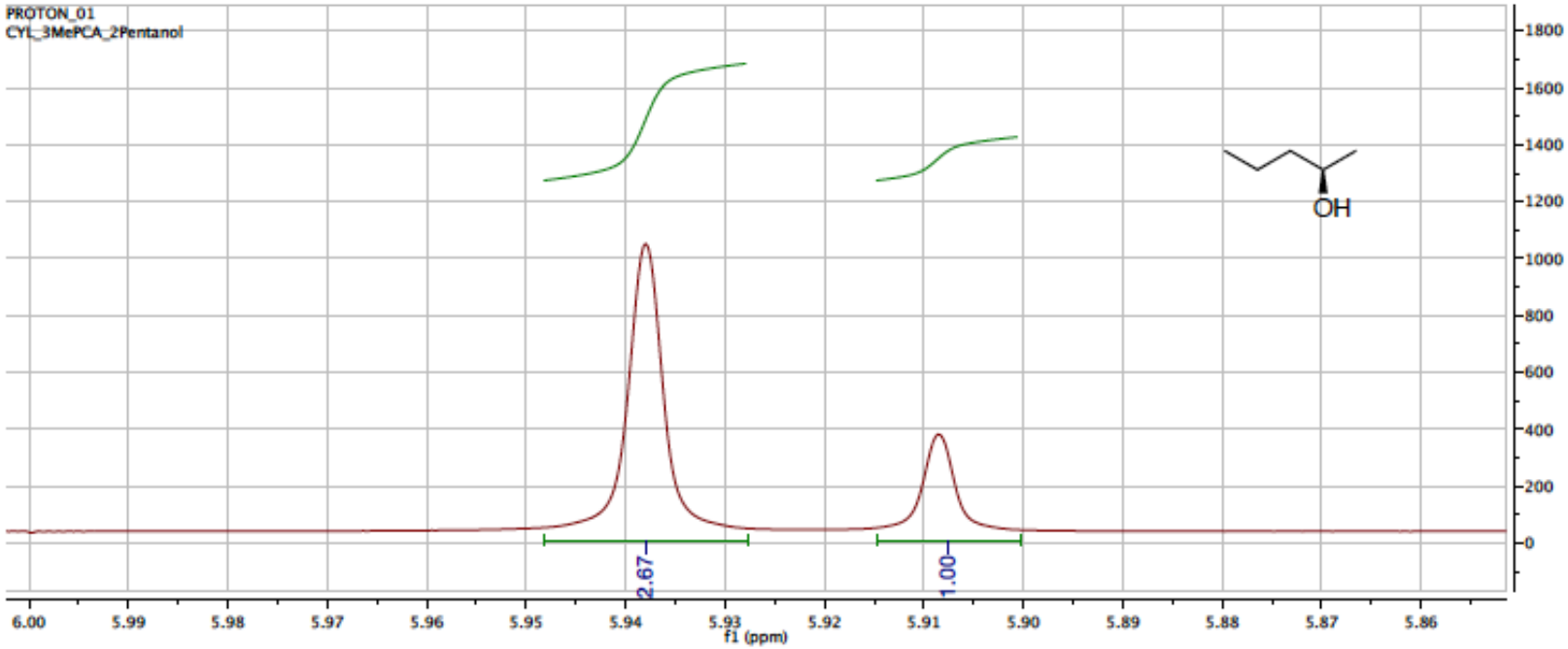


**Figure 3.38** [1]HNMR spectrum of 2-pentanol with 3-methylpyridine-2-carbaldehyde assembly.

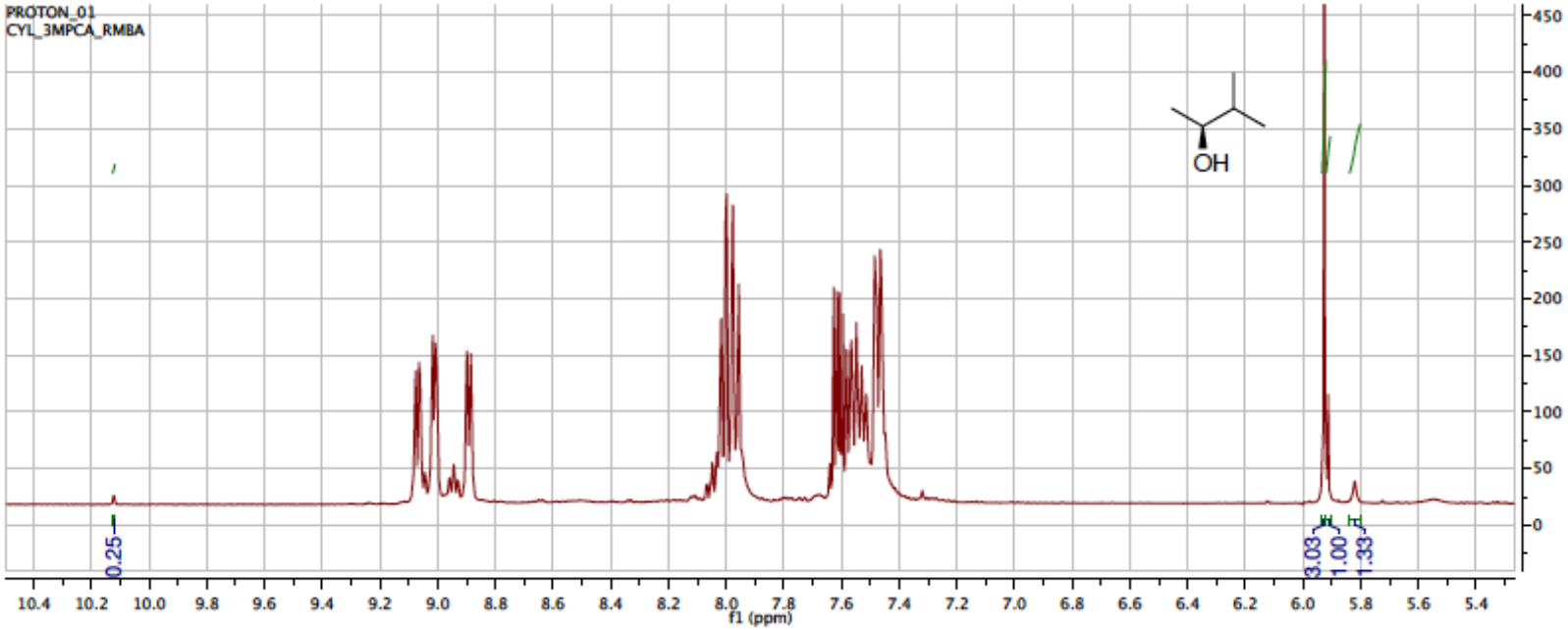


**Figure 3.39** [1]HNMR spectrum of 3-methyl-2-butanol with 3-methylpyridine-2-carbaldehyde assembly.

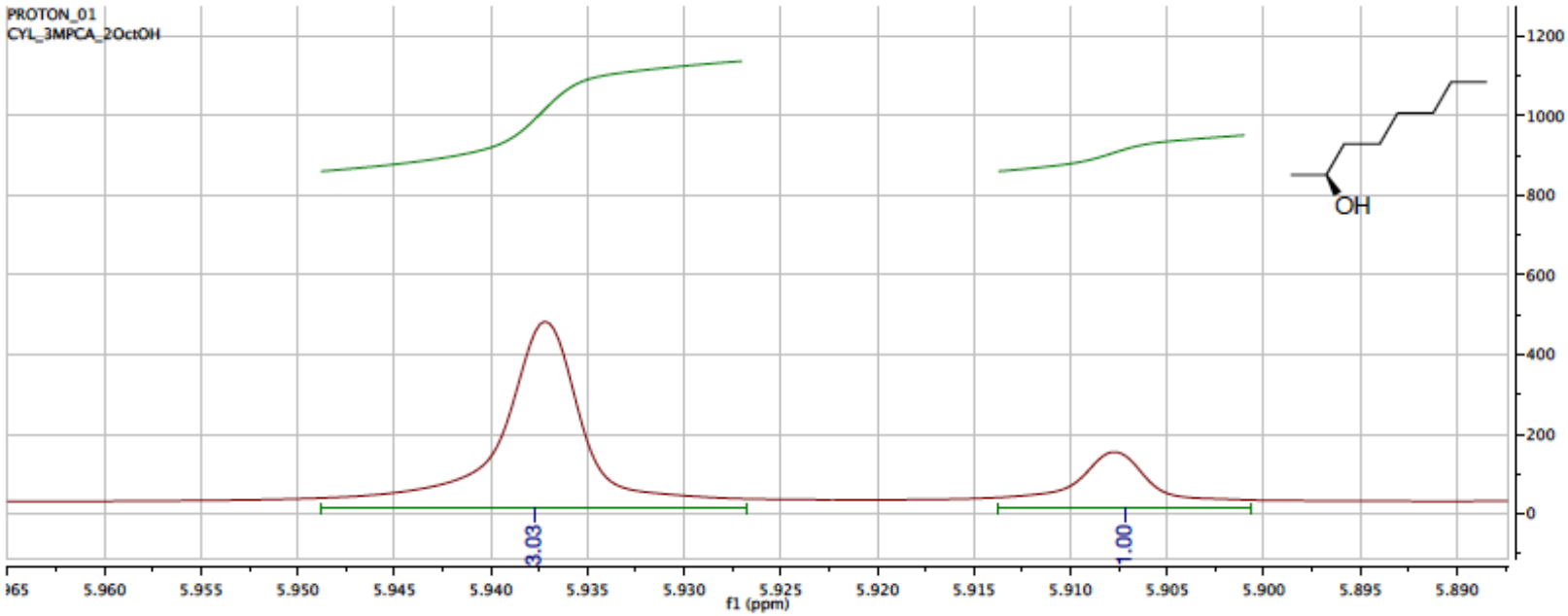


**Figure 3.40** [1]HNMR spectrum of 2-octanol with 3-methylpyridine-2-carbaldehyde assembly.

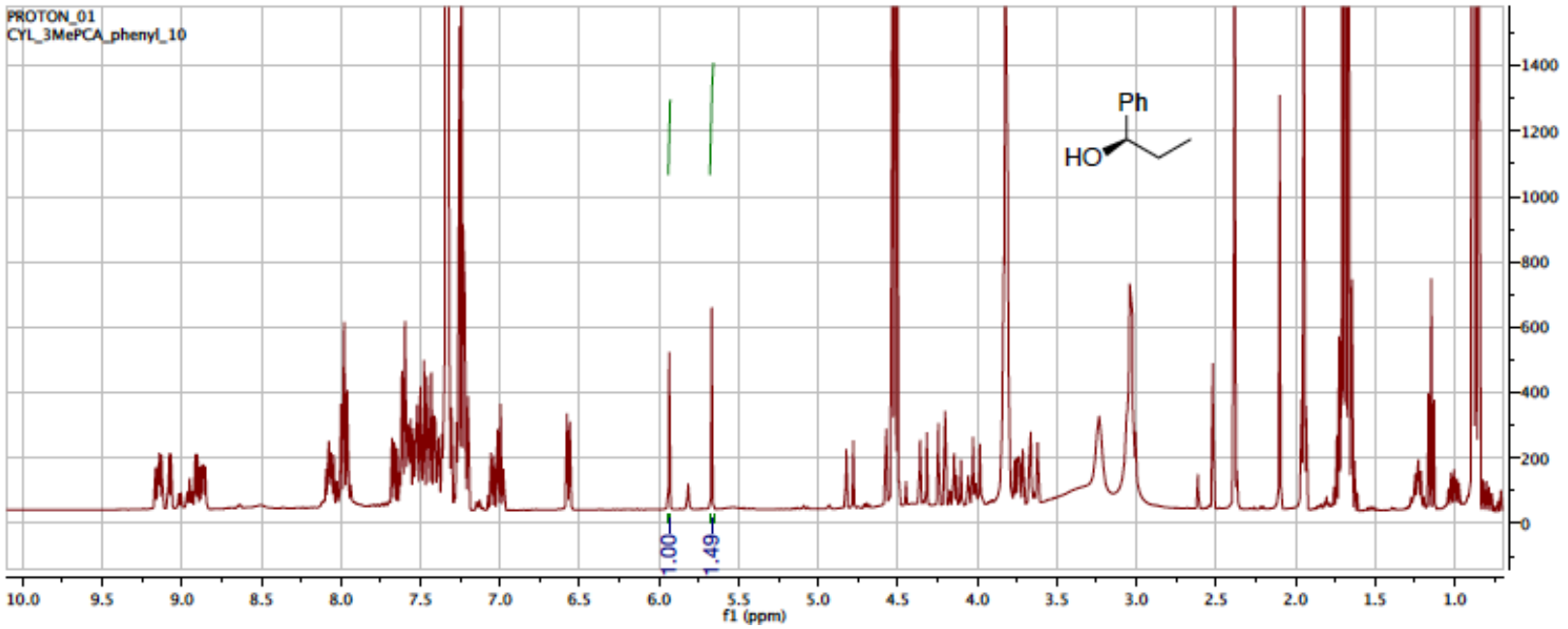


**Figure 3.41** [1]HNMR spectrum of 1-phenylpropranol with 3-methylpyridine-2-carbaldehyde assembly.

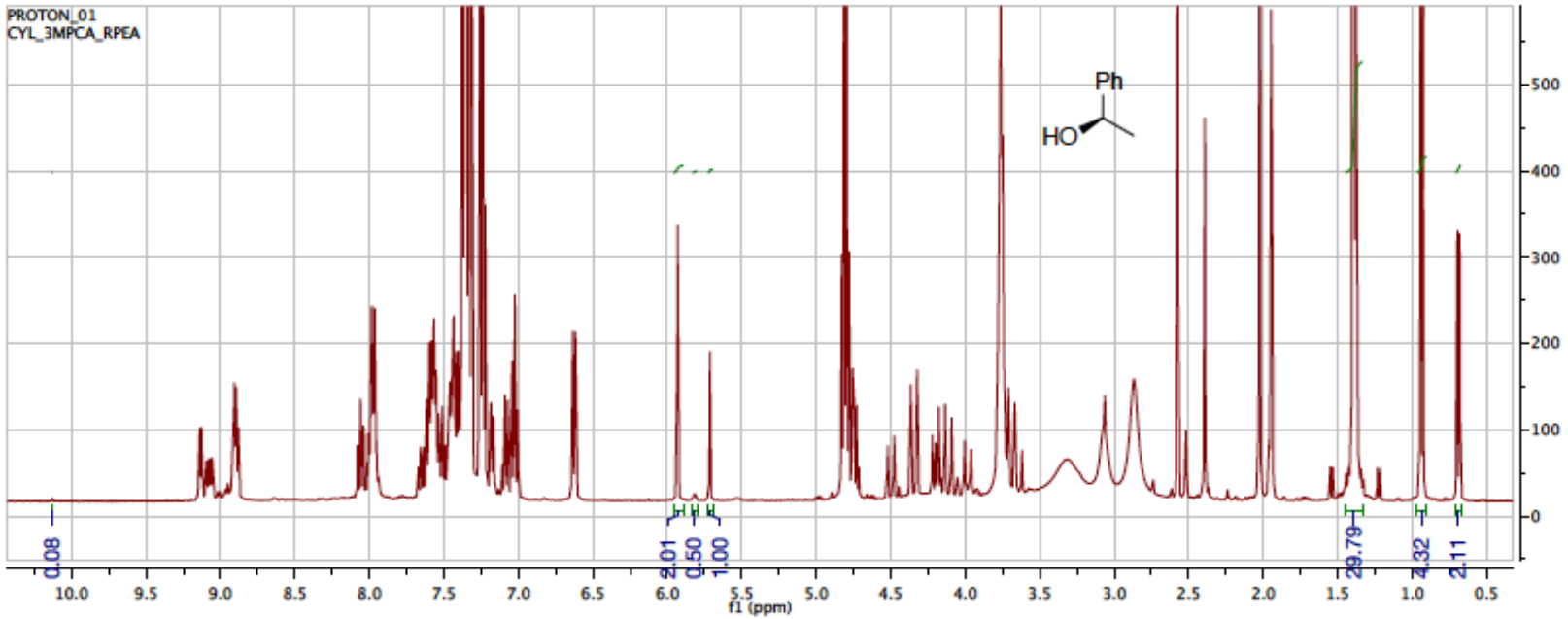


**Figure 3.41** [1]HNMR spectrum of 1-phenylethanol with 3-methylpyridine-2-carbaldehyde assembly.

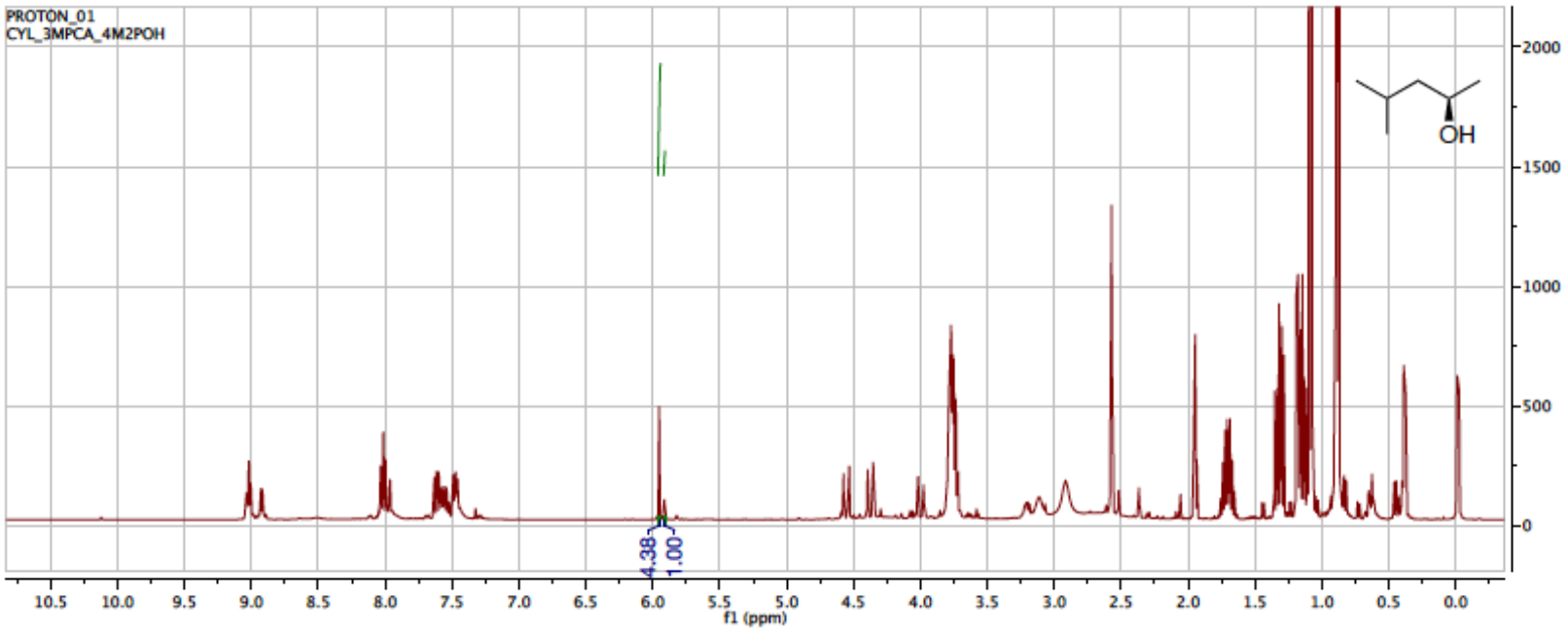


**Figure 3.42** [1]HNMR spectrum of 4-methyl-2-pentenol with 3-methylpyridine-2-carbaldehyde assembly.

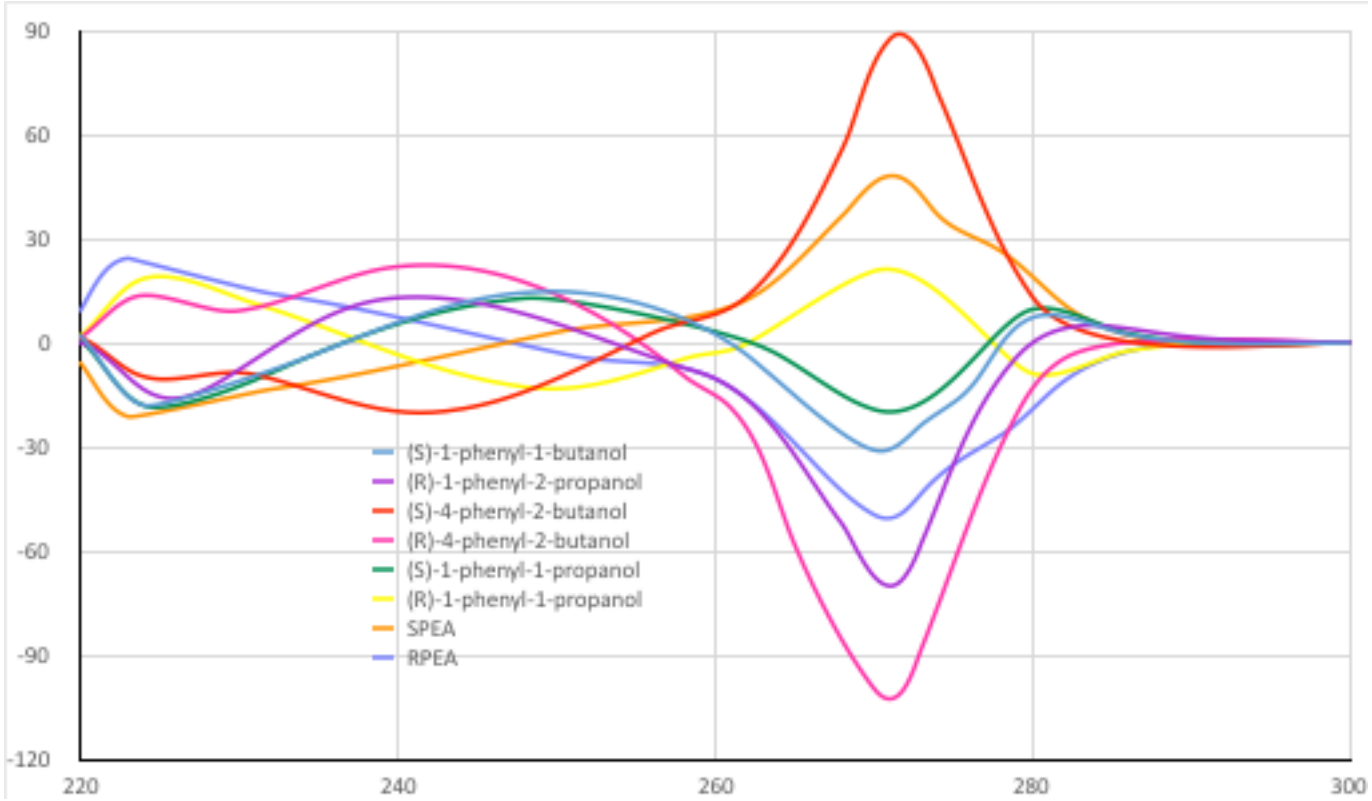


**Figure 3.43** CD spectra of R and S alcohols in 3-methypyridine-2-carbaldehyde assembly. The alcohols includes 1-phenyl-1-butanol, 1-phenyl-2-propanol, 4-phenyl-2-butanol,1-phenyl-1-propanol, and 1-phenylethanol.

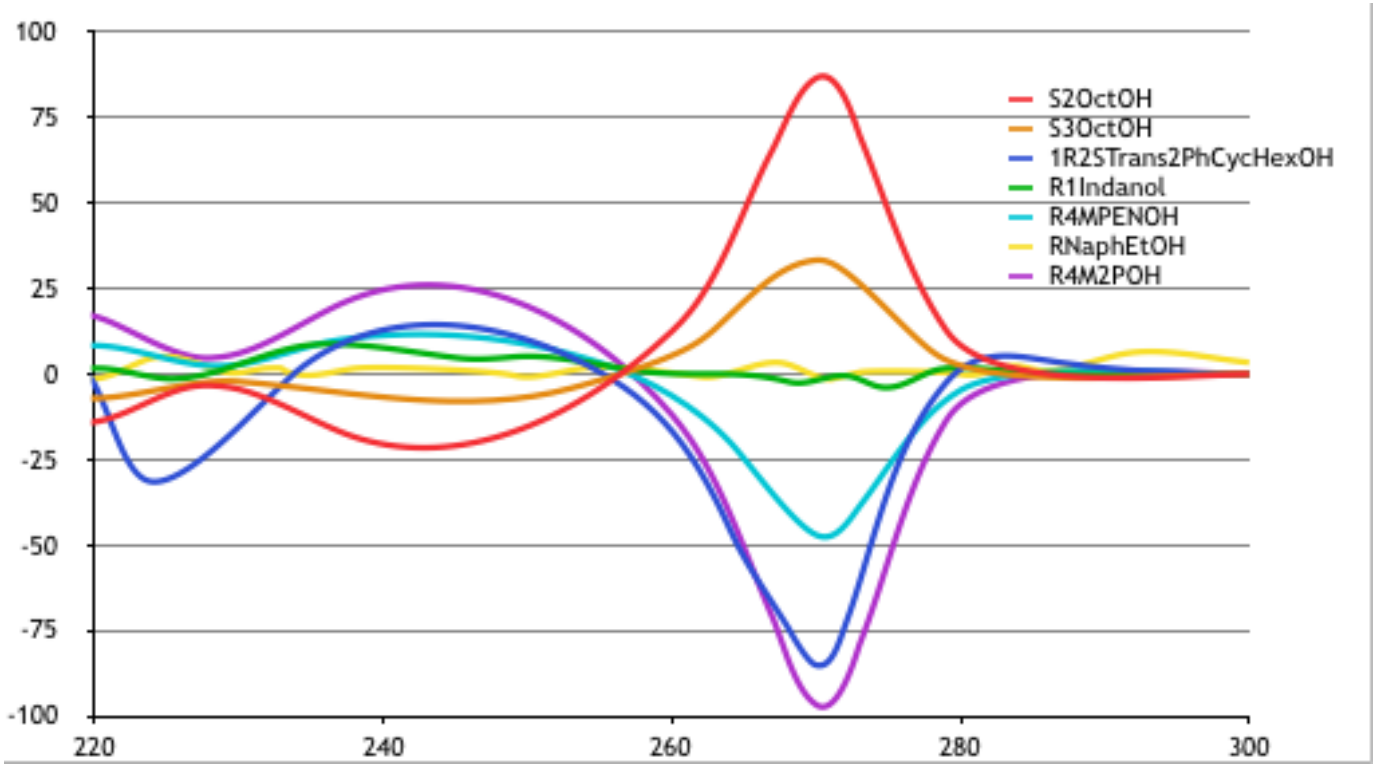


**Figure 3.44** CD spectra of R and/or S alcohols in 3-methypyridine-2-carbaldehyde assembly. The alcohols includes 2-octanol, 3-octanol, (1R,2S)-2-phenylcyclohexanol, 1-indanol, 4-methylpentenol, naphthylethanol, 4-methyl-2-pentanol.

## 5. REFERENCES


1) J. F. Traverse, J. F. Traverse, M. L. Snapper and M. L. Snapper, *Drug Discov. Today*, 2002, **7**, 1002–12.
2) G. Gübitz, *Chromatographia*, 1990, **30**, 555–564.
3) G. Subramanian, *Chiral Separation Techniques: a practical approach*, Wiley-VCH, New York, 2nd edn., 2001.
4) V. Schurig, *J. Chromatogr. A*, 2001, **906**, 275–299.
5) G. Gübitz and M. G. Schmid, *Chiral Separations: Methods and protocols*, Humana Press, Totowa, NJ, 2004.
6) C. J. Welch, M. Biba and P. Sajonz, *Chirality*, 2007, **19**, 34–43.
7) P. Sajonz, X. Gong, W. R. Leonard Jr., M. Biba and C. J. Welch, *Chirality*, 2006, **18**, 803–813.
8) E. L. Regalado, P. Zhuang, Y. Chen, A. a. Makarov, W. a. Schafer, N. McGachy and C. J. Welch, *Anal. Chem.*, 2014, **86**, 805–813.
9) L. Zhu and E. V Anslyn, *J. Am. Chem. Soc.*, 2004, **126**, 3676–3677.
10) E. Holmes, D. Das and J. W. Canary, *J. Am. Chem. Soc.*, 2007, **129**, 1506–7.
11) S. H. Shabbir, L. a Joyce, G. M. da Cruz, V. M. Lynch, S. Sorey and E. V. Anslyn, *J. Am. Chem. Soc.*, 2009, **131**, 13125–31.
12) L. A. Joyce, M. S. Maynor, J. M. Dragna, G. M. da Cruz, V. M. Lynch, J. W. Canary and E. V Anslyn, *J. Am. Chem. Soc.*, 2011, **133**, 13746–52.
13) L. You, J. S. Berman and E. V Anslyn, *Nat. Chem.*, 2011, **3**, 943–948.
14) L. You, S. R. Long, V. M. Lynch and E. V Anslyn, *Chem. Eur. J.*, 2011, **17**, 11017–23.

15) L. You, G. Pescitelli, E. V Anslyn and L. Di Bari, *J. Am. Chem. Soc.*, 2012, **134**, 7117–25.

16) P. Metola, E. V. Anslyn, T. D. James and S. D. Bull, *Chem. Sci.*, 2012, **3**, 156.

17) Wolf and K. W. Bentley, *Chem. Soc. Rev.*, 2013, **42**, 5408–24.

18) K. W. Bentley and C. Wolf, *J. Am. Chem. Soc.*, 2013, **135**, 12200–12203.

19) H. H. Jo, R. Edupuganti, L. You, K. N. Dalby and E. V Anslyn, *Chem. Sci.*, 2015, **6**, 158–164.

20) J. G. Aston, S. C. Shumann, H. L. Fink and P. M. Doty, *J. Am. Chem. Soc.*, 1941, **63**, 2029–2030.

21) R. Stonard, D. A. Trainor, M. Nakatani and K. Nakanishi, *J. Am. Chem. Soc.*, 1983, **105**, 130–131.

22) M. Charton, *J. Org. Chem.*, 1978, **43**, 3995–4001.

23) M. W. Giuliano, C.-Y. Lin, D. K. Romney, S. J. Miller and E. V. Anslyn, *Adv. Synth. Catal.*, 2015, **357**, 2301–2309.

# Chapter 4

## 1.INTRODUCTION

Stereoisomers are known to possess different biological activity and reactivity, which is of special interest to the pharmaceutical industry. In the case of thalidomide,[1] the (R)-enantiomer is effective in relieving nausea, while the (S)-enantiomer is teratogenic and causes birth defects. Therefore, advancements in asymmetric synthesis have been a major focus in organic chemistry. The goal of asymmetric synthesis is to develop methods for synthetic transformations that yield high enantiomeric excesses.[2-4] In order to facilitate asymmetric syntheses, introduction of a chiral agent, usually a chiral catalyst, is needed to direct enantioselective product formation.

The traditional approach for asymmetric catalyst development starts by designing a catalyst for a transformation of interest, which is then synthesized and tested. The success of the catalyst is determined by measuring the enantiomeric excess (*ee*) of the products. Based on the results, structural changes to the catalyst are studied to optimize the *ee*. This process is repeated iteratively until a desired *ee* has been achieved. In recent years, with the advent of combinatorial chemistry and parallel synthesis, large number of asymmetric catalysts can be designed, synthesized, and tested simultaneously. This process is known as high-throughput experimentation (HTE).[5] Due to the large quantity of analytes being generated in high frequency, an analysis technique that can match the speed of HTE is crucial for maintaining efficiency.

Currently, the most popular method for enantiomeric excess determination is high performance liquid chromatography (HPLC) or supercritical fluid chromatography (SFC) with a chiral column.[6-8] Although chiral chromatographic methods are associated with relatively high accuracies, exhibiting average errors of 1 to 2%, the major drawback of these methods is the analysis time.[9] Each column can only analyze one sample at a time

and averages about 150 samples over 24 hours.[10] Efforts toward overcoming this bottleneck have attempted to multiplex HPLC columns[5,11,12] or perform multiple properly spread injections for continuous analysis.[13] These methods, however, do not achieve the desired efficiency to match HTE. In addition, chiral columns are costly and specific for different classes of analytes. For these reasons, there is a need to develop a faster analysis technique for *ee* determination.

Optical spectroscopy techniques like circular dichroism (CD) spectroscopy are attractive due to their short analysis time. CD is the difference in absorbance between right and left circularly polarized light by a chiral analyte.[14] One form of CD is exciton-coupled circular dichroism (ECCD). ECCD can be observed when two or more excited chromophores are held in proximity. As seen in **Figure 4.1**, the coupling of transitions dipoles led to the formation of two different energy levels as described by Davydov splitting.[15-16] This splitting would result in two spectra of the same sign, and often, the curves add constructively to each other yielding a single local maximum with twice the magnitude. In addition, a defining characteristic of ECCD is bisignate curves referred to as Cotton effects.[17] When the bisignate curve has a negative slope at the longest wavelength of the signal (**Figure 4.1b** top), it is designated as a positive Cotton effect. Similarly, a negative Cotton effect refers to a positive slope at the longest wavelength. In addition to these properties, Cotton effects are associated with the absolute configuration of chiral species (*i.e.* when the chromophores are arranged clockwise, a positive Cotton effect is observed). Lastly, another feature of the Cotton effect is that the point where the signal crosses the x-axis corresponds to the UV-Vis absorbance maximum of the chormophores (**Figure 4.1b** bottom).

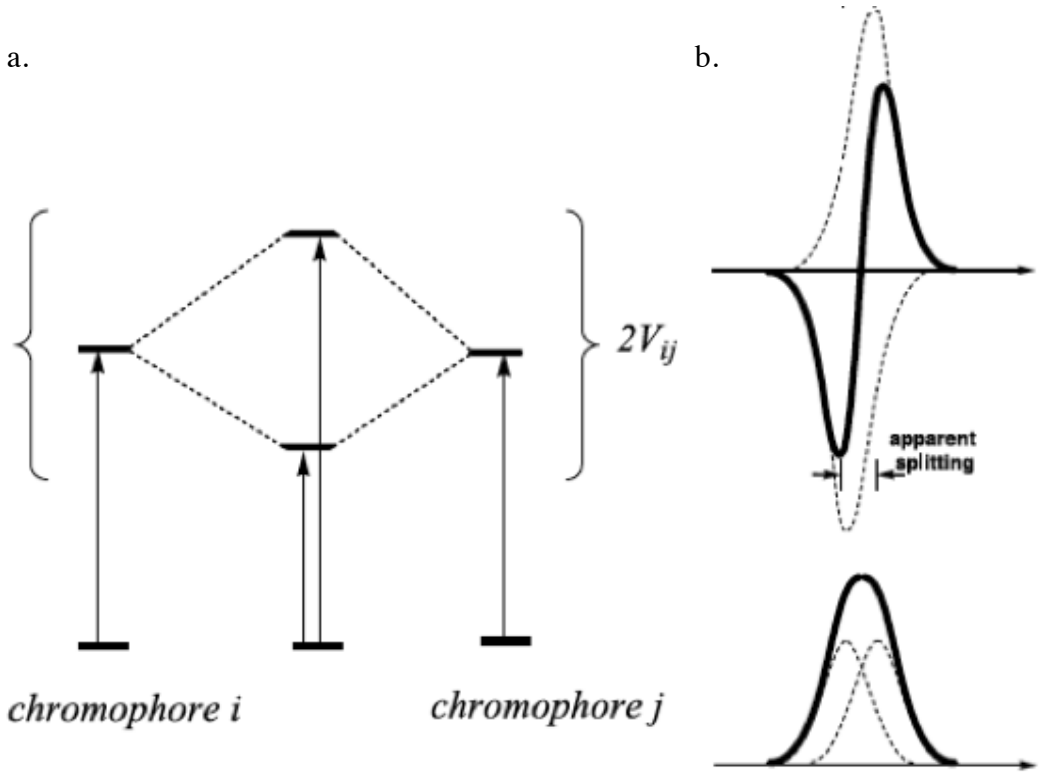


**Figure 4.1** a) Davydov splitting, observed when two chromphores *i* and *j* are coupled. b) The ECCD spectrum (top) and the UV-Vis spectrum (bottom) of a coupled excited system with two identical

Assays to determine enantiomeric excess that utilize ECCD have been investigated by several research groups.[18-29] One example of a chiral host system, developed by the Canary group, uses a bisquinoline host complex for chiral primary amine absolute configuration determination (**Scheme 4.1**).[19] The host helical twist was found to be dependent on the substituents and on the presence of a chelating moiety at the stereocenter. In addition to using quinoline as the host chromophores, Canary and coworkers further derivatized the chromophores by attaching a porphyrin on the ligands.[21] This extension in conjugation not only gives a drastically larger ECCD signal but also a bathochromic shift of the absorption maximum.

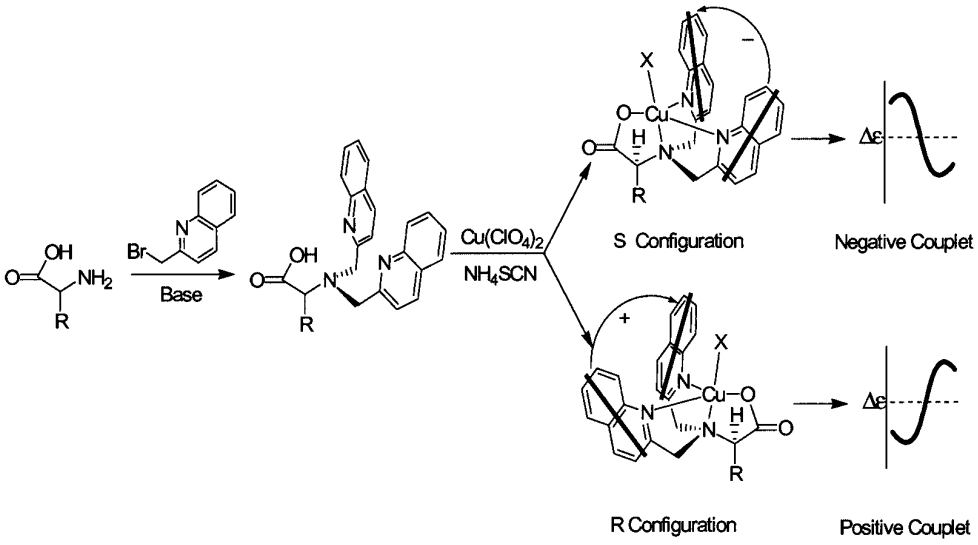


**Scheme 4.1** Chiral primary amine absolute configuration determination complex developed by Canary.

Recently, our group has developed several ECCD-based optical enantiomeric excess sensing techniques for chiral carboxylate, amine, and alcohol moieties.[30-32] The chiral carboxylate sensing method, done in collaboration with the Canary group, involves binding of a chiral carboxylate guest with the achiral [(BQPA)$Cu^{II}$] host **1**. The binding event of a chiral host induces chirality in the achiral complex (**Scheme 4.2**). Such a phenomenon was first described by Pfeiffer for resolution of chiral coordination complexes.[33] The incorporation of a chiral guest to a racemic metal complex perturbs the equilibrium of enantiomeric complexes. As a result, one of the newly formed diastereomeric metal complexes is preferred. In the case of host **1**, the binding of a chiral carboxylate results in the preferential formation of one of the helices. This detection system was able to rapidly determine the *ee* and absolute configuration of chiral carboxylates with an average error of 3%.

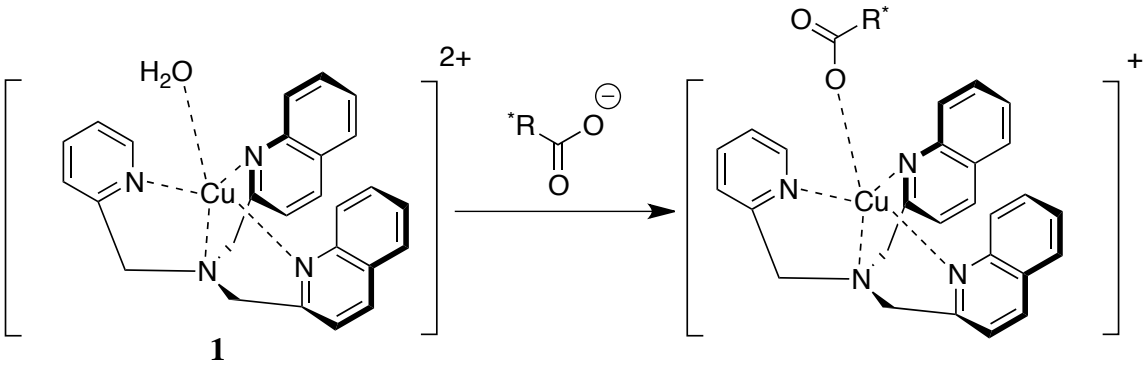


**Scheme 4.2** Chirality is transferred to the achiral carboxylate-sensing host upon coordination of the chiral analyte.

The chiral alcohol assay involved a multi-component assembly formed under equilibrium conditions followed by an acid-promoted hemiaminal ether formation (**Scheme 4.3**). Similar to the biasing towards one diastereomeric carboxylate host complex shown in **Figure 3**, the same scenario is observed for the chiral alcohol assembly. Depending on the enantiomer of the chiral alcohol used in the hemiaminal ether formation, one of the diastereomeric host assemblies is formed preferentially. The chiral alcohol assembly was found to be able to perform *ee* analyses and absolute configuration designation.

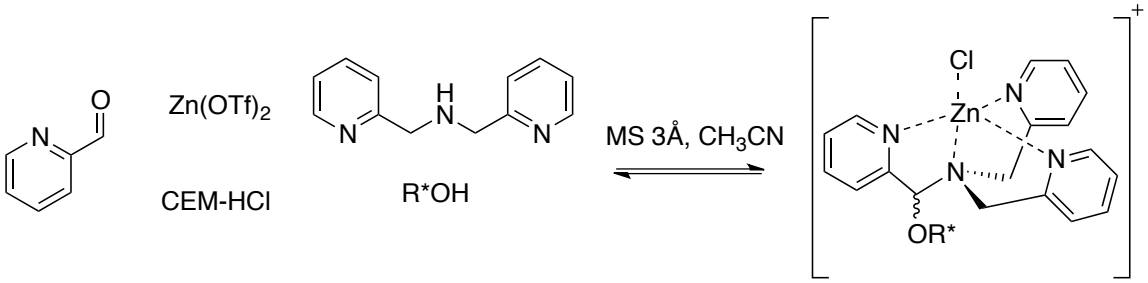


**2**

**Scheme 4.3** Formation of the multicomponent alcohol assembly; the incorporation of chiral alcohol to the assembly is promoted by CEM-HCl.

The goal of research described herein is to develop a fast and reliable screening method for enantiomeric excess determination of various chiral analytes. Specifically, further studies are required for demonstrating flexibility and improving the analytical power of our group's general strategies. To test the applicability of our chiral carboxylate host, this project seeks to use this host for analysis of nonclassical chiral carboxylates. Up to this point, only point chiral molecules have been used to demonstrate the carboxylate *ee* sensing capability of our host. It is hypothesized that nonclassical (*e.g.* axial or planar) chiral carboxylates will behave similarly to classical chiral carboxylates and impart the same perturbation in the equilibrium of the two helices. To test this hyphothesis, a biphenyl-based axial chiral carboxylate and a ferrocene-based planar chiral carboxylate are to be synthesized and analyzed using the assay shown in **Scheme 4.2**.

For improvement of analytical power of the chiral alcohol sensing method, the research aims to enhance the ECCD signal of the hemiaminal ether alcohol assembly shown in **Scheme 4.3**. First, signal enhancement by further perturbation of equilibrium was explored. This was carried out by introducing a second chiral analyte to the assembly. Similar to the case of **1**, because of the open coordination site on **2**, it was hypothesized that introducing chirality through coordination would alter the equilibrium of diastereomers. The scenario in which the second chiral analyte favors the same helicity as the chiral alcohol would result in an enrichment of the predominant diastereomer. Hence, a larger ECCD signal for the corresponding helicity was anticipated. In addition, the project seeks to enhance the ECCD signal through extending ligand conjugation or attaching chromophores  We hypothesized that extending conjugation would result in enhanced an ECCD signal.[21] Previous work on the alcohol complex has shown that steric factors, specifically Charton steric parameters, of the chiral alcohol substituents have high predictive power for diastereomeric ratio (*dr*).[32] This dependence should become more

apparent as the steric bulk of the ligands increases, thus resulting in increased sensitivity to small substituent steric differences of the analyte.

## 2. Results and Discussion

### 2.1 Non-classical Chiral Analyte Applicability

#### *2.1.1 Synthesis of Planar Chiral Ferrocene Carboxylic Acid*

Methylated ferrocene carboxylic acid was synthesized and esterified in moderate yield from commercially available materials following closely to the procedures of Breuninger *et al*. and Weissensteiner *et al*. (**Scheme 4.4**).[34-35] Column chromatography of diastereomeric ferrocene esters yielded fractions with *dr* ranging from 95:5 to 1:39. The separated diastereomeric ferrocene esters was saponified to give the methylated ferrocene carboxylic acid at various *ee*.

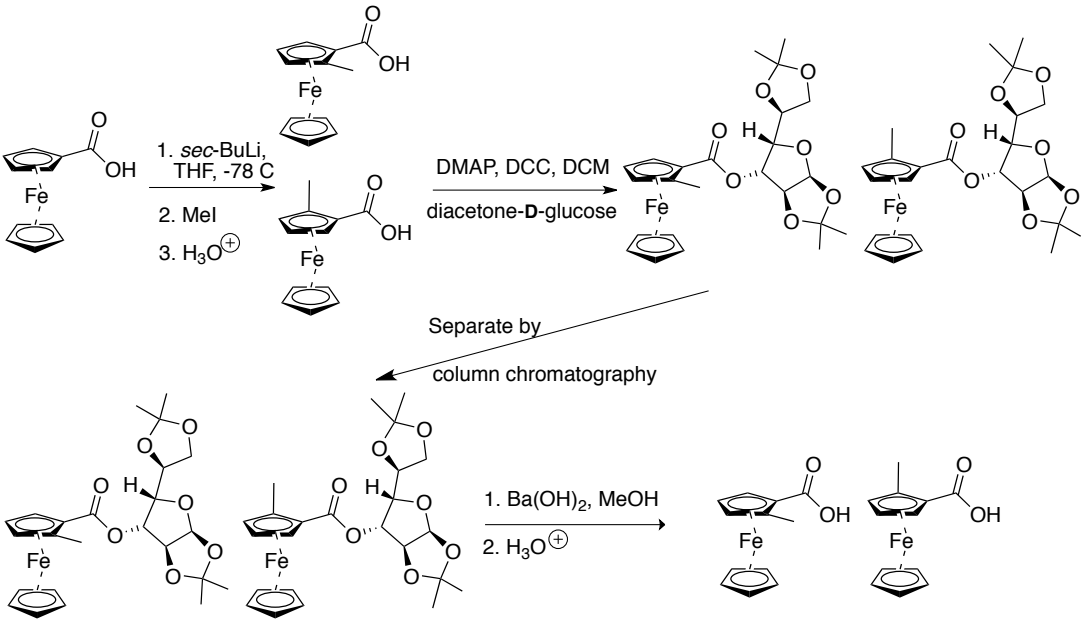


**Scheme 4.4** Synthetic route for planar chiral ferrocene carboxylic acid.

### *2.1.2 CD Analysis of Planar Chiral Ferrocene Carboxylic Acid*

The synthesized planar chiral ferrocene carboxylic acid was subjected to the chiral carboxylate sensor. The CD signal of the chiral ferrocene overlapped and overwhelmed the CD signal of the [(BQPA)$Cu^{II}$] host. Further investigation of less CD active non-classical chiral species such as allene is needed.

### *2.1.3 CD Analysis of Axial Chiral Biphenyl Carboxylic Acid*

The analytes were prepared by the Miller group at Yale and analyte *ee* was confirmed with chiral HPLC spectra (**Figure 4.2**). Carboxylate hosts were prepared following our previously established protocol.[30] Because carboxylic acid **3** has a CD signal near carboxylate host ECCD signal, excess of **3** would cause the $\lambda_{max}$ to change. To avoid this, the CD spectra were recorded at one to one equivalent between host **1** and carboxylic acid **3** (**Figure 4.3a**). The carboxylate **3** has $\lambda_{max}$ of 236 nm. Even at one equivalent the effect of 3 can be seen as made evident by the shift of $\lambda_{max.}$ Though this might be problematic, the linearity between CD at 291nm and the *ee* was confirmed as seen in **Figure 4.3b**. This linearity agreed with our hypothesis that the chirality of a nonclassical chiral molecule can be transferred to an achiral host via coordination.

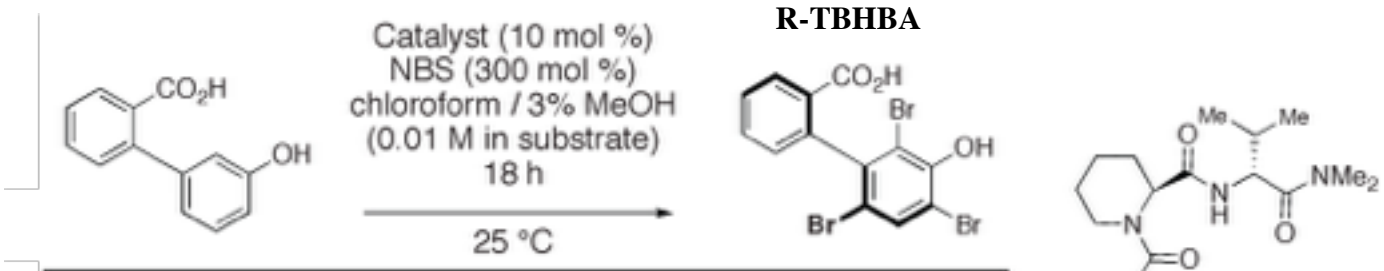


| Entry | Catalyst | Yield (%) | E.r. |
|---|---|---|---|
| 1 | Boc-β-Dmaa-Pro-(D)Val-(*R*)-αMba | 90 | 75.0:25.0 |
| 2 | Boc-β-Dmaa-Pip-(D)Val-(*R*)-αMba | 87 | 90.0:10.0 |
| 3 | Boc-β-Dmaa-Pip-(D)Phe-(*R*)-αMba | 73 | 86.5:13.5 |
| 4 | Boc–β-Dmaa-Pip-(D)Tle-(*R*)-αMba | 85 | 89.0:11.0 |
| 5 | Boc-β-Dmaa-Pip-(D)Ile-(*R*)-αMba | 65 | 82.5:17.5 |
| 6 | Boc-β-Dmaa-Pip-(L)Val-(*R*)-αMba | 95 | 75.0:25.0 |
| 7 | Boc-β-Dmaa-Pip-(D)Val-(*S*)-αMba | 80 | 75.0:25.0 |
| 8 | Boc-β-Dmaa-Pip-(D)Val-$NMe_2$ | 90 | **92.0:8.0** |
| 9 | Boc-β-Dmaa-Pip-(D)Val-OMe | 90 | 65.0:35.0 |

**Figure 4.2** The brominated axial chiral biphenyl carboxylic acid prepared by Miller group. The R stereoisomer is shown in the figure.

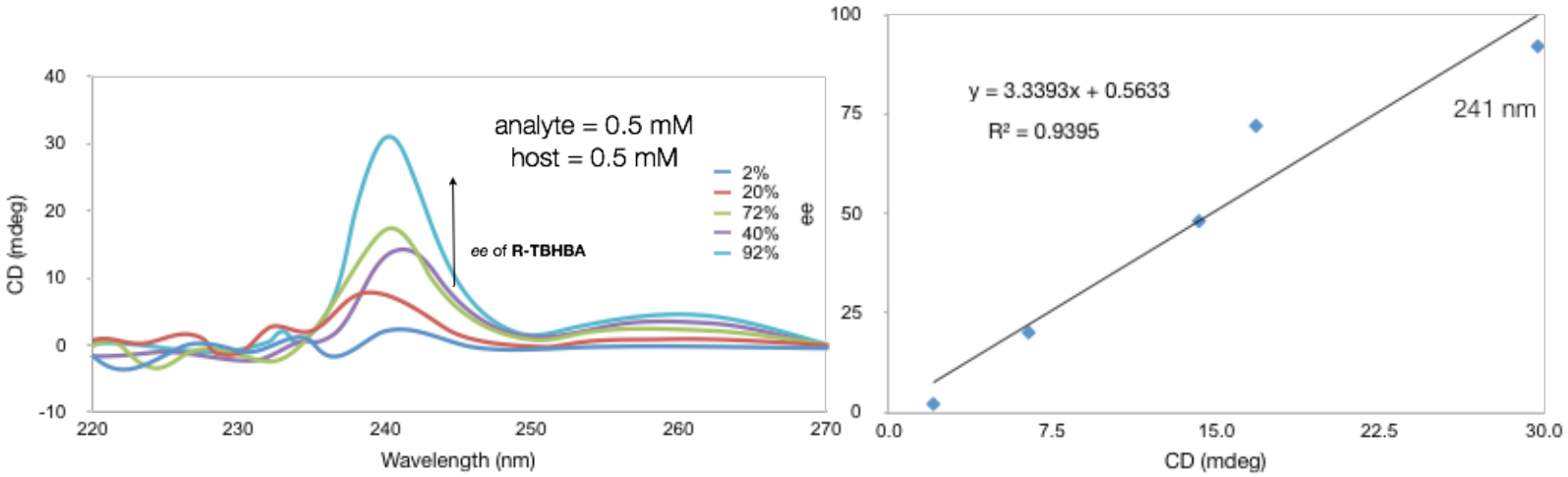


**Figure 4.3** a) CD spectra of each carboxylic acid samples. The spectra were taken with **1** (0.5mM) and **3** (0.5mM) in HEPES buffer (75% acetonitrile, 25% water) at pH 7.4. b) *ee* of the solution plotted against the CD spectrum at 239 nm.

## 2.2 Signal Enhancement Through Second Chiral Analyte Induction

The chiral alcohol multicomponent assembly (**Scheme 4.3, 2**) was formed at 50 mM following a published procedure with (S)-1-phenylethanol as the chiral alcohol.[31] The following experiments were monitored using $^{1}$H NMR and mass spectrometry (MS). Previous work had demonstrated success in transferring chirality by coordination using chiral carboxylates,[30] thus chiral carboxylates were investigated as a possible candidate for this purpose. Because of the acidic nature of assembly formation conditions, assemblies were subjected to 2 equivalents of base to favor the formation of carboxylates. The $^{1}$H NMR results showed that the assembly remained intact after addition of Hünig's base and 2,6-lutidine. Once the assembly stability under basic conditions was confirmed, the effect of chiral carboxylate coordination was investigated. To test this, samples were prepared with 2 equivalents of Hünig's base followed by addition of (S)-2-phenylpropanoic acid (0.25 to 1.5 equiv. at 0.25 increment). A small upfield shift of the hemiaminal ether methine was observed upon the initial addition of carboxylic acid. However, this shift did not persist with addition of more equivalents of acid. Moreover, MS studies on the samples showed no corresponding mass for the carboxylate coordinated hemiaminal ether assembly. This apparent change in assembly environment without carboxylate coordination could be explained through additional hydrogen bonding made possible by the introduction acid. Since there was a lack of coordination activity with carboxylates, amines were investigated as possible candidates to coordinate. As seen in **Table 1,** the MS results show no apparent coordinating activity. Interestingly, the mass indicative of aminal formation was found in the MS study with (R)-3,3-dimethyl-2-butylamine. Carboxylic acids could behave similarly leading to the formation of hemiaminal esters, which was examined by subjecting several carboxylic acids to host **2** in the absence of alcohol. Not surprisingly, MS studies

confirmed that the less nucleophilic carboxylic acids did not form hemiaminal esters. Lastly, chiral anionic acids were used as acid promoters for hemiaminal ether formation. By using a chiral anionic acid, such as shown on the last two rows of **Table 4.1**, which is itself chiral, the additional introduction of a second chiral analyte was avoided. The MS results showed no corresponding mass with coordinated chiral anions, which can be explained by the sterically hindered chiral anions making the coordination to the assembly unfavorable.

| Species | Equivalents | Result |
|---|---|---|
| Hünig's base<br>2,6-Lutidine | 2 | Complex remained intact |
| Hünig's base + (S)-2-phenylpropanoic acid | 2 of base and 0.25-1.5 (0.25 increment) | No corresponding mass |
| DBU<br>alpha-methylbenzylamine<br>(R)-3,3-dimethyl-2-butylamine<br>N,N-dimethylaniline | 2 | No corresponding mass |
| Isobutyric acid<br>Pentenoic acid<br>3-chloropropanoic acid | 2 | No corresponding mass |
| (R) and (S)-1,1'-binaphthyl-2,2'-diyl-hydrogenphosphate | 1 | No corresponding mass |
| Camphorsulfonic acid | 1 | No corresponding mass |

**Table 4.1** Results of studies for second analyte introduction to chiral alcohol assembly.

## 2.3 Dynamic Range Enhancement Through Ligand Alteration

### *2.3.1 Heterocyclic Ligand Syntheses*

In order to test whether ligand conjugation extension would result in enhanced signal, isoquinoline-1-carboxyaldehyde (**4**), phenanthridine-6-carboxyaldehyde (**5**), 1-(isoquinolin-1-yl)-*N*-(pyridin-2-ylmethyl)methanamine (**7**), 1-(pyridin-2-yl)-*N*-(quinolin-2-ylmethyl)methanamine (**8**), and bis(quinolin-2-ylmethyl)amine (**9**) were synthesized with satisfactory to low yields following literature procedures (**Scheme 4.5**).[36-42] The synthesized heterocyclic ligands were then subjected to assembly formation conditions.

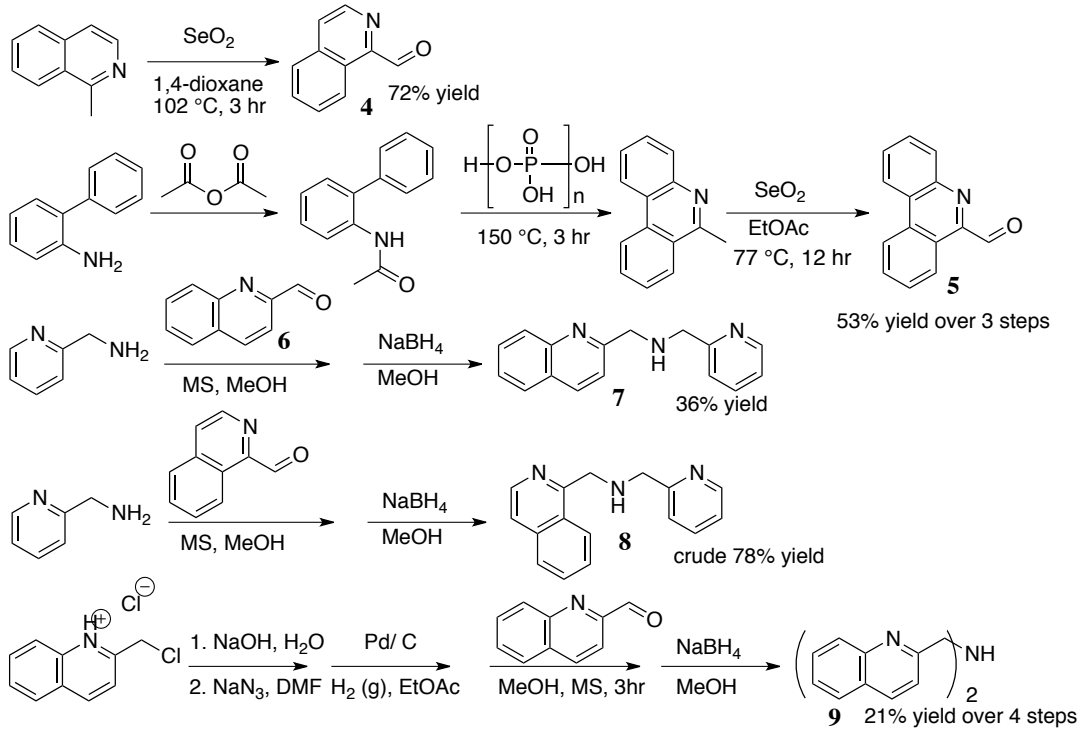


**Scheme 4.5** Synthetic routes for ligands with extended conjugation.

### *2.3.2 Multicomponent Assembly Formation with Extended-Conjugation Ligands*

To test the signal enhancement hypothesis through ligand conjugation extension, the synthesized ligands were used to form different combinations of the multicomponent assemblies following a published protocol.[31] The complex formation was confirmed by MS. Amine **7** was found to be poorly soluble in the complex formation solvent (acetonitrile), therefore complex formation with **7** was not attempted. As seen in **Figure 7**, all the attempted complexes formed except **ZnPhenDPA** and **ZnQQP**. This result can be attributed to the hydrogen on the 4 position of aldehyde **5** blocking the coordination center Zn metal (hydrogen shown in **Scheme 4.6** for clarity). Similarly, for complex **ZnQQPA**, the hydrogens from aldehyde **6** and amine **7** (both shown in **Scheme 4.6**) are both within the vicinity of Zn, thereby inhibiting complex formation.

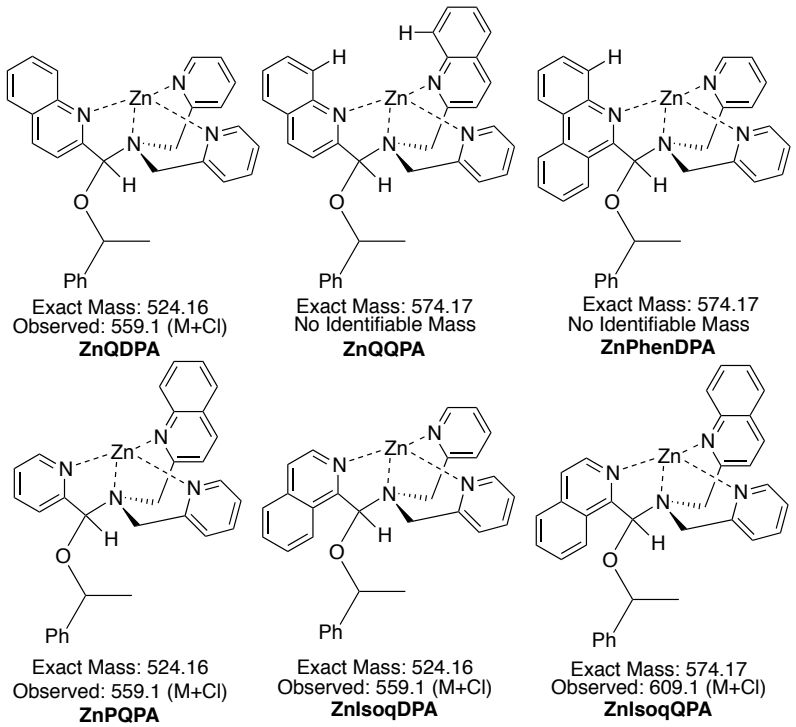


**Scheme 4.6** Extended conjugation ligand complex formation and MS study results.

Once the formation of the complexes had been confirmed by MS, CD studies were carried out with the newly formed complexes. No significant signal strength from the CD studies was observed except with complex **ZnIsoqQPA** (**Figure 4.4** right). Further investigation using $^{1}$H NMR showed that the alcohol incorporation rate for **ZnIsoqQPA** was 43%, while incorporation ranged from 1 to 6% for the other complexes. This minimal hemiaminal ether formation suggests that the majority of our host remained as racemates thus leading to the observed low CD signal. With the alcohol incorporation rate normally at around 90% for host **2**, the CD signal observed for **ZnIsoqQPA** agrees with our hypothesis (**Figure 4.4** left). The extended ligand size enhanced the sensitivity of analyte substituent sterics. This heightened sensitivity resulted a larger CD signal at low hemiaminal ether formation.

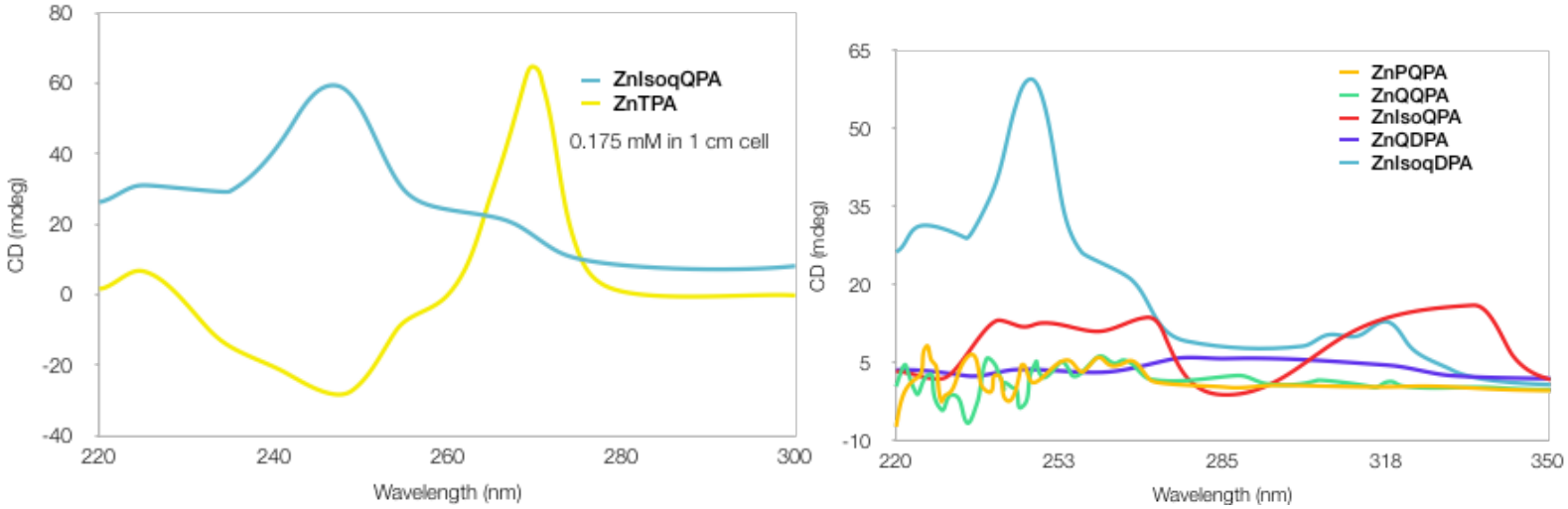


**Figure 4.4** CD spectra of complexes formed with synthesized extended conjugation ligands; the samples were prepared at 0.175 mM in acetonitrile and taken with a 1 cm cell.

### *2.3.3 Chromophoric Ligand Syntheses*

As an attempt to form the multicomponent assembly with bathochromic $CD_{max}$, we turned our attention to installing pyridine-2-carbaldehyde ligands on chromophores. Several chromophores were synthesized as potential ligands for this purpose including fluorescein, rhodamine, 4,4-difluoro-4-bora-3a,4a-diaza-s-indacene (BODIPY), and coumarin (**Scheme 4.6**, **4.7**, and **4.8**).[43-45] Fluorescein and rhodamine were scrapped due to poor solubility, and coumarin dyes were found to degrade under the assembly formation conditions.

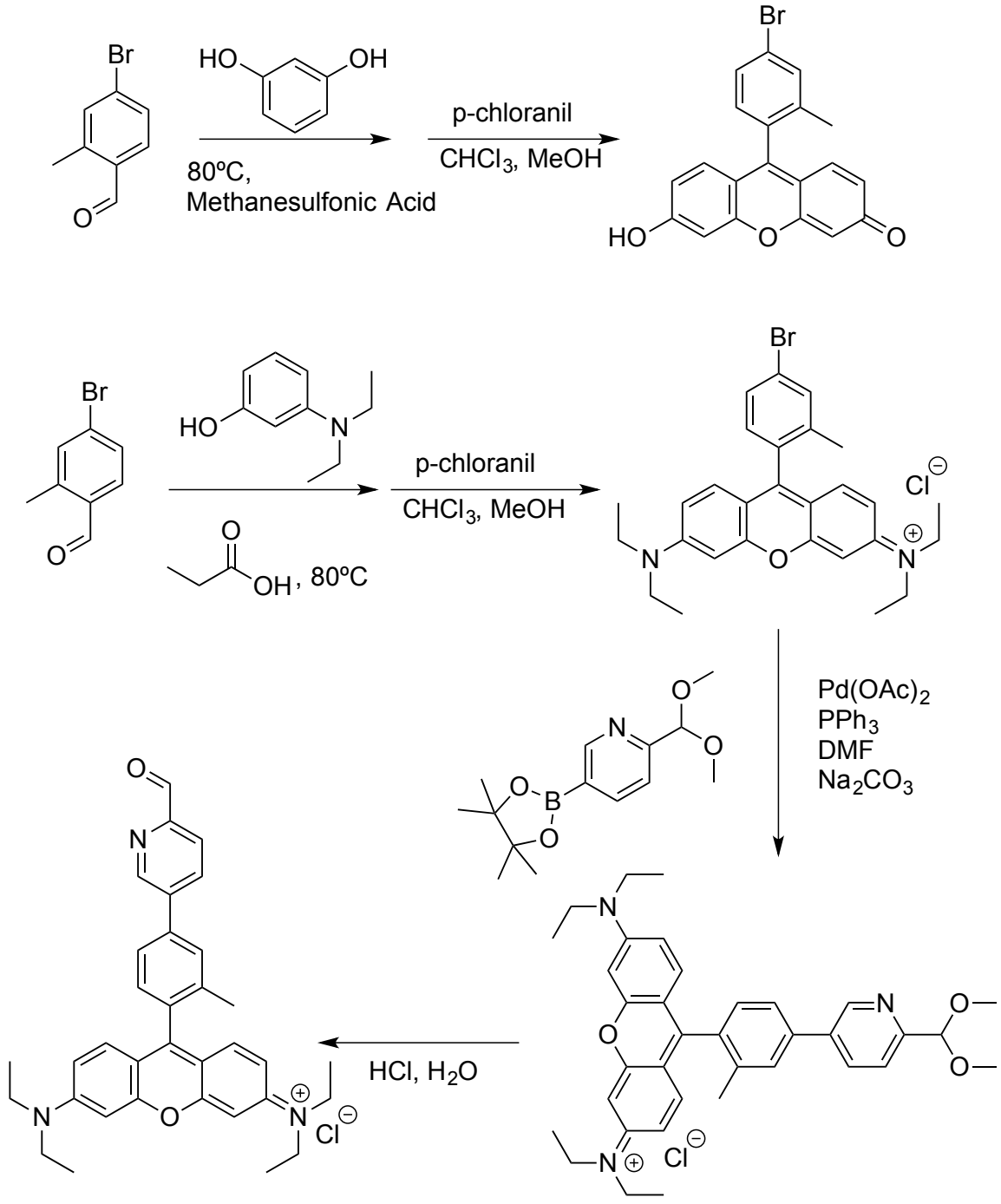


**Scheme 4.6** Synthetic routes for the bromofluorescein and pyridylrhodamine dye.

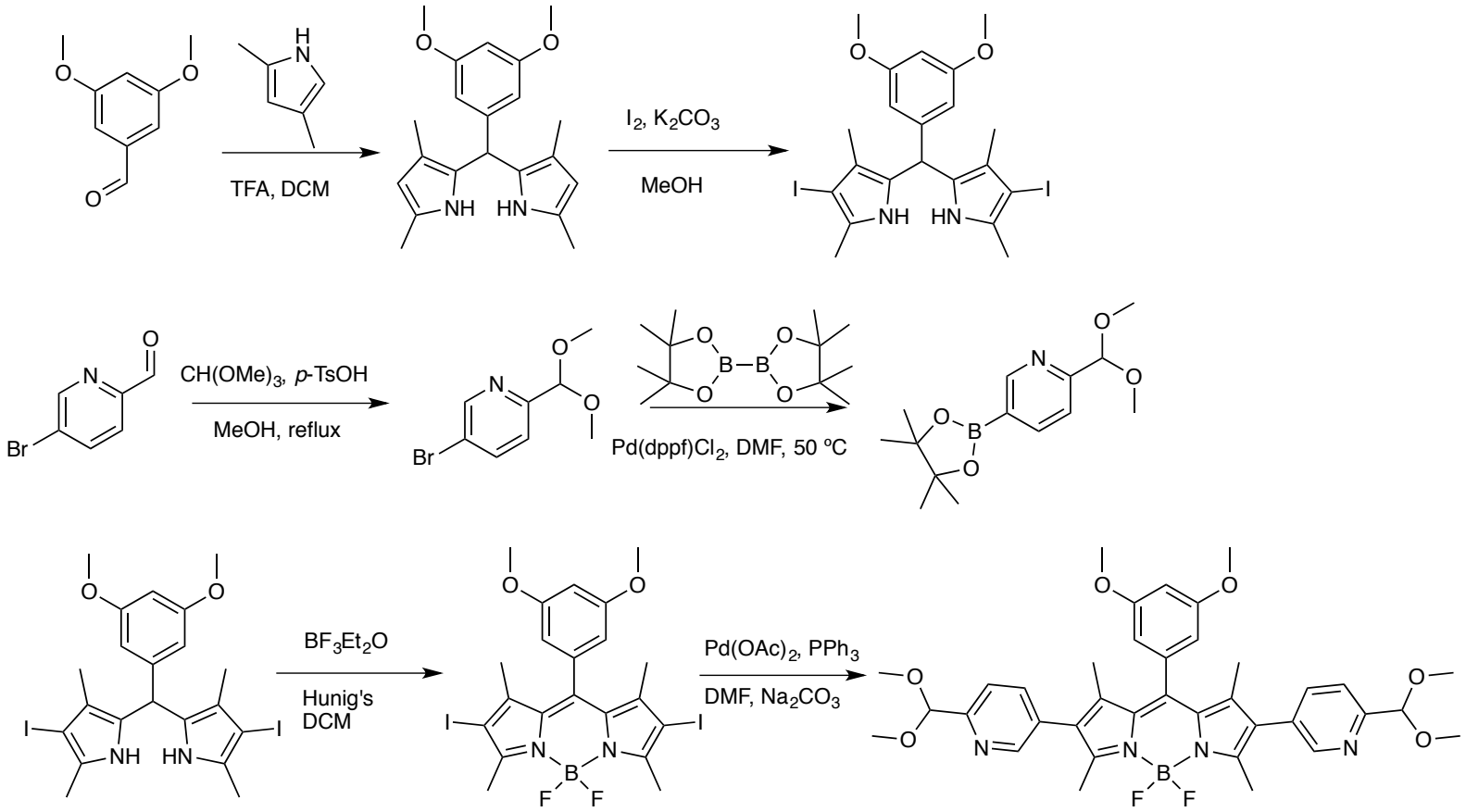


**Scheme 4.7** Synthetic route for the pyridyl-BODIPY dye. Note the protected acetal is shown above, the deprotection step offers a way to access the mono- or the di-pyridinecarbaldehyde BODIPY dyes.

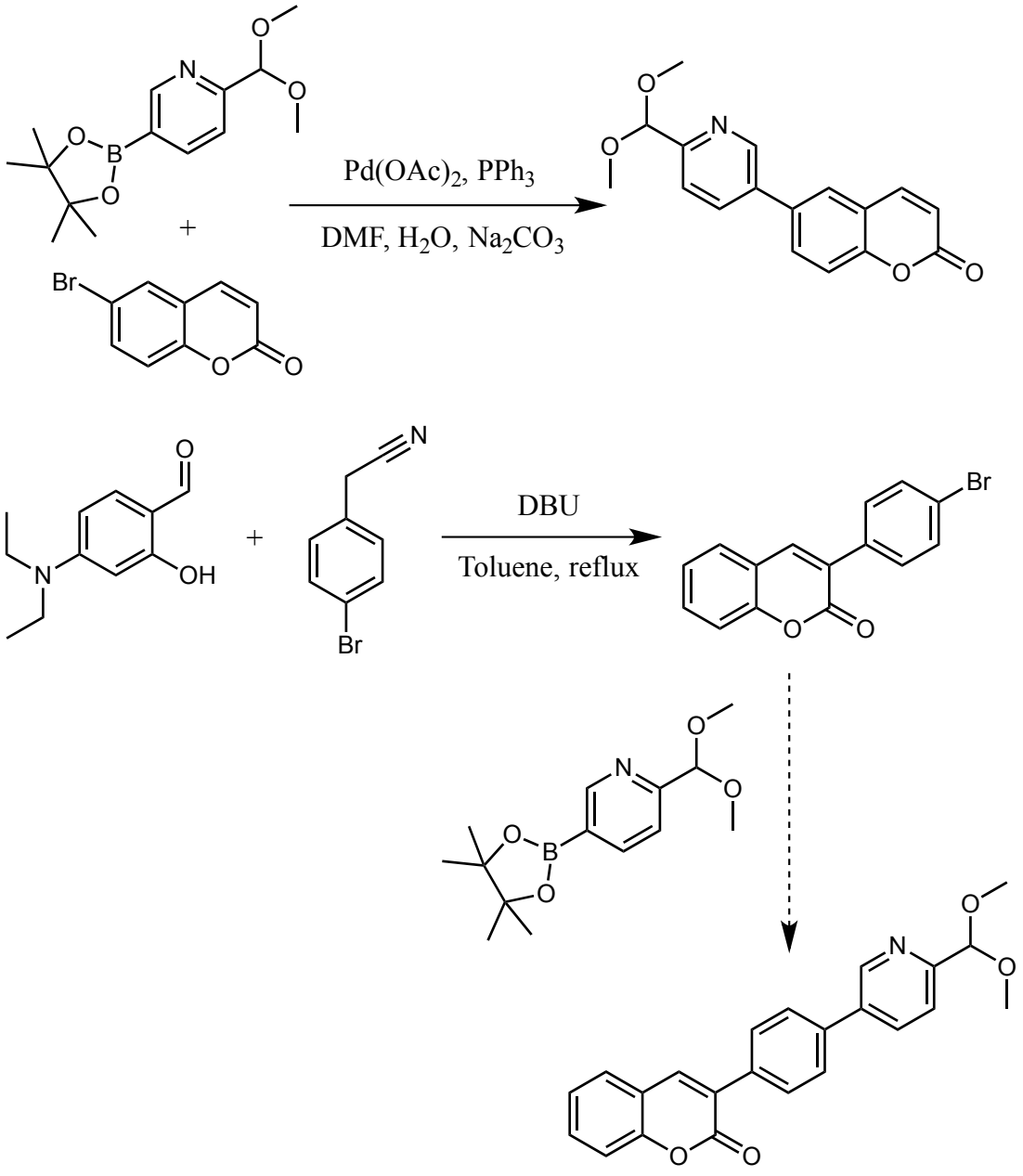


**Scheme 4.8** Synthetic routes for pyridyl-coumarin dyes. The coumarin based dyes were found to degrade under assembly formation condition, thus the synthesis was halted.

### *2.3.4 BODIPY Survivability Investigation*

Due to the presence of $Zn^{2+}$ and CEM-HCl in the assembly formation condition, the elevated acidity in the solution could potentially be deleterious for BODIPY dye. To confirm the stability of the dye towards these species, the dye was subjected to the assembly formation condition and monitored with UV-VIS at 0, 2, and 24 hours time points (**Figure 4.5**). The samples were prepared with 1 mM BODIPY, 50 mM $Zn(OTf)_2$, and 50 mM CEM-HCl in acetonitrile. No significant change in absorbance was observed after subjecting the dye to $Zn^{2+}$ and CEM-HCl.

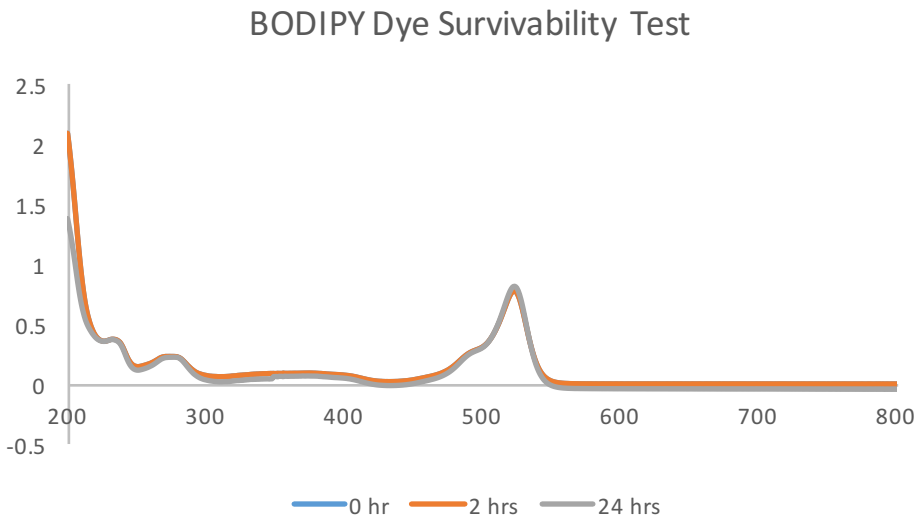


**Figure 4.5** BODIPY was subjected to CEM-HCl and $Zn^{2+}$ in acetonitrile and monitored at 0, 2, and 24 hours time points.

### *2.3.5 Assembly Formation with 5,5'-(10-(3,5-dimethoxyphenyl)-5,5-difluoro-1,3,7,9-tetramethyl-5*H*-4[$^4$,5[$^4$-dipyrrolo[1,2-*c*:2',1'-*f*][1,3,2]diazaborinine-2,8-diyl)dipicolinaldehyde (DPABODIPY)*

The synthesized **DPABODIPY** dye was subjected to the multicomponent alcohol assembly formation condition. The assembly was formed with **DPABODIPY** (1 equiv.), di-(2-picolyl)amine (**DPA**) (2.4 equiv.), $Zn(OTf)_2$ (2 equiv.), CEM-HCl (1 equiv.), and phenethylalcohol (10 equiv.) in DMSO at 50 mM. The assembly formation was monitored using $^1$HNMR. The lack of aldehyde proton peak in $^1$HNMR spectra indicated the condensation between the dye and **DPA**. Due to the complicated spectra, however, hemiaminal ether methine or hemiaminal methine proton peaks were not identified. This mixture was later found to be not CD active. Further investigation is needed to elucidate the lack of CD active species and the appropriate assembly formation conditions with **DPABODIPY**.

## 3. CONCLUSION

The chiral carboxylate array for *ee* determination using host **1** has been applied to an axial chiral molecule, and a linear relationship between the CD signal and *ee* was observed. Next, the host **1** will be applied to a planar chiral ferrocene carboxylic acid. In the future, applicability towards other nonclassical chiral molecules will be investigated. Despite the difficulties with signal enhancement through introduction of a second analyte, encouraging results were obtained from using ligands with extended conjugation. Further investigation of steric effects from the ligands will be particularly important for optimization. In addition, with the success of isoquinoline ligands, structurally similar ligands will be investigated.

## 4. EXPERIMENTAL AND CHARACTERIZATION

### 4.1 Syntheses

#### *4.1.1 Synthesis of (R)-and (S)-2-(methyl)ferrocene carboxylic acid*

This synthesis followed closely to literature procedures by Breuniger and Breit.[34] Ferrocene carboxylic acid (2.64g, 11.45 mmol) in dried THF (70 mL) was cooled to -78°C. Addition of *sec*-BuLi (22.9 mmol, 1.4 M in cyclohexane) was done over 10 minutes. The reaction was then left stirring at -78°C for 3 hours. Iodomethane (1.73g, 12.2 mmol) was added dropwise to the stirring reaction mixture, then the reaction was allowed to warm to room temperature. The reaction was left stirring in room temperature for 72 hours. The reaction was acidified with HCl (2M) until pH 2 followed by ether extraction (30 mL*5). The organic extract was dried ($MgSO_4$), filtered, and concentrated *in vacuo* to give a brown oil. The product was then purified using Combiflash Rf-200 UV-Vis Automated Flash Chromatography System with Redi*Sep*® Rf C18 reverse phase column ($H_2O$: MeCN; started at 5% MeCN end with 95% MeCN over 12 minutes). The isolated product was lyophilized to give an orange fluffy solid (1.52g, 49%yield). The purified product (0.213g, 0.77 mmol) was mixed with diacetone-**D**-glucose (0.261g, 1.00 mmol), DMAP (0.086g, 0.77 mmol), and DCC (0.191g, 0.924 mmol) in DCM (10 mL). The reaction was left stirring overnight. The reaction was filtered and concentrated *in vacuo* to give 0.212g of maroon oil (54% yield). Kinetic resolution on the esterified product was carried out on the crude product with column chromatography (silica; Hexane:EtOAc, 4:1). The *dr* of separated fractions were calculated using $^1$H NMR, and each fraction was sponified with $Ba(OH)_2$ (excess) in MeOH.

$^1$H-NMR of methylated ferrocene carboxylic acid (400MHz, $CD_3Cl_3$): δ (ppm) 2.23 (s, 3H), 4.14 (s, 5H), 4.27 (t, 1H), 4.38 (t, 1H), 4.65 (dd, 1H).

### *4.1.2 Carboxylate Host 1 Synthesis*

BQPA (0.196g, 0.5 mmol) was synthesized following literature procedure[36] and dissolved in dried MeOH (10 mL). $Cu(ClO_4)_2$ (0.185g, 0.5 mmol) was dissolved in dried MeOH (5 mL) and added dropwise to the stirring BQPA solution. After stirring for 10 minutes, the reaction was poured into $Et_2O$ (50mL), where light blue precipitate was observed. The suspension was left stirring for an hour and the precipitate was collected by vacuum filtration. Yield: 0.213 g, 65.4% yield. ESI-MS: m/z 452.22(Cu+BQPA); calculated 453.11.

### *4.1.3 Synthesis of isoquinoline-1-carboxyaldehyde 4*

The synthesis followed literature procedure by Long *et al*.[42] 1-Methylquinolin (0.300 g, 2.1 mmol) and $SeO_2$ (0.323 g, 2.91 mmol) were dissolved in 1,4-dioxane (20 mL) and refluxed for 1.5 hour under nitrogen. The reaction mixture was filtered through Celite and concentrated *in vacuo*. Product was purified using column chromatography (silica; hexanes: EtOAc, 5:1 v/v) to give 72% yield.

$^1$H-NMR (400MHz, $CD_3CN$): δ (ppm) 7.76 (m, 2H), 7.90 (m, 2H), 8.73 (d, 1H), 9.27 (m, 1H), 10.35 (s, 1H).

### *4.1.4 Synthesis of phenanthridine-6-carbaldehyde 5*

This synthesis procedure followed the protocol by Pierre and Cladwell.[38,40] 2-Aminobiphenyl (1.01 g, 5.97 mmol) was dissolved in acetic anhydride (1.52 g, 14.5 mmol) and stirred for 10 minutes. One equivalent of acetic anhydride (0.59 g, 5.97 mmol) was added to the reaction followed by 30 minutes stirring. The reaction was then poured over ice where precipitation was observed. The solids were collected by vacuum filtration and washed with water. The solids were left dried in air overnight yielding 1.12 g (89% yield). The solid (0.701 g, 3.32 mmol) was then dissolved in polyphosphoric acid (10 mL) and

stirred at 150°C for 2.5 hours. The reaction mixture was then cooled to 0°C and basified using NaOH (1M) to pH 10. The reaction was extracted with DCM (4*30 mL), dried ($MgSO_4$), then concentrated in vacuo. The product was purified with column chromatography (silica; DCM:MeOH, MeOH starting at 0% and end at 10%) to give a white/orange solid. The solid was then stirred with EtOAc (20mL) with $SeO_2$ (0.516 g, 4.65 mmol) followed by 12 hours refluxing. The reaction mixture was extracted with water (pH 4, 50mL*4) followed by basifying the aqueous layer to pH 10. The basified extract was extracted with chloroform (50 mL*4). The organic layer was dried ($MgSO_4$) and concentrated to give a white solid (0.362 g, 53% yield).

$^1$H-NMR (400MHz, $CD_3CN$): δ (ppm) 7.78 (dd, 1H), 7.82 (m, 2H), 7.91 (dd, 1H), 8.32 (m, 1H), 8.63 (m, 1H), 8.68 (m, 1H), 9.43 (dd, 1H), 10.42 (s, 1H).

### *4.1.5 Synthesis of (2-pyridylmethyl) (2-quinolylmethyl)amine 7*

This synthesis procedure followed the protocol published by Rompel and coworkers.[41] 2-quinolinecarboxyaldehyde (1.000g, 6.35 mmol) and 2-aminomethylpyridine (0.688g, 6.35 mmol) was mixed in MeOH (20 mL) with MS. The reaction was left stirring for 3 hours. Then, the reaction was filtered and cooled to 0°C followed by $NaBH_4$ (0.336 g, 8.89 mmol) addition. The reaction was then left stirring in room temperature overnight. The reaction was then acidified to pH 1 (2M HCl) and extracted with chloroform (30 mL*4). The aqueous layer was basified to pH 10 (1M NaOH) and extracted with chloroform (30 mL*4). The organic layer was concentrated *in vacuo* to give a dark maroon oil. The crude product was then purified using column chromatography (alumina, 1% MeOH in DCM) to give 0.569 g of red oil (36% yield).

$^{1}$H-NMR (400MHz, $CD_3CN$): δ (ppm) 3.94 (s, 2H), 4.07 (s, 2H), 7.02 (dd, 1H), 7.24 (d, 1H), 7.32 (td, 1H), 7.48 (td, 1H), 7.56 (td, 1H), 7.65 (dd, 1H), 7.96 (t, 1H), 8.46 (dd, 1H).

### *4.1.6 Synthesis of (2-isoquinolylmethyl) (2-pyridylmethyl)amine 8*

This synthesis procedure followed closely to the protocol published by Rompel and coworkers.[41] 2-Isoquinolinecarboxyaldehyde (0.486 g, 3.05 mmol) and 2-aminomethylpyridine (0.330 g, 3.05 mmol) was mixed in MeOH (20 mL) with MS. The reaction was left stirring for 3 hours. Then, the reaction was filtered and cooled to 0°C followed by $NaBH_4$ (0.115 g, 3.05 mmol) addition. The reaction was then left stirring in room temperature overnight. The reaction was then acidified to pH 1 (2M HCl) and extracted with chloroform (30 mL*4). The aqueous layer was basified to pH 10 (1M NaOH) and extracted with chloroform (30 mL*4). The organic layer was concentrated *in vacuo* to give a dark maroon oil (crude).

### *4.1.7 Synthesis of bis(2-quinolylmethyl)amine 9*

2-chloromethylquinoline (5.026 g, 23.47 mmol) was dissolved in DI water and then treated with 1 equivalent of NaOH (1 M). The precipitate was collected and recrystallized in hexanes. The recrystallized product was then dissolved in DMF (30mL), mixed with $NaN_3$ (7.631g, 117.4 mmol), and left stirring overnight. The reaction mixture was washed with water (30 mL) and extracted with EtOAc (30 mL *3). The organic extract was then concentrated to give about 20 mL of the product with EtOAc. Pd/C (10 wt%, 0.249 g, 2.34 mmol) was then added to the mixture, and the reaction was left stirring overnight under $H_2$ in atmosphere. The product mixture was concentrated *in vacuo* to give a purple oil. This purple oil was then mixed with 2-quinolinecarboxyaldehyde (3.689g, 23.47 mmol) and MS in MeOH (20 mL) for 3 hours. The reaction was then filtered, cooled to 0 °C, followed by

$NaBH_4$ (1.154g, 30.51 mmol) addition, and left stirring at room temperature overnight. The reaction was acidified to pH 1 (2M HCl) and extracted with chloroform (30 mL*4). The aqueous layer was then basified to pH 10 (1M NaOH) and extracted with chloroform (30 mL*4). The organic layer was dried ($MgSO_4$), filtered, and concentrated *in vacuo*. The crude product was purified using column chromatography (alumina, 1% MeOH in DCM) to yield 1.474 g (21% yield).

$^1$H-NMR (400MHz, $CD_3CN$): δ (ppm) 4.91 (s, 4H), 7.28 (d, 2H), 7.53 (dd, 2H), 7.72 (dd, 2H), 7.82 (dd, 2H), 8.07 (d, 2H), 8.14 (d, 2H).

### *4.1.8 Synthesis of 5,5'-((3,5-dimethoxyphenyl)methylene)bis(2,4-dimethyl-1*H*-pyrrole)*

3,5-dimethoxybenzaldehyde (427.1 mg, 2.57mmol), 2,4-dimethylpyrrole (514 mg, 5.40 mmol), and TFA (catalytic) was mixed in dried DCM for 24 hours under Argon. The reaction was diluted with DCM and washed with saturated $NaHCO_3$. The organic layer was dried ($MgSO_4$), filtered, and concentrated in vacuo to give a maroon oil. This crude oil was used without any purification for the next step.

### *4.1.9 Synthesis of 5,5'-((3,5-dimethoxyphenyl)methylene)bis(3-iodo-2,4-dimethyl-1*H*-pyrrole)*

The crude oil (836.8 mg) was mixed with $I_2$ (1.657 g) and $K_2CO_3$ (1.227g) in MeOH for 12 hours at 0°C. After removal of MeOH, the residue was dissolved in $CHCl_3$. The solution was then washed with saturated $Na_2S_2O_3$ (aq.) followed by drying over $MgSO_4$. The washed organic solution was concentrated in vacuo to give a brown oil (2.123 g). This crude oil was carried forward to next step without further purification.

### *4.1.10 Synthesis of 10-(3,5-dimethoxyphenyl)-5,5-difluoro-2,8-diiodo-1,3,7,9-tetramethyl-5H-4[$^4$,5[$^4$-dipyrrolo[1,2-c:2',1'-f][1,3,2]diazaborinine*

The crude brown oil (2.123 g) was dissolved in dried DCM and Hunig's base (21.93 mL). The reaction was then cooled to 0 ℃ followed by dropwise addition of $BF_3Et_2O$. The reaction was left stirring for 2 hours at 0 ℃. The reaction was quenched with $H_2O$ (20 mL) and the organic layer was washed with 2N NaOH (15 mL*3) and $H_2O$ (20 mL). The organic layer was dried ($MgSO_4$), filtered, and concentrated in vacuo to give an aubergine oil. The crude oil was purified with flash chromatography (silica; $CHCl_3$:EtOH(0.5 %), first fluorescent fraction) to give the pure dye (4% yield).

$^1$H-NMR (400MHz, $CDCl_3$): δ (ppm) 1.54 (s, 6H), 2.62 (s, 6H), 3.78 (s, 6H), 6.39 (d, 2H), 6.56 (t, 1H).

### *4.1.12 Synthesis of 5-bromo-2-(dimethoxymethyl)pyridine*

5-bromo-2-picolinaldehyde (0.5 g), p-TsOH (13 mg), and methylorthoformate (0.87 mL) were refluxed for 3 hours in dried MeOH. After the MeOH was removed, the reaction was dissolved in $CHCl_3$ and washed with sat. $NaHCO_3$. The organic layer was dried with $MgSO_4$, filtered, and concentrated in vacuo to give a yellow oil. The product was characterized with $^1$H-NMR.

$^1$H-NMR (400MHz, $CDCl_3$): δ (ppm) 3.40 (s, 6H), 5.35 (s, 1H), 7.46 (d, 1H), 7.86 (d, 1H), 8.68 (s, 1H).

### *4.1.13 Synthesis of 2-(dimethoxymethyl)-5-(4,4,5,5-tetramethyl-1,3,2-dioxaborolan-2-yl)pyridine*

5-bromo-2-(dimethoxymethyl)pyridine (412. 7 mg), Bis(pinacolato)diboron (543 mg) was mixed in DMF (10 mL, degassed) and saturated with $N_2$ for 10 min. Meanwhile, a mixture of $Pd(dppf)Cl_2$ (73 mg) and KOAc (524 mg) was °mixed in DMF (2 mL, degassed) and saturated with $N_2$ for 10 min. The two mixtures were added together and

stirred for 28 hours at 50 °C under argon. After removal of DMF, the residual was suspended in diisopropyl ether and filtered through celite. The filtrate was concentrated in vacuo and the residual was suspended in hexanes and the suspension was filtered through celite. The filtrate was concentrated in vacuo to give a light yellow oil. The product was characterized with $^1$H-NMR.

$^1$H-NMR (400MHz, $CDCl_3$): δ (ppm) 1.36 (s, 12H), 3.40 (s, 6H), 5.35 (s, 1H), 7.54 (d, 1H), 8.11 (d, 1H), 8.94 (s, 1H).

### *4.1.11 Synthesis of 2,8-bis(6-(dimethoxymethyl)pyridin-3-yl)-10-(3,5-dimethoxyphenyl)-5,5-difluoro-1,3,7,9-tetramethyl-5H-4[$^4$,5[$^4$-dipyrrolo[1,2-c:2',1'-f][1,3,2]diazaborinine*

The diiodo-BODIPY dye (30 mg) and 2-(dimethoxymethyl)-5-(4,4,5,5-tetramethyl-1,3,2-dioxaborolan-2-yl)pyridine (31.2 mg) were mixed in degassed DMF-$Na_2CO_3$ (aq.) (10 mL-2mL(2N)) followed by addition of triphenylphosphine (2.29 mg) and PdOAc (1.14 mg). The mixture was further saturated with $N_2$ for 10 min. The reaction was then left stirring for 2 hours at 70 °C under argon. After the removal of solvents, the reaction was re-suspended in DCM. The insoluable material was removed with celite and the filtrate was concentrated in vacuo to give a fluorescent red oil. The crude product was carried forward to the deprotection step without any purification.

### *4.1.12 Acetal deprotection of 2,8-bis(6-(dimethoxymethyl)pyridin-3-yl)-10-(3,5-dimethoxyphenyl)-5,5-difluoro-1,3,7,9-tetramethyl-5H-4[$^4$,5[$^4$-dipyrrolo[1,2-c:2',1'-f][1,3,2]diazaborinine*

The crude product from previous step was dissolved in 4N HCl/THF (1:1 10 mL) and stirred at room temperature for 12 hours. The mixture was diluted with $CHCl_3$ and washed with 10% $K_2CO_3$ solution and water. The organic layer was dried ($MgSO_4$), filtered, and concentrated in vacuo. The residue was purified by flash chromatography on silica gel (Hexanes:EtOAc 1:1) to give both the mono- and di- aldehyde dyes.

## 4.2 CD Analyses

### *4.2.1 CD Studies of biphenyl 3*

CD spectra were taken with Jasco J-815 CD Spectrometer with Starna Type 21 1-mm quartz cuvette at 25 °C. Buffer solutions was prepared by dissolving 4-(2-hydroxyethyl)-1-piperazineethanesolfonic acid (HEPES) in 75% acetonitrile and 25% water to give 20 mM concentration at pH= 7.4. The prepared biphenyl samples were mixed with host at 1 to 1 equivalent, and the samples made at 0.5 mM.

### *4.2.2 CD Studies of conjugation extended ligands*

CD spectra were taken with Jasco J-815 CD Spectrometer with Starna Type 21 1-cm quartz cuvette at 25 °C. The assembly was prepared by mixing pyridine-2-carbaldehye or derivative of (1 equiv.), di(2-picolyl)amine (1.2 equiv.), $Zn(OTf)_2$ (1 equiv.), chloroethylmorpholin-HCl (1 equiv.), and chiral alcohol (5 equiv.) at 50 mM aldehyde concentration in acetonitrile. The samples were diluted to 0.25 mM before taking its CD spectra.

## 5.REFERENCE


1) Blaschke, G.; Kraft, H. P.; Fickentscher, K.; Kohler, F. *Arzneimittel-Forsch* **1979**, *29-2*, 1640. b) Teo, S. K.; Colburn, W. A.; Tracewell, W. G.; Kook, K. A.; Stirling, D. I.; Jaworsky, M. S.; Scheffler, M. A.; Thomas, S. D.; Laskin, O. L. *Clin. Pharmacokinet*. **2004**, *43*, 311. 55
2) Lin, G.-Q.; Li, Y.-M.; Chan, A. S.-C. *Principles and applications of asymmetric synthesis*; John Wiley & Sons: New York, 2001.
3) Christmann, M.; Bräse, S. *Asymmetric synthesis : the essentials*; Wiley-VCH: Weinheim, 2007.

4) de Vries, J. G.; Lefort, L. *Chemistry – A European Journal* **2006**, *12*, 4722.

5) Welch, C.; Biba, M.; Sajonz, P. *Chirality*. **2007**, *19*, 34-43.

6) Gubitz, G. *Chromatographia* **1990**, *30*, 555.

7) Subramanian, G. *Chiral separation techniques : a practical approach*; 2nd completely rev. and updated ed.; Wiley-VCH: Weinheim ; New York, **2001**.

8) Schurig, V. *J Chromatogr A* **2001**, *906*, 275.

9) Gübitz, G.; Schmid, M. G. *Chiral separations : methods and protocols*; Humana Press: Totowa, N.J., 2004.

10) Traverse, J. F.; Snapper, M. L. *Drug Discov Today* **2002**, *7*, 1002.

11) Sajonz, P.; Gong, X.; Leonard, W. R., Jr.; Biba, M.; Welch, C. J. *Chirality* **2006**, *18*, 803.

12) Sajonz, P.; Schafer, W.; Gong, X.; Shultz, S.; Rosner, T.; Welch, C. *J. Chromatogr. A* **2007**, *1145*, 149.

13) Welch, C.; Gong, X.; Schafer, W.; Pratt, E.; Brkovic, T.; Pirzada, Z.; Cuff, J.; Kosjek, B. *Tetreahedron: Asym.*, **2010**, 1647-1681.

14) Nagai, Y.; Kusumi, T. *Tetrahedron Lett*. **1995**, *36*, 1853.

15) Arnold, S.; Whitten, W.; Damask, A. *Phys. Rev. B* **1971**, 3452-3457.

16) Davydov, A. S. *Theory of molecular excitons*; McGraw-Hill: New York,, 1962..

17) Berova, N.; Nakanishi, K.; Woody, R.. W. Circular Dichroism Principles and Applications. Wiley-VCH; New York, NY, 2000.

18) Jang, W.; Lee, C.; Yoon, H. *Chem. Eur. J*. **2012**, *18*, 12479-12486.

19) Holmes, A. E.; Zahn, S.; Canary, J. W. *Chirality* **2002**, *14*, 471.

20) Zhang, J.; Holmes, A. E.; Sharma, A.; Brooks, N. R.; Rarig, R. S.; Zubieta, J.; Canary, J. W. *Chirality* **2003**, *15*, 180.

21) Holmes, A. E.; Das, D.; Canary, J. W. *J. Am. Chem. Soc*. **2007**, *129*, 1506.

22) Canary, J. W.; Mortezaei, S.; Liang, J. A. *Coordin. Chem. Rev.* **2010**, *254*, 2249-2266.

23) Zahn, S.; Canary, J. W. *Org. Lett.* **1999**, *1*, 861.

24) Hor, K.; Gimple, O.; Schreier, P.; Humpf, H. U. *J. Org. Chem.* **1998**, *63*, 322.

25) Matile, S.; Berova, N.; Nakanishi, K.; Novkova, S.; Philipova, I.; Blagoev, B. *J. Am. Chem. Soc.* **1995**, *117*, 7021.

26) Matile, S.; Berova, N.; Nakanishi, K.; Fleischhauer, J.; Woody, R. W. *J. Am. Chem. Soc.* **1996**, *118*, 5198.

27) Tabei, J.; Shiotsuki, M.; Sanda, F.; Masuda, T. *Macromolecules* **2005**, *38*, 9448.

28) Gawronski, J.; Grajewski, J.; Drabowicz, J.; Mikolajczyk, M. *J. Org. Chem.* **2003**, *68*, 9821.

29) Dalisay, D. S.; Tsukamoto, S.; Molinski, T. F. *J. Nat. Prod.* **2009**, *72*, 353.

30) Joyce, L.; Maynor, M.; Dragna, J.; da Cruz, G.; Lynch, V.; Canary J.; Anslyn, E. *J. Am. Chem. Soc.* **2011**, *133*,13746-13752.

31) You, L.; Berman, J.; Anslyn, E. *Nat. Chem.* 2011, 3. 943-948.

32) You, L; Berman, J.; Lucksanawichien, A.; Anslyn, E. *J. Am. Chem. Soc.* **2012**, *134*, 7126-7134.

33) Pfeiffer, P.; Quehl, K.; Tappermann, F. *Ber. Dtsch. Chem. Ges. B* **1930**, *63B*, 1301.

34) Bernhard Breit and Daniel Breuninger. *Synthesis* **2005**, 2782-2786.

35) Zirakzadeh, A.; Schuecker, R.; Weissensteiner, W. *Tetrahedron: Asym.* **2010**, 1494-1502.

36) Wei, N.; Murthy, N.; Chen, Q.; Zubieta, J.; Karlin, K. *Inorg. Chem.* **1994**, *33*, 1953-1965.

37) Yoshinobu, T.; Katsuya, Y.; Yoshitaka, H.; Yoshinobu; G. *Heterocycles* **2003**, *60*, 953-958.

38) Cladwell, A. *J. Chem. Soc.* **1952**, 2035-2041.

39) Weitz, E.; Chang, J.; Rosenfield, A.; Pierre, V. *J. Am. Chem. Soc.* **2012**, *134*, 39, 16099-16102.

40) Mundinger, S.; Jokob, U.; Bichovski, P.; Bannwarth, W. *J. Org. Chem.* **2012**, *77*, 8968-8979.

41) Baldeau, S; Slinn, C.; Krebs, B.; Rompel A. *Inorganica Chimica Acta* **2004**, *357*, 3295-3303.

42) Cao, B.; Wang, Y.; Ding, K.; Neamati, N.; Long, Y. *Organic and Biomolecular Chemistry,* **2012**, *10*, 1239-1245.

# Chapter 5

## 1. Introduction

High throughput screening (HTS) of asymmetric catalysis reactions has been adopted in both academic and industrial settings.[1–3] Even though HTS has become possible with development of multiplexed instrumentation such as HPLC-CD, HPLC-MS, HPLC-UV, and MISER HPLC-MS,[4–16] the need for optimizing methods for each reaction leaves the analysis of samples a bottleneck of this process. This mismatch in efficiency between the analytical and synthetic tools has driven the development of chiroptical based sensors that are more compatible with the workflow of HTS.[17–19]

A chiral optical sensor works by coordinating or binding to the chiral analyte, which generates CD active species or modulates the optical spectra.[20] Due to the nature of sensor-analyte interaction, the sensors often are only capable of reporting the enantiomeric excess (ee) of stereocenter with similar functional groups. For example, Dragna et al[21] reported a 3-hydroxy-2-picolinealdehdye and Fe(II) based sensor for chiral amines (**Scheme 5.1a**). The bidentate imine ligand, generated from condensing a chiral amine with a picolinaldehyde, forms a CD active complex after coordination with Fe(II). Thus, this sensor complex is only capable of chiroptical sensing for nucleophilic amines or hydrazines. Similarly, You et al[22] developed a multicomponent dynamic assembly that is capable for sensing of chiral secondary alcohols (**Scheme 5.1b**). The assembly is orthogonal to stronger nucleophiles. For example, amines could disrupt the assembly equilibrium via zinc coordination and thereby hinder the formation of the key iminium intermediate.

Often, biologically active natural products contain more than one stereocenters, thus transformations that introduces more than one stereocenter with high enantio-selectivity is particularly of interest. To enable HTS for these transformations, we describe

herein our efforts to develop a platform capable of determining two stereocenters. In addition to developing ee determination sensors for aminoalcohols, we engineered a CD well plate reader for fast analysis.

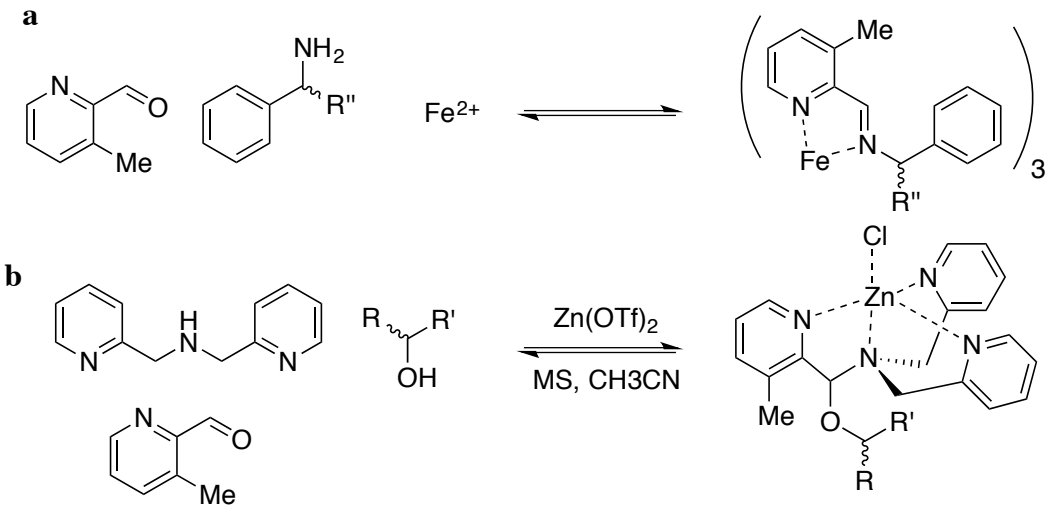


**Scheme 5.1** The multicomponent dynamic chemoselective assemblies that have been used to determine ee of **a)** chiral primary amines and **b)** chiral secondary alcohols or secondary amines.

## 2. Results and Discussion

### 2.1 Circular Dichroism Well Plate Reader Quality Control

Part of the effort to develop a faster screening platform for enantiomeric excess (ee) determination was the instrumentation. We collaborated with Hinds Instruments® to commercialize the first circular dichroism well plate reader. A large part of the technology followed the same principle as the previously published proof of concept paper.[23] Improvements in the instrumentation design, particularly how the well plate is positioned inside the instrument is a large focus of our work. Additionally, the integrity of the quartz well plates purchased from Hellma® was interrogated using Exicor® Microimager.

#### *2.1.1 Amine Assembly*

The instrument was able to read the amine assembly formed with 3-methylpyridine-2-carbaldehyde, methylbenzylamine, and Fe(II) with high fidelity to the JASCO instrument (Figure 5.1). In our previous publication the same assembly was shown to have comparable CD at 480 nm to 600 nm range, therefore only the region between 200 nm to 350 nm was investigated.

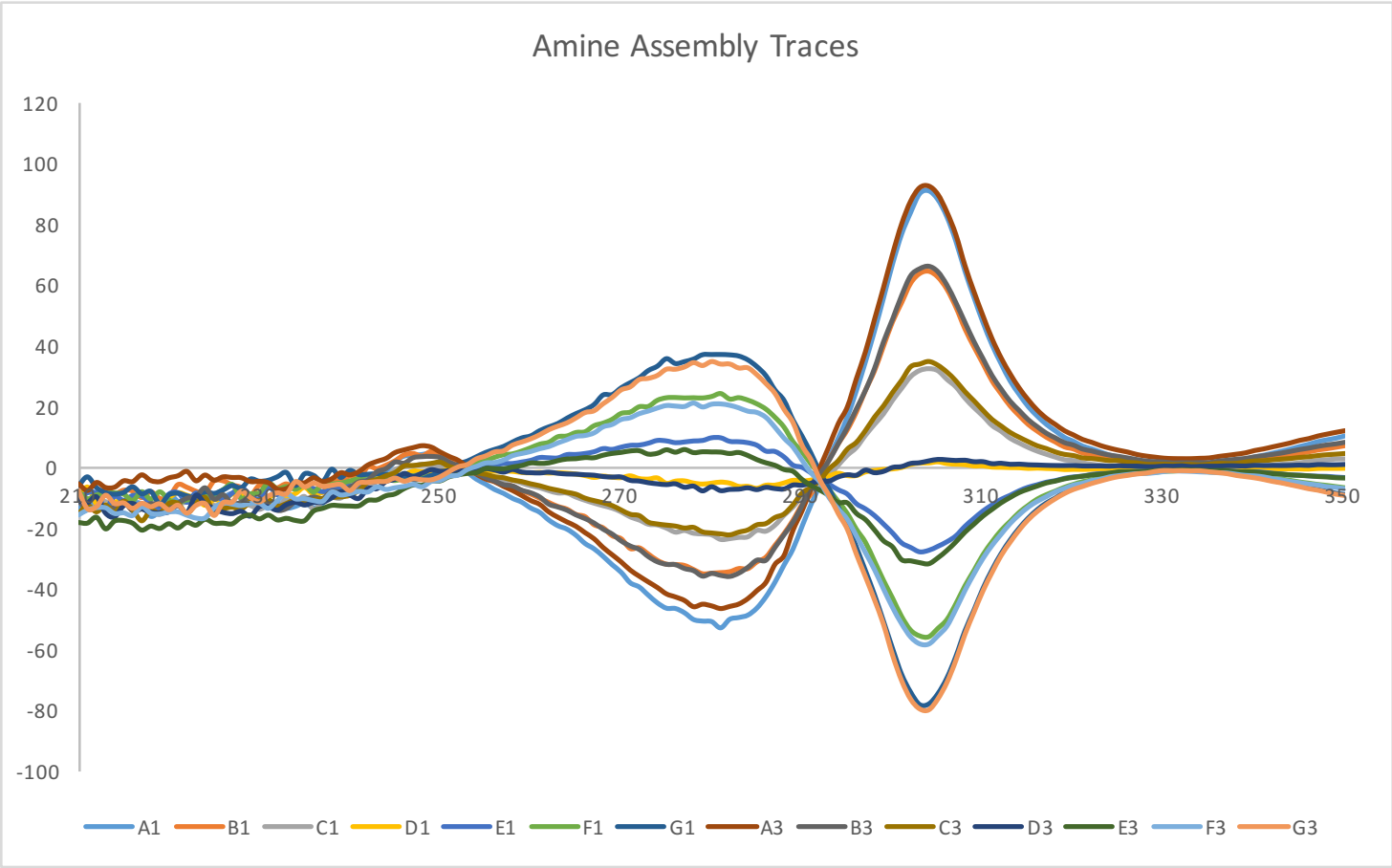


**Figure 5.1** CD spectra of the MLCT bands of the Fe(II) (0.03 mM) assembly with 3-methylpyridine-2-carbaldehyde (0.15 mM) and methylbenzylamine (0.15 mM) at various ee in acetonitrile in a 96-well quartz plate from 220 to 350 nm.

### *2.1.2 Alcohol Assembly*

The instrument was not able to read the alcohol assembly formed with 3-methylpyridine-2-carbaldehyde, di(2-picolyl)amine, chloroethylmorpholine-HCl, 1-phenylethanol, and Zn(II) with high accuracy at the same concentration (**Figure 5.2**). It was speculated that at the original concentration (0.2 mM) very little light can pass through the sample resulting in large errors observed by the detector. Once the pathlength for the well plate was halved (half of the amount of sample to the well plate), higher accuracy was observed (**Figure 5.3**). For JASCO results see chapters 2-4.

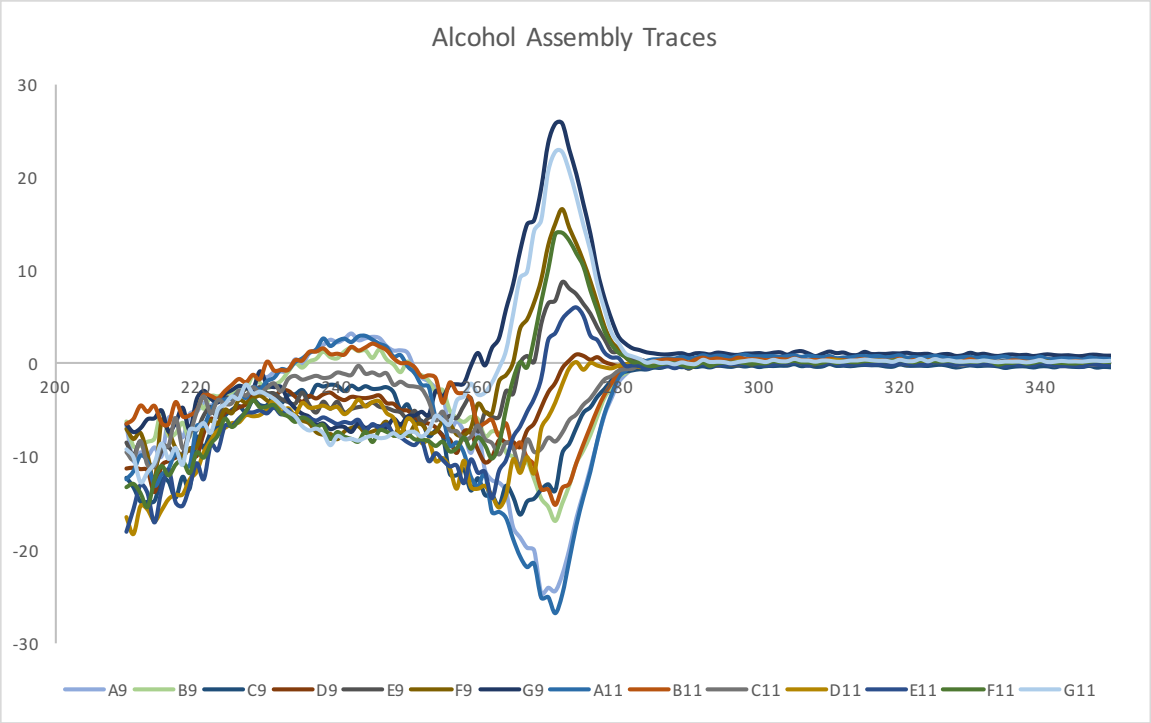


**Figure 5.2** CD spectra of the alcohol assembly form with Zn(II), 3-methylpyridine-2-carbaldehyde, di(2-picolyl)amine, chloroethylmorpholine-HCl, and 1-phenylethanol at 0.2 mM at various ee in acetonitrile in a 96-well quartz plate from 220 to 350 nm.

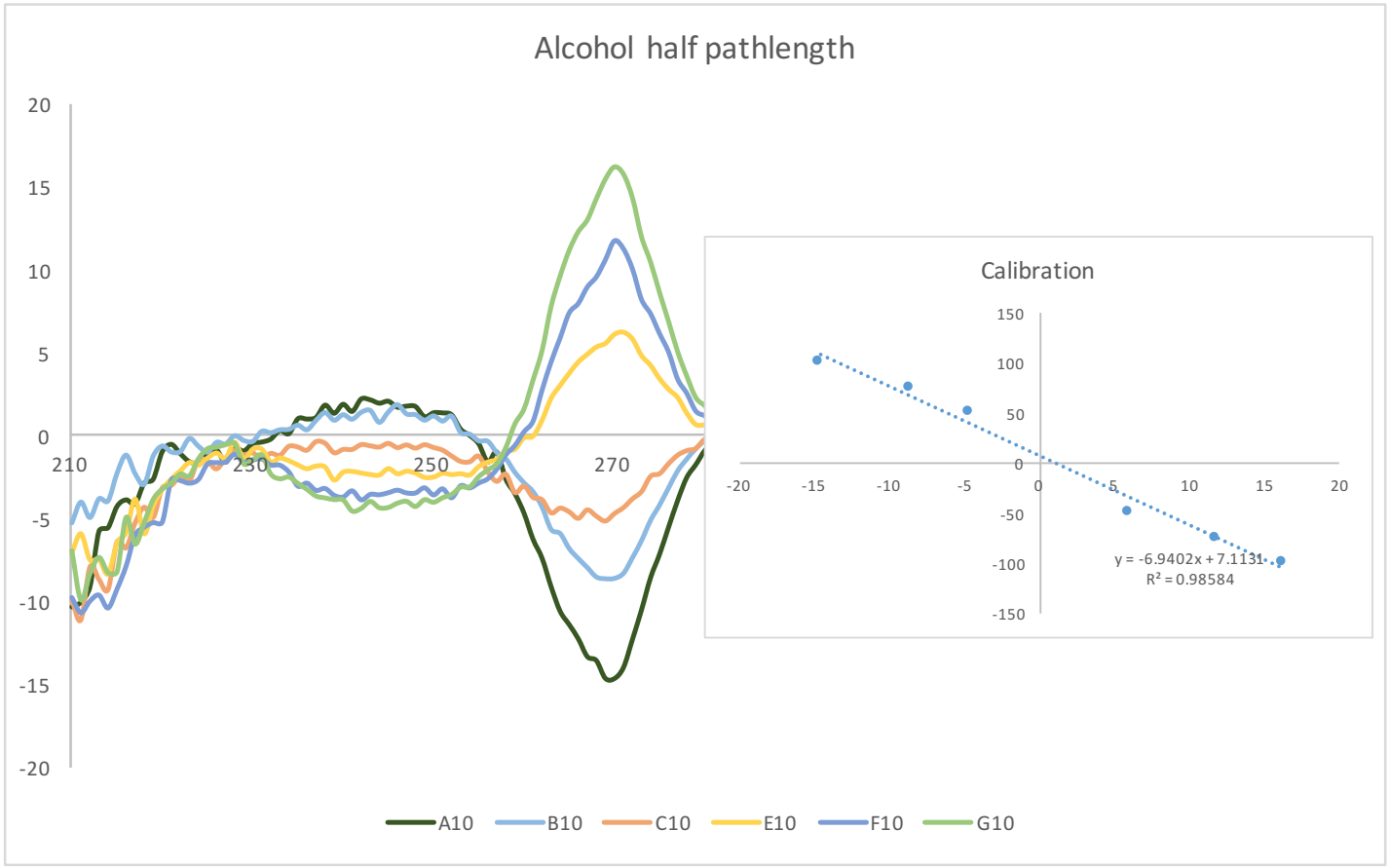


**Figure 5.3** CD spectra and the calibration curve of the alcohol assembly form with Zn(II), 3-methylpyridine-2-carbaldehyde, di(2-picolyl)amine, chloroethylmorpholine-HCl, and 1-phenylethanol at 0.2 mM at various ee in acetonitrile in a 96-well quartz plate from 220 to 350 nm at halved pathlength.

### *2.1.3 Hellma® Quartz Well Plates Birefringence*

During the quality control process, we found that fused silica well plate would not work for the sensors in the low UV region. Therefore, two quartz well plates from Hellma® were procured. The quartz well plates were made by attaching the top well part to a solid bottom. The synthetic quartz used offers high chemical resistance, UV transmission, and thermal stability. However, inherent birefringence of the quartz material might be problematic if not controlled. Thus, we measured the plate birefringence with the Hinds Instruments' Exicor Microimager (**Figure 5.4**). As seen in the heat map, one well plate (**Figure 5.4 a**) suffers from minor birefringence for the wells around the plate perimeter while the other one (**Figure 5.4 b**) was pretty great.

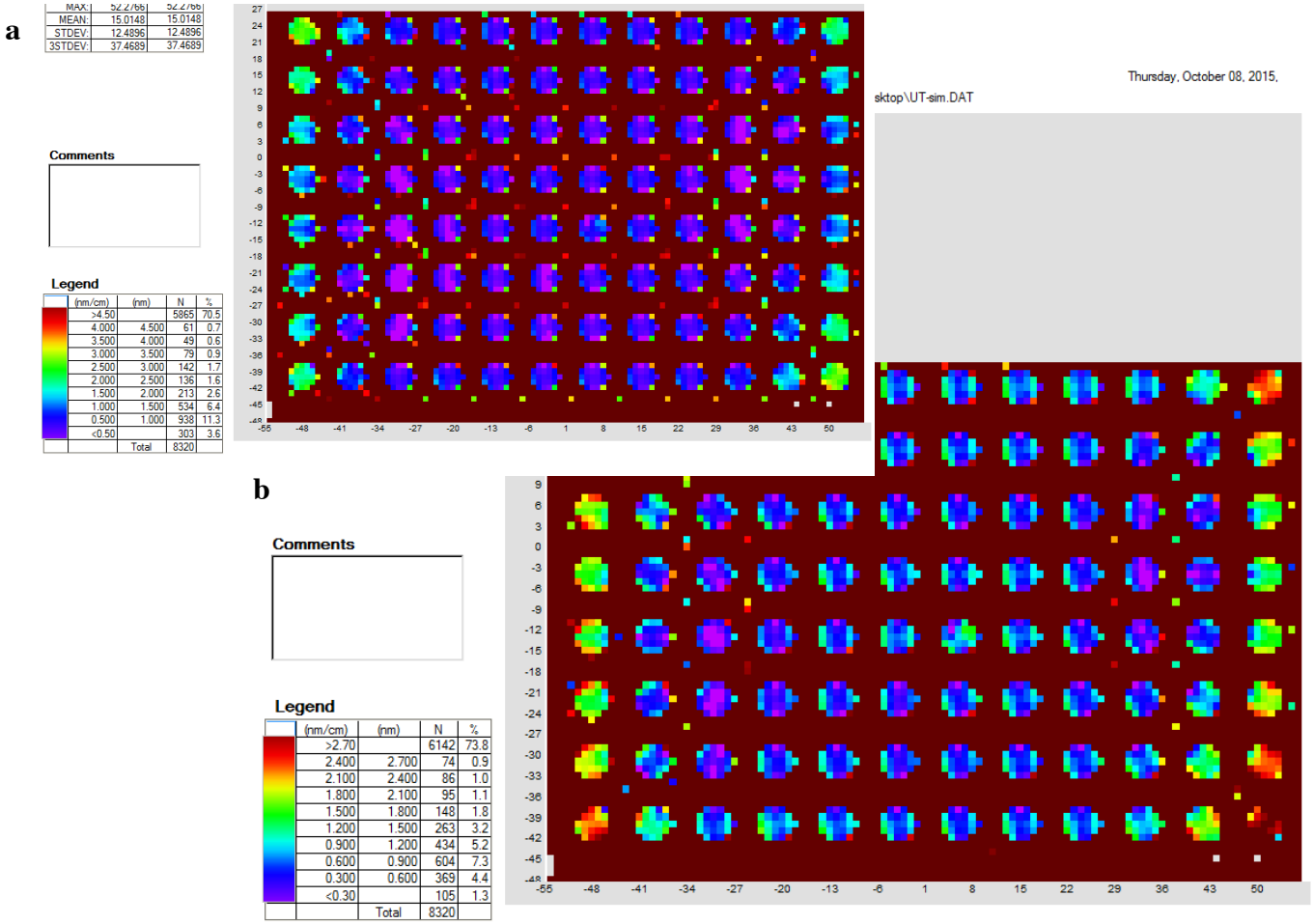


**Figure 5.4** Birefringence reading of the two quartz well plates from Hellma®. Both of the well plates suffered from minor birefringence for the well around the plate perimeter with one being slightly worse than the other one (red is high birefringence and purple/blue is low).

## 2.2 Concurrent Assembly Development

### *2.2.1 Concurrent Formation of the Amine and Alcohol Assembly for ee Determination*

To explore the potential of forming the amine and alcohol assembly and measuring the CD of both assemblies concurrently, we started out by attempting to form the alcohol assembly first, then add the components for the formation of amine assembly. This sequence turned out to be detrimental for the alcohol assembly, presumably due to the fast extraction of Zn(II) from the alcohol assembly by an amine. When we reversed the order, where we pre-formed the amine assembly, we found that the alcohol sensor assembled.

After establishing that the two assemblies were formed in the same mixture, measuring ee and the associated errors with these two systems concurrently were investigated. The absorbance for the two assembly overlaps near the $CD_{max}$ for alcohol assembly. To compensate for this increased absorbance, the assemblies' concentrations were adjusted (40% reduction of alcohol and 60% reduction of amine). Expectedly, these changes in concentration decreased our dynamic range because of Beer's law.

To start, calibration curves were built for phenethyl alcohol and benzylmethyl-amine using the cooresponding assemblies (**Figure 5.4** and **Figure 5.5**). The two calibration curves were generated at the adjusted concentration (0.12 mM alcohol and 0.012 mM amine), and with the other sensing assembly present at zero ee. Once the calibrations were generated, we tested it against samples with unknown alcohol and amine ee (**Figure 5.6** and **Table 5.1**). As seen in **Figures 5.4** and **5.5**, the amine assembly's CD spectrum overlaped with the alcohol assembly's CD from 290 nm and below. Therefore, to calculate the ee of the chiral alcohol and amine in this mixture, we needed to determine the ee of the chiral amine first by looking at the calibration curve constructed above 290nm. Once the amine ee was determined, the CD contribution of the chiral amine at 270 nm was

determined using a second calibration curve. This calculation allows us to isolate the chiral alcohol assembly CD at 270 nm, which can then be used to calculate the ee of chiral alcohol. As seen in **Table 5.1**, the average error for ee determination is 4.7 for the amine and 10.7 for the alcohol. This increase in error for alcohol ee determination can be attributed to the necessary propagation from determining the amine ee to amine CD, which was used to calculate alcohol CD which was then used to calculated the alcohol ee.

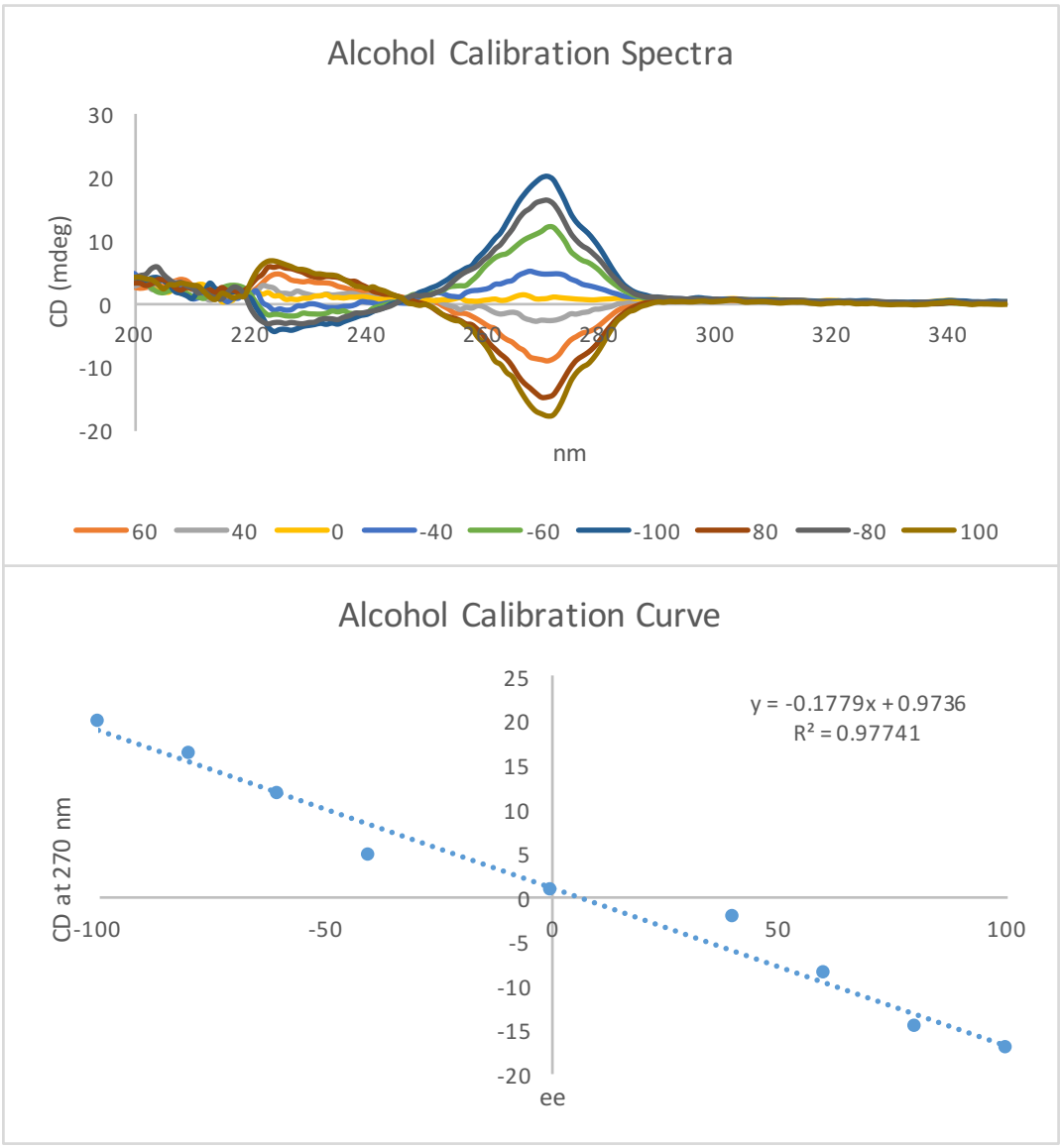


**Figure 5.4** CD spectra and the calibration curve of the alcohol assembly form with Zn(II), 3-methylpyridine-2-carbaldehyde, di(2-picolyl)amine, chloroethylmorpholine-HCl, and 1-phenylethanol at 0.12 mM at various ee in acetonitrile in a 96-well quartz plate from 200 to 350 nm. These measurement was done in the presence of amine assembly (0.012 mM) with racemic amine analyte.

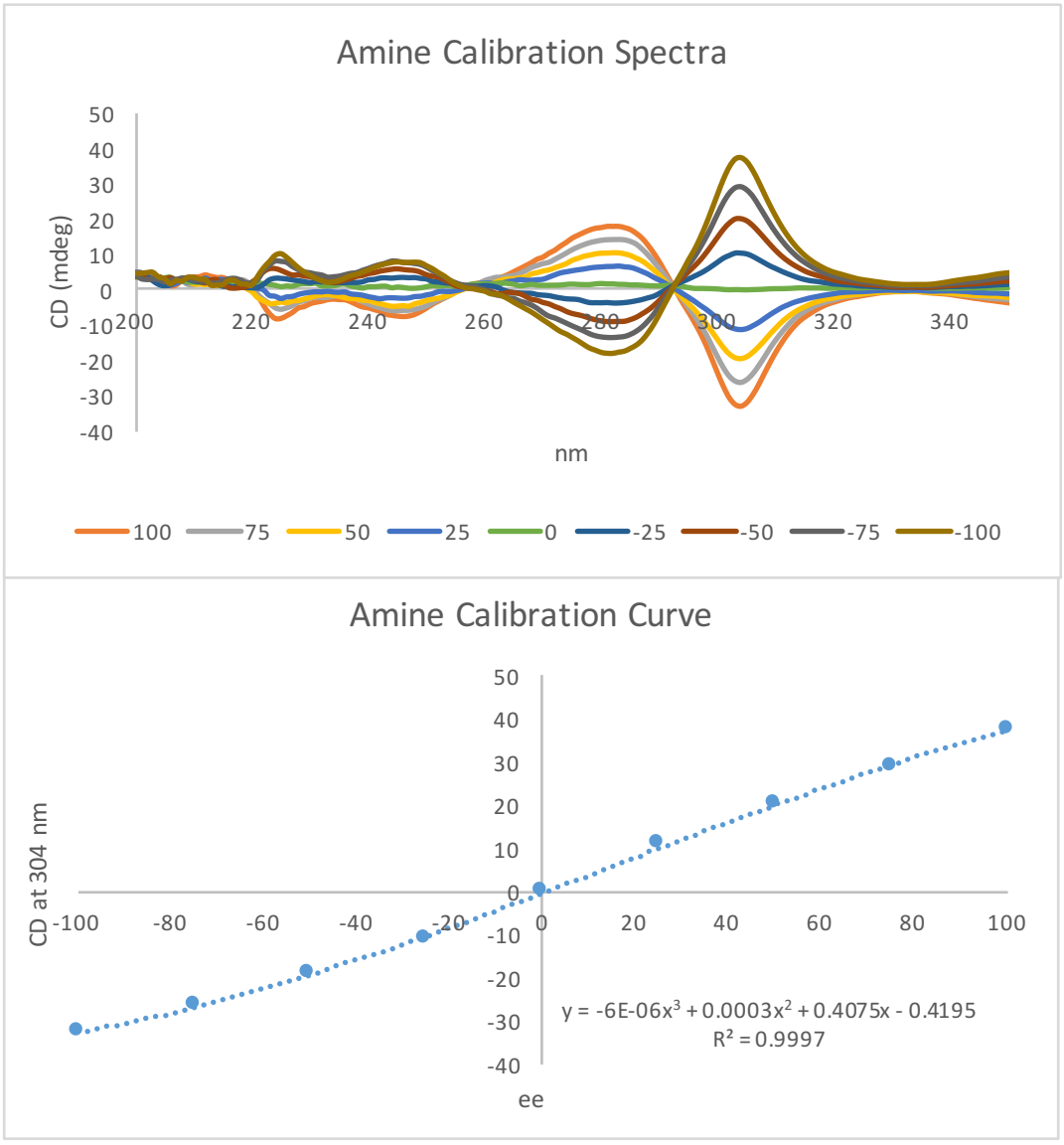


**Figure 5.5** CD spectra of the MLCT bands of the Fe(II) (0.012 mM) assembly with 3-methylpyridine-2-carbaldehyde (0.06 mM) and methylbenzylamine (0.06 mM) at various ee in acetonitrile in a 96-well quartz plate from 220 to 350 nm. These measurement was done in the presence of alcohol assembly (0.12 mM) with racemic amine analyte.

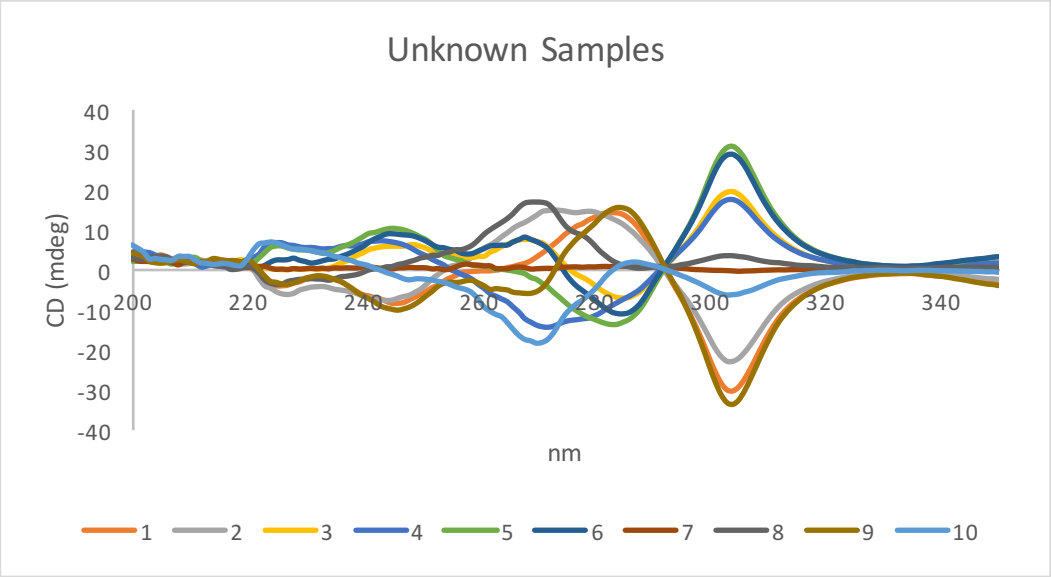


**Figure 5.6** CD spectra of samples with unknown mixtures of chiral 1-phenylethanol and methylbenzylamine.

| Sample | CD 304 nm | Calculated ee | Actual ee | Error | Calculated CD at 270nm | CD 270 nm | Corrected CD | Calculated ee | Actual ee | Error |
|---|---|---|---|---|---|---|---|---|---|---|
| 1 | -30.24 | -88.90 | -72.00 | 16.90 | 8.30 | 3.29 | -5.00 | 32.85 | 19.36 | 13.49 |
| 2 | -22.80 | -61.62 | -58.00 | 3.62 | 6.29 | 13.60 | 7.31 | -34.83 | -40.56 | 5.73 |
| 3 | 19.50 | 48.31 | 46.00 | 2.31 | -3.79 | 7.28 | 11.06 | -55.45 | -50.50 | 4.95 |
| 4 | 17.53 | 43.38 | 40.00 | 3.38 | -3.30 | -13.46 | -10.15 | 61.15 | 49.50 | 11.65 |
| 5 | 31.30 | 80.96 | 92.00 | 11.04 | -7.00 | -1.89 | 5.10 | -22.68 | -20.64 | 2.04 |
| 6 | 29.40 | 75.25 | 74.00 | 1.25 | -6.44 | 7.33 | 13.77 | -70.30 | -60.42 | 9.88 |
| 7 | -0.22 | 1.31 | 0.00 | 1.31 | 0.77 | 0.41 | -0.37 | 7.37 | -0.67 | 8.04 |
| 8 | 3.43 | 9.94 | 7.00 | 2.94 | -0.05 | 16.89 | 16.94 | -87.73 | -80.24 | 7.49 |
| 9 | -33.66 | -103.05 | -100.00 | 3.05 | 9.22 | -5.35 | -14.57 | 85.42 | 59.57 | 25.85 |
| 10 | -6.04 | -13.00 | -14.00 | 1.00 | 2.11 | -18.26 | -20.37 | 117.26 | 98.94 | 18.32 |
| | | | average | 4.68 | | | | | average | 10.74 |

**Table 5.1** The ee determination results for the unknown samples with the calibration curves generated in Figure 5.4 and 5.5. The amine 270 nm calibration curve is not shown.

### *2.2.2 Running the Amine and Alcohol Assembly for 2-Aminocyclohexanol*

Once it was shown that the amine and alcohol assembly can be used concurrently to determine the ee of a secondary alcohol and primary amine, we turned our attention to chiral 2-aminocyclohexanols. In our preliminary studies comparing the CD spectra of the *cis*- and *trans*- aminoalcohol enantiomers, the diastereomers do have different magnitudes of CD maximum (**Figure 5.7**). This means that we will need additional information to better our estimations of the aminoalcohol ee (see Appendix).

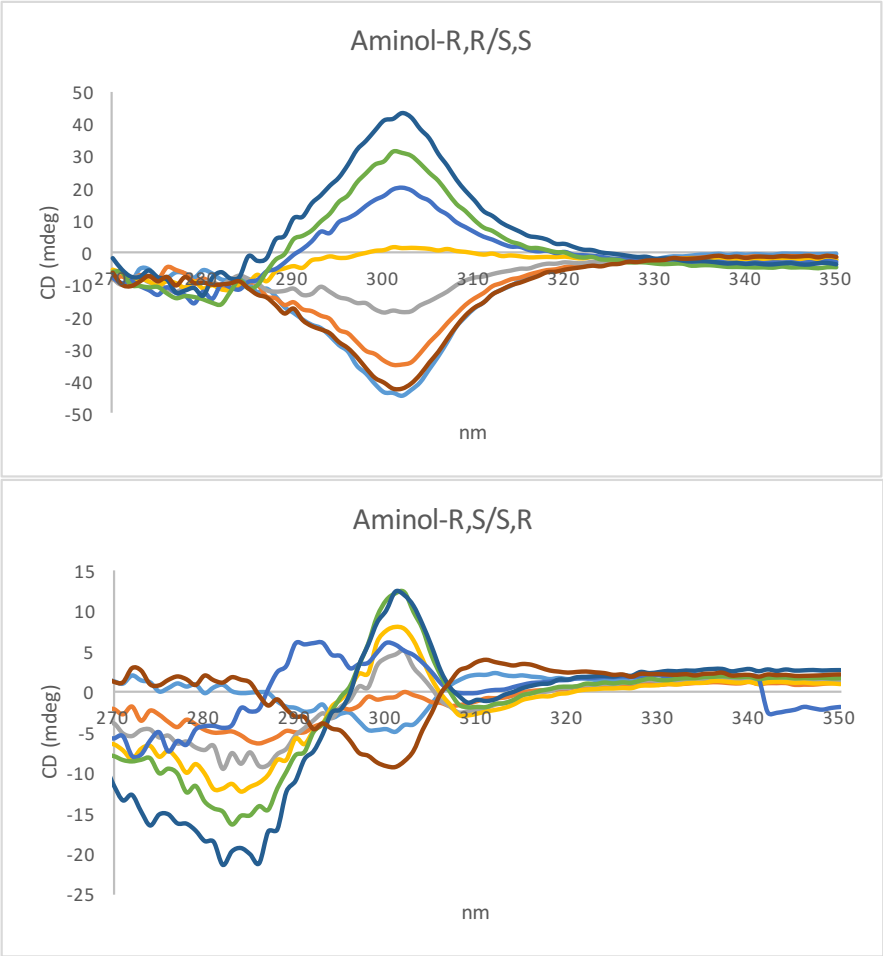


**Figure 5.7** The amine assembly CD spectra for the *trans*- (top) and *cis*- (bottom) enantiomers of 2-aminocyclohexanol. The difference in the magnitude of CD maximum suggested additional information is needed.

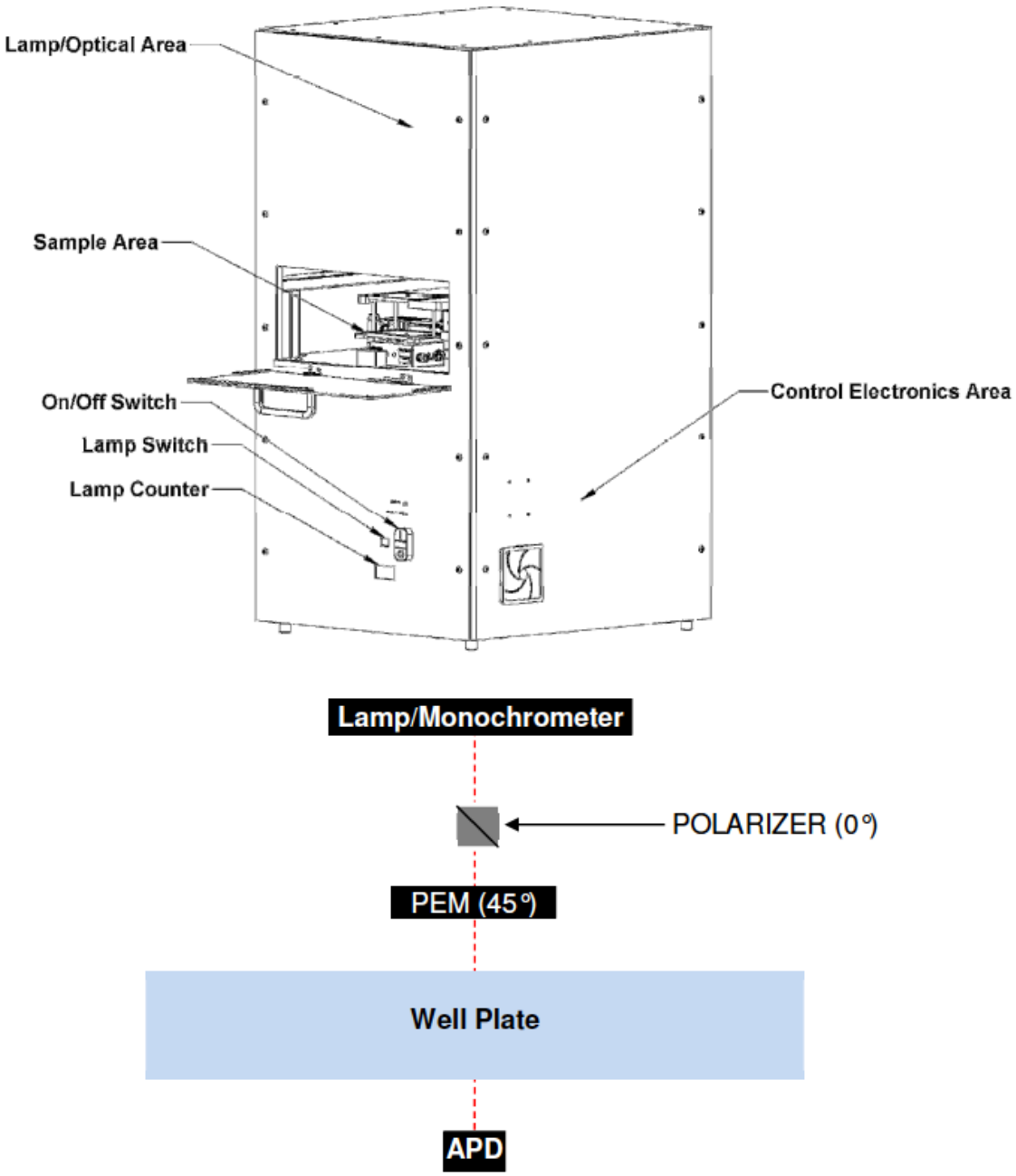


**Figure 5.8** Fast CD well plate reader main component schematics.

### 3. RELATING EE TO DR

Enantiomeric excess (ee) or ratio (er) is commonly used to quantify the relative amount of enantiomers in a mixture. For molecules with two or more stereocenters, additional descriptors such as diastereomeric ratio (dr) is used to further elucidate the amount of diastereomers in the mixture. Given a scenario where diketones are sequentially reduced to an alcohol and amine (**Scheme 5.2**), four different stereoisomers are generated. In this theoretical scenario, the first transformation sets the alcohol stereocenter (shown in maroon in **Scheme 5.2**) while the second sets the amine stereocenter (blue in **Scheme 5.2**). Out of the four stereoisomers, A (R,R) and C (S,R) are the enantiomeric pair of the anti-diastereomers, and B (R,S) and D (S,S) are the enantiomeric pair of the syn- diastereomer. With the ee sensors presented above, we could determine the er at the alcohol (er1) and amine (er2) position.

$$er1 = \frac{A + B}{C + D}$$

$$er2 = \frac{A + C}{B + D}$$

These values can be seen as two known values that relates the quantity of unknown stereoisomers. To relate these ers to the dr of this mixture of stereoisomers (defined as the syn diastereomer over the anti), an additional relationship is needed to restrict the solution (see appendix for the full proof).

$$dr = \frac{(er1 \times er2) + 1}{(er1 + er2)} \; when \; A \cdot D = B \cdot C$$

This relationship between the ers and dr deviates from the true value when the product of the enantiomeric pair of each diastereomer are not equal. In other terms, the dr calculated using above relationship is closest to the true value when the one or two of the transformations in the scenario are not highly stereoselective.

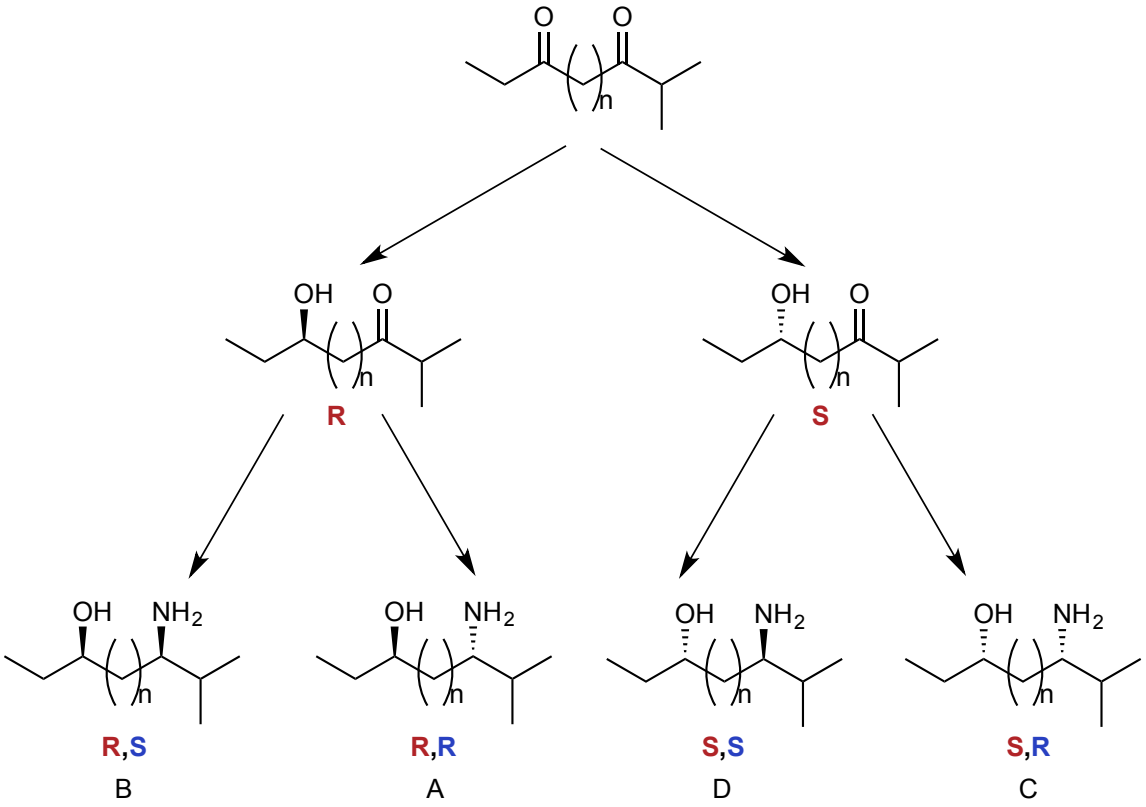


**Scheme 5.2** A theoretical scenario where a diketone is sequentially reduced to an aminoalcohol, where the first transformation sets the alcohol stereocenter and the second transformation sets the amine stereocenter. The four possible stereoisomers (A-D) of the aminoalcohols are shown on the bottom. The stereocenter designations are also shown where maroon letter denotes the alcohol stereocenter and blue letter denotes amine stereocenter.

To further investigate this deviation, a set of randomly generated data (matrix of 5000 by 4, Python 3) was use to calculate dr and ers. The generated ers are then used to calculate theoretical dr (drc) values according to the relationship described above. Three dimensional scatterplots of the two ers and the difference between dr and drc are generated for visualization (**Figure 5.9**).

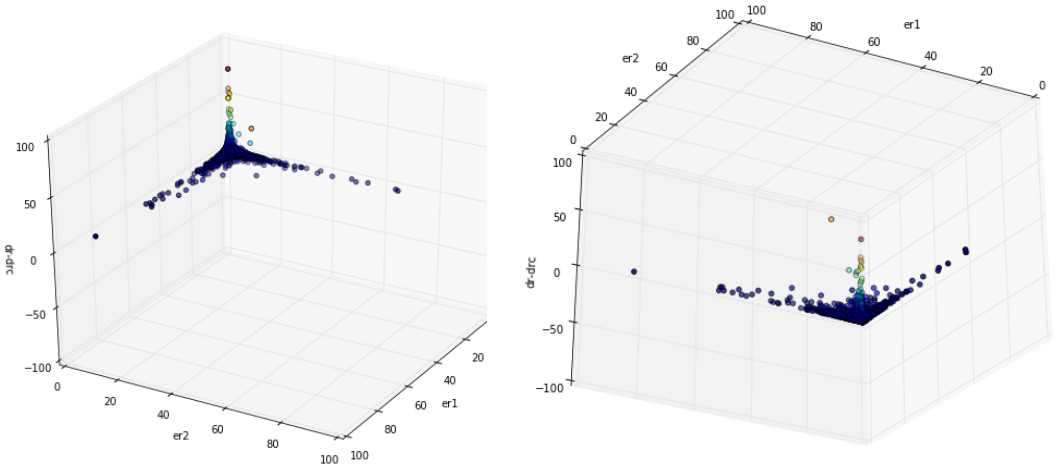


**Figure 5.9** Three dimensional scatterplot of the generated er values (x- and y- axis) and the deviation of dr value calculated with the relationship derived in the text.

## 4. Conclusion

At this point, we have developed a fast CD well plate reader and a sensing system that is capable of determining the ee of two stereocenters on two different molecules. In our case, we have chosen a primary amine and a secondary alcohol, but this approach could be expended to other functionalities. Carrying further, we will need to demonstrate this sensing system will work on a molecule with two stereocenters before implementing this sensing platform to screen asymmetric aminohydroxylation.

## 5. Reference


1) Bentley, K. W.; Zhang, P.; Wolf, C. *Sci. Adv.* **2016**, 1.
2) McNally, A.; Prier, C. K.; MacMillan, D. W. C. *Science*. **2011**, *334*, 1114.
3) Santanilla, A. B.; Regalado, E. L.; Pereira, T.; Shevlin, M.; Bateman, K.; Campeau, L.; Schneeweis, J.; Berritt, S.; Shi, Z.; Nantermet, P.; Liu, Y.; Helmy, R.; Welch, C. J.; Vachal, P.; Davies, I. W.; Cernak, T.; Dreher, S. D. *Science*. **2015**, *347*, 443.
4) Vistuba, J. P.; Piovezan, M.; Pizzolatti, M. G.; Rebelo, A. M.; Azevedo, M. S.; Vitali, L.; Costa, A. C. O.; Amadeu Micke, G. *J. Chromatogr. A* **2013**, *1274*, 159.
5) Bellomo, A.; Celebi-Olcum, N.; Bu, X.; Rivera, N.; Ruck, R. T.; Welch, C. J.; Houk, K. N.; Dreher, S. D. *Angew. Chemie Int. Ed.* **2012**, *51*, 6912.
6) Duursma, A.; Minnaard, A. J.; Feringa, B. L. *Tetrahedron* **2002**, *58*, 5773.
7) Joyce, L. a.; Sherer, E. C.; Welch, C. J. *Chem. Sci.* **2014**, *5*, 2855.
8) Friest, J. A.; Broussy, S.; Chung, W. J.; Berkowitz, D. B. *Angew. Chemie Int. Ed.* **2011**, *50*, 8895.
9) Gao, X.; Kagan, H. B. *Chirality* **1998**, *124*, 120.

10) Guo, J.; Wu, J.; Siuzdak, G.; Finn, M. G. *Angew. Chemie Int. Ed.* **1999**, *38*, 1755.

11) Evans, M. A.; Morken, J. P. *J. Am. Chem. Soc.* **2002**, *124*, 9020.

12) Wolf, C.; Hawes, P. A. *J. Org. Chem* **2002**, 2727.

13) Reetz, M. T.; Kühling, K. M.; Wilensek, S.; Husmann, H.; Häusig, U. W.; Hermes, M. *Catal. Today* **2001**, *67*, 389.

14) Reetz, M. T.; Becker, M. H.; Kühling, K. M.; Holzwarth, A. *Angew. Chemie - Int. Ed.* **1998**, *37*, 2647.

15) Reetz, M. T.; Eipper, A.; Tielmann, P.; Mynott, R. *Adv. Synth. Catal.* **2002**, *344*, 1008.

16) Taran, F.; Gauchet, C.; Mohar, B.; Meunier, S.; Valleix, A.; Renard, P. Y.; Créminon, C.; Grassi, J.; Wagner, A.; Mioskowski, C. *Angew. Chemie - Int. Ed.* **2002**, *41*, 124.

17) Jo, H. H.; Lin, C.; Anslyn, E. V. *Acc. Chem. Res.* **2014**, *47*, 2212.

18) Leung, D.; Kang, S. O.; Anslyn, E. V. *Chem. Soc. Rev.* **2012**, *41*, 448.

19) Wolf, C.; Bentley, K. W. *Chem. Soc. Rev.* **2013**, *42*, 5408.

20) Leung, D.; Anslyn, E. V. *J. Am. Chem. Soc.* **2008**, *130*, 12328.

21) Dragna, J. M.; Pescitelli, G.; Tran, L.; Lynch, V. M.; Anslyn, E. V.; Di Bari, L. *J. Am. Chem. Soc.* **2012**, *134*, 4398.

22) You, L.; Berman, J. S.; Anslyn, E. V. *Nat. Chem.* **2011**, *3*, 943.

23) Anslyn, E. V; Kahr, B.; Nichols, S. M.; Metola, P. *Chem. Sci.* **2014**, *5*, 4278.

# Appendix

This section shows the mathematical manipulation that relates the two enantiomeric ratio (er) values of to a value that can be used to estimate diastereomeric ratio (dr) value. In this system, four stereoisomeric (A-D) species have been generated from two sequential reactions. For the chemical scheme, see chapter five section three.

$$er1 = \frac{x}{y} = \frac{A + C}{B + D}$$
$$er2 = \frac{u}{v} = \frac{A + B}{C + D}$$
$$dr = \frac{A + D}{B + C}$$

$$xu + yv = A^2 + AC + AB + 2BC + BD + CD + D^2$$

$$xv + yu = B^2 + BD + AB + 2AD + CA + CD + C^2$$

multiply the numerator and denominator with (A+D) (C+B), we get

$$\frac{(er1 \cdot er2) + 1}{er1 + er2} = \frac{xu + yv}{xv + yu} = \frac{(A^2 + AC + AB + 2BC + BD + CD + D^2)(C + B)(A + D)}{(B^2 + BD + AB + 2AD + CA + CD + C^2)(A + D)(C + B)}$$

then multiply out the first two terms to get

$$= \frac{(A^2C + AC^2 + ABC + BCD + C^2D + CD^2 + 2BC^2 + A^2B + AB^2 + ABC + BCD + B^2D + BD^2 + 2B^2C)(A + D)}{(A^2C + AC^2 + ABD + ACD + C^2D + CD^2 + 2AD^2 + A^2B + AB^2 + ABD + ACD + B^2D + BD^2 + 2A^2D)(C + B)}$$

rearrange the terms

$$= \frac{(A^2C + AC^2 + C^2D + CD^2 + A^2B + AB^2 + B^2D + BD^2 + 2ABC + 2BCD + 2BC^2 + 2B^2C)(A + D)}{(A^2C + AC^2 + C^2D + CD^2 + A^2B + AB^2 + B^2D + BD^2 + 2ABD + 2ACD + 2A^2D + 2AD^2)(C + B)}$$

we can see that most of the terms are the same in the above expression with the exception of last five, so isolate them to get

$$= \frac{(S + 2ABC + 2BCD + 2BC^2 + 2B^2C)(A + D)}{(S + 2ABD + 2ACD + 2A^2D + 2AD^2)(C + B)}$$

where S is the common sum in the expression. Looking at the four leftover terms, if the last for sums equal to each other, then

$$\frac{xu + yv}{xv + yu} = dr = \frac{A + D}{B + C}$$

in other words, if the below relationship is true, then the above is true

$$2ABD + 2ACD + 2A^2D + 2AD^2 = 2ABC + 2BCD + 2BC^2 + 2B^2C$$

simplify and factor terms out to get the following expression

$$(BC)(A + B + C + D) = (AD)(A + B + C + D)$$

then, if BC=AD,

$$\frac{xu + yv}{xv + yu} = dr = \frac{A + D}{B + C}$$

## Bibliography

Jaroch, S.; Weinmann, H.; Zeitler, K. Asymmetric organocatalysis. *Chem. Med. Chem.* **2007**, *2*, 1261–1264.

Lin, G.-Q.; Li, Y.-M.; Chan, A. S. C. *Principles and Applications of Asymmetric Synthesis*; John Wiley & Sons, 2003.

Christmann, M.; Bräse, S. *Asymmetric Synthesis*; Wiley-VCH, 2008.

Tsukamoto, M.; Kagan, H. B. Recent advances in the measurement of enantiomeric excesses. *Advanced Synthesis & Catalysis* **2002**.

Finn, M. G. Emerging methods for the rapid determination of enantiomeric excess. *Chirality,* **2002**, *14*, 534–540.

Welch, C. J.; Szczerba, T.; Perrin, S. R. Some recent high-performance liquid chromatography separations of the enantiomers of pharmaceuticals and other compounds using the Whelk-O 1 chiral stationary phase. *J. Chromatogr. A* **1997**, *758*, 93–98.

Welch, C. J.; Grau, B.; Moore, J.; Mathre, D. J. Use of chiral HPLC-MS for rapid evaluation of the yeast-mediated enantioselective bioreduction of a diaryl ketone. *J. Org. Chem.* **2001**, *66*, 6836–6837.

Welch, C. J.; Fleitz, F.; Antia, F.; Yehl, P. Chromatography as an enabling technology in pharmaceutical process development: expedited multikilogram preparation of a candidate HIV protease inhibitor. *Org. Process Res. Dev.* **2004**, *8*, 186– 191.

Sigman, M. S.; Jacobsen, E. N. Schiff base catalysts for the asymmetric Strecker reaction identified and optimized from parallel synthetic libraries. *J. Am. Chem. Soc.*

**1998**, *120*, 4901– 4902.

Wolf, C.; Hawes, P. A. A high-throughput screening protocol for fast evaluation of enantioselective catalysts. *J. Org. Chem.* **2002**, *67*, 2727–2729.

Pu, L. Fluorescence of organic molecules in chiral recognition. *Chem. Rev.* **2004**, *104*, 1687–1716.

Wolf, C.; Bentley, K. W. Chirality sensing using stereodynamic probes with distinct electronic circular dichroism output. *Chem. Soc. Rev.* **2013**, *42*, 5408–5424.

Bentley, K. W.; Wolf, C. Stereodynamic chemosensor with selective circular dichroism and fluorescence readout for in situ determination of absolute configuration, enantiomeric excess, and concentration of chiral compounds. *J. Am. Chem. Soc.* **2013**, *135*, 12200–12203.

Zhu, L.; Anslyn, E. V. Facile quantification of enantiomeric excess and concentration with indicator-displacement assays: an example in the analyses of alpha-hydroxyacids. *J. Am. Chem. Soc.* **2004**, *126*, 3676–3677.

Zhu, L.; Zhong, Z.; Anslyn, E. V. Guidelines in implementing enantioselective indicator-displacement assays for alpha-hydroxycarboxylates and diols. *J. Am. Chem. Soc.* **2005**, *127*, 4260–4269.

Zhu, L.; Shabbir, S. H.; Anslyn, E. V. Two methods for the determination of enantiomeric excess and concentration of a chiral sample with a single spectroscopic measurement. *Chem. Eur. J.* **2007**, *13*, 99–104.

Shabbir, S. H.; Joyce, L. A.; da Cruz, G. M.; Lynch, V. M.; Sorey, S.; Anslyn, E. V. Pattern-based recognition for the rapid determination of identity, concentration,

and enantiomeric excess of subtly different threo diols. *J. Am. Chem. Soc.* **2009**, *131*, 13125–13131.

Shabbir, S. H.; Regan, C. J.; Anslyn, E.V. A general protocol for creating high-throughput screening assays for reaction yield and enantiomeric excess applied to hydrobenzoin. *Proc. Nat. Acad. Sci.* **2009**, *106*, 10487.

Folmer-Andersen, J. F.; Lynch, V. M.; Anslyn, E. V. Colorimetric enantiodiscrimination of alpha-amino acids in protic media. *J. Am. Chem. Soc.* **2005**, *127*, 7986–7987.

Folmer-Andersen, J. F.; Kitamura, M.; Anslyn, E. V. Pattern-based discrimination of enantiomeric and structurally similar amino acids: an optical mimic of the mammalian taste response. *J. Am. Chem. Soc.* **2006**, *128*, 5652–5653.

Leung, D.; Folmer-Andersen, J. F.; Lynch, V. M.; Anslyn, E. V. Using enantioselective indicator displacement assays to determine the enantiomeric excess of alpha-amino acids. *J. Am. Chem. Soc.* **2008**, *130*, 12318–12327.

Leung, D.; Anslyn, E. V. Transitioning enantioselective indicator displacement assays for alpha-amino acids to protocols amenable to high-throughput screening. *J. Am. Chem. Soc.* **2008**, *130*, 12328–12333.

Coomans, D.; Massart, D. L.; Kaufman, L. Optimization by statistical linear discriminant analysis in analytical chemistry. *Anal. Chim. Acta*. **1979**, *112*, 97-122.

Li, Y.; Jiang, J. H.; Chen, Z. P.; Xu, C. J. Robust linear discriminant analysis for chemical pattern recognition. *J. Chemom.* **1999**, *13*, 3-13.

Ringnér, M. What is principal component analysis? *Nat. Biotechnol.* **2008**, 26, 303-304.

Nieto, S.; Lynch, V. M.; Anslyn, E. V.; Kim, H. High-throughput screening of identity,

enantiomeric excess, and concentration using MLCT transitions in CD spectroscopy. *J. Am. Chem. Soc.* **2008**, *130*, 9232-9233.

Nieto, S.; Lynch, V. M.; Anslyn, E. V.; Kim, H.; Chin, J. Rapid enantiomeric excess and concentration determination using simple racemic metal complexes. *Org. Lett.* **2008**, *10*, 5167–5170.

Dezhahang, Z.; Merten, C.; Poopari, M. R.; Xu, Y. Vibrational circular dichroism spectroscopy of two chiral binaphthyl diphosphine ligands and their palladium complexes in solution. *Dalton Trans.* **2012**, *41*, 10817–10824.

Nieto, S.; Dragna, J. M.; Anslyn, E. V. A facile circular dichroism protocol for rapid determination of enantiomeric excess and concentration of chiral primary amines. *Chem. Eur. J.* **2010**, *16*, 227–232.

Leung, D.; Anslyn, E. V. Rapid determination of enantiomeric excess of α-chiral cyclohexanones using circular dichroism spectroscopy. *Org. Lett.* **2011**, *13*, 2298–2301.

Dragna, J. M.; Pescitelli, G.; Tran, L.; Lynch, V. M.; Anslyn, E. V.; Di Bari, L. In situ assembly of octahedral Fe(II) complexes for the enantiomeric excess determination of chiral amines using circular dichroism spectroscopy. *J. Am. Chem. Soc.* **2012**, *134*, 4398–4407.

Pérez-Fuertes, Y.; Kelly, A. M.; Johnson, A. L.; Arimori, S.; Bull, S. D.; James, T. D. Simple protocol for NMR analysis of the enantiomeric purity of primary amines. *Org. Lett.* **2006**, *8*, 609–612.

Pérez-Fuertes, Y.; Kelly, A. M.; Fossey, J. S.; Powell, M. E.; Bull, S. D.; James, T. D.

Simple protocols for NMR analysis of the enantiomeric purity of chiral primary amines. *Nat. Protoc.* **2008**, *3*, 210–214.

Metola, P.; Anslyn, E. V.; James, T. D.; Bull, S. D. Circular dichroism of multi-component assemblies for chiral amine recognition and rapid *ee* determination. *Chem. Sci.* **2012**, *3*, 156-161.

Berova, N.; Di Bari, L.; Pescitelli, G. Application of electronic circular dichroism in configurational and conformational analysis of organic compounds. *Chem. Soc. Rev.* **2007**, *36*, 914–931.

Zahn, S. S.; Canary, J. W. J. Absolute configurations of N,N-dialkyl alpha-amino acids and beta-amino alcohols from exciton-coupled circular dichroism spectra of Cu(II) complexes. *Org. Lett.* **1999**, *1*, 861–864.

Zhang, J.; Holmes, A. E.; Sharma, A.; Brooks, N. R.; Rarig, R. S.; Zubieta, J.; Canary, J. W. Derivatization, complexation, and absolute configurational assignment of chiral primary amines: application of exciton-coupled circular dichroism. *Chirality,* **2003**, *15*, 180–189.

Huang, X. X.; Nakanishi, K. K.; Berova, N. N. Porphyrins and metalloporphyrins: versatile circular dichroic reporter groups for structural studies. *Chirality,* **2000**, *12*, 237–255.

Balaz, M.; De Napoli, M.; Holmes, A. E.; Mammana, A.; Nakanishi, K.; Berova, N.; Purrello, R. A cationic zinc porphyrin as a chiroptical probe for Z-DNA. *Angew. Chem. Int. Ed.* **2005**, *44*, 4006–4009.

Matile, S.; Berova, N.; Nakanishi, K.; Novkova, S.; Philipova, I.; Blagoev, B. Porphyrins:

Powerful Chromophores for Structural Studies by Exciton-Coupled Circular Dichroism. *J. Am. Chem. Soc.* **1995**, *117*, 7021–7022.

Furusho, Y.; Kimura, T.; Mizuno, Y. Chirality-Memory Molecule: AD 2-Symmetric Fully Substituted Porphyrin as a Conceptually New Chirality Sensor. *J. Am. Chem. Soc.* **1997**, *119*, 5267-5268.

Tanasova, M.; Yang, Q.; Olmsted, C. C. An Unusual Conformation of α-Haloamides Due to Cooperative Binding with Zincated Porphyrins. *Eur. J. Org. Chem.* **2009**, 4242-4253.

Borovkov, V. V.; Lintuluoto, J. M.; Inoue, Y. Supramolecular chirogenesis in zinc porphyrins: mechanism, role of guest structure, and application for the absolute configuration determination. *J. Am. Chem. Soc.* **2001**, *123*, 2979–2989.

Li, X.; Borhan, B. Prompt determination of absolute configuration for epoxy alcohols via exciton chirality protocol. *J. Am. Chem. Soc.* **2008**.

Li, X.; Burrell, C. E.; Staples, R. J.; Borhan, B. Absolute configuration for 1,n-glycols: a nonempirical approach to long-range stereochemical determination. *J. Am. Chem. Soc.* **2012**, *134*, 9026–9029.

Tartaglia, S.; Padula, D.; Scafato, P.; Chiummiento, L.; Rosini, C. A chemical/computational approach to the determination of absolute configuration of flexible and transparent molecules: aliphatic diols as a case study. *J. Org. Chem.* **2008**, *73*, 4865–4873.

Ghosn, M. W.; Wolf, C. Chiral amplification with a stereodynamic triaryl probe: assignment of the absolute configuration and enantiomeric excess of amino

alcohols. *J. Am. Chem. Soc.* **2009**, *131*, 16360–16361.

Ghosn, M. W. M.; Wolf, C. C. Synthesis, conformational stability, and asymmetric transformation of atropisomeric 1,8-bisphenolnaphthalenes. *J. Org. Chem.* **2011**, *76*, 3888–3897.

Yoon, H.; Lee, C.-H.; Jang, W.-D. Absolute stereochemical determination of chiral carboxylates using an achiral molecular tweezer. *Chem. Eur. J.* **2012**, *18*, 12479–12486.

Fujiwara, T.; Taniguchi, Y.; Katsumoto, Y.; Tanaka, T.; Node, M.; Ozeki, M.; Yamashita, M.; Hosoi, S. Induced circular dichroism in chiralN-methyl amides possessing an achiral binaphthyl chromophore and its application to absolute configuration determination of aliphatic chiral amines. *Tetrahedron:Asymmetry* **2012**, *23*, 981–991.

Iwaniuk, D. P.; Wolf, C. A stereodynamic probe providing a chiroptical response to substrate-controlled induction of an axially chiral arylacetylene framework. *J. Am. Chem. Soc.* **2011**, *133*, 2414–2417.

Wezenberg, S. J.; Salassa, G.; Escudero-Adán, E. C.; Benet-Buchholz, J.; Kleij, A. W. Effective chirogenesis in a bis(metallosalphen) complex through host-guest binding with carboxylic acids. *Angew. Chem. Int. Ed.* **2011**, *50*, 713–716.

Cysewski, R.; Kwit, M.; Warzajtis, B.; Rychlewska, U.; Gawroński, J. Synthesis, conformation and chiroptical properties of diaryl esters of tartaric acid. *J. Org. Chem.* **2009**, *74*, 4573–4583.

Kim, H.; So, S. M.; Yen, C. P.-H.; Vinhato, E.; Lough, A. J.; Hong, J.-I.; Kim, H.-J.;

Chin, J. Highly stereospecific generation of helical chirality by imprinting with amino acids: a universal sensor for amino acid enantiopurity. *Angew. Chem. Int. Ed.* **2008**, *47*, 8657–8660.

Berova, N.; Pescitelli, G.; Petrovic, A. G.; Proni, G. Probing molecular chirality by CD-sensitive dimeric metalloporphyrin hosts. *Chem. Commun.* **2009**, 5958–5958.

Barman, S.; Anslyn, E. V. Rapid determination of enantiomeric excess of α-chiral aldehydes using circular dichroism spectroscopy. *Tetrahedron.* **2014**, *70*, 1357–1362.

Joyce, L. A.; Maynor, M. S.; Dragna, J. M.; da Cruz, G. M.; Lynch, V. M.; Canary, J. W.; Anslyn, E. V. A simple method for the determination of enantiomeric excess and identity of chiral carboxylic acids. *J. Am. Chem. Soc.* **2011**, *133*, 13746–13752.

Joyce, L. A.; Canary, J. W.; Anslyn, E. V. Enantio-and Chemoselective Differentiation of Protected α-Amino Acids and β-Homoamino Acids with a Single Copper (II) Host. *Chem. Eur. J.* **2012**, *18*, 8064-8069.

You, L.; Berman, J. S.; Anslyn, E. V. Dynamic multi-component covalent assembly for the reversible binding of secondary alcohols and chirality sensing. *Nature. Chem.* **2011**, *3*, 943–948.

You, L.; Pescitelli, G.; Anslyn, E. V.; Di Bari, L. An exciton-coupled circular dichroism protocol for the determination of identity, chirality, and enantiomeric excess of chiral secondary alcohols. *J. Am. Chem. Soc.* **2012**, *134*, 7117–7125.

You, L.; Berman, J. S.; Lucksanawichien, A.; Anslyn, E. V. Correlating sterics parameters and diastereomeric ratio values for a multicomponent assembly to

predict exciton-coupled circular dichroism intensity and thereby enantiomeric excess of chiral secondary alcohols. *J. Am. Chem. Soc.* **2012**, *134*, 7126–7134.

Pu, L. Enantioselective fluorescent sensors: a tale of BINOL. *Acc. Chem. Res.* **2012**, *2*, 150-163.

Wen, K.; Yu, S.; Huang, Z.; Chen, L.; Xiao, M.; Yu, X.; Pu, L. Rational Design of a Fluorescent Sensor to Simultaneously Determine Both the Enantiomeric Composition and the Concentration of Chiral Functional Amines. *J. Am. Chem. Soc.* **2015**, *137*, 4517-4524.

Wang, C.; Wu, E.; Wu, X.; Xu, X.; Zhang, G.; Pu, L. Enantioselective fluorescent recognition in the fluorous phase: Enhanced reactivity and expanded chiral recognition. *J. Am. Chem. Soc.* **2015**, *137*, 3747-3750.

Bentley, K. W.; Zhang, P.; Wolf, C. Miniature high-throughput chemosensing of yield , ee , and absolute configuration from crude reaction mixtures. *Sci. Adv.* **2016**, 2.

Bentley, K. W.; Nam, Y.; Murphy, J.; Wolf, C. Chirality Sensing of Amines, Diamines, Amino Acids, Amino Alcohols, and hydroxy Acids with a single probe. *J. Am. Chem. Soc.,* **2013**, *135*, 18052-18055.

De Los Santos, Z.; Ding, R.; Wolf, C. Quantitative chirality sensing of amines and amino alcohols via Schiff base formation with a stereodynamic UV/CD probe. *Org. Biomol. Chem.,* **2016**, *14*, 1934-1939.

Bentley, K. W.; Wolf, C. Comprehensive Chirality Sensing: Development of Stereodynamic Probe with a Dual (Chir)optical Response. *J. Org. Chem.* **2014**, *79*, 6517- 6531.

de Vries, J. G.; Lefort, L. *Chemistry – A European Journal* **2006**, *12*, 4722.

Anslyn, E. V; Kahr, B.; Nichols, S. M.; Metola, P. *Chem. Sci.* **2014**, *5*, 4278.

Welch, C.; Biba, M.; Sajonz, P. *Chirality*. **2007**, *19*, 34-43.

Gubitz, G. *Chromatographia* **1990**, *30*, 555.